Application Artificial Forecasting Techniques in Cost Management (review)

Dr. Faiq Mohammed Sarhan Al-Zwainy
Assist Professor
Department of Civil Engineering
College of Engineering
Alnahrain University
faiq_faiqmohmed@yahoo.com

Neran Taher Hadal
M.Sc.Student
Department of Civil Engineering
College of Engineering
Baghdad University
neran_taher68@yahoo.com

ABSTRACT

For the duration of the last few many years many improvement in computer technology, software program programming and application production had been followed with the aid of diverse engineering disciplines. Those trends are on the whole focusing on synthetic intelligence strategies. Therefore, a number of definitions are supplied, which recognition at the concept of artificial intelligence from exclusive viewpoints. This paper shows current applications of artificial intelligence (AI) that facilitate cost management in civil engineering tasks. An evaluation of the artificial intelligence in its precise partial branches is supplied. These branches or strategies contributed to the creation of a sizable group of fashions such as difficulty evaluation, interpretation and prediction of various parameters. A list of decided on, updated fashions is provided, that challenge cost control for civil engineering initiatives. The models are analyzed in keeping with the pastime, discipline of operation, enter and output statistics and the techniques and strategies they implant. It will become clean that arterial Intelligence may be the destiny vital tool for each engineer and it's going to lead to sizable upgrades within the construction area.

Keywords: Artificial intelligence applications, Civil Engineering, Cost Management

تطبيقات تقنيات التنبؤ الذكية في ادارة الكلفة (استعراض)

د. فائق محمد سرحان الزويني
استاذ مساعد
كلية الهندسة / القسم المدني
جامعة النهرين

نيران طاهر هذال
طالبة ماجستير
كلية الهندسة / القسم المدني
جامعة بغداد

الخلاصة

طوال العقود القليلة الماضية اصبحت عدة تطورات في علم الحاسوب , البرمجيات وتطبيق وانتاج هذه البرامج تم اعتماده بمن قبل تخصصات هندسية متنوعة تركز هذه التطورات عموما على تكنلوجيا الذكاء الاصطناعي , لذلك عد من التعاريف قد تم تقديمها والتي تركز على مفهوم الذكاء الاصطناعي من وجهات نظر مختلفة . يعرض هذا البحث تطبيقات موجودة للذكاء الاصطناعي والتي تقوم بتسهيل ادارة التكاليف في مشاريع الهندسة المدنية . تحليل الذكاء الاصطناعي في فروعه الجزئية الخاصة قد تم تقديمه . هذه الفروع والمناهج اسهمت في ابتكار مجموعة كبيرة (او هامة) من النماذج التي تهتم (او تتعلق) بالتحليل ,التفسير و التنبؤ لمتغيرات متعددة, لقد تم تجهيز نماذج منتقاة حديثة والتي تتعلق بادارة التكاليف لمشاريع الهندسة المدنية . النماذج تم تحليلها وفقا لنشاط , ميدان العمليات , بيانات الادخال والاخراج والنظريات التي قاموا بترسيخها . لقد اصبح واضحا ان الذكاء الاصطناعي سيكون الاداة الاساسية المستقبلية لكل مهندس وسوف يقود الى تطورات كبيرة ومهمة في قطاع الانشاءات .

الكلمات الرئيسية : تطبيقات الذكاء الصناعي. الهندسة المدنية، ادارة الكلفة.

1. INTRODUCTION

Cost estimate is the most essential preliminary process for any construction project. So, construction cost estimations have the largest part of the research work in construction management. Estimation of cost is the important initial process to any construction project. For the construction industry, cost estimation is the process of predicting the costs required to perform the work within the scope of the project **Holm at el., 2005.** Accurate estimation for cost is crucial to confirm the successful completion for a construction project. Estimating construction cost is an example of a knowledge-intensive engineering task **French at el., 2003.** That is, it depends on the expertise of the human professional. Engineers require several years for developing the required expertise to conduct the process of cost estimation. Here the main problem is that the expertise of engineers is often not authenticated or documented. Hence, this expertise is disposed to subjectivity (i.e., it is defined to an extent for one's personal opinion). So, according to **Shane et al., 2009,** the accuracy and comprehensiveness for cost estimation are delicate subjects and can be simply affected by several different parameters; furthermore, each parameter must be well addressed in order to keep an acceptable level of the accuracy during the process. So, estimating construction cost to a reasonable degree of accuracy is generally impossible to achieve manually.

On the other hand, many problems are got by the inaccurate cost estimation, such as construction delay **Parmee, 2003.** Change order, or even business bankruptcy with the worst scenarios. The two factors, first the impossibility to conduct the cost estimation manually and second the effects of the incorrect cost estimation so encourage researchers besides construction companies to investigate smart solutions to handle the cost estimation problem.

2. CONSTRUCTION COST ESTIMATING

Good estimate depends on various factors including estimator's experience, time given to the estimator, and the wide range of assumptions regarding the project **Jrade and Alkass, 2007**. Construction cost estimating includes collecting, analyzing, and summarizing for all available data of a project **Holm et al., 2005**.

The construction cost estimate is a forecast of the whole cost for a construction project also it's estimator's responsibility for helping the owner of project to plan and to budget for the project construction **Choi, 2004.** At different stages of construction, three different types of estimates are used: conceptual, semi-detailed, and the detailed cost estimates **Holm et al., 2005**. The difference between the three methods of estimating is explained in **Table2**.

This paper will focus on conceptual cost estimating. Major difficulties which arise as conducting cost estimation through the conceptual phase are the lack of preliminary information, the lack of database of costs for road works, and lack of limited date cost estimation methods. Additional difficulties arise as a result of larger uncertainties caused by engineering solutions, environmental issues, and socio-economical. Parametric cost estimation or the estimation based on the historic database is extensively used in developed countries during the conceptual estimate phase. However, developing countries meet difficulties related to the creation of database of a road work costs that may be used for the cost estimation in either the conceptual stage or in the feasibility study to a project cycle **Jamshid, 2005.**

3. PURPOSE OF COST ESTIMATE

The early planning process is an important factor leading to project success. In recent decades, researchers and participants in construction industry have recognized the potential impact of

early planning to final project outcomes. Therefore, they started to put more emphasis on early planning process, where the project definition in **Wang, et al., 2012.**

The cost estimate becomes one of the main elements of information for decision making at preliminary stage of construction. Thus, the improving of cost estimation techniques will ease more effective control of costs and time in construction projects **Kim, et al., 2004**.

Actually, estimates are made and used for several different purposes including tendering phase, feasibility studies, and avoidance misuse of funds through the project, etc. The first purpose of cost estimation is to make an accurate and a reliable cost prediction of the construction project.

On the other hand, the cost which is predicted depends on requirements of customer and upon the information besides data available. Stated that the purpose of an estimate is to postulate the costs required to complete project in accordance with the contract plans and specification **Abdal-Hadi, 2010**.

Likewise and Weatney cited in **Jitendra, et al., 2011** outlined the purpose of cost estimate through the following points:

1. Provides an assessment of capital cost for a specified piece of project.
2. It can help to prioritize and classify projects of development with respect to a complete business plan.
3. Through defining the scope for work besides its associated estimation cost the base for planning and control is formed
4. Determines what resources to commit to the project with providing much of the basic information (hours, resources, tasks, and durations) which is needed for preparing a schedule.
5. When resources are well matched to actual needs, projects can be easily managed and controlled.
6. Provides the financial input required to prepare a cash flow curve.
7. Customers expect actual development costs to be in line with estimated costs.
8. Can be used to assess the impact of changes and support re-planning.

4. CONSTRUCTION COST FACTORS

According to **Shane et al., 2009** and **Ahiaga-Dagbui and Smith, 2012,** any construction cost estimation should be developed based on specific parameters such as type of project, material costs, size of project, likely design with scope changes, ground conditions, type of client, duration, and tendering method. So, in this paper these factors have been introduced as a measure to compare between the cost estimation plans.

Various different factors which affect cost estimation when constructing projects can be clustered into two distinct groups **Akinci and Fischer,1998** :

1) Estimator-Specific Factors and
2) Design and Project-Specific Factors.

4.1 Estimator Specific Factors

A cost estimator is one of the three gatherings: contractor, consultant, or owner. Based on the estimator's background and experience, cognitive biases or errors in cost estimates may occur accordingly **Akinci and Fischer, 1998.** In many cases, a cost estimator makes decisions established on the probable gains, or losses, of a project and not necessarily established on the actual outcome of the decision. Moreover, the individual estimator may customize pricing based upon best local practices, which differ from country to country.

4.2 Design and Project-Specific Factors

The factors are project size, ground conditions, type of project, material costs, type of client, expected design and scope changes, tendering method duration, **Shane et al., 2009** .

5. THE COST ESTIMATING METHODS

Estimates are done by humans not by tools; tools are means that are used by the analysts while dependable expert systems which can estimate the costs are still unfound. The estimates are based on the comparisons and they are based on the company data base. A handbook on costs that may allow the creation of a data base related to its activity still does not exist. In order to estimate, the technical knowledge of background, tools, products, technologies and the used means for production must be acquired. A number of estimating methods distinguished mainly by level of accuracy that is desired for the results, these include:

1. Analogy method
2. Parametric method
3. Analytical method

The method is not chosen randomly, so there must be a logic of the information clearly available, and it is worth considering progress of the project then what method may require for starting function.

5.1 Analogy Method

5.1.1 General principle

Analogy method of estimating of cost functions by comparing the suggested project to priory similar completed projects that the cost and functional definition is known.

So by comparison, a judgment must be got through the characteristics for two completed projects. Then this judgment must be worked out in a way which can be explained in terms of cost and the method must decrease the maximum of subjectivity.

This method has a principle that is implementing an extrapolation of like cases (source case) and a present case (target case). A source cases are abstracted by historical databases of project.

The construction of the target case may be different from source case. The case basis must be improved continuously by some new treated cases.

5.1.2 Conclusion on analogy method

As the use of Analogy method gives increase to certain concerns it is worth for stating its weaknesses

a. Analogy method leaves room to subjectivity, and such observation is largely hard, by putting the trust on the detailed level that limited enough in comparison with accomplishment which is finished and known.
b. Analogy method supposes that the comparisons that are made are valid, and such fact leads, to search for recent projects owing to the need of keeping pace with the rapidly developing technologies, but, this is not at all times attainable on one hand, so on the other hand, uniformity of projects stands a difficulty to find local completions to standardized the data on other hand.
c. It suggests that the progress and production logics must be the same to capable to assess the different; this is a serious problem in the measuring where an advanced level of estimate is required for the study. However, there exist no magic methods that can avoid asking such kind of question!

In fact, this method provides in a timely and responsive manner accurate estimate via low costs when it is rigorously applied. Also it allows having quick studies of sensitivity while it is worked

on coefficients of analogy. It can therefore be used as input for comparison of principles for solutions studied in the analysis of value. However, one must not expect extraordinary precision.

5.2 Parametric Method

5.2.1General principle and classification of parametric methods

Estimating of cost model that is used in design phase needs to be in coherence with project definition report. It is then better to consider the concept of product architecture. It is not known yet how these products will be produced, but a number of physical characteristics or parameters like the mass, the volume, the energy absorbed or number of input-output can be accessed and this is obtained for the information purposes at beginning of development phase.

Parametric estimate has been built specifically to create the costs to estimate from these parameters. For management, it must go from the high techniques that characterizes product and owned with the engineering design to economic necessary data.

The two types of parametric methods that are highlighted are distinguished both through their design and their usage.

a. Cost list.
b. Statistical models or the cost estimates formula.

This method includes more complex calculations than calculations for analogy method.

This method only works on the family products (or projects) with identical structure that is differing only in size. Here calculations are computerized on a spreadsheet for example Excel. The application of parametric assessment can be used or reached within an unskilled operator on the contrary, the development of cost estimation formula is complex and requires an expert experienced in statistical calculation

5.2.2 Conclusions on the parametric method

- It is more complex calculations than analogy method.
- It works on family products (or projects) with identical structure different only in size.
- The calculations are computerized on a spreadsheet for example Excel.
- The application of parametric assessment can be usde within an unskilled operator, on the contrary, the development of cost estimation.

5.3 Analytical Method

5.3.1 General principle

The analytical method is the oldest, the most classic and the most widespread among other cost estimating methods. It requires very detailed information on the product to encode and on its development process.

The most complex form for this method is to decompose each activity into the elementary tasks so that the time is known. This method makes it possible to calculate the actual cost of past achievements and to build up a data bank.

The projects that have already been completed must be a source of experience for better anticipation and management of costs and risks of a new project.

5.3.2 Conclusions on analytical method

The method permits to have accurate estimate of costs. However, it requires much detailed information on both the product and tools used in a given operative range. The analytical method is therefore focused on as being chosen to be the subject of our studies although it requires the manager to be rigorous, since it is more detailed than others and it does not represent any subjectivity.

6. INTELLIGENT CONSTRUCTION PROJECT COST ESTIMATION METHODS

In this section, analysis of the surveyed intelligent construction cost estimation methods was conducted. These methods have been categorized into five groups, based on the intelligent technique that is used in each group:

1) Machine-learning (ML).
2) Knowledge -based systems (KBS).
3) Evolutionary systems (ES).
4) Agent-based system (ABS).
5) Hybrid systems (HS).

At the first step, each group is explored to highlight their strengths and weaknesses. Subsequently, the methods are analysed in depth in terms of coverage of construction cost estimation techniques. In each proposal, four key questions have been highlighted for analysis. These questions are:

(1) Which intelligent technique is used?

(2) How the input datasets are collected?

(3) How the proposed method is validated?

(4) Which construction cost estimation factors are covered?

In the following subsections, firstly, the intelligent techniques employed are discussed, where the findings of which are considered as an answer to the first question. Secondly, each proposal is analysed individually, which answers question 2. The content of **Table 2,** illustrates the answer of question 1, while the content of **Table 3** illustrates the answer of question 2.

6.1 Machine Learning (ML) Systems

ML systems have been defined as a construction of a system that can learn from data. In general, the main strengths of ML are (i) the ability to deal with uncertainty, (ii) the ability to work with incomplete data, and (iii) the ability to judge new cases based on acquired experiences from similar cases. On the other hand, the main weakness of ML is the lack of technical justification; that is, the causes beyond the decision are not available. This type of decision is called a black box decision. However, in the construction management, the artificial neural network (ANN) and the support vector machine (SVM) are the most common ML techniques. In the next paragraph, the construction cost estimation proposals that are based on ML are analysed.

One of the earliest papers to introduce the benefits and the implementation of ANN in the civil engineering community is published by, **Flood and Kartam, 1994**. This research has opened the door for many proposals that suggest ML as the preferred method to tackle various challenges in the construction industry.,**Petroutsatou et al., 2012** introduced the ANN as a technique for early cost estimation of road tunnel construction. The data collection strategy of this research was based on structured questionnaires from different tunnel construction sites. **Wilmot and Mei, 2005** introduced an ANN model for highway construction costs. This research used the following factors as a base for cost estimation: price of labor, price of material, price of equipment, pay item quantity, contract duration, contract location, quarter in which the contract

was let, annual bid volume, bid volume variance, number of plan changes, and changes in standards or specifications. The main contribution of this work was that it covered all required factors**. ,Jafarzadeh et al., 2014** proposed the ANN method for predicting seismic retrofit construction costs. This study selected data from 158 earthquake-prone schools. The validation of this method is not clear**. An et al., 2007** proposed SVM for assessing conceptual cost estimates. Although this proposal is introduced as an assessment tool, still it might be considered as a cost estimation method. The method was developed on the basis of data from 62 completed building construction projects in Korea. Furthermore, **Hola and Schabowicz, 2010** developed an ANN model for determining earthworks' execution times and costs. Basically, this model was developed on the basis of a database created from several studies that were carried out during large-scale earthwork operations on the construction site of one of the largest chemical plants in central Europe.

Son et al., 2012 developed a hybrid prediction model that combines principal component analysis (PCA) with a support vector regression (SVR) predictive model for cost performance of commercial building projects. They used 64 related variables to define the pre-project planning stage. They developed their dataset based on information from 84 building projects in South Korea. **Cheng and Hoang, 2014** developed cost estimation at completion technique using least squares support vector machine. The data sets that are used in this research were collected from 13 reinforced concrete building projects executed between 2000 and 2007 by one construction ompany headquartered in Taiwan.

6.2 Knowledge - Based Systems (KBS)

This category includes any technique that uses logical rules for deducing the required conclusions. The main strengths of KBS are (i) the ability to justify any result and (ii) uncomplicated methods (i.e., it is relatively easy to develop (KBS). On the other hand, the limitations of KBS are (i) the difficulty of self-learning and (ii) time consumption during the rule acquisition process. Expert system and case-based reasoning are the common techniques used in KBS. The accuracy of case-based reasoning is highly dependent on the number of selected cases. Recently, KBS has been combined with other techniques to handle the limitation of the self-learning process. However, this mixture will be discussed in more details in the section of this paper that deals with hybrid systems.

Ji et al., 2012, proposed case-based reasoning to prepare strategic and conceptual estimations for construction budgeting. The data for this project were collected from 129 military barrack projects. **Choi et al., 2014** proposed a cost prediction model for public road planning. The research data had been collected from a total of 207 real public road projects. **Choi et al., 2014** used rough-set theory to control the data collection and a genetic algorithm to optimize the rough-set model. Their work was classified as CBS since the authors implemented the case-based reasoning component in their cost estimation**. Kim K. J. and Kim K., 2010** developed a cost estimation model using KBR. This research overcomes the uncertainty in choosing the correct case by using a genetic algorithm. For this research, data were collected from 65 projects that constructed 585 bridges over a 5-year period.
Kim, 2013 developed a cost estimation model based on case-based reasoning and analytical hierarchy process (AHP). In this project, data have been selected from literature and only 13 studies have been analyzed. **Kim, 2013** developed his model based on data from high-way construction projects. The validation has been conducted based on case study that contains data from 48 construction projects.

6.3 Evolutionary Systems (ES)

ES is a group of intelligent systems concerned with continuous optimization with heuristics. As the results of ES are generated based on specific heuristics, they are very difficult to generalize, which is considered to be the main limitation of ES. The ability to solve complicated and uncertain problems is the main motivation for researchers to use ES. Evolutionary systems are used mainly as optimization tools where there are many solutions; however, the ES algorithm assists in obtaining the correct solution. **Rogalska et al., 2008** proposed a method based on genetic algorithm to deal with the problem of construction project scheduling. **De Albuquerque Et Al., 2012** developed a tool for estimating the cost of concrete structures. This tool is developed based on genetic algorithm. The cost has been estimated in all construction phases, such as manufacture, transport, and erection. **Afshar et al., 2009** developed a multicolony ant algorithm to solve the time/cost multiobjective optimization problem. This method estimated both direct and indirect costs. **Zhang and ng, 2012** developed a decision support system (DSS) for cost estimation based on ant colony system**, Zhang and Ng, 2012** used synthetic data to develop their DSS and they do validate their system by comparing it with a standard academic project. However, validation is done. Still validation with real projects provides more accurate results.

6.4 Agent- Based Systems (ABS)

ABS has been considered as one of the main tracks in artificial intelligence, simulating the actions and interactions of autonomous agents with a view of assessing their effects on the system as a whole. In ABS, the generalization of extracted results is the main challenge. **Karakas et al., 2013** developed a multivalent system (MAS) that simulates the negotiation process between contractor and client regarding risk allocation and sharing of cost overruns in construction projects. This MAS was tested by interviewing eight professionals from the construction industry. In addition, **Rojas and Mukherjee, 2006** developed a general multivalent simulation framework that can be used as an effective training environment. This framework could be used to estimate direct and indirect costs for construction projects.

6.5 Hybrid Systems (HS)

HS is defined as a collection of techniques used together to solve a specific problem. Usually, researchers use HS to overcome the techniques' individual limitations. Implementation of HS could represent a challenge, due to the unavailability of computational tools that could support its implementation. **Cheng et al., 2013** proposed a hybrid intelligence system for estimating construction cost. This hybrid system was developed based on support vector machine (SVM) and differential evolution (DE). In this proposal, data were collected across a number of public projects in Taiwan. **Kim et al., 2005** proposed hybrid models of ANN and GA for cost estimation of residential buildings, in order to predict preliminary cost estimates. In **Kim et al.**'s proposal, data were collected from residential buildings constructed in the years between 1997 and 2000 in Seoul, Korea**. Yu and Skibniewski, 2010** proposed integrating a neurofuzzy system with conceptual cost estimation to discover cost-related knowledge from residential construction projects. The data used in this proposal was based on historical data from previous construction projects collected by the ministry of construction of PRC in the years between 1996 and 2002. Most recently, **Cheng et al., 2009** proposed web-based conceptual cost estimates for construction projects, using an evolutionary fuzzy neural inference model. Data were collected from 28 construction projects spanning the years from 1997 to 2001 in Taiwan.

Table 2 shows the comparison of surveyed proposals, based on two issues. The first issue is the intelligent technique used in a proposal. The second issue is the type of validation that is used to

prove the applicability of the proposal. **Table 3** shows the comparison of surveyed proposals, based on design and project-specific factors used to estimate construction cost in each proposal. The letter "y" means that this factor has been considered in this proposal, while the letter "N" means that this factor has not been considered. It is very obvious that there is no proposal that satisfies all the design and project-specific factors.

7. HISTORICAL COST DATA

The preparing of cost estimates normally requires usage of historical data on the construction costs. The data historical cost will be valuable for cost estimation only when they are collected then organized in a technique that is compatible with the future applications. Organizations that are engaged in estimation of cost continually ought to keep a file for the own use. The information need to be updated with the respect to changes which will inevitably occur. The format of the cost data, such as the unit costs of various items, must be organized according to current standard of the use in the organization.

The data historical cost must be used cautiously and changes in relative prices that may have substantial impacts on the construction costs that have increased in the relative price. Unluckily, systematic changes over the long period of time and for such factors are hard to predict. The errors in analysis serve to introduce uncertainty in the cost estimates. Of course it is difficult, to forecast all problems that may occur in construction as well as operation of facilities. Some evidence to estimate costs of construction and operating have tended to persistently minimize the actual costs. So this is by reason of the effects in costs for greater than anticipated increases, changes in design through the construction process. A lot of data is required to construction cost estimating on building elements, equipment, material, labor, as well as other related information.

These data need to be organized in a way that they can be easily accessed. One way to solve the problem is to use a database for storage of the data. A database is a storage facility or a collection of related records or documents.

Databases are designed, constructed, and populated with information data for a specific purpose then has an intended group for users and some applications by which the users are interested. The estimating software is designed to estimate adopts database technology for storing all the information that necessary for the estimating.

Some of the reasons for using databases are **Phuwadol, 2010**:

1. Compactness: The Databases help for maintaining the large quantities of data, and therefore completely replace voluminous the paper files.
2. The Speed: Searches for a specific piece of information or data in the database are faster than the sorting through paper piles.
3. Less drudgery: It is dull work to keep files by hand; so by using a database fully eliminates such maintenance.
4. Currency: Database systems can easily be updated and so provide accurate information all the time and on demand.

8. CONCLUSIONS

This centered evaluation of the continuing strategies screen the prolonged and growing adoption of AI within the management of Civil Engineering initiatives and particularly task cost management. It has become obvious inside the previous couple of years that each software of AI has its strong and susceptible points. As quickly as those factors had been identified, the brand new methods are targeted on hybrid structures. The latter ones are structures which integrate two or more one-of-a-kind AI. The preceding analysis, concluded that the most commonplace and

appropriate processes of artificial intelligence, which can be used to expand fashions for production projects are Fuzzy good judgment, Neural Networks, support vector machine and Genetic Algorithms. Those techniques combined with data and particularly regression evaluation may want to produce predicting fashions easy to use, and at the equal time green and correct. Subsequently, because the hardware is becoming extra robust and green, and at the same time applications aim at a total integration, the resulting systems will exhibit remarkable overall performance.

In this paper, a survey and analysis have been done on extraordinary proposals as a way to address the trouble of growing production cost estimation based totally on clever techniques. A systematic methodology has been designed to enforce this survey. The method of the offered paper becomes based on parts. The first component turned into worried with a literature survey to have a look at the present day nation of sensible answers in the construction industry. Concerning this relies, the journals that specialize in both statistics technology and construction management are chosen solely. Period is enough to surround the instructions of research in a selected place. The second one part became involved with analysis of the proposals accrued inside the first element. Four key questions were selected to analyze every concept. This paper offers contributions to this vicinity of understanding: (1) an analysis of construction price estimation proposals and (2) a well-known survey methodology that may be utilized in any destiny surveys that deal with construction price estimation. Consistent with the effects of this studies paper, the studies gaps which have been deduced from this survey are as follows. (1) there may be a critical necessity for a price estimation method that covers all estimation elements from each type; that is, there's a need for one approach that includes all “estimator precise” and “design and challenge-particular” elements. In desk 1, it is obvious that no proposal has a complete row of “Y.” (2) there is a real need for a widespread validation method which can be used to determine the accuracy stage of a value estimation proposal. (3) there are many proposals that be afflicted by a loss of medical justification for the consequences, that is, loss of describing how technically the outcomes had been executed.

REFERENCE

- Abdal-Hadi, M., 2010**.,** *Factors Affecting Accuracy of Pre-tender Cost Estimate in Gaza Strip*., **.** Master thesis in construction management, The Islamic University of Gaza Strip.

- Afshar A., Ziaraty A. K., Kaveh A., and Sharifi F.,2009, *No Dominated Archiving Multicolony Ant Algorithm In Time Cost Trade-Off Optimization*, Journal of Construction Engineering and Management, vol. 135, no. 7, pp. 668–674.

- Akinci B. And Fischer M.,1998, *Factors Affecting Contractors Risk Of Cost Overburden***,** Journal of Management in Engineering, vol. 14, no. 1, pp. 67–76.

- An S.-H., .Park U.-Y, Kang K.-I., Cho M.-Y., and Cho H.-H.,***2007,*** *Application of Support Vector machines in Assessing Conceptual Cost Estimates*, Journal of Computing in Civil Engineering, vol. 21, no. 4, pp. 259–264.

- Cheng M.-Y., Tsai H.-C., and Hsieh W.-S.,2009, *Web-Based Conceptual Cost Estimates for Construction Projects Using Evolutionary Fuzzy Neural Inference Model***,** Automation in Construction, vol. 18, no. 2, pp. 164–172.

- Cheng M.-Y. and Hoang N.-D., **2**014**,** *Interval estimation of construction cost at completion using least squares support vector machine***,** Journal of Civil Engineering and Management, vol. 20, no. 2, pp. 223–236.

- Cheng M.-Y., Hoang N.-D., and Wu Y.-W.,2013, *Hybrid Intelligence Approach Based on LS-SVM and Differential Evolution for Construction Cost Index Estimation: A Taiwan Case Study* **,***Automation in Construction*, vol. 35, pp. 306–313.

- Choi S., Kim D. Y., Han S.H., and Kwak Y. H.,2014, *Conceptual Cost Prediction Model for Public Road Planning Via Rough Set Theory and Case-Based* .

- Choi, Ying-Kit.,2004, *Principles of Applied Civil Engineering Design. New York*: American Society of Civil Engineers.

- de Albuquerque A. T., El Debs M. K., and Melo A. M. C.,2012, *A Cost Optimization-Based Design of Precast Concrete Floors Using Genetic Algorithms*, Automation in Construction, vol. 22, pp. 348–356.

- Flood I. and Kartam N., 1994, *Neural Networks in Civil Engineering. Principles and Understanding*, Journal of Computing in Civil Engineering, vol. 8, no. 2, pp. 131–148

- French S., Fischer M., Kunz J., and Paulson B.,2003, *A generic Feature-Driven Activity-Based Cost Estimation Process***,** Advanced Engineering Informatics, vol. 17, no. 1, pp. 23–39.

- Hola B. and Schabowicz K.,2010, *Estimation Of Earthworks Execution Time Cost By Means Of Artificial Neural Networks***,** Automation in Construction, vol. 19, no. 5, pp. 570–579.

- Holm L., Schaufelberger J. E., Griffin D., and Cole T., 2005, *Construction Cost Estimating Process and Practices*, Pearson Education, Upper Saddle River, NJ, USA.

- Jafarzadeh R., Ingham J. M., Wilkinson S., Gonz´alez V., and Aghakouchak A. A.,2014, *Application of Artificial Neural Network Methodology for Predicting Seismic Retrofit Construction Costs*, Journal of Construction Engineering and Management, vol. 140, no. 2.

- Jamshid S., 2005**,** *Cost Estimation of Highway Projects in Developing Country: Artificial Neural Network Approach. Graduate Project*, Department of Civil and Environmental Eng., Saitama University.

- Ji S.-H., Park M., and Lee H.-S.,2012, *Case Adaptation Method of Case-Based Reasoning for Construction Cost Estimation in Korea*, Journal of Construction Engineering and Management, vol. 138, no. 1, pp. 43–52.

- Jitendra, Vikas, Kuldeep & Samiksha, 2011, *Cost Prediction Using Neural Network Learning Techniques***,** IJCSMS International Journal of Computer Science and Management Studies.

- Jrade, Ahmad, and Sabah Alkass., 2007, *Computer-Integrated System for Estimating the Costs Of Building Projects.* Journal of Architectural Engineering 13.4.

- Karakas K., Dikmen I., and Birgonul M. T.,2013, *Multiagent System to Simulate Risk-Allocation and Cost-Sharing Processes in Construction Projects***,** Journal of Computing in Civil Engineering, vol. 27, no. 3, pp. 307–319.

- Kim G. H., Seo D. S., and Kang K. I.,2005, *Hybrid Models of Neural Networks and Genetic Algorithms for Predicting Preliminary Cost Estimates***,** Journal of Computing in Civil Engineering, vol. 19, no. 2, pp. 208–211.

- Kim K. J. and Kim K., 2010, *Preliminary Cost Estimation Model Using Case-Based Reasoning and Genetic Algorithms,* Journal of Computing in Civil Engineering, vol. 24,no. 6, pp.499–505.

- Kim S., 2013, *Hybrid Forecasting System Based on Case-Based Reasoning and Analytic Hierarchy Process for Cost Estimation***,** Journal of Civil Engineering and Management, vol. 19, no. 1, pp. 86–96.

- Kim, G.-H., An, S.-H. & Kang, K.-I., 2004**.** *Comparison of Construction Cost Estimating Models Based on Regression Analysis, Neural Networks, and Case-Based Reasoning*. Building and Environment, February, Volume 39, p. 1235 – 1242.

- Parmee I. C., 2003, *Computational Intelligence and Civil Engineering- Perceived Problems and Possible Solutions,* in Towards a Vision for Information Technology in Civil Engineering.

- Petroutsatou K., Georgopoulos E., Lambropoulos S., and Pantouvakis J. P., 2012, *Early Cost Estimating 0f Road Tunnel Construction Using Neural Networks***,** Journal of Construction Engineering and Management, vol. 138, no. 6, pp. 679–687.

- PhuwadolSamphaongoen, B.S.,2010**,***A Visual Approach to Construction Cost Estimating***,** A MS.c Thesis submitted to the Faculty of the Graduate School, Marquette University.

- Rogalska M., Bozejko W., and Hejducki Z., 2008, *Time Cost Optimization Using Hybrid Evolutionary Algorithm in Construction Project Scheduling,* Automation in Construction, vol. 18, no. 1, pp. 24–31.

- *Rojas E. M.* And Mukherjee A.,2006, *Multi-Agent Framework For General-Purpose Situational Simulations In The Construction Management Domain***,** Journal of Computing in Civil Engineering, vol. 20, no. 3, pp. 165–176.

- Shane J. S., Molenaar K. R., Anderson S., and Schexnayder C.,2009, *Construction Project Cost Escalation Factors***,** Journal of Management in Engineering, vol. 25, no. 4, pp. 221–229.

- Son H., , and Kim C.,2012, *Hybrid Principal Component Analysis And Support Vector Machine Model For Predicting The Cost Performance Of Commercial Building Projects Using Preproject Planning Variables***,** Automation in Construction, vol. 27, pp. 60–66.

- Wang, Y., Yu, C. & Chan, H., 2012. *Predicting Construction Cost and Schedule Success Using Artificial Neural Networks Ensemble And Support Vector Machines Classification Models.* International Journal of Project Management, Volume 30, p.470–478.

- Wilmot C. G. and Mei B., 2005, *Neural Network modeling Of Highway Construction Costs***,** Journal of Construction Engineering and Management, vol. 131, no. 7, pp. 765–771.

- Yu W.-D. and Skibniewski M. J.,2010, Integrating Neurofuzzy System With Conceptual Cost Estimation To Discover Cost-Related Knowledge From Residential Construction Projects, Journal of Computing in Civil Engineering, vol. 24, no. 1, pp. 35–44.

- Zhang Y. and Ng S. T.,2012, *An Ant Colony System Based Decision Support System For Construction Time-Cost Optimization***,** Journal of Civil Engineering and Management, vol. 18, no. 4, pp. 580– 589.

Table 1. Three types of construction cost estimating methods.

Type of Estimate	Construction Development	Expected Error
Conceptual	Programming and schematic design	± 10-20%
Semi-Detailed	Design development	± 5-10%
Detailed	Plans and specification	± 2-4%

Table 2. Comparison of proposals based on technique and validation

Proposal	Technique	Validation
Wilmot and Mei	ML, ANN	Comparison with methods for assessing conceptual cost estimates
An et al	ML,SVM	Comparison with methods for assessing conceptual cost estimates
Petroutsatou et al.	ML, ANN	By comparison with other models in literature
Jafarzadeh et al.	ML, ANN	Have not been mentioned
Hola andSchabowicz	ML, ANN	Have not been mentioned
Son et al.	ML,SVM	Comparison with other techniques such as ANN and a decision tree (DT)
Cheng and Hoang	ML,SVM	Have not been mentioned
Ji et al	KBS: case-based reasoning	Using case study
Choi et al.	KBS: case-based reasoning	By comparison with previous conceptual cost estimation studies
K. J. Kim and K.	KBS: case-based	Have not been mentioned

Kim	reasoning	
Karakas et al.	ABS: MAS	Interview with expert
Rojas and Mukherjee	ABS: multiagent	Have not been mentioned
kim	KBS: case-based reasoning and analytical hierarchy process	Case study
de Albuquerque et al.	ES: genetic algorithm	Have not been mentioned
Rogalska et al.	ES: hybrid genetic evolutionary algorithm	By comparing the result with case studies from literature
Afshar et al.	ES: ant colony	By comparing the results with case studies in construction optimization
Zhang and Ng	ES: ant colony	By comparing the results with an academic benchmark
Cheng et al.	HS: SVM and DE	By comparing the result with other methods
Kim et al.	HS: ANN and GA	Have not been mentioned
Yu and Skibniewski	HS: ANN and fuzzy system	By using a case study of residential building construction projects in China
Cheng et al.	HS: ANN, GA, and fuzzy system	Have not been mentioned

Table 3. Comparison of the proposals based on design and project-specific factors.

Work	Project size	Project type	Ground conditions	Type of client	Likely design and scope changes	Contract type	Material costs	Duration	Tendering method
Wilmot and Mei	Y	Y	Y	Y	Y	Y	Y	Y	N
An et al	Y	Y	Y	Y	Y	N	N	N	N
Petroutsatou et al.	Y	Y	Y	Y	Y	Y	Y	N	N
Jafarzadeh et al.	Y	Y	Y	Y	Y	N	N	N	N
Hola andSchabowicz	Y	Y	Y	N	N	N	Y	Y	Y
Son et al.	Y	Y	N	Y	Y	N	N	Y	N
Cheng and Hoang	Y	Y	Y	N	N	N	N	Y	N
Ji et al	Y	Y	Y	N	Y	N	Y	N	N

Choi et al.	Y	Y	Y	Y	N	N	N	N	N
K. J. Kim and K. Kim	Y	Y	Y	Y	N	N	N	N	N
Karakas et al.	N	N	Y	Y	Y	N	Y	N	N
Rojas and Mukherjee	Y	Y	Y	N	N	N	N	N	N
kim	Y	Y	Y	N	N	N	N	N	Y
deAlbuquerque	Y	Y	Y	N	N	N	Y	N	N
Rogalska et al.	Y	Y	Y	N	N	N	N	N	N
Afshar et al.	Y	Y	Y	N	N	Y	Y	Y	Y
Zhang and Ng	Y	Y	Y	N	N	N	N	N	N
Cheng et al.	Y	Y	Y	N	N	N	Y	Y	N
Kim et al.	Y	Y	Y	N	N	N	Y	Y	N
Yu and Skibniewski	Y	Y	Y	Y	N	N	Y	Y	N
Cheng et al.	Y	Y	Y	Y	N	N	Y	Y	N

Non-Linear Behavior of Strengthened Steel-Concrete Composite Beams with Partial Interaction of Shear Connectors

Dr. Ali Ihsan Salahaldin
Lecturer
Civil Engineering Department
College of Engineering
University of Kirkuk
E-Mail: ali.ihsan@uokirkuk.edu.iq

Shaho Mahmoud Hama
Assistant Lecturer
Civil Engineering Department
College of Engineering
University of Anbar
E-Mail: shaho_m83@yahoo.com

ABSTRACT

In this research a theoretical study has been carried out on the behavior and strength of simply supported composite beams strengthened by steel cover plate taking into consideration partial interaction of shear connectors and nonlinear behavior of the materials and shear connectors. Following the procedure that already has been adopted by **Johnson (1975)**, the basic differential equations of equilibrium and compatibility were reduced to single differential equation in terms of interface slip between concrete slab and steel beam. Furthermore, in order to consider the nonlinear behavior of steel, concrete and shear connectors, the basic equation was rearranged so that all terms related to materials are isolated in the equation from the main variable (interface slip). The exact solution was obtained by considering appropriate boundary conditions according to load types and location. A computer program has been written using MATLAB R2013a to simplify the process of computation of section properties where the load applied iteratively from zero to ultimate capacity of the beam, and the results are compared with available experimental results which show good agreement.

As the composite section reaches its ultimate capacity in bending and lower flange start yielding due to excessive loading, cover plate are furnished in order to increase load carrying capacity of beam. In the process of strengthening, using of cover plate as a percent of the area of lower flange of steel section equal to 41%, 82% and 164% will increase the beam carrying capacity by 15%, 30% and 43% respectively; also using the same above mentioned area of cover plate will reduce the central deflection by 59%, 72% and 80% respectively.

Keywords: composite beams, partial interaction theory, nonlinear materials.

التصرف اللاخطي للعتبات المقواة والمركبة من الحديد والخرسانة المتصلة جزئياً باستخدام رباطات القص

د. علي احسان صلاح الدين
كلية الهندسة - جامعة كركوك

شاهو محمود حمه
كلية الهندسة - جامعة الانبار

الخلاصة

يقدم البحث نموذجاً نظرياً لسلوك العتبات المركبة البسيطة الإسناد والمقواة باستخدام الصفائح الفولاذية, أخذاً بنظر الاعتبار التصرف اللاخطي لعناصر المقطع المركب (الخرسانة والفولاذ ورباطات القص) بالإضافة إلى اعتماد نظرية التداخل الجزئي لرباطات القص. متبعا نظرية جونسون تم اختصار المعادلات التفاضلية الرئيسية للتوازن والتوافق بين عناصر المقطع المركب إلى معادلة تفاضلية واحدة بدلالة الانزلاق بين الحديد والخرسانة. بالاضافة الى ذلك ، تم فصل المتغيرات المتعلقة بخصائص المقطع المركب من اجل اخذ التصرف اللاخطي للمواد بنظر الاعتبار.

عند وصول المقطع المركب إلى تحمله الأقصى نتيجة الأحمال المسلطة عليه تصل مادة الشفة السفلى للعتبة الفولاذية الى الخضوع لذا يتم إضافة الشرائح الفولاذية أسفل العتبة لزيادة قابلية تحملها. تم كتابة برنامج بلغة الماتلاب بنسخة R2013a من اجل تسهيل حساب خصائص المواد حيث تمت مقارنة النتائج المستحصلة من الدراسة الحالية مع النتائج العملية المنشورة في البحوث سابقة وقد وجد تقارب جيد معها. إن تقوية الشفة السفلى في مقطع الحديد بزيادة السمك يؤدي الى زيادة في مقدار تحمل العتبة المركبة وانخفاض في قيمة كلٍ من الانزلاق الأقصى في النهاية العتبة والهطول في منتصف العتبة المركبة في نفس المستوى من التحميل (بدون التقوية). حيث وجد ان زيادة مساحة مقطع حديد التقوية (الصفائح الفولاذية) بمقدار 41% ,

82% و164% (كنسبة من مساحة مقطع الشفة السفلى) يؤدي إلى زيادة تحمل المقطع بنسب 15% ,30% و 43% على التوالي, وانخفاض في الهطول عند منتصف العتبة المركبة بمقدار 59%, 72% و80% على التوالي.

1. INTRODUCTION

Composite construction, especially for multi-store buildings and bridges, has achieved a high market share in several European countries, USA, Canada and Australia. This is mainly due to a reduction in construction depth, to savings in steel weight and to rapid construction programs. The simplest form of composite steel – concrete beam consists of steel I–beams and an upper concrete slab connected together by shear connectors as shown in **Fig. 1**.

A fundamental point for the structural behavior and design of composite beams is the level of connection and interaction between the steel section and the concrete slab. The term "full shear connection" relates to the case in which the connection between the components is able to fully resist the forces applied to it. Partial composite action occur when the number of shear connectors is less than required to achieves full interaction between slab and steel beam**.**

Mechanical shear connectors are required at the steel-concrete interface and these connectors are necessary to transmit longitudinal shear along the interface, and to prevent separation of steel beam and concrete slab at the interface. The first interaction theory that takes account of slip effects was initially formulated by **Newmark in 1951**, based on elastic analysis of composite beams assuming linear material and shear connector behavior. Using the same element presented by Newmark, **Johnson in 1975** proposed a partial interaction theory for simply supported beams, in which the analysis was based on elastic theory. The composite beam was assumed to be in linear elastic materials. The discrete connection was assumed to be smeared along the beam, so that the connector strength and stiffness can be quoted per unit length of beam. **In 1985, Roberts** tackle the problem of incomplete interaction for composite beams in more details. The solution arrived at the four simultaneous differential equations in terms of four independent displacements which are the horizontal and vertical displacements in each component of the composite section. **In 1990, Al-Amery and Roberts** made a new development in this field where allowance has been made for the simultaneous slip and separation at the interface and the nonlinear behavior for the concrete, steel and connectors.

The researches in this field was continued to cover sandwich composite beams. **In 2007 Al-Amery et al** presented two researches on behavior of multi-layer composite beams with partial interaction of shear connectors, while **Sayhood and Mahmood (2011)** tackle the problem of non-linear behavior of composite slim floor beams with partial interaction. The main differential equations were written in term of interface slip while **Dogan and Roberts (2010)** drive the basic equations in term of axial forces that transmitted between composite section layers.

The aim of this research is developing analytical solution for nonlinear behavior of simply supported composite beam with partial connection.

2. ASSUMPTIONS

The basic assumptions of conventional beam theory were used in which plane sections are assumed to remain plane after bending. The connection is assumed to have negligible thickness and possess finite normal and tangential stiffness, and it will resist the uplift forces and prevent the separation between the steel and concrete. Also, the concrete is assumed to have no tensile strength and all the tensile forces beyond neutral axis are transmitted through connectors to steel beam.

3. THE MODELS

In this study non-linear analysis of composite beam subjected to different loads has been adopted. The reason for choosing typical composite beam is that it is one of the most common flexure elements, and at the same time is simple enough to allow for closed-form analysis.
The second order differential equations obtained by **Johnson in 1975**, were derived as follows. The material properties are isolated in separate terms in order to simplify the process of computing the inelastic properties of these components.

3.1 Equilibrium Equations

An element of a composite steel and concrete beam, length (dx), shown in **Fig. 2**, is subjected to moments (M), shear forces (V) and axial forces (F). Subscripts (c) and (s) denote the concrete and steel respectively, and the local (x-z) axes pass through the centroids of the two materials.
Longitudinal equilibrium of either the steel or concrete gives,

$$\frac{dF}{dx} = -q \tag{1}$$

Taking moments about the center of the concrete element alone gives,

$$\frac{dM_c}{dx} + V_c = q.\frac{h_c}{2} \tag{2}$$

The term ($dv_c/2$) has been neglected because it very small value.
Similarly for the steel element

$$\frac{dM_s}{dx} + V_s = q.\frac{h_s}{2} \tag{3}$$

Also, the term ($dv_s/2$) has been neglected for the same reason above mentioned. Hence,

$$V_c + V_s = N \tag{4}$$

Where N is the total vertical shear at a section, distance (x) from the support
From Eq. (2), Eq. (3) and Eq. (4),

$$\frac{dM_c}{dx} + \frac{dM_s}{dx} + N = q.\,d_1 \tag{5}$$

in which (d_1) is the distance between the centroids of the two components. The applied external moment (M) is equal to the sum of the individual moments that each element can carry together with the composite couple, so,

$$M = M_c + M_s + F.d_1 \tag{6}$$

3.2 Compatibility Equations

Assuming equal curvatures for the two materials gives,

$$\frac{d^2w_c}{dx^2} = \frac{d^2w_s}{dx^2} = \frac{d^2w}{dx^2} \tag{7}$$

From elastic beam theory,

$$\frac{d^2w}{dx^2} = \frac{d^2w_c}{dx^2} = \frac{M_c}{E_cI_c} \tag{8}$$

$$\frac{d^2w}{dx^2} = \frac{d^2w_s}{dx^2} = \frac{M_s}{E_sI_s} \tag{9}$$

Differentiating Eq. (8) and Eq. (9) once with respect to (x) and substituting for ($\frac{dM_c}{dx}$) and ($\frac{dM_s}{dx}$) in Eq. (5), and rearranging gives,

$$\frac{d^3w}{dx^3}.(E_c.I_c + E_s.I_s) + N = q \cdot d_1 \quad (10)$$

The shear flow q is related to the slip (u_{cs}) by the equation,

$$q = \frac{K \cdot u_{cs}}{S} \quad (11)$$

Substituting for q into Eq. (10) and rearranging, give,

$$\frac{d^3w}{dx^3} = \frac{1}{(E_c.I_c + E_s.I_s)}\left(\frac{K \cdot u_{cs}. d_1}{S} - N\right) \quad (12)$$

Strains of the concrete and steel, (ε_c) and (ε_s), at the interface can be expressed as,

$$\varepsilon_c = \frac{1}{2} h_c \cdot\frac{d^2w}{dx^2} - \frac{F}{E_c.A_c} \quad (13)$$

$$\varepsilon_s = \frac{1}{2} h_s \cdot\frac{d^2w}{dx^2} + \frac{F}{E_s.A_s} \quad (14)$$

The interface slip strain ($\frac{du_{cs}}{dx}$) is given by,

$$\frac{du_{cs}}{dx} = \varepsilon_c - \varepsilon_s \quad (15)$$

Eq. (13) and Eq. (14), give,

$$\frac{du_{cs}}{dx} = d_1.\frac{d^2w}{dx^2} - F\left(\frac{1}{E_c.A_c} + \frac{1}{E_s.A_s}\right) \quad (16)$$

Differentiating Eq. (16) once with respect to (x), yield into;

$$\frac{d^2u_{cs}}{dx^2} = d_1.\frac{d^3w}{dx^3} - \frac{dF}{dx}\left(\frac{1}{E_c.A_c} + \frac{1}{E_s.A_s}\right) \quad (17)$$

Substituting for ($\frac{d^3w}{dx^3}$) and ($\frac{dF}{dx}$) from Eq. (12), Eq. (1) and Eq. (11) and rearranging Eq. (17) becomes.

$$\frac{d^2u_{cs}}{dx^2} - \frac{K \cdot u_{cs}}{S}\left[\frac{1}{E_c.A_c} + \frac{1}{E_s.A_s} + \frac{d_1^2}{(E_c.I_c + E_s.I_s)}\right] = - N.\left(\frac{d_1}{(E_c.I_c + E_s.I_s)}\right) \quad (18)$$

Let,

$$\alpha_1^2 = \frac{K}{S}\left[\frac{1}{E_c.A_c} + \frac{1}{E_s.A_s} + \frac{d_1^2}{(E_c.I_c + E_s.I_s)}\right] \quad (19)$$

$$\beta_1 = \frac{d_1}{(E_c.I_c + E_s.I_s)}.\frac{1}{\alpha_1^2} \quad (20)$$

Hence, substituting in Eq. (18), will give the basic differential equation in terms of interface slip:-

$$\frac{d^2u_{cs}}{dx^2} - \alpha_1^2.u_{cs} = -\alpha_1^2.\beta_1.N \quad (21)$$

The iterative solution of this equation considering material non linearity will give the values of the interface slip along the beam span.

In which (α_1) and (β_1) are functions of the section and material properties, (N) is the vertical shear force in the beam at a distance (x) from the support.

4. THE SOLUTION OF THE DIFFERENTIAL EQUATION

The general solution for the differential Eq. (21) can be obtained mathematically as usual; then, the constants can be defined after specifying the suitable boundary conditions.

4.1 Case1: Point Loads:

For a simply supported beam subjected to a point load (P) applied at distance (L_1) and (L_2) from the ends of the beam, as shown in **Fig. 3**.

The differential equation obtained by Johnson can be solved after expressing the shear forces to the left and right of the load, as given below:

$$N^L = -P\frac{L_2}{L} \quad \text{(to the left of point load)} \quad (22)$$

$$N^R = +P\frac{L_1}{L} \quad \text{(to the right of point load)} \quad (23)$$

where superscripts L and R denote left and right of the load. Solving Eq. (21) for the two parts of the beam (to the left and right of the point load) gives:

$$u_{cs}^{\ L} = K_1.\sinh(\alpha_1.x)+K_2.\cosh(\alpha_1.x) - \beta_1.P(\frac{L_2}{L}) \quad (24)$$

$$u_{cs}^{\ R} = K_3.\sinh(\alpha_1(x-L_1))+K_4.\cosh(\alpha_1(x-L_1)) + \beta_1.P(\frac{L_1}{L}) \quad (25)$$

in which (K_1) to (K_4) are arbitrary constants of integration. The four boundary conditions needed to determine these constants are:

$$u_{cs}^L = u_{cs}^R \quad \text{when } x = L_1 \quad (26)$$

$$\frac{du_{cs}^{\ L}}{dx} = \frac{du_{cs}^R}{dx} \quad \text{when } x = L_1 \quad (27)$$

$$\frac{du_{cs}^{\ L}}{dx} = 0 \quad \text{when } x = 0 \quad (28)$$

$$\frac{du_{cs}^R}{dx} = 0 \quad \text{when } x = L \quad (29)$$

Applying these boundary conditions, (K_1) to (K_4) can be determined as follows:

$$K_1 = 0 \quad (30)$$

$$K_2 = \beta_1.P\frac{\sinh(\alpha_1.L_2)}{\sinh(\alpha_1.L)} \quad (31)$$

$$K_3 = \beta_1.P\frac{\sinh(\alpha_1.L_1).\sinh(\alpha_1.L_2)}{\sinh(\alpha_1.L)} \quad (32)$$

$$K_4 = -\beta_1.P\frac{\sinh(\alpha_1.L_1).\cosh(\alpha_1.L_2)}{\sinh(\alpha_1.L)} \quad (33)$$

Substituting for (K_1) to (K_4) into Eq. (24) and Eq. (25) gives the final solution for a simply supported beam subjected to concentrated load, as shown below:

$$u_{cs}^{L} = \beta_1.P\frac{\sinh(\alpha_1.L_2)}{\sinh(\alpha_1.L)}.\cosh(\alpha_1.x) - \beta_1.P(\frac{L_2}{L}) \quad (34)$$

$$u_{cs}^{R} = -\beta_1.P\frac{\sinh(\alpha_1.L_1)}{\sinh(\alpha_1.L)}.\cosh(\alpha_1(L-x)) + \beta_1.P(\frac{L_2}{L}) \quad (35)$$

4.2 Case2: Uniformly Distributed Loads:

Using Johnson's approach for a simply supported beam of span (L) subjected to a uniformly distributed load (ρ) , the vertical shear force at distance (x) from the left hand support as shown in **Fig. 4**, is given by,

$$N = \rho.x - \rho\frac{L}{2} \quad (36)$$

Substituting for (N), the general solution of the differential Eq. (21) can be obtained as:

$$u_{cs} = K_5.\sinh(\alpha_1.x)+K_6.\cosh(\alpha_1.x) + \beta_1.\rho(x-\frac{L}{2}) \quad (37)$$

in which (K_5) and (K_6) are arbitrary constants. The boundary conditions can be expressed in terms of the slip (u_{cs}) as the axial strains and curvature equal to zero at supports:

$$\frac{du_{cs}}{dx} = 0 \qquad \text{when } x = 0 \text{ and } x = L \quad (38)$$

Alternatively due to symmetry, one of the conditions expressed by Eq. (38) can be replaced by:

$$u_{cs} = 0 \qquad \text{when } x = L/2 \quad (39)$$

Substituting these boundary conditions into Eq. (37), the constants K_5 and K_6 can be determined and the particular solution for this case is:

$$u_{cs} = -\frac{\beta_1.\rho}{\alpha_1}\sinh(\alpha_1.x) + \frac{\beta_1.\rho}{\alpha_1}\tanh(\frac{\alpha_1.L}{2}).\cosh(\alpha_1.x) + \beta_1.\rho(x-\frac{L}{2}) \quad (40)$$

5. BASIC DIFFERENTIAL EQUATIONS

When the material properties (E) are considered to be constant (linear analysis) Eq. (40) can be solved directly. The equation can be used to get the slip and axial force along the beam. Alternatively, if the material properties are non-linear functions of strain, the above equations require specifying these properties at each loading stage. This can be achieved by dividing the cross sectional area of the concrete and steel shape into a number of layers having areas (A_c^i) and (A_s^j) at a distance (z_c^i) and (z_s^i) from the origin of coordinates, respectively, and using the summation over the appropriate area. The appropriate values of (E_c^i) and (E_s^j), for the layers (A_c^i) and (A_s^j) are the secant values determined from the assumed stress-strain curves, corresponding to the strains (ε_c^i) and (ε_s^j) in center of layers (A_c^i) and (A_s^j), respectively. Therefore, for concrete, (E_c^i) corresponds to a strain (ε_c^i) at the center of the corresponding layer and is given by,

$$\varepsilon_c^i = z_c^i \cdot \frac{d^2w}{dx^2} - \frac{F}{\sum_{i=1}^{n_1} E_c^i.A_c^i} \quad (41)$$

Similarly for steel shape,

$$\varepsilon_s^j = - z_s^j \cdot \frac{d^2w}{dx^2} + \frac{F}{\sum_{j=1}^{n_2} E_s^j.A_s^j} \quad (42)$$

in which n_1 and n_2 are the total number of layers in the concrete and steel shape respectively.

The corresponding stress (σ) for each layer can be obtained using appropriate secant (E) values at the center of each layer. Hence,

$$\sigma_c^i = E_c^i.\varepsilon_c^i \quad (43)$$

$$\sigma_s^j = E_s^j.\varepsilon_s^j \quad (44)$$

The non-linear behavior of the stud connectors has been introduced in this formulation through Eq. (53) in which shear stiffness of the connectors (Ks) can be defined from the relative value of the slip. After substituting Eq. (41) and Eq. (42) into the basic equilibrium and compatibility equations Eq. (18) and rearranging them, the new form of the differential Eq. (21), in term of interface slip including the influence of the non-linear material and shear connector behavior is,

$$\frac{d^2u_{cs}}{dx^2} - \frac{K_s.u_{cs}}{S}.\left[\frac{1}{\sum_{i=1}^{n_1} E_c^i.A_c^i} + \frac{1}{\sum_{j=1}^{n2} E_s^j.A_s^j} + \frac{d_1^2}{\left(\sum_{i=1}^{n_1} E_c^i.I_c^i + \sum_{j=1}^{n2} E_s^j.I_s^j\right)}\right] = N.\left[\frac{d_1}{\left(\sum_{i=1}^{n_1} E_c^i.I_c^i + \sum_{j=1}^{n_2} E_s^j.I_s^j\right)}\right] \quad (45)$$

Now letting

$$\alpha_2^2 = \frac{K_s}{S}.\left[\frac{1}{\sum_{i=1}^{n_1} E_c^i.A_c^i} + \frac{1}{\sum_{j=1}^{n_2} E_s^j.A_s^j} + \frac{d_1^2}{\left(\sum_{i=1}^{n_1} E_c^i.I_c^i + \sum_{j=1}^{n_2} E_s^j.I_s^j\right)}\right] \quad (46)$$

$$\beta_2 = \left[\frac{d_1}{\left(\sum_{i=1}^{n_1} E_c^i.I_c^i + \sum_{j=1}^{n_2} E_s^j.I_s^j\right)}\right].\frac{1}{\alpha_2^2} \quad (47)$$

Then, the final form of the differential Eq. (21) becomes,

$$\frac{d^2u_{cs}}{dx^2} - \alpha_2^2.u_{cs} = -\alpha_2^2.\beta_2.N \quad (48)$$

and Eq. (40) becomes,

$$u_{cs} = -\frac{\beta_2.\rho}{\alpha_2}\sinh(\alpha_2.x) + \frac{\beta_2.\rho}{\alpha_2}\tanh(\frac{\alpha_2.L}{2}).\cosh(\alpha_2.x) + \beta_2.\rho(x-\frac{L}{2}) \quad (49)$$

6. MATERIAL PROPERTIES

The performance of any structure under load depends to a large degree on the stress-strain relationship of the material from which it is made. In the following a description of the constitutive relationships for the materials comprising composite beams is given.

Concrete

In American code for structural concrete, the compressive strength of the concrete is usually based on standard (150 mm * 300 mm) cylinders cured under standard laboratory conditions and tested at a specified rate of loading at 28 days of age. Another widely used model for the stress strain relationship of the concrete in compression is that proposed in the **BS8110**, as shown in **Fig. 5** where the variation of the curved portion of the stress-strain relationship is given by,

$$\sigma = 5500\sqrt{f_{cu}}\,.\,\varepsilon - 11.3*10^{6}.\varepsilon^{2} \quad (f_{cu} \text{ is in N/mm}^2) \tag{50}$$

The above equation is used in this study

Steel section

Hot rolled steel sections were used extensively as structural material because of their significant properties such as high strength as compared to any other building material and also ductility which is the ability to deform substantially in either tension or compression before failure. **Fig. 6** shows a suitable mathematical model for representing the behavior of structural steel as a practical strain limit. This model which is proposed by **BS8110**, consists of elastic, perfectly plastic portions. In the present study the strain hardening is not taken into account.

Shear connectors

In composite beam design, headed stud shear connectors are commonly used to transfer longitudinal shear forces across steel-concrete interface. Present knowledge on the load–slip behavior and the shear capacity of the shear stud in composite beam is limited to data obtained from the experimental push-off tests, **Lam, and El-Lobody, 2005**.

Al-Amery, and Roberts, 1990, developed a model for shear connectors and carried out parametric study to end up with the following exponential form in which one point on the load-slip curve is required (values of slip and corresponding load) to model that curve as follows,

$$Q = Q_u\,.\,\left(1 - e^{-\phi.u_{cs}}\right) \tag{51}$$

$$\phi = \left(1/\overline{u_{cs}}\right).\ln\left[Q_u/(Q_u - \overline{Q})\right] \tag{52}$$

in which (ϕ) is a constant and ($\overline{Q}$) is the midrange load from experimental curve and ($\overline{u_{cs}}$) is the corresponding slip. The tangent stiffness, K_s, is given by differentiating Eq. (51) once with respect to slip value,

$$K_s = dQ/du_{cs} = Q_u.\phi\left(1 - e^{-\phi.u_{cs}}\right) \tag{53}$$

This model has been used in the present study, as shown in **Fig. 7**.

7. APPLICATIONS

In order to validate the theoretical representation of the partial interaction behavior of simply-supported composite beam, the formulation presented in the previous sections has been applied to a practical section and the results are compared with the experimental values reported by previous researchers.

The computer program presented in this study for non-linear analysis of composite beams with partial connection is used to investigate various loading conditions. Also, a convergence study is carried out since a numerical method has been employed in the solution. A computer program has been written using MATLAB R2013a to simplify the process of computation the section

properties. The full loading history was covered in the program to describe the complete behavior of the composite beam from zero to full yielding loading of strengthened beam.

7.1 Example 1

The example which is presented by **Al-Amery, and Roberts, 1990** was used herein for validating the accuracy of the proposed method of analysis and to examine the effect of some properties on the behavior of simply supported composite beam.

A study was made on the behavior of 9 m span simply supported composite beam having the cross-section dimensions shown in **Fig. 8** and **Fig. 4**. For simplicity, the beam was assumed to be supported during construction, so that the construction strains ε_c, was zero, and subjected to a uniformly distributed load. The free strains ε_f, were also assumed zero.

Concrete slab: Width of concrete slab = 1800 mm, depth of concrete slab = 150 mm, cross sectional area = 270000 mm^2, d_1 =281 mm, initial modulus of elasticity = 30000 MPa, ultimate compressive strength=30 MPa.

Steel beam: Flange width = 153mm, flange thickness = 16 mm, web height = 380 mm, web thickness = 9.4 mm, cross sectional area = 8500 mm^2, initial modulus of elasticity = 200000 MPa, yield stress = 280 Mpa.

Shear connector: The connection between the concrete slab and steel beam was assumed to be produced by pairs of headed studs of 19-mm diameter, l00-mm long, with a spacing of 240 mm. The ultimate shear strength of a single stud, Q_u, was taken as 100 kN while the slip $\bar{u}_{cs}$ corresponding to a shear force $\bar{Q}$ = 62 kN was taken as 0.5 mm **(see Fig. 7)**. This gave an initial tangent value of Ks = 1.935 kN/mm.

It should be noted that the concrete slab was divided into ten equal strips. Each flange of the steel beam was divided into eight equal strips and the web of the steel beam was divided into twenty equal strips.

To illustrate the application of the formulation that was developed at the previous sections, a comparison is made between current study model and Al-Amery and Roberts model. Load-deflection relationships and slip distributions between the concrete slab and steel beam obtained from analysis are shown in **Fig. 9** and **Fig. 10**, respectively, for a simply supported composite beam with partial interaction.

These curves show good agreement between two types of analysis of composite beam where the method developed by Al-Amery and Roberts depends on four independent variables (tow horizontal displacement u_c and u_s) and (two vertical displacement w_c and w_s) while Johnson approach depends on only one independent variable that is slip u_{cs}.

From the examination of load-deflection curve in **Fig. 9** conclusion can be made that beam behaves in almost linear shape up to 50 kN/m, then partial yielding starts in the steel section from lower stand which causes respective increasing in deflection with small increasing in beam load carrying capacity, maximum load recorded was (ρ_u=78 kN/m), at 0.93%ρ_u deflection equal to 175 mm at mid span.

Examination of **Fig.10** represents the relation of applied external load with maximum slip which occurs at the end of span. The vertical applied load is converted to horizontal shear flow that is transmitted between steel section and concrete slab according to traditional beam theory. In the beginning the connector shows linear response to applied load until ρ = 60 kN/m then the nonlinear effect starts between ρ = 60 kN/m and 78 kN/m.

Strain and stress profiles throughout the depth of the simply supported composite beam corresponding to different levels of the applied uniformly load are shown in **Fig. 11** and

Fig. 12.The load increments are taken as percentage of ultimate load (78 kN/m) as; 90% and 93%.

The discontinuous strain profiles indicate the existence of slip at the interface between the concrete and steel, while the stress profiles indicate the spread of plasticity.

7.2 Example 2

Chapman and Balakrishnan, 1964 tested a series of simply supported composite beams. EII is one of the tested beam, with 5.5 m, which was used herein to carry out a second validation test of the proposed analysis method and **Fig. 13** illustrates the cross-section of this beam.

Concrete slab: Width of concrete slab = 1220 mm, depth of concrete slab = 153 mm, cross sectional area = 186660 mm2, d_1 = 162.9 mm, Initial modulus of elasticity = 26700 MPa, ultimate compressive strength = 50 MPa.

Steel beam: flange width = 153 mm, flange thickness = 18.2 mm, web height = 268.6 mm, web thickness = 10.16 mm, cross sectional area =8300 mm^2, initial modulus of elasticity = 205000 MPa, Yield stress = 265 Mpa.

Shear connector: the connection between the concrete slab and steel beam was assumed to be produced by pairs of headed studs of 12.5mm diameter, 50mm long, with a spacing of 110 mm.

The concrete slab was divided into ten equal layers. Each flange of steel beam was divided into eight equal layers and web of steel beam was divided into twenty equal layers.

Fig.14 shows the load-deflection curves for the beam. The results show very good agreement between the experimental test and the theoretical nonlinear analysis as the difference is less than 5% in ultimate load carrying capacity or corresponding deflection.

On the other hand examining the slip behavior along the beam as shown in **Fig.15** clarifies obvious difference between theoretical and experimental test results. This can be explained due to the behavior of point load, where both maximum values of shear force (equal to P/2) and bending moment (equal to pL/4) occur at the region of mid-span simultaneously resulting in high principle stresses. At the early stage of loading, the connectors show almost equal horizontal displacement as the equal shear force is transmitted in the interface of concrete and steel. As the load increases the maximum principle stresses occur in the inclined axis depending on the value of two types of stresses (shear and bending), therefore the inclined principle forces which slope up ward will bend the connector in the experimental tested beam and may cause crashing of concrete at the region of mid-span. Therefore this difference between experimental and theoretical analysis is recorded as shown in **Fig. 15**.

8. DESCRIPTION OF THE BEHAVIOR OF COMPOSITE BEAM OF EXAMPLE 1

After the proposed method has been checked by comparison of results with another model the full behavior of simply supported composite beam can be described as follows.

8.1 Deflection

The deflection along the composite beam can be computed taking into account the nonlinear behavior of steel, concrete, connector, and partial interaction theory. The differences are computed at different load increments. The load increments are taken as percentage of ultimate load capacity of beam (ρ_u =78 kN/m) as follows; 87% and 93%, in order to clarify the result in different scales; the results are shown in the **Fig. 16**.

The maximum deflection is located at mid span. The central deflection is increased with increasing applied uniform load as 122.7 and 175.1 mm for 87% and 93% ρ_u percentage of ultimate load, respectively.

8.2 Interface Slip

The distribution of slip is computed for different load increments. The load increments are as follows; 87% and 93% ρ_u as shown graphically in **Fig. 17**.

The value of maximum slip occurs at the supports and it increases with increasing of applied uniform load as, 4.12 and 11.1 mm for load 87% and 93% ρ_u.

9. BEHAVIOR COMPOSITE BEAM OF EXAMPLE 2 STRENGTHENED WITH COVER PLATE

In some circumstances as, after designing and using a structure for many years it is required to increase load carrying capacity due to different reasons. In the other hand yielding of beam may occur due an expected additional loading. In both cases strengthening of composite beam is required by any available producers to withstand the new conditions taking in consideration the load history of the composite the existing pre-slip at interface and yielding the bottom flange of steel beam which is indicate the failure of composite structure.

In the design of composite structure according to related design code, the design is often made of the section in the bases of tension failure of steel component of the cross section. The tension failure allows for high ductility of structure members and prevents sudden failure of the beams. Therefore if it is required to strengthen any member, it is essential to increase the area of steel in the process of increasing load carrying capacity of the beam. Different techniques of strengthening of structure members have been used such as using CFRP sheets that are glued to the lower flange of the steel section by special type of epoxy or using external prestressing technique of composite member applying force on straight or inclined strand and provide required anchorage at the ends of the beams.

In this research the strengthening of composite member was carried out by welding steel cover plate to lower flange of steel beams. The steel beam and plate are fully connected while partial interaction of the shear connector is considered in the analysis of overall section. Also it's assumed that the plate is attached to the beam after the full yielding of lower flange and the welded plate while the web is the elastic zone.

A computer program is designed to stop temporarily after reaching yield stress and strain, and then the required thickness of plate is added along the beam taking into consideration the transverse dimension to the centroid of cross section. After that the program will continue running taking in consideration all previous loading steps, strains and stresses in the member. The results are shown in **Fig. 18**.

Load-deflection curve for simply supported composite beam had already been tested by **Chapman, and Balakrishnan, 1964.** The original load carrying capacity of beam was 530 kN with central deflection equal to 76.41 mm. Strengthening the beam with cover plate of (153 x 7.5), (153 x 15) and (153 x 30) mm will increase beam capacity by 15 %, 30%, 43% respectively, as shown in **Fig. 19**

Also the distribution of slip with the applied point load (530 kN) is found for different thicknesses of cover plate as shown graphically in **Fig. 19** The maximum slip at the support decreases with increasing of thickness of cover plate as follow: 0.577, 0.511, 0.473, 0.446 and 0.424 mm for 0, 7.5, 15, 22.5 and 30 mm, respectively.

10. CONCLUSIONS

Based on results of the present study, the following conclusions can be drawn,

1. Nonlinear analysis of steel, concrete and shear connecter has been derived for strengthened simply supported composite member, and verified with experimental work.
2. In the process of strengthening, using area of steel equal to 41%, 82% and 164% of the existing lower flange area will increase the beam carrying capacity by 15%, 30% and 43%.
3. Also using the same above mentioned area of steel cover plate will reduce the central total deflection by 59%, 72% and 80%.
4. It is found by increasing the area of cover plate at the same applied load value of 530 kN. The value of maximum deflection will reduce by, 76.4 , 67.76 ,61.57 and 52.94mm for plate thickness 0 ,7.5 ,15 and 30 mm respectively
5. Also it is found by increasing the area of cover plate at the same applied load value of 530 kN the value of maximum slip will be reduced as fallows; 0.5772, 0.5113, 0.4732 and 0.4239 mm respectively.

REFERENCES

- Al-Amery, R. I. M. and Roberts, T. M., 1990, *Nonlinear Finite Difference Analysis of Composite Beams with Partial Interaction*, International Journal of Computers and Structures, Vol. 35, No.1, PP. 81-87.

- Al-Amery, R. I. M., Ali Z. M. and Aziz Kh. I., 2007, *Behavior of Multi-Layer Composite Beams with Partial Interaction "Part I "*,Iraqi Journal of Civil Engineering, 8th Issue, June.

- Al-Amery, R. I. M., Ali Z. M. and Aziz Kh. I., 2007, *Behavior of Multi-Layer Composite Beams with Partial Interaction "Part II "*,Iraqi Journal of Civil Engineering, 9th Issue, December.

- BS8110: Part-1: 1997, *Structural use of concrete*, Code of Practice for Design and construction. British Standard Institution, London.

- Chapman, J. C. and Balakrishnan, S., 1964, *Experiments on Composite Beams*, Structural Eng., Vol. 42, No. 11, pp. 369-383, (Cited according to **Yam and Chapman**,**1968**)

- Dogan, O. and Roberts, T. M., 2010, *Comparison of experimental internal forces with full and partial interaction theories in steel-concrete-steel sandwich beams*, International Journal of the Physical Sciences, Vol. 5, No. 15, pp. 2322-2334.

- Johnson, R. P. and May, I. M., 1975, *Partial Interaction Design of Composite Beams*, the Structural Engineer, Vol. 53, No. 8, Aug., pp. 305-311.

- Lam, D. and El-Lobody, E., 2005, *Behavior of Headed Stud Shear Connectors in Composite Beam*, ASCE, Journal of Structural Engineer., Vol. 131, No. 1, pp. 96–107.

- Newmark, N. M., Siess, C. P. and Viest I. M., 1951, *Tests and Analysis of Composite Beams with Incomplete Interaction*, Proc. Society for experimental stress analysis, Vol. 9, No. 1.

- Roberts, T. M., 1985, *Finite Difference Analysis of Composite Beams with Partial Interaction*, Computers and Structures, Vol. 21, No. 3, pp.469-473.

- Sayhood E. K. and Mahmood M. Sh., 2011, *Non-Linear Behavior of Composite Slim Floor Beams with Partial Interaction*, European Journal of Scientific Research, Vol.56 No.3, pp.311-325.

- Yam, L. C. P. and Chapman, J. C., 1968, *The Inelastic Behavior of Simply Supported Composite Beams of Steel and Concrete*, Proceedings Institution of Civil Engineers, Vol. 41, December, pp. 651-683.

NOMENCLATURE

A_c	cross section area of concrete slab.
A_s	cross section area of steel beam.
d_1	distance between centroids of concrete and steel section in a composite beam.
E_c , E_s	young modulus of the concrete and steel beam respectively.
f_{cu}	cubic compressive strength of concrete.
f_y	yield strength of steel.
h_c	total depth of concrete beam.
h_s	total depth of steel beam.
I	second moment of inertia.
I_c	second moment of inertia of concrete.
I_s	second moment of inertia of steel beam.
K	shear stiffness of the connection in the composite beam.
K_1-K_6	constant of integration.
K_s	normal and shear stiffness per unit length
L	span of composite beam.
M	applied bending moment.
M_c	bending moment in the concrete.
M_s	bending moment in the steel beam.
N	applied shear force at a section of the composite beam.
n_1	number of layers of concrete.
n_2	number of layers of steel beam.
P	applied point load.
q	longitudinal shear force per unit length at the interface.
S	spacing of shear connectors
T	normal force per unit length at the interface.
u_{cs}	slip at the interface.
V	applied shear force.
V_c	shear force at the concrete slab.
V_s	shear force at the steel beam.
w	displacement in z direct ion
α & β	function of section and material properties of a composite beam.
ε	strain.

ε_{cu} ultimate concrete crushing strain.
ε_o strain at maximum stress.
ε_y steel yield strain.
ϕ constant.
ρ applied load per unit length.
σ stress.

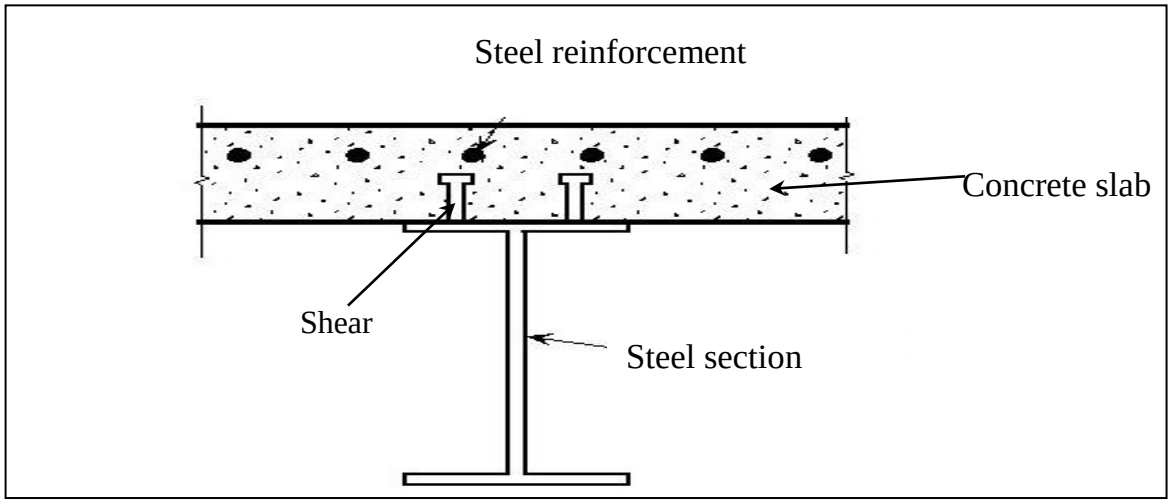

Figure 1 .Typical composite beam consist of steel section and concrete slab.

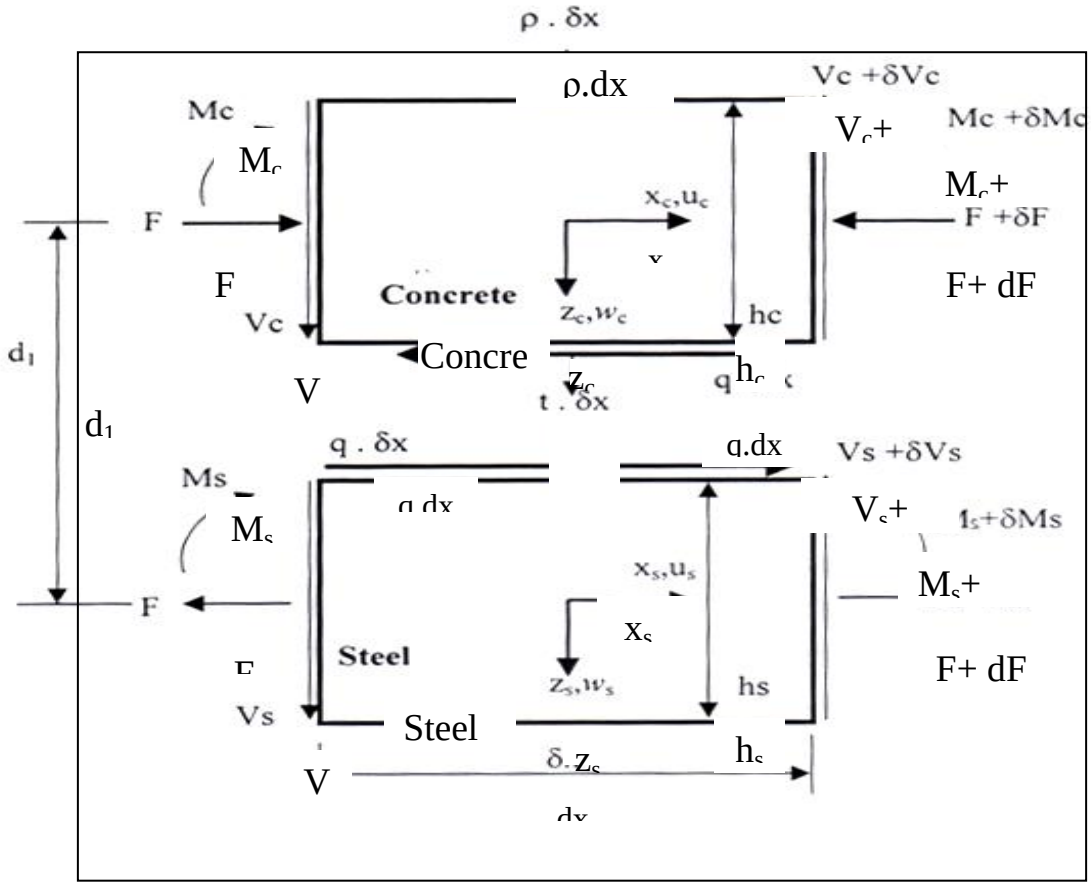

Figure 2 Elevation of element of composite beam

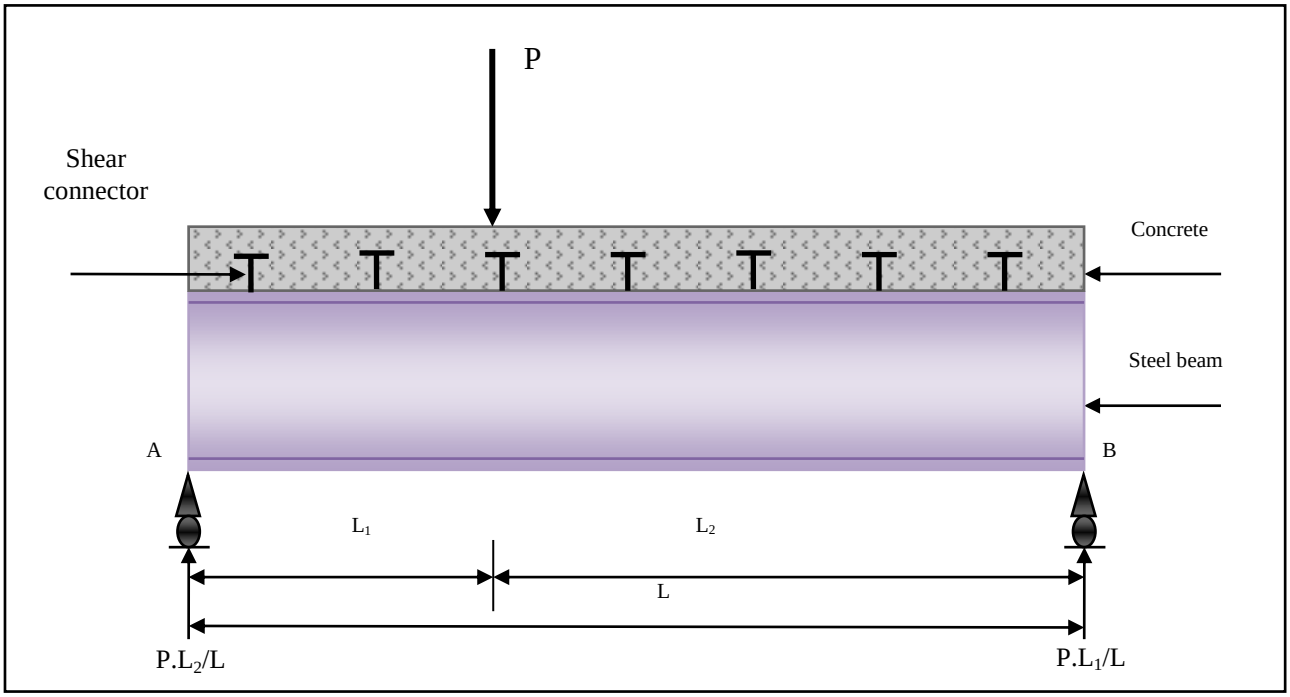

Figure 3. Typical composite beam subjected to point load.

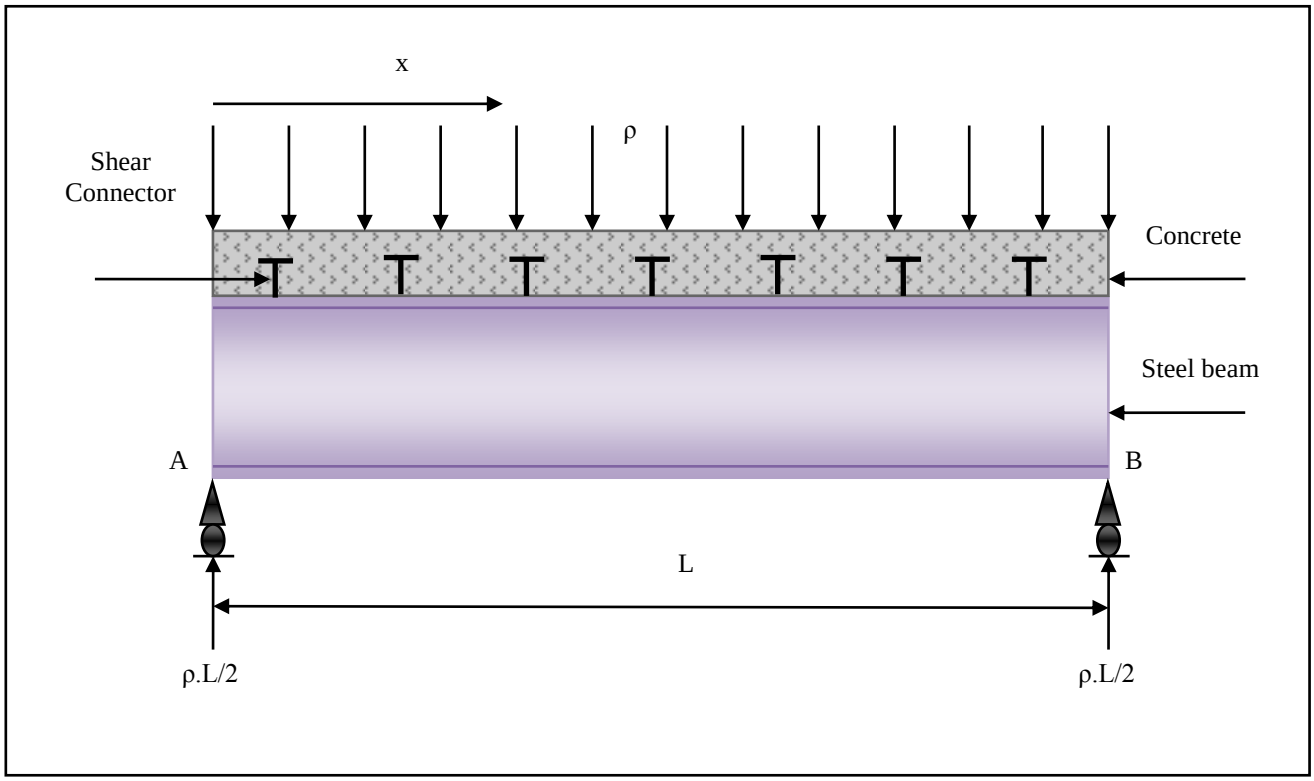

Figure 4 Typical composite beam subjected to uniformly distributed load.

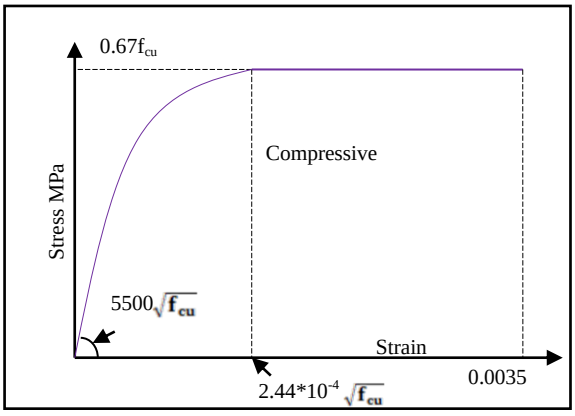

Figure 5 BS 8110 compressive stress-strain curve for concrete.

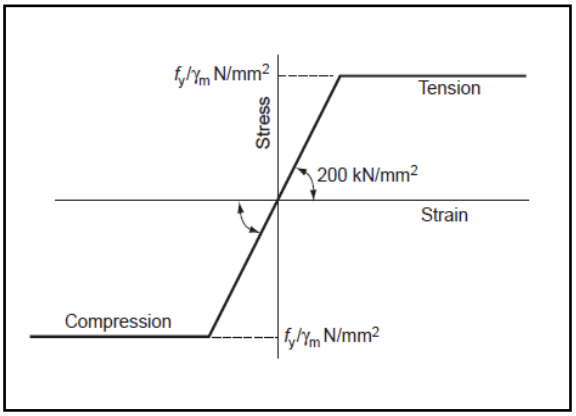

Figure 6 Idealized stress-strain curve for steel.

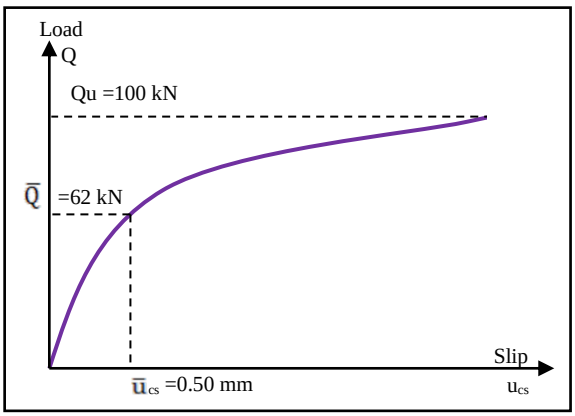

Figure.7 Shear force versus slip curve for shear connectors. **Al-Amery, and Roberts, 1990**

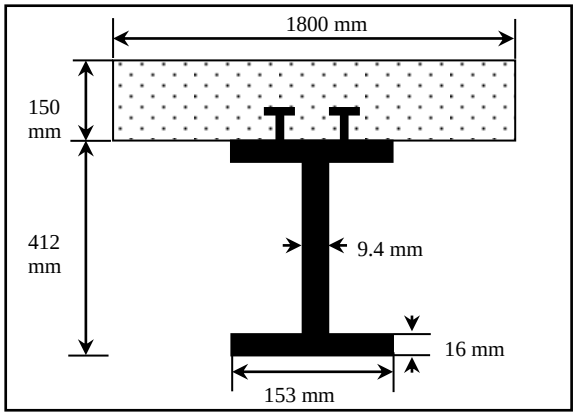

Figure 8 Composite beam-cross-section dimensions of example one

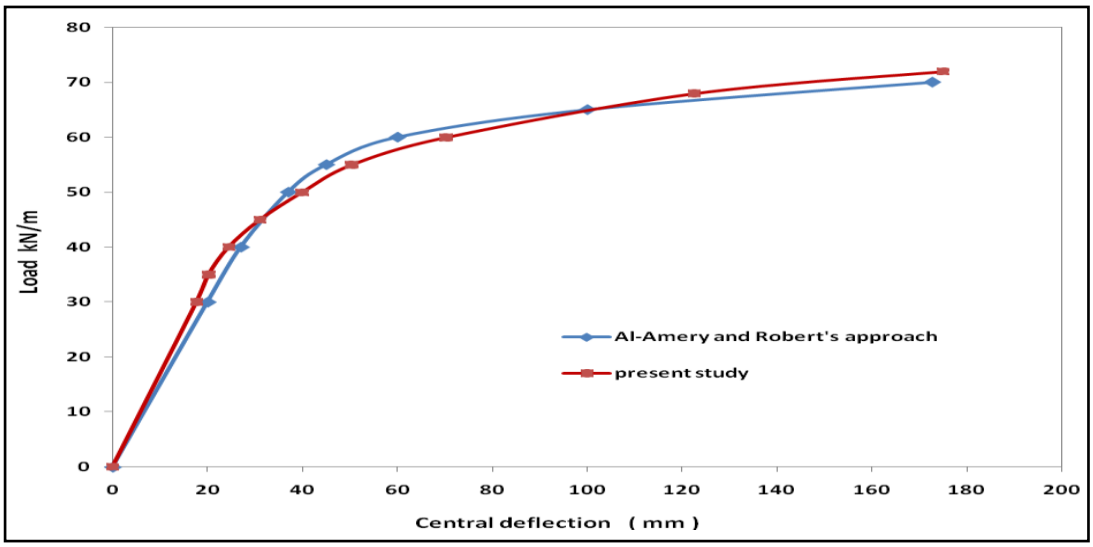

Figure 9 Load-deflection of the beams of example one.

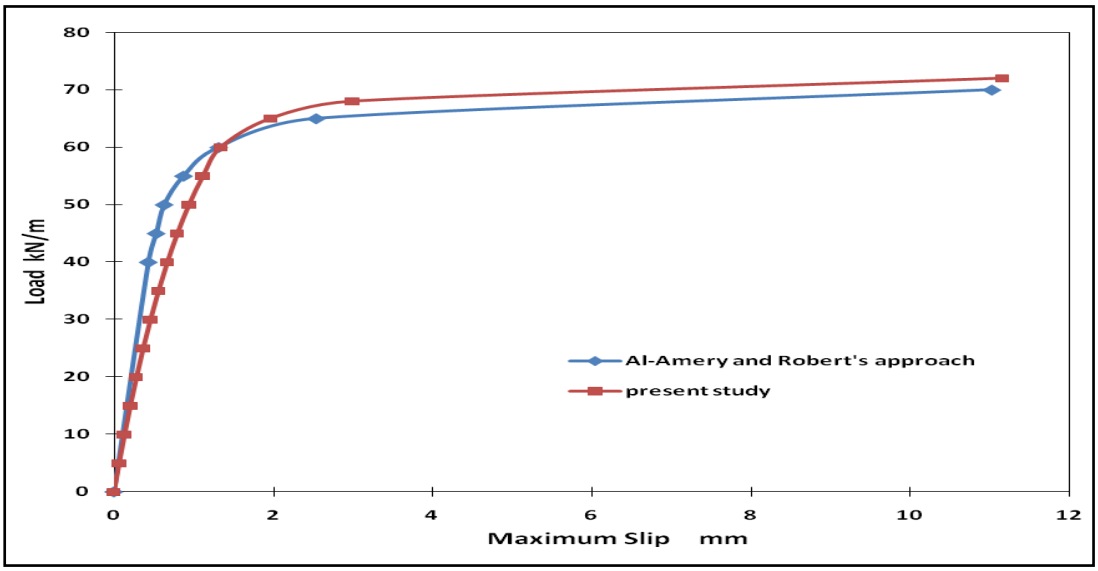

Figure 10 Load-slip curve of the beams of example one.

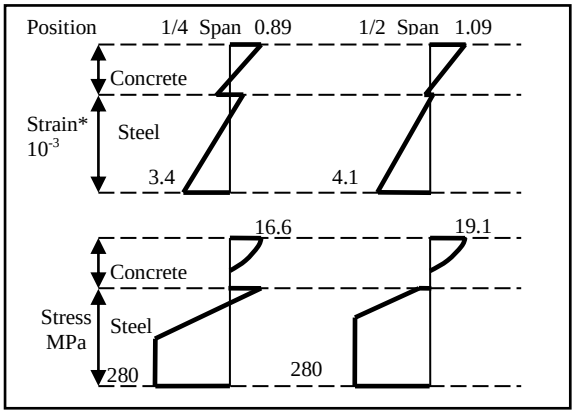

Figure 11 Strain and stress profiles at load levels 90% ρ_u.

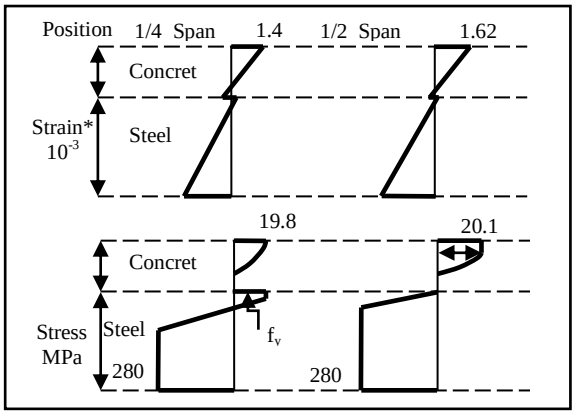

Figure 12 Strain and stress profiles at load levels 93% ρ_u.

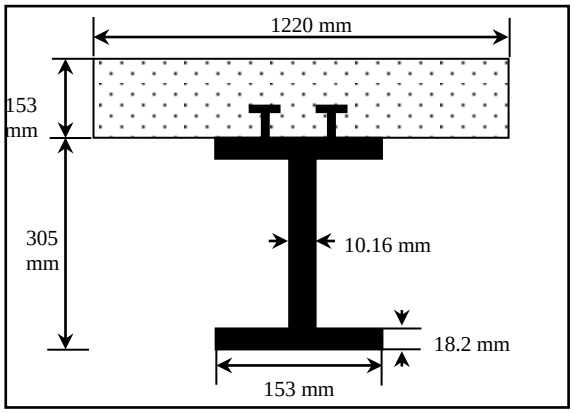

Figure 13 Composite beam cross-section dimensions of example two

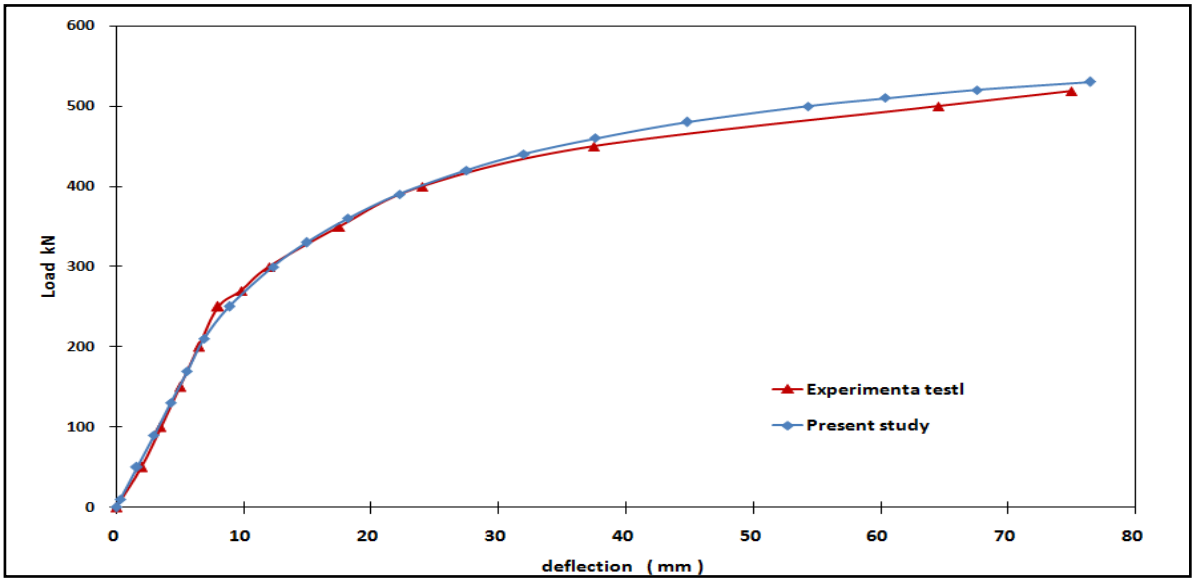

Figure 14 Load-deflection curve of beam EII **(Chapman and Balakrishnan, 1964)**.

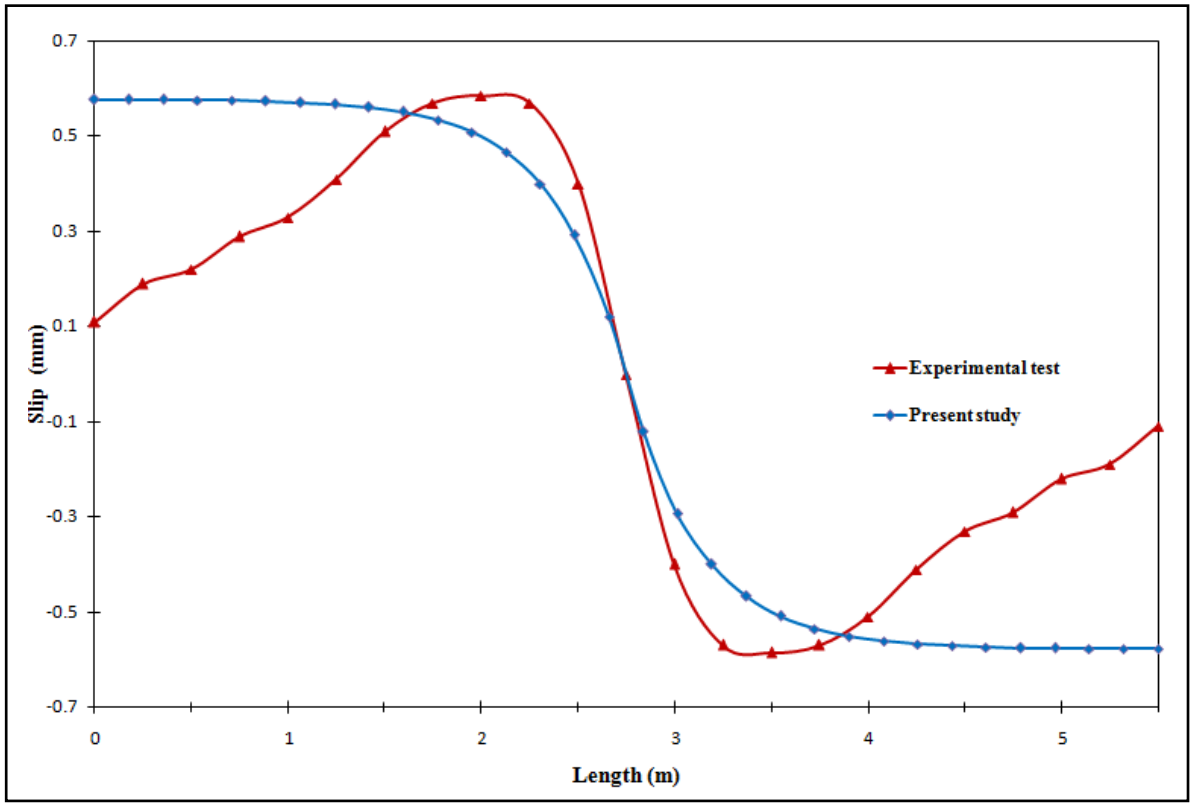

Figure 15 Slip along the span at load 450 kN for the second example.

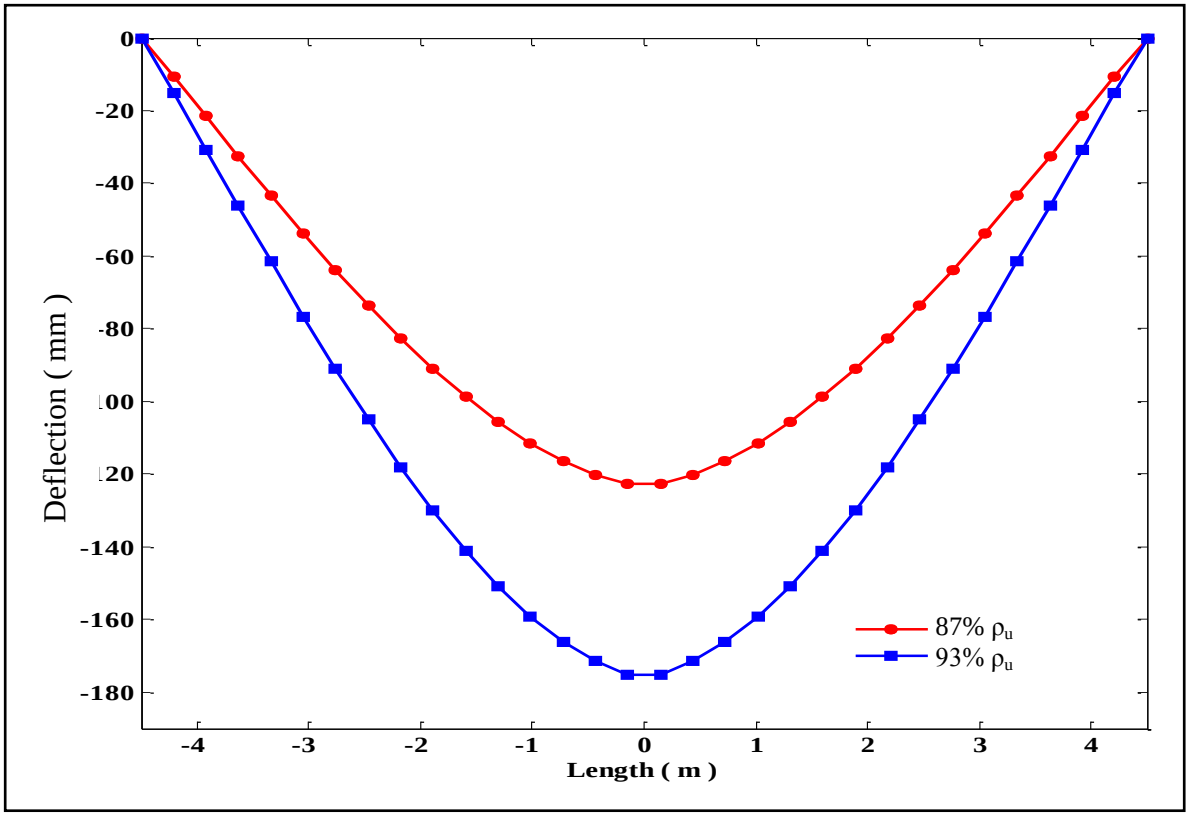

Figure 16 Deflection of example one along span at 87% ρu and at 93% ρu.

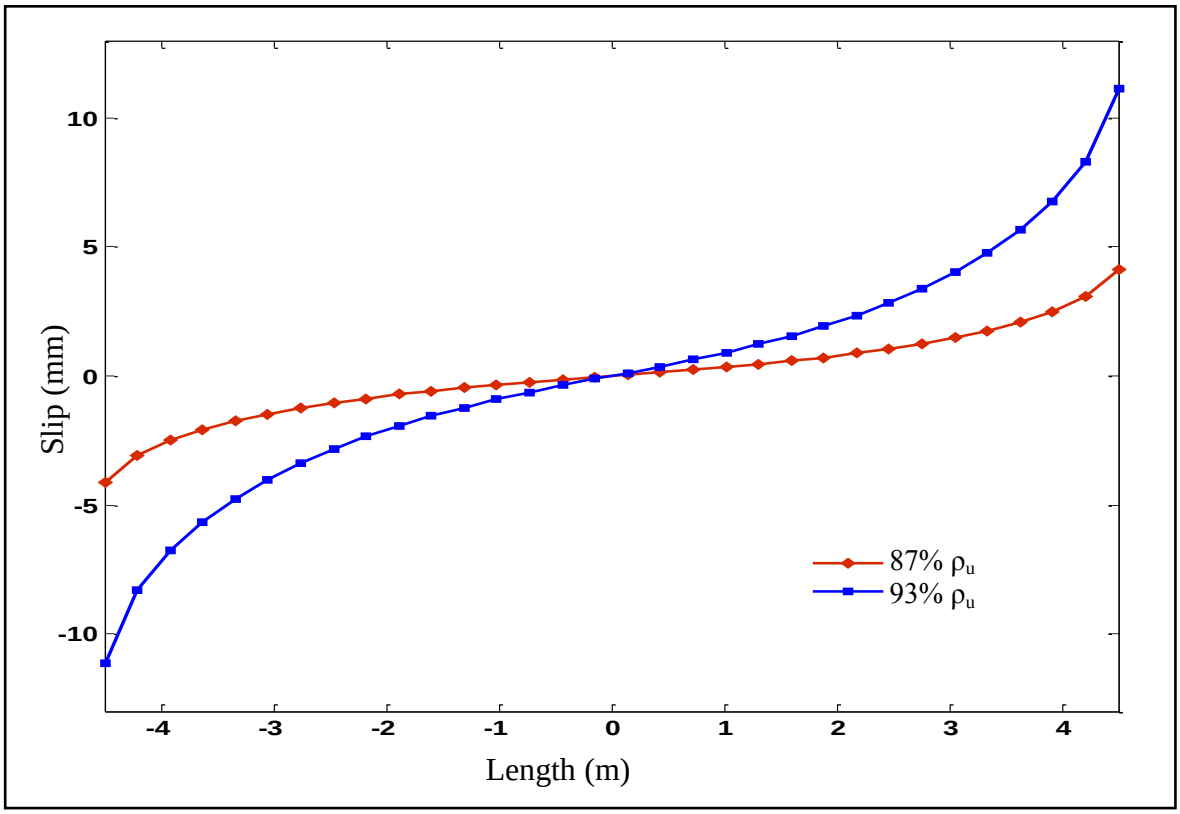

Figure17 Slip of example one along span at 87% ρu and at 93% ρu.

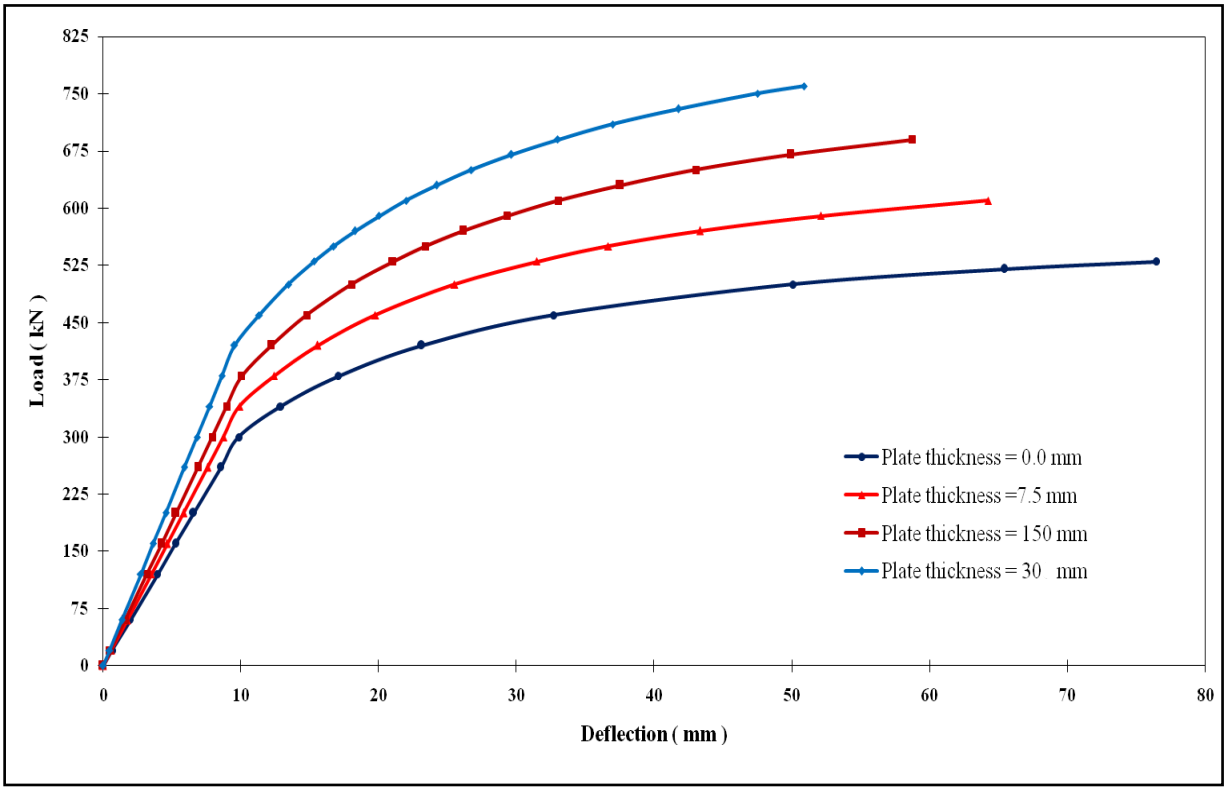

Figure 18 Load-deflection curve of strengthened composite beam of example two with various cover plates.

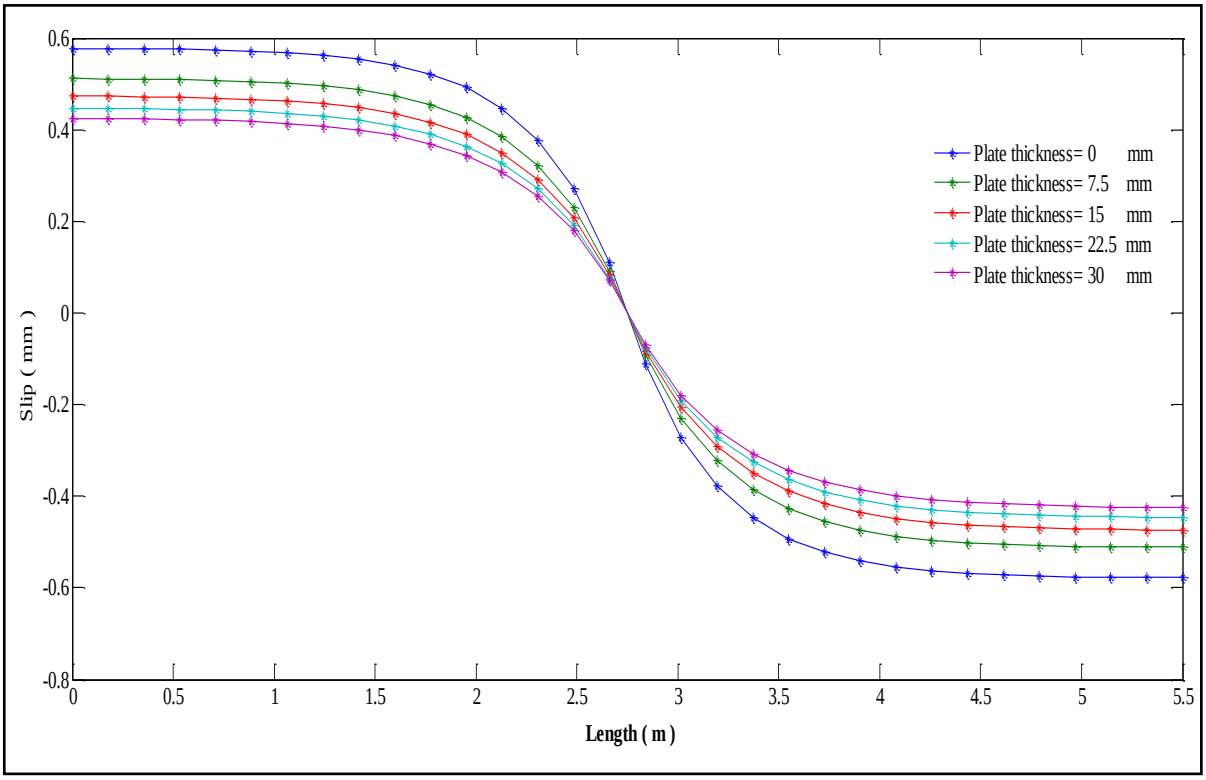

Figure 19 Slip distributions along beam of example two with various plate thicknesses at load 530 kN

Behavior of Reinforced Concrete Deep Beams Strengthened with Carbon Fiber Reinforced Polymer Strips

Dr. Ali Hussein Ali Al-Ahmed
Lecturer
College of Engineering – University of Baghdad
ali_hussein_alahmed@yahoo.co.uk

Mohammed Hazim Mohammed Al-Jburi
M.Sc. Structures
Ministry of Higher Education and Scientific Research
mohammed_hazim2013@yahoo.com

ABSTRACT

This research is concerned to investigate the behavior of reinforced concrete (RC) deep beams strengthened with carbon fiber reinforced polymer (CFRP) strips. The experimental part of this research is carried out by testing seven RC deep beams having the same dimensions and steel reinforcement which have been divided into two groups according to the strengthening schemes. Group one was consisted of three deep beams strengthened with vertical U-wrapped CFRP strips. While, Group two was consisted of three deep beams strengthened with inclined CFRP strips oriented by 45^o with the longitudinal axis of the beam. The remaining beam is kept unstrengthening as a reference beam. For each group, the variable considered was the center to center spacing between strips (orthogonal spacing) which are (100 mm, 125 mm and 150 mm). Based on the experimental results it is found that the strengthening deep beams with CFRP strips by the two strengthening schemes, the mid-span deflection was decreased and both first cracking and ultimate loads capacities were increased compared to reference deep beam. For beams having the same spacing between strips, the enhancement occurred by using vertical U- wrapped scheme was somewhat better than using inclined scheme but it needs to use additional numbers of CFRP strips. The percentages increase in first cracking and ultimate loads were (50.0%, 46.0% and 20.5%) and (14.6%, 13.3% and 12.2%) respectively for beams strengthened with vertical U-wrapped scheme. While these percentages were changed to (36.5%, 18.0% and 12.5%) and (12.5%, 10.4% and 8.6%) for beams strengthened with inclined scheme. These results were obtained for center to center spacing between strips of (100 mm, 125 mm and 150 mm) respectively. The analytical part of this research was also adopted using the ACI 440 Code provisions to calculate the additional shear resistance carried by the CFRP strips. Good agreement was obtained between the experimental and analytical results.

Key words: carbon fiber reinforced polymer, strengthening, deep beams, strips

سلوك العتبات الخرسانية المسلحة العميقة المقواة بأشرطة الألياف الكاربونية

د. علي حسين علي أل احمد
مدرس
كلية الهندسة / جامعة بغداد

محمد حازم محمد الجبوري
ماجستير انشاءات
وزارة التعليم العالي والبحث العلمي

الخلاصة

يهتم هذا البحث بالتحري عن سلوك العتبات الخرسانية العميقة المقواة باشرطة الالياف الكاربونية. تضمن الجانب العملي من هذا البحث فحص سبعة عتبات عميقة لها نفس الابعاد وحديد التسليح وتم تقسيمها الى مجموعتين حسب نمط التقوية. تالفت المجموعة الاولى من ثلاثة عتبات عميقة تم تقويتها باشرطة الالياف الكاربونية الشاقولية على شكل حرف U. بينما تالفت المجموعة الثانية من ثلاثة عتبات عميقة ايضا ولكن باستخدام اشرطة الالياف الكاربونية المائلة بزاوية 45^o عن المحور الافقي للعتبة. اما العتبة المتبقية فتركت بدون تقوية كعتبة مرجعية لأغراض المقارنة. المتغير الذي تم اعتماده لكل مجموعة هو المسافات المتعامدة بين مراكز اشرطة الالياف الكاربونية التي كانت بواقع (100 ملم, 125 ملم و 150 ملم). وجد من النتائج العملية ان تقوية العتبات العميقة باستخدام اشرطة الالياف الكاربونية لنمطي التقوية قد قلل من الهطول في منتصف العتبات

وكذلك ازداد حمل التشقق الاولي وقوة التحمل الاقصى للعتبات العميقة مقارنة مع العتبة المرجعية. كذلك وجد بانه لنفس المسافات المتعامدة بين اشرطة الالياف الكاربونية ان التحسن الحاصل باستخدام نمط التقوية باشرطة الالياف الكاربونية على شكل حرف U كان اكثر نوعا ما من التحسن الحاصل باستخدام نمط التقوية باشرطة الالياف الكاربونية المائلة ولكنها تحتاج الى زيادة في عدد اشرطة الالياف الكاربونية المستخدمة. كانت نسب الزيادة في حمل التشقق الاولي والحمل الاقصى (50.0%, 46.0% و 20.5%) و (14.6%, 13.3% و 12.2%) على التوالي عند استخدام نمط التقوية باشرطة الالياف الكاربونية على شكل حرف U. بينما تغيرت هذه النسب الى (36.5%, 18.0% و 12.5%) و (12.5%, 10.4% و 8.6%) على التوالي عند استخدام نمط التقوية باشرطة الالياف الكاربونية المائلة. تم حساب هذه النسب للمسافات المتعامدة بين مراكز اشرطة الالياف الكاربونية (100 ملم, 125 ملم و 150 ملم) على التوالي. تبنى الجانب التحليلي من هذا البحث استخدام علاقات المدونة الامريكية ACI 440 Code لحساب التعزيز الحاصل لقوه القص الناجم من التقوية باستخدام الالياف الكاربونية حيث وجد ان هنالك تقارب جيد بين النتائج العملية والتحليلية.

الكلمات الرئيسية : الالياف الكاربونية, تقوية، عتبات عميقة، اشرطة

1. INTRODUCTON

Reinforced concrete (RC) deep beams are very useful members and are widely used in buildings, bridges and infrastructures. The deep beam is a beam having a large height (***h***) comparable with its span length (***l***). To consider a beam is deep, the span length to height ratio (***l/h***) should be less than a certain value. The **ACI-318 Code, 2014**, considers a beam is deep if (***l/h***) ratio is less than or equal to 4.

In the continuous development in science and technology, strengthening of RC structures may be needed due to additional loads that may be imposed or due to deterioration of RC structures as a result of steel corrosion or concrete cracking. There are many ways that may be used to improve this traditional concept in different structural members such as using fiber concrete instead of normal concrete, coating beams with bonded steel plates or fiber reinforced polymer (FRP) materials, **Shanafel,** and **Horn, 1985; Neale, 2000**.

Uses of FRP materials becomes an acceptable solution for strengthening and repairing in the field of civil engineering across the globe and are widely used for strengthening and retrofitting of RC structures because they have different properties such as light weight, resistance to chemicals and non-corrosive non-magnetic nature. Also, the formability of FRP produces their enforcement technique which is very simple to install, **Alkhrdaji, et al., 2000; Neale, 2000; Li, et al., 2002; Ludovico, 2002.**

Three types of FRP are mainly used for strengthening and rehabilitation of RC structures, Glass Fiber Reinforced Polymer (GFRP), Aramid Fiber Reinforced Polymer (AFRP) and Carbon Fiber Reinforced Polymer (CFRP). Among these three types, CFRP is found to be most efficient to increase the capacity of RC beams, **Li, et al., 2002, Abdel-Jaber, et al., 2003; Feng,** and**, Yuan, 2008.** Using CFRP sheets or strips is more suitable for applications that have complex geometrical arrangement like curved beams or beams having higher level of reinforcement. These are typically fattened with an epoxy resin in-situ, which likewise acts to bind the fibers to the structure. The comparatively high modulus of the carbon fiber materials makes them more suitable to promote the serviceability of steel structures, **Barros,** and **Dias, 2003; Mitali,** and **Gajjar, 2012; Liu, et al., 2012.**

2. EXPERIMENTAL PROGRAM .

2.1 Introduction

The main purpose of this research is to investigate the behavior RC deep beams strengthened with CFRP strips. The primary variables considered are the strengthening schemes of CFRP strips and the center to center spacing between strips. Two schemes of strengthening using CFRP

strips were adopted. These schemes are vertical U-wrapped CFRP strips and inclined CFRP strips oriented by 45° with the longitudinal axis of the beam.

Standard tests were carried out to determine the properties of materials used in this research. In addition, instrumentation, experimental setup and testing procedures adopted throughout this investigation are presented.

2.2 Deep Beams Details

In this research work, seven simply supported RC deep beams were cast and tested up to failure by applying two-point loading. Six of these beams were strengthened with CFRP strips (strip width= 50 mm). While, the remaining deep beam (denoted as DB1) is kept unstrengthening as a reference beam. All tested beams having the same dimensions [total length =1100 mm, width (***b***) = 150 mm and height (***h***) =240 mm]. The center to center distance between supports (span=***l***) was 950 mm which results a span to height ratio (***l/h***) equals to 3.96 which lies within the ACI Code limits. All beams were designed to fail in shear. These deep beams were reinforced with 2ϕ16 mm and 1ϕ12 mm steel bars at the bottom side of beams. While, ϕ 6 mm is used as stirrups spaced each 100 mm. In addition, a skin reinforcement of 1ϕ6 mm was added at mid height of the beam cross section at both side faces. Also, 2ϕ6 mm steel bars were located at the top of beams. **Fig. 1** shows full details of a typical tested beam.

The strengthened deep beams were divided into two groups according to the strengthening schemes. Group one was consisted of three deep beams denoted as DB2, DB3 and DB4 strengthened with vertical U-wrapped CFRP strips having spacing of (100, 125, and 150 mm) center to center between strips respectively. While, Group two was consisted of three deep beams denoted as DB5, DB6 and DB7 strengthened with inclined CFRP strips oriented by 45° with the longitudinal axis of beam having the same spacing above orthogonal to strips as shown in **Fig. 2**. Also, **Table 1** presents the description of tested beams conducted in this study.

2.3 Materials Used for Casting Beams

2.3.1 Cement

Ordinary Portland cement type (I) was used for concrete mix. This cement was tested chemically and physically according to the **Iraqi Specifications No. 5, 1984** for Portland cement.

2.3.2 Fine aggregate

Natural sand from Al-Akhaidher quarries was used throughout this study. This sand has a maximum particles size of (4.75mm). The sand washed with water and then dried and it was confirmed to the **Iraqi specification No.45, 1984**.

2.3.3 Coarse aggregate

Crushed gravel from Al-Sodor region with maximum size of 15 mm was used throughout this research. The crushed gravel was washed and it was conform to the **Iraqi specification No.45, 1984**.

2.3.4 Steel reinforcement

Three sizes of deformed steel bars were utilitied in the investigation having diameters of ϕ6 mm, ϕ12 mm and ϕ16 mm. These steel bars were tested according to the **ASTM standard A615, 2001**. The yield stress (f_y) for ϕ6 mm steel bars was 420 MPa. While for ϕ12 mm and ϕ16 mm steel bars, the yield stress was 460 MPa.

2.3.5 CFRP strips

CFRP type Sika Wrap Hex-230 and epoxy based impregnating resin of type Sikadur-330 were used in this study for externally strengthening the deep beams. The CFRP strips having width of 50 mm and thickness of 0.15 mm. Based on a data sheet given by the manufactured company, the ultimate tensile strength and the modulus of elasticity for the CFRP strips used throughout this research were 3400 MPa and 230000 MPa respectively.

2.4 Concrete Compressive Strength

In the present study, normal weight concrete was used for casting the specimens. After several trial mixes, the cylindrical compressive strength (f'_c) was 17.3 MPa. This value is slightly larger than the minimum recommended value that mentioned in the **ACI-318 Code, 2014**.

2.5 Preparation of Specimens

For casting the specimens, seven wooden molds were prepared and fabricated into the required beam dimensions. These molds were oiled and then the reinforcement cages were put into the required positions as shown in **Fig. 3**. After 28 days of curing, all specimens were white painted to recognize cracks during the test. Scraper machine was used to rough the surface of the beams at specified location of CFRP strips to make good cohesion between concrete surface and CFRP strips. The epoxy mix has been applied to the surface of concrete, and then the CFRP strips were pasted on the concrete surface as shown in **Fig. 4**.

2.6 Test Rig Components and Loading Procedure

All deep beams were tested up to failure by using a hydraulic testing machine available at the Civil Engineering Department Laboratory of the University of Bagdad. All beams were mounted on two steel rollers (supports) available at the laboratory and attached to the bottom face of the beams with distance of 950 mm measured center to center between supports. After mounting the specimens on the supports, a single dial gauge was fixed on the lower bed of the testing frame and attached to the bottom face of the beams at mid span.

A special system was achieved for applying two-point loading. This system was fabricated by welding two stiff steel angles with the bottom flange of IPE200 section. Then 2ϕ25 mm steel bars with distance of 300 mm center to center between them were also welded with these angles as shown in **Fig. 5**. A hydraulic jack having a capacity of 500 kN was put on the top flange of IPE200. Then a load cell with capacity of 200 kN was used with a hydraulic jack and the system was attached the testing frame at the top. Small amount of external load was applied until the specimen got stable on the supports. After that, reading of the load cell is reset and load was statrted to be applied gradually with a step of 5 kN. At each load step, mid span deflection was recorded. Also a magnifier was used to note the appearance of first crack for all tested beams. **Fig. 6** shows the setup of tested beams with devices used throughout the test.

3. EXPERIMENTAL RESULTS

3.1 Cracking and Ultimate Loads Test Results

All tested beams were characterized by the formation of diagonal shear cracks near supports. These diagonal cracks were propagated with an angle of 45^o until they reached the top surface of beams then failure occurred. At stages of loading close to failure load, debonding of some CFRP strips where the cracks passed through occurred. **Fig. 7** shows all tested deep beams after failure.

Table 2 summarizes the experimental first cracking and ultimate loads results. From this table it can be noticed that strengthening deep beams with CFRP strips has a significant effect on increasing the first cracking load and slightly increases the ultimate load compared to reference

deep beam. For the first scheme of strengthening (vertical U-wrapped strips) which is represented by beams of group one, the maximum percentage increase in first cracking and ultimate loads were 50.0% and 14.6% respectively for deep beam DB2 which has been strengthened with 10-U wrapped strips spaced each 100 mm center to center of strips. While, for the second scheme of strengthening (inclined strips) which is represented by the beams of group two, the maximum percentage increase in first cracking and ultimate loads were 36.5% and 12.5% for deep beam DB2 which has been strengthened with 6-inclined strips spaced each 100 mm center to center orthogonal to strips. Also, from this table it can be noticed that as the spacing between strips is decreased, the percentages increasing in first cracking and ultimate loads are increased for both schemes of strengthening.

By comparing the results obtained from **Table 2** for both strengthening schemes, it may be noticed that for the same spacing between strips there is a small different in percentage increase in ultimate load compared to reference deep beam. Hence, for the same spacing between strips U-scheme of strengthening need more amount of CFRP strips than inclined scheme of strengthening. So that, the inclined scheme of strengthening may be more economic than the U-scheme of strengthening.

3.2 Load-Mid Span Deflection Response

Figs. 8 & 9 show the load-mid span deflection response for beams of Group one (deep beams strengthened with vertical U-wrapped CFRP strips) and beams of Group two (deep beams strengthened with inclined CFRP strips) respectively compared to reference deep beam (DB1). From these figures, it can be noticed that the deflection is decreased as the center to center spacing between strips is decreased for the entire range of loading of each group. This is because of increased stiffness for beams strengthened with CFRP strips when the spacing between strips was decreased. **Table 3** summarizes the experimental deflection values at mid-span of tested beams corresponding to a load level of (96 kN) which represents the ultimate load of the reference deep beam (DB1). From this table it can be noticed that the percentages decrease in deflections were 24.76%, 19.05% and 13.33% for beams strengthened with U-wrapped strips spaced at 100 mm, 125 mm and 150 mm respectively. While, the percentages decrease in deflection were 20.00%, 12.38% and 7.62% for beams strengthened with inclined strips having the same spacing above compared to reference deep beam.

Figs. 10, 11 & 12 were plotted to show the load-mid span deflection response for strengthened beams having the same spacing center to center between CFRP strips but differ in strengthening scheme (i.e U-wrapped and inclined strips). These figures correspond to center to center spacing between strips of 100 mm, 125 mm and 125 mm respectively. From these figures, it can be noticed that for beams strengthened with vertical U-wrapped CFRP strips had stiffer response than beams strengthened with inclined strips. This is because the U-wrapped strengthening scheme might made beams more confined than the inclined strengthening scheme.

4. ANALYTICAL INVESTIGATION BASED ON THE ACI-440 CODE PROVISIONS

The **ACI-440 Code, 2008** provides an expression to calculate the additional shear strength provided by the FRP strips (V_f) as given by Eq. (1). Also **Fig. 13** reveals the dimensional variables used in this equation.

$$V_f = \frac{A_{fv} \times f_{fe} \times (\sin\alpha + \cos\alpha) \times d_{fv}}{s_f} \quad \text{(N)} \qquad 1$$

where

A_{fv} =area of FRP strip within spacing (s_f) given by Eq. (2)
f_{fe} = effective stress in FRP strip given by Eq. (3)
α = angle of FRP strip orientation about x- axis
d_{fv} = effective depth of FRP strip (distance from center of flexural reinforcement to the extreme fiber of strips
s_f = spacing center to center between strips in the horizontal direction

$$A_{fv} = 2 \times t_f \times w_f \quad (\text{mm}^2) \qquad 2$$

where
t_f = FRP strip thickness (mm)
w_f = FRP strip width (mm)

$$f_{fe} = \varepsilon_{fe} \times E_f \quad (\text{MPa}) \qquad 3$$

where
ε_{fe} = effective strain in FRP strip given by Eq. (4)
E_f = modulus of elasticity of FRP strip (MPa)

$$\varepsilon_{fe} = k_v \times \varepsilon_{fu} \leq 0.004 \qquad 4$$

where
ε_{fu} = rupture strain of FRP strip given by Eq. (5)
k_v = bond dependent coefficient given by Eq. (6)

$$\varepsilon_{fu} = \frac{f_{fu}}{E_f} \qquad 5$$

where
f_{fu} = ultimate tensile strength of FRP strip (MPa)

$$k_v = \frac{K_1 K_2 L_e}{11900\varepsilon_{fu}} \qquad 6$$

where
K_1 = modified concrete factor given by Eq. (7)
K_2 = modified FRP scheme factor given by Eq. (8)
L_e = active bond length of FRP strip given by Eq. (9)

$$K_1 = \left(\frac{f'_c}{27}\right)^{\frac{2}{3}} \qquad 7$$

$$K_2 = \frac{d_{fv} - 2L_e}{d_{fv}} \quad \text{for two sides bonded} \qquad 8\text{-a}$$

$$K_2 = \frac{d_{fv} - L_e}{d_{fv}} \quad \text{for U-wrapped bonded} \qquad 8\text{-b}$$

$$L_e = \frac{23300}{(n_f \times t_f \times E_f)^{0.58}} \quad (\text{mm}) \qquad 9$$

where
n_f = modular ratio of elasticity given by Eq. (10)

$$n_f = \frac{E_f}{E_c} \quad (10)$$

where
E_c = modulus of elasticity of concrete given by Eq. (11)

$$E_c = 4700\sqrt{f_c'} \quad \text{(MPa)} \quad (11)$$

Eq. (1) is applied to reference deep beam DB1 to compute the percentage increase in ultimate load for both U-wrapped and inclined strengthening schemes. A comparison between the experimental and the analytical results is listed in **Table 4**. From this table it can be noted that good agreement between the experimental and the theoretical results is obtained by using the ACI 440-Code provisions. Also, this table reveals that for both strengthening schemes having the same orthogonal spacing center to center between CFRP strips, the experimental and analytical results showed a convergence in the ultimate load results. As the U-wrapped strengthening scheme have more number of CFRP strips than the inclined strengthening scheme, so that it may be concluded that using inclined strips is more economic than using U-wrapped strips.

5. CONCLUSIONS

1. Based on experimental results it is found that strengthening deep beams by two schemes of strengthening using CFRP (vertical U-wrapped scheme and inclined scheme oriented by 45^o), the mid-span deflection was decreased and both first cracking load and ultimate load capacities were increased compare to the reference deep beam.
2. For strengthening beams having the same spacing between strips, the enhancement occurred using vertical U- wrapped scheme was somewhat better than using inclined scheme but it needs to use more numbers of CFRP strips.
3. When using U-wrapped CFRP strengthening scheme, the percentages increase in first cracking loads were (50.0%, 46.0% and 20.5%) for deep beams having center to center spacing between strips of (100 mm, 125 mm and 150 mm) respectively compared to reference beam without strengthening. While when using inclined CFRP strengthening scheme, the percentages increases in first cracking loads were (36.5%, 18.0% and 12.5%) for deep beams having the same spacing above compared to reference beam.
4. The percentages increase in ultimate loads were (14.6%, 13.3% and 12.2%) and (12.5%, 10.4% and 8.6%) for U-wrapped strengthening scheme and inclined strengthening scheme respectively compared to reference beam without strengthening. These results were obtained for center to center spacing between strips of (100 mm, 125 mm and 150 mm) respectively.
5. Under a load level representing the ultimate load of reference deep beam DB1, the percentages decrease in deflections were 24.76%, 19.05% and 13.33% for beams strengthened with U-wrapped strips spaced at 100, 125 and 150 mm respectively. While, the percentages decrease in deflections were 20.00%, 12.38% and 7.62% for beams strengthened with inclined strips having the same spacing above compared to reference deep beam.
6. Based on theoretical analysis according to the ACI 440 Code provisions, good agreement was obtained between the experimental and theoretical results.
7. From the experimental and analytical results it is found for the same center to center spacing between strips there is a convergence in ultimate results for both styles of strengthening. Also, as

U-scheme of strengthening needs more amount of CFRP strips than inclined scheme of strengthening. Hence, the use of inclined scheme of strengthening may be more economic than using the vertical U-scheme of strengthening.

REFERENCES

- Abdel-Jaber, M. S., Walker, P. R., and Hutchinson, A. R., 2003, *Shear Strengthening of Reinforced Concrete Beams Using Different Configurations of Externally Bonded Carbon Fiber Reinforced Plates*, Materials and Structural Journal, Vol. 36, No. 5, June, PP. 291-301.
- ACI Committee 318, 2014, *Building Code Requirements for Reinforced Concrete and Commentary (ACI 318-14 and ACI 318R-14)*, American Concrete Institute, Detroit, USA.
- ACI Committee 440.2R, 2008, *Guide for the Design and Construction of Externally Bonded FRP Systems for Strengthening Concrete Structures*, American Concrete Institute, Detroit, USA.
- Alkhrdaji, T., Nanni, A., and Mayo, R., 2000, *Upgrading Missouri Transportation Infrastructure: Solid Reinforced-Concrete Decks Strengthened with Fiber- Reinforced Polymer Systems*, Transportation Research Record No. 1740, National Academy Press, Washington, D.C., USA, PP. 157-163.
- ASTM Designation A615/A615M-01b, 2001, *Standard Specifications for Deformed and Plain Billet-Steel Bars for Concrete Reinforcement*, Annual Book of ASTM Standards, American Society for Testing and Materials, Philadelphia, Pennsylvania, vol. 1.04.
- Barros, J. A. O., and Dias, S. J. E., 2003, *Shear strengthening of reinforced concrete beams with laminate strips of CFRP*, Proceedings of the International Conference Composites in Constructions, CCC2003, Cosenza, Italy, Vol. 16, No. 19, September, PP. 289-294.
- Feng, L. J., and Yuan, L. J., 2008, *Properties comparison of four FRP materials and the applications of them in reinforcement of civil engineering*, Shanxi Architecture, Vol. 4. PP. 172-173.
- Iraqi Specification No. 5, 1984, *Portland Cement*, Baghdad.
- Iraqi Specification No. 45, 1984, *Natural Sources for Gravel That is Used in Concrete and Construction*, Baghdad.
- Li, Y., Lin, C., and Sung, Y., 2002, *Compressive Behavior of Concrete Confined by Various Types of FRP Composite Jackets*, Mechanics of Materials, Vol. 35, No. 3-6, PP. 603-619.
- Liu, X. H., Wang, X. K., and Wang, X. Z., 2012, *Study on the Shear Behavior of RC deep beam strengthening by FRP*, Civil Engineering & Architecture College, Liaoning University of Technology, Jinzhou, China, 2nd International Conference on Electronic & Mechanical Engineering and Information Technology, PP. 445-448.
- Ludovico, M. D., 2002, *Experimental Behavior of Pre-Stressed Concrete Beams Strengthened with FRP*, Center for Infrastructure Engineering Studies, University of Missouri- Rolla, PP. 197.
- Mitali, R. P., and Gajjar, R. K., 2012, *Shear Strengthening of RC Beams using CFRP*, International Journal of Advanced Engineering Technology, Vol. 3, No. 1, PP. 338-342.
- Neale, K. W., 2000, *FRPs for Structural Rehabilitation: A Survey of Recent Progress*, Progress in Structural Engineering and Materials, Vol. 2, PP. 133-138.

- Shanafel, G.O., and Horn W. B., 1985, *Guidelines for Evaluation and Repair of Pre-stressed Concrete Bridge Members*, NCHRP Report No. 280, Transportation Research Board, Washington D.C., USA.

NOMENCLATURE

A_{fv} area of FRP strip within spacing (s_f)
CFRP carbon fiber reinforced polymer
d_{fv} effective depth of FRP strip
E_c modulus of elasticity of concrete
E_f modulus of elasticity of FRP strip
f_c' cylindrical compressive strength of concrete
f_{fe} effective stress in FRP strip
f_{fu} ultimate tensile strength of FRP strip
f_y yield stress of steel reinforcement
h overall depth of the section
K_1 modified concrete factor
K_2 modified FRP scheme factor
k_v bond dependent coefficient
l span center to center of beam
L_e active bond length of FRP strip
n_f modular ratio of elasticity
RC reinforced concrete
s_f spacing center to center between strips in the horizontal direction
t_f thickness of FRP strip
V_f additional shear force carried by FRP strips
W_f width of FRP strip
ε_{fe} effective strain in FRP strip
ε_{fu} rupture strain of FRP strip
α angle of FRP orientation about x-axis

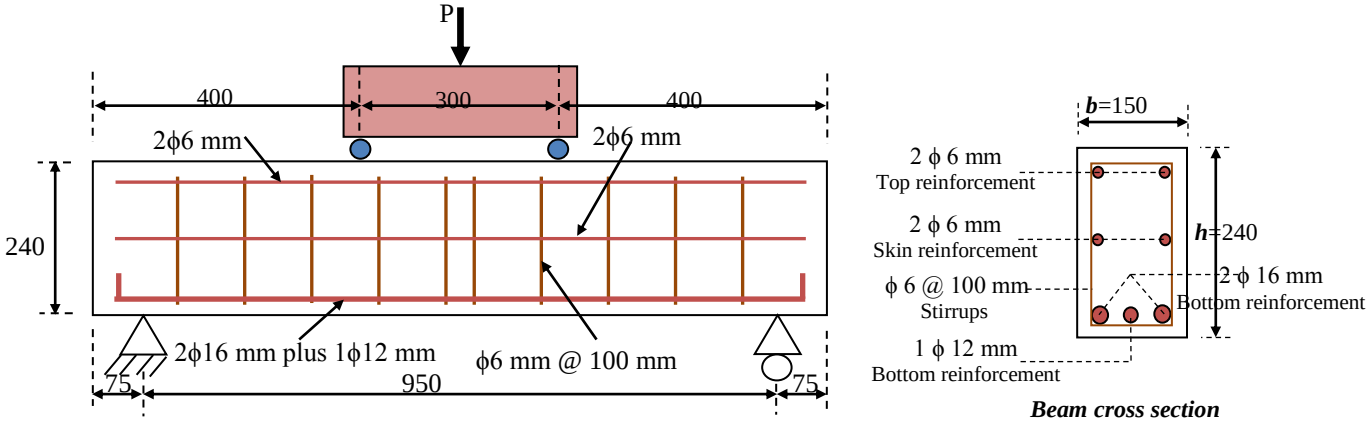

Figure 1. Layout of a typical tested deep beam (all dimensions are in mm).

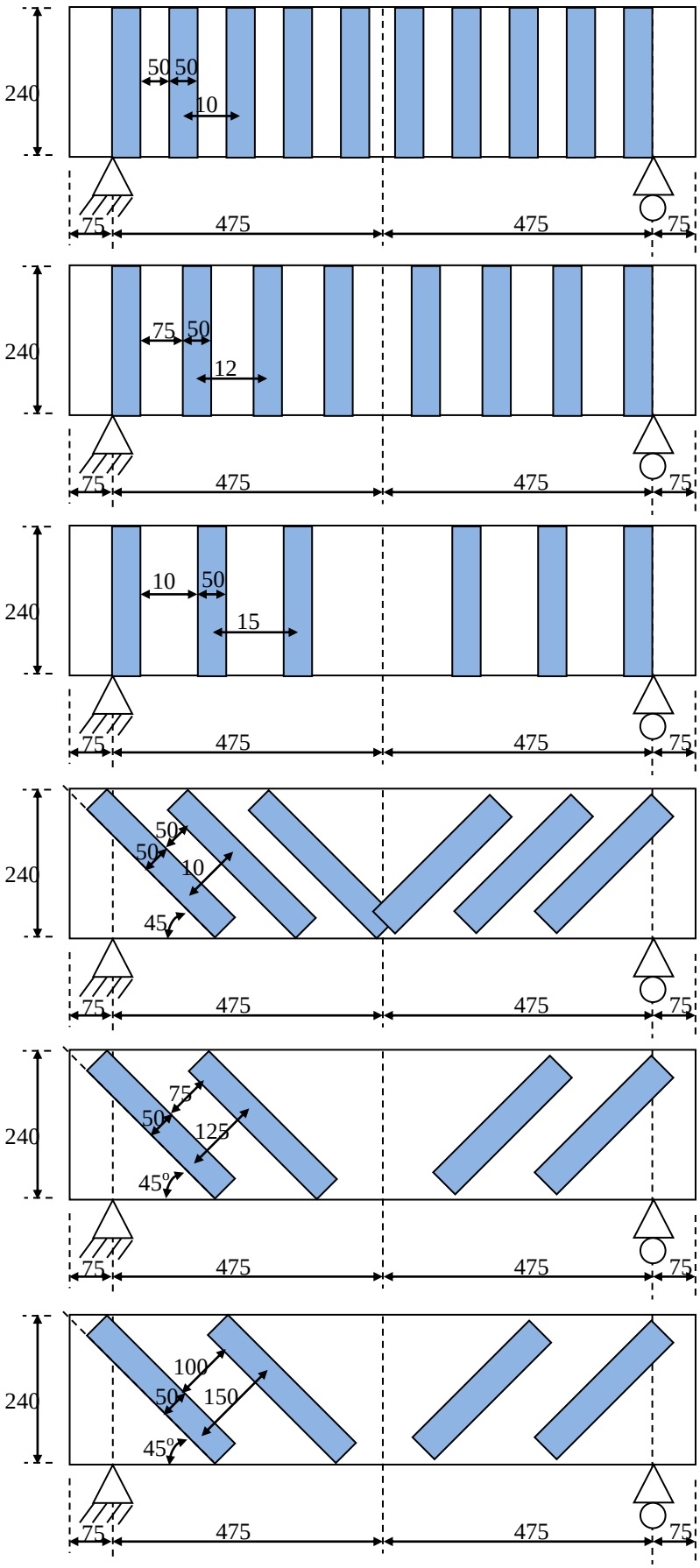

Figure 2. Strengthening schemes and tested beams designations (all dimensions are in mm).

Figure 3. Mold fabrication and reinforcement cage of a typical tested beam.

Figure 4. Roughing concrete surface and applying epoxy at CFRP strips location of a typical tested beam.

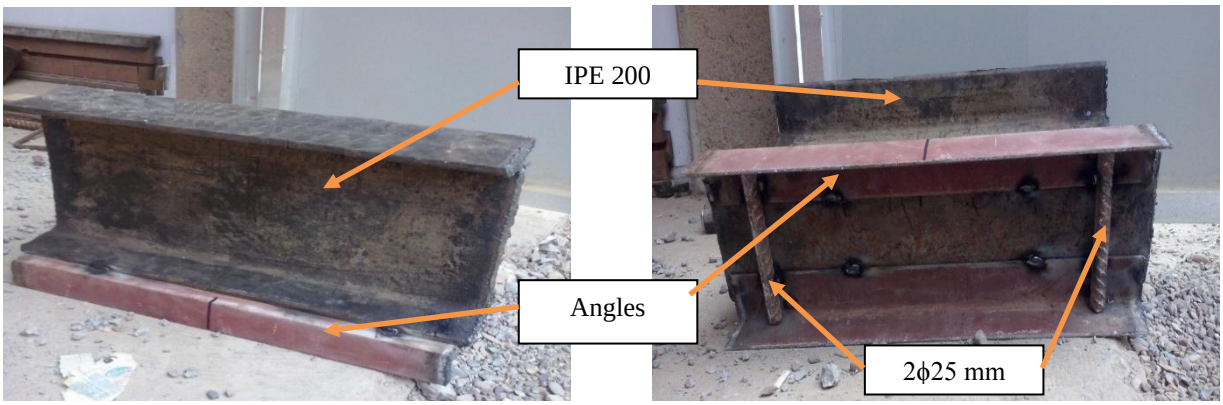

Figure 5. Fabricated system used for applying the load on tested beams.

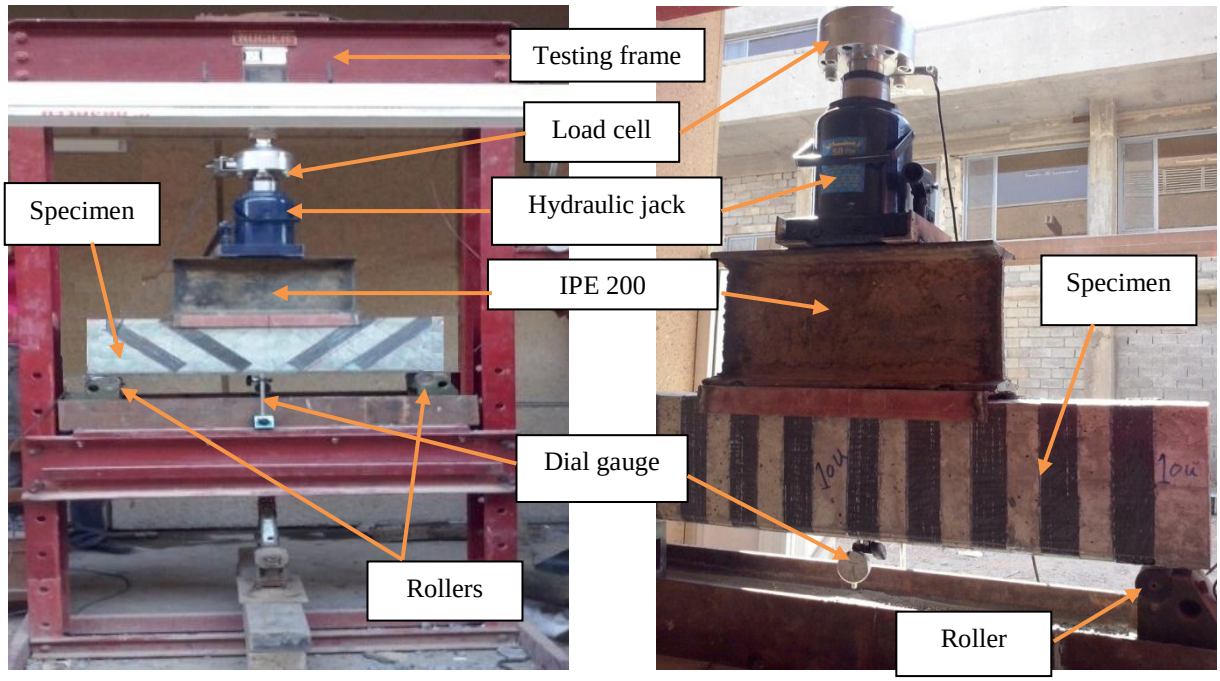

Figure 6. Setup of typical tested beams.

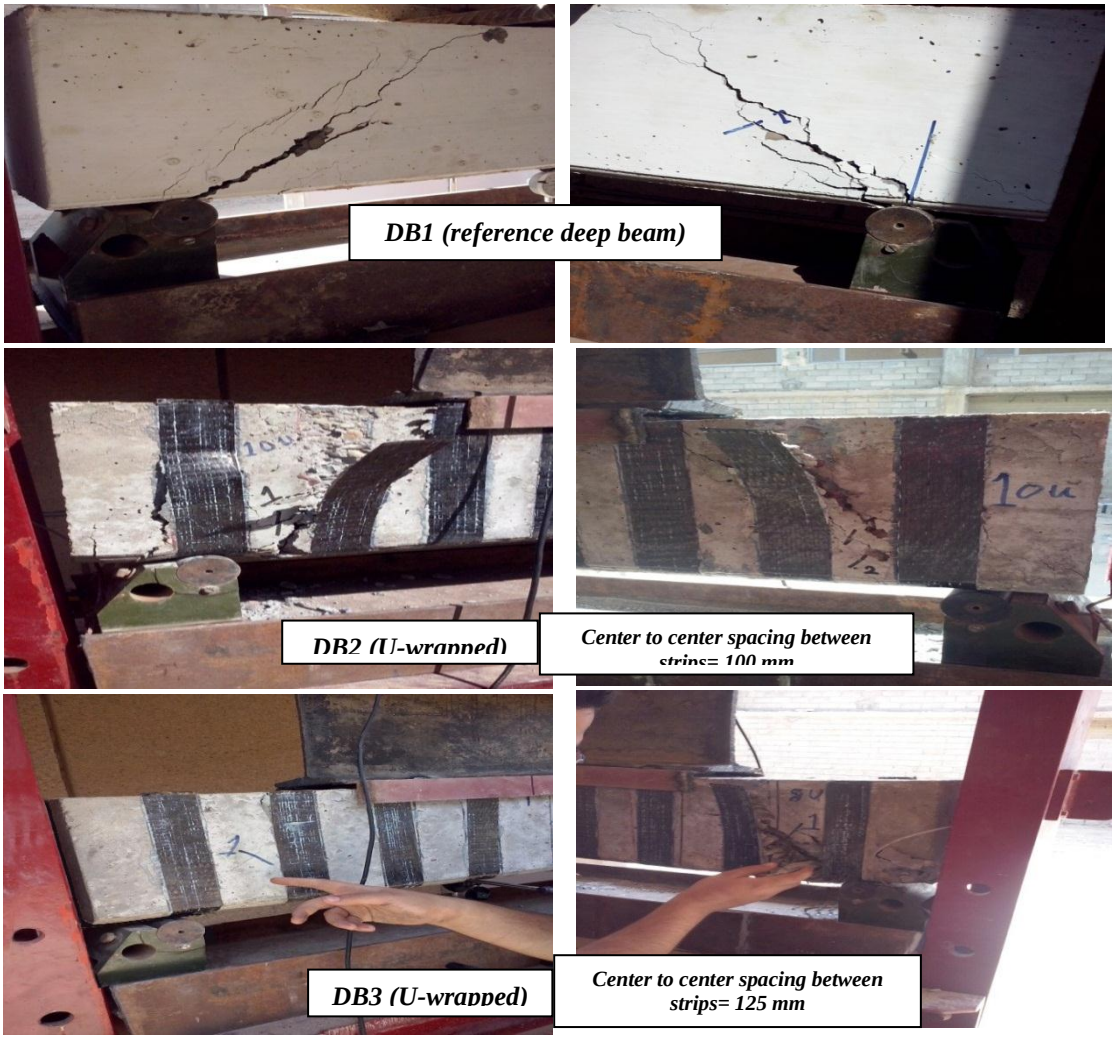

Figure 7. Tested beams after failure.

Figure 7. Continue.

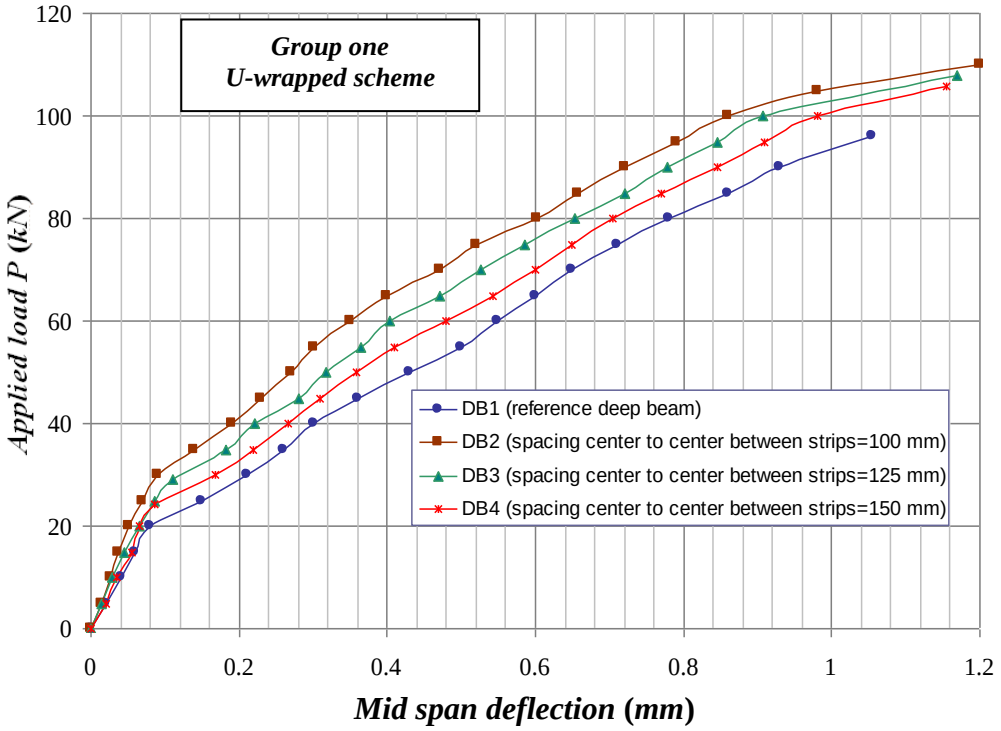

Figure 8. Load-mid span deflection for beams of Group one.

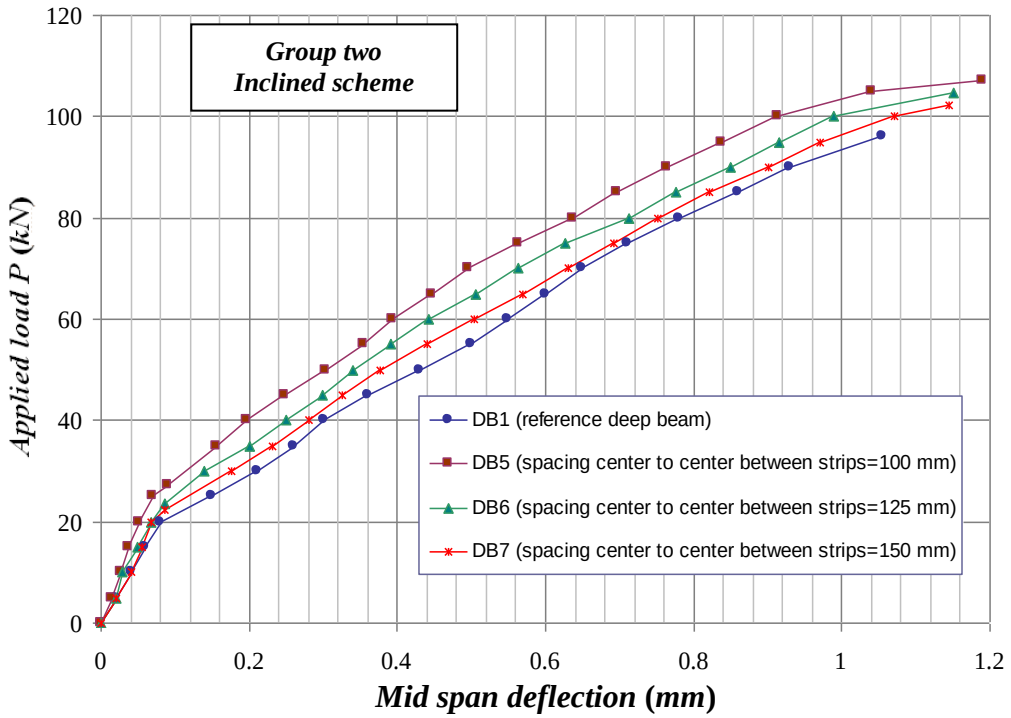

Figure 9. Load-mid span deflection for beams of Group two.

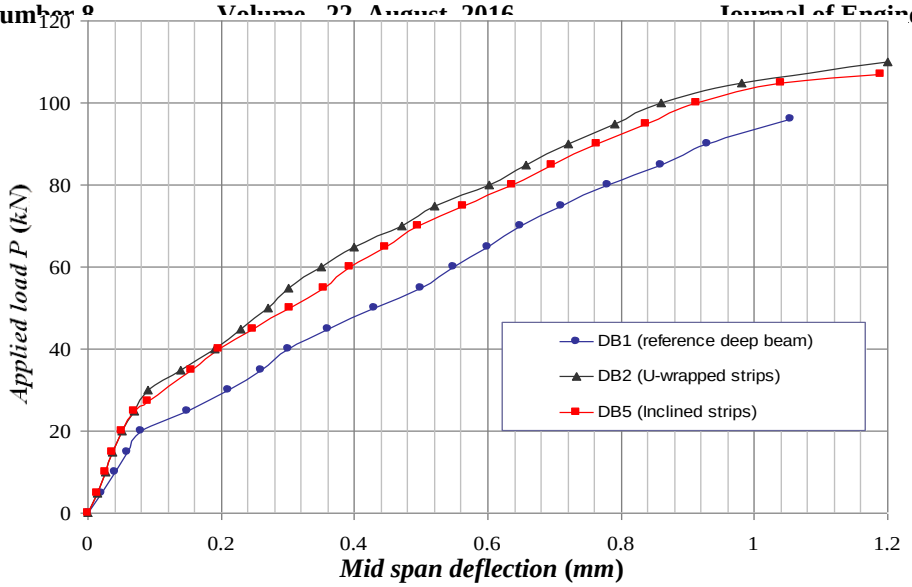

Figure 10. Load-mid span deflection for beams with center to center spacing between strips= 100 mm.

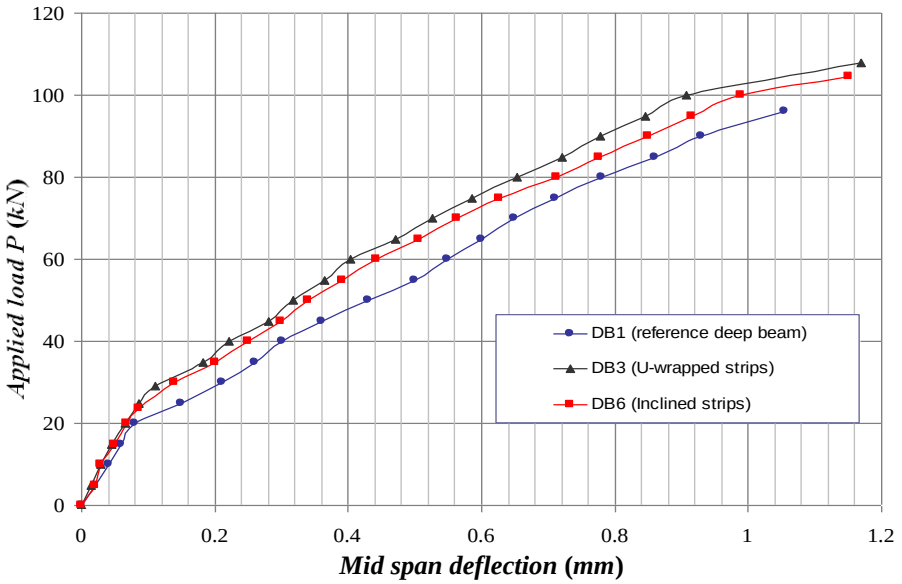

Figure 11. Load-mid span deflection for beams with center to center spacing between strips= 125 mm.

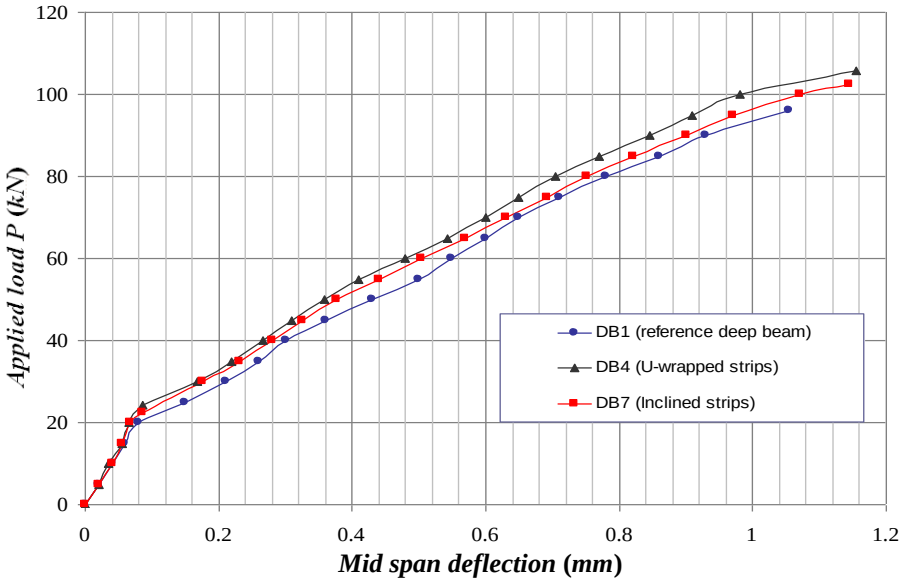

Figure 12. Load-mid span deflection for beams with center to center spacing between strips= 100 mm.

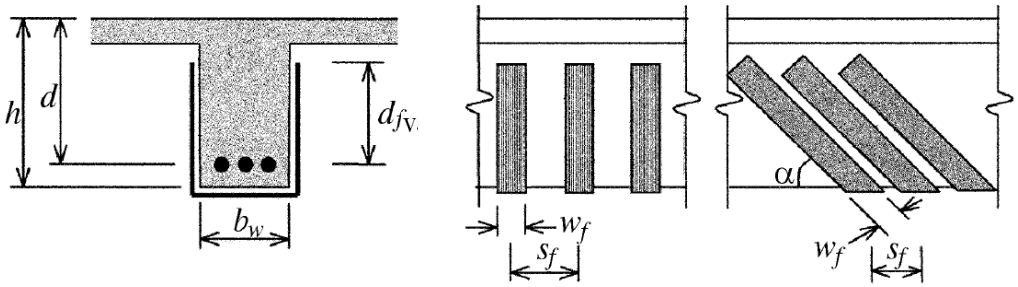

Figure 13. Illustration of the dimensional variables used for calculating the additional shear strength provided by FRP strips, **ACI 440 Code, 2008**.

Table 1. Tested beams designation and strengthening schemes.

Group No.	***Beam designation***	***Beam type***	***CFRP Strengthening scheme***	***Center to center spacing between CFRP Strips (mm)***
-	DB1	Reference	-	-
Group one	DB2	Strengthened	U- wrapped (10 strips)	100
	DB3	Strengthened	U- wrapped (8 strips)	125
	DB4	Strengthened	U- wrapped (6 strips)	150
Group two	DB5	Strengthened	Inclined with 45˚(6 strips)	100 (orthogonal inclined)
	DB6	Strengthened	Inclined with 45˚(4 strips)	125 (orthogonal inclined)
	DB7	Strengthened	Inclined with 45˚(4 strips)	150 (orthogonal inclined)

Table 2. First cracking and ultimate loads of tested deep beams.

Beam designation		***Center to center spacing between Strips (mm)***	***First cracking load P_{cr} (kN)***	***% Increase in first cracking load***	***Ultimate load P_u (kN)***	***% Increase in ultimate load***
Reference	DB1	-	20.0	-	96.0	-
Group one (U-wrapped strips)	DB2	100	30.0	50.0	110.0	14.6
	DB3	125	29.2	46.0	107.8	13.3
	DB4	150	24.1	20.5	105.7	12.2
Group two (Inclined strips)	DB5	100 (orthogonal inclined)	27.3	36.5	107.1	12.5
	DB6	125 (orthogonal inclined)	23.6	18.0	104.6	10.4
	DB7	150 (orthogonal inclined)	22.5	12.5	102.3	8.6

$$\% \ Increase = \frac{P(strengthened) - P(reference)}{P(reference)} \ x\ 100$$

Table 3. Mid span deflection values at ultimate load level of tested deep beams.

Beam designation		*Center to center spacing between Strips (mm)*	*Mid-span* deflection (mm)*	*% Decrease in mid-span deflection*
Reference	DB1	-	1.05	-
Group one (U-wrapped strips)	DB2	100	0.79	24.76
	DB3	125	0.85	19.05
	DB4	150	0.91	13.33
Group two (Inclined strips)	DB5	100 (orthogonal inclined)	0.84	20.00
	DB6	125 (orthogonal inclined)	0.92	12.38
	DB7	150 (orthogonal inclined)	0.97	7.62

***** *Corresponding to a load level of (96 kN) which represents the ultimate load of the reference deep beam (DB1)*

% Decrease = $\frac{deflection(strengthened)-deflection(reference)}{deflection(reference)}$ *x 100*

Table 4. Experimental and analytical percentages increase in ultimate load.

Beam designation		*s^* (mm)*	*s_f^{**} (mm)*	*V_f^{***} (kN)*	*% Increase in† ultimate load (analytically)*	*Experimental ultimate load P_u (kN)*	*% Increase in†† ultimate load (experimentally)*
Reference	DB1	-	-	-	-	96.0	-
Group one (U-wrapped strips)	DB2	100	100	5.97	12.44	110.0	14.6
	DB3	125	125	4.78	9.96	107.8	13.3
	DB4	150	150	3.98	8.29	105.7	12.2
Group two (Inclined strips)	DB5	100	141	5.56	11.58	107.1	12.5
	DB6	125	177	4.43	9.23	104.6	10.4
	DB7	150	212	3.70	7.71	102.3	8.6

***** *Orthogonal spacing center to center between strips*

****** *Horizontal spacing center to center between strips*

******* *By applying Eq. (1)*

† *% Increase in ultimate load (analytically)* = $\frac{2\times V_f}{P_{u(reference\ deep\ beam)}}$ *x 100*

†† *% Increase in ultimate load (experimentally)* = $\frac{Pu(strengthened)-Pu(reference)}{Pu(reference)}$ *x 100*

Performance Evaluation of the Investment Projects during the Implementation Phase (Najaf province as a case study)

Kadhim Raheem Erzaij
Asst.prof
Baghdad University-College of Engineering
Baghdad email: Kadhum69@yahoo.com

Dhefaf Madlool Aljanabei
Baghdad University-College of Engineering
email:dhefafaljanaby@yahoo.com

ABSTRACT

The construction project is a very complicated work by its nature and requires specialized knowledge to lead it to success. The construction project is complicated socially, technically and economically in its planning, management and implementation aspects due to the fact that it has many variables and multiple stakeholders in addition to being affected by the surrounding environment. Successful projects depend on three fundamental points which are cost-time, performance and specifications. The project stakeholder's objective to achieve best specifications and the cost-time frame stipulated in the contract.

The question is, was the optimum implementation accomplished? The provision for the success of the project is how are the daily activities managed by the three stakeholders of the project (contractor, owner, and consultant) and their technical and practical capability to attain the balance of the project fundamental points (cost, time and quality) taking into account the project objectives that were set by the owner. Despite the way, logical framework management and project's major steps there is a group of elements which become major measures to determine the success or failure of the project, the research interested in these elements by a thorough study of references related to the success of a constructional project. To reinforce the theoretical study a field assessment of the housing project; this led to the recognition of the major elements that caused breaches of the evaluation criteria.

The closed questionnaire and the regular forms based on the data and information collected through the theoretical review and the closed questionnaire to conclude and examine some concepts related by assessing the quality of building materials used in residential investment projects through the stages (planning - design-implementation)

Through the research a lot of deductions were made, the most important is that there cannot be an evaluation system without having a holistic monitoring system in Iraq. It was also deduced that the most important source of project failure is not allocating enough time to the planning phase. Some other recommendations and suggestions for future studies were made also.

Key words: evaluation**,** investment**,** Implementation**,** performance …etc.

تقييم الاداء المشاريع الاستثمارية خلال مرحلة التنفيذ (محافظة النجف حالة دراسية)

كاظم رحيم رزيج
استاذ مساعد
جامعة بغداد - كلية الهندسة
Baghdad email: Kadhum69@yahoo.com

ضفاف مدلول الجنابي
باحثة
جامعة بغداد - كلية الهندسة
email:dhefafaljanaby@yahoo.com

الخلاصة

إن المشروع الإنشائي بطبيعته هو عمل معقّد جداً، ويتطلب معرفة متخصصة لتقوده نحو النجاح. فالمشروع الإنشائي معقّد إجتماعياً وتقنياً وإقتصادياً في التخطيط والإدارة والتنفيذ وذلك لكثرة المتغيرات وتعدد الأطراف فضلا عن تأثره بشكل مباشر بالبيئة المحيطة به.تعتمد المشاريع الناجحة على ثلاثة مرتكزات أساسية هي الكلفة والوقت وتحقيق المواصفات. تهدف أطراف المشروع الى تحقيق المواصفات والأداء الوظيفي الأفضل ضمن الوقت والكلفة المتعاقد عليها ولكن يبقى السؤال القائم، هل تم

التوصل الى الحالة المثالية لتنفيذ المشروع ؟ إن نجاح المشروع يبقى رهينة بالعمل اليومي ضمن نشاطات المشروع وبكيفية إدارة هذه النشاطات من الأطراف الثلاثة المشتركة (المقاول، صاحب العمل، الإستشاري) ومقدرتهم العلمية والعملية في الوصول الى توازن مرتكزاته الثلاثة (الكلفة والوقت والنوعية)، مع الأخذ بنظر الإعتبار الأهداف الرئيسة التي وضعها صاحب العمل للمشروع. بغض النظر عن الطريقة أو إطار العمل وإدارته وبغض النظر عن عدد الخطوات الرئيسية ، إن نجاح اي مشروع أو فشله يعتمد على مجموعة مشتركة من العوامل التي تمثل معايير رئيسية لذا إهتم البحث بدراسة هذه المعايير وذلك من خلال دراسة شاملة للأدبيات ذات الصلة بمعايير نجاح المشروع الإنشائي. ولغرض دعم الدراسة النظرية تم إجراء دراسة ميدانيه تمثلت من خلال مسح ميداني لـ مشروع سكني والتعرف على اهم العوامل التي تسببت في حدوث التجاوزات على أهداف التقييم، القيام باستبيان مغلق وتحليل ثم تصميم استمارة الاستبيان المغلق النظامية بالاعتماد على ما جمع من بيانات ومعلومات من خلال الدارسة النظرية ،للتعرف والتحقق من بعض الامور المتعلقة بواقع تقييم نوعية مواد البناء المستخدمة في المشاريع الاستثمارية السكنية خلال مراحل (التخطيط - التصميم-التنفيذ). من خلال البحث تم التوصل الى العديد من الإستنتاجات أهمها: إنه لايمكن إن يكون هنالك نظام للتقييم دون وجود نظام متابعة متكامل. كما واستنتج البحث الى إن أهم مصادر فشل المشروع هو عدم منح العملية التخطيطية الوقت الكافي ، فضلا عن مجموعة من التوصيات والمقترحات لدراسات وبحوث مستقبلية.

1. INTRODUCTION

The Iraqi economy is one of the economies of the developing countries which depend on one resource for income (oil). After the large economic transformations produced by going towards the market economy and not depending on one origin of fund, the variety of the origins of the income, such as investment was directed to.

Any economic project starts with an idea designed to add new value to the national capital by directing part of the financial and human resources to create a unit of new economic able to create other values in order to achieve the interests of the owner of the project on the one hand and on the other hand increase the national income and that which drives the economy national forward in terms of the interaction of the project with its own environment, public and activation of all economic sectors associated with the project and the availability of the basic principles of investment which should be available in order to polarize the investors through issuing law of investment No.13 of the year 2006 for the sake of developing the process of economic and social development to bring the modern scientific experiences, develop the staff, find work opportunities for the Iraqis through encouraging the process of investment and widening its base and supporting the process of erecting the investment projects of the economic and development profits .

2. EVALUATION AND INVESTMENT

2.1 Definition of Evaluation

Evaluation, as a concept, can be defined as "a set of processes conducted in order to compare between the results obtained with the preset objectives of the project, so that future decisions can improve the remaining part of the project or other future projects. No doubt, this requires that project objectives should be clearly determined during planning stage. A comparison should be made between the results of the work activities and these objectives using scientific and practical measures "One of the main objectives of project evaluation is to compare between results and preset objectives. This sheds the light on a major problem in project assessment that is project objectives should be well-understood and specified as they were set during the planning stage. Project objectives should satisfy the following requirements**, RPS &INAC, R., 2000.**

2.2 The Role of Evaluation in a Project Life Cycle

The process of evaluation consists of consecutive steps for a certain project as shown below**, Westland, 2006.**

1. The project planner should have good knowledge of the project objectives which have to be measurable quantatively, by time and qualitatively.
2. Upon defining the objectives a comprehensive plan should be made for the project. Before adopting, the plan should be evaluated through the feasibility studies of the project.

3. During the project implementation, the work should be supervised, followed up and assessed in order to make the required changes timely.
4. After the completion of project, the results are evaluated against objectives; the figure below shows the role of assessment in project life cycle.

2.3 Relation between Performance Evaluation and Planning

Planning, as defined by (Weick, 1995) is a vision of the desired future and the means required to achieve it**, Weick,1995.**

Planning also is defined by (Simon and Schuster, 1994) as a set of formal actions aiming to achieve clear results in the form of an integrated system for decisions**, Simon, and Schuster, 1994.**

2.4 Relation between Performance Evaluation and Monitoring

Monitoring involves making sure whether everything is carried out according to the preset plan, regulations and principles. Monitoring aims at highlighting the weakness points and errors to deal with them and to make sure they will not occur again. The monitoring is applicable to many things including laborers and operations**.**

Dervavux and Coulaud (1999) considered that the purpose behind supervision is to ensure that the decisions taken by the top management are followed effectively and efficiently in order to improve the company performance**, Westal , and Joy Frechtling, 2002.**

Elements of monitoring include quantity, methods, cost, and time. Process of monitoring involves the following steps**, Simon, and Schuster, 1994.**

1. Defining of supervision criteria and measures.
2. Measuring performance and comparing it with criteria.
3. Correction of any deviation from criteria and plans.

2.5 Relation between follow up and Evaluation

Assessment during implementation is (the comparison between the current situation and the planned path for project). Also, evaluation is the final resultant of what follow up system has reached. Following up process can be defined as a function that is carried out by the administration of project in order to validate that work proceeds according to the preset objectives efficiently and sufficiently and within the time schedule**, O'Reilly, 2005.** It is also has been defined as "the activity carried out by the management to follow up the implementation policy previously set up and evaluating it and finally to correct any weakness it might undergoes so that the desired objectives are achieved".

Based on the above, follow up generates the performance criteria which will be used to measure the progress towards reaching the objectives. That is through the determination whether the resources of the project are used in a proper way that leads towards achieving the objectives**, O'Reilly, 2005.**

2.6 Reasons of Construction Project washout

Many studies have been performed to tackle such question in order to answer it. These studies have reached too many conclusions which focus on two reasons, project management and human factors. In general, most of the studies have classified the causes of failure of construction projects into three groups:

1. There is no realistic estimation of cost and duration of the project as well as wrong distribution of resources because of the weak planning of the project**, Vorster, and Michael, 2005.**
2. Project objectives are not clear neither realistic? Moreover, there is no agreement on project delivery.
3. The project is not well studied. This includes weakness in the implementation support, lack of expertise as well as the lack of pursuance by project owner.

4. Voster, Michael C (2005) defined the reasons of project failure in addition to the percentages of their effects on the project failure as shown in Table (1).

2.7 Success Factors of a Construction Project

The success factors of any construction project are: time, cost, and quality which together represent the corners of the project management triangle which are shown in **Fig.1, Smith, 2002.**

2.8. INVESTMENT

Foreign investment is a term that is usually used when a normal person or juristic person utilizes its expertise, efforts or money to perform economic project either alone or jointly with a natural or juristic person, with local or foreign investor, or jointly with government or its citizens. The host country has the right to direct investors towards certain economic activities according to its needs. In Iraq, this direction comes through the Modified Investment Law No (13) of 2006**, Iraqi Law, 2006,** which deal with several sectors? The sectors included in the mentioned law are; housing, tourism, industry, health, education, agriculture, and recreational sectors. This happens together with other relevant legislations such as Article (15) of tax law of 2006 related to exemption from tax which designed to attract and encourage foreign capitals to invest in several diverse fields.

Investment can also be defined in another way as (the transfer of foreign capital, knowledge and advanced technical and administrative technology so as to generate economic, social, and administrative development that can lead to develop and revive the host country through the new companies and in participation with national capital**.**

The research will cover investment and development experienced in Egypt and Iraq.

2.9 Investment and its Objectives in Egyptian Law

Egypt had a law No. 65 of 1977 "Arab Investment Law" but was not active because of the socialist orientation at that period and the political system instability**, The Investment Egyptian Law, 1977.** The latest investment law which is still working in Egypt was PRESIDENTIAL. M. D, No. 1144 of 2002**, PRESIDENTIAL. M. D, 2002.**

In an attempt to encourage Arab and foreign investment operating in Egypt, the law offered guarantees to the investor against changes in the country social system and the changes in the economic policy. The investor irrespective of his nationality or place of residence enjoyed these guarantees.

These guarantees were as follows:

1. The project real estate cannot be expropriated either wholly or partially unless for public interest and according to the law. Compensation should be fair and according to market value.
2. Companies that invest foreign or Arab monies were considered private companies even if the Egyptian money used in the investment belongs to the public sector, that is, the newly established companies were subjected to legislations on private companies, in other words, the law on private properties even if the Egyptian money used in the investment belongs to the public sector, thus facilitating the measures and providing flexibility to ensure project success.
3. Among the guarantee was the project invested money cannot be sequestrated, frozen, confiscated or placed under receivership without court order. In other words, these measures were limited to extrajudicial punishment. Any court order was valid.

In addition, the Egyptian law on investment introduces a number of exemptions for the benefit of investors as stipulated in Article (20) of Law No 230 0f 1989 as shown below:

1. Investment projects enjoyed exemptions from the Company Establishment Law.
2. The number of board members was not limited, therefore according to this exemption projects were not bounded by a certain number of members of the board.
3. Exemption from the provision requiring the participation of employees in project management as stated by Article 82 of the Company Law

4. Exemption from the provision requiring a majority of Egyptians in management board as stated by Article 93 of the Company Law.

Additional exemptions that mentioned herein were only given as examples.

Among the factors which encouraged investors to invest in Egypt which were contained in Law 1144 of 2002 on investment were a number of tax exemptions granted to investors as shown below.

1. 15-year tax exemptions for housing projects. The exemption can be extended for another five years on the recommendation of Investment Board.
2. 10-year tax exemptions for project set up in new areas and new urban communities. This exemption can be extended for another two years on the recommendation of Investment Board.
3. Tax exemptions for already existing projects in order to increase their productivity which is covered by tax exemptions if the development and expansion were achieved.
4. 3-year tax exemptions for already existing projects in order to correct financial position according to the terms to be laid down by Investment Board.
5. Income tax exemption was made to encourage investment in corporations.
6. Tax exemption for land reclamation projects and for some project with special importance to Egyptian economy.

A brief exposition of the Egyptian legislations as mentioned above aims to attract Arab and foreign investment to Egypt. The investment was encouraged through several impetuses including guarantees and tax exemptions. All objectives and the legislator aims were analyzed and concluded from issuing Law 1144 of 2002 and the manner to realize them as follows**,**

PRESIDENTIAL. M. D, 2002.

The Egyptian investor was granted the same privileges as those granted to Arab and foreign investors.

1. The investor would have to deal with only one body through the newly established Board of Investment which was assigned to deal with all matters related to newly established or existing projects
2. Investment in the field of priority are encouraged and upheld.
3. The Egyptian legislator aimed to reduce unemployment and encourage investment which recruits a large number of employees
4. The Egyptian legislator aims to advanced management, technical, and technological systems.
5. Freeing the Egyptian economy from dependence of the public sector and directing towards privatization so that foreign investors would have confidence in Egyptian investors and thus they cooperate.
6. The Egyptian legislator aimed to reduce the deficit in the balance of payment**, Law No. 8 of 1997.**

These targets are reached from analyzing Law 1144 of 2002 which will be helpful to countries which intend to invest in developing countries.

2.10 Investment and its Objectives in Iraqi Law

The Iraqi Investment Law No. 13 was issued in 2006.The Iraqi Investment Law explained the advantages and guarantees for each investor and facilities for all investment projects in all sectors as follow:

The investor irrespective of his/her nationality shall enjoy all privileges, facilitations and guarantees and will be subject to the obligations stated in this law. The Iraqi and foreign investor shall have the right for, the purposes of housing projects, the use of the land for a sum to be determined between him and the land owner without land speculation according to conditions set forth by the National Commission for Investment and the approval of the Council of ministers.

The Commission will facilitate the allocation of the required lands for the housing projects. The housing units shall be allocated for ownership by the Iraqis after the completion of the project.
The factors which encouraged investors to invest in Iraq are as follows:

2.10.1 The project that has obtained an investment license from the Commission shall enjoy exemption from taxes and fees for a period of (10) ten years as of the date of commencing commercial operations in accordance with the areas of development defined by the Council of Ministers at the suggestion of the national commission for Investment based on the degree of economic development and the nature of the investment project.

2.10.2 The Council of Ministers shall have the right to propose draft laws to extend or grant exemptions in addition to the exemptions stipulated in paragraph (First) of this Article, or provide incentives, guarantees or other benefits to any project or sector or region and for the years and percentages it deems appropriate in accordance with the nature of the activity, its geographical location and its contribution to manpower employment and its effect on driving the economic development, and for considerations of national interest.

2.10.3 The National Commission for Investment has the right to increase the years of tax and fees exemption in a way directly proportional to the increase in the Iraqi Investor share in the project to reach fifteen years if the Iraqi Investor share in the project was more than 50%**, The Investment Iraqi law, 2006.**

2.11 Methods of Comparison between Projects

2.11.1 Economic Methods

The economic methods used in comparison vary depending upon the target of project which in turn varies with whether the project is public or private. With respect to public projects, comparison depends on some factors among which are**:**

2.11.1.1 The importance of the project in line with the national economy

Projects can be differentiated according to project importance to the national economy:

1. The importance of the project in economic development:
The importance of the project and its relation with economic development vary with the project nature, target and size. Industrial projects are typically more effective on national development than agricultural ones. Industrial projects in turn vary in importance and effect on national development. Heavy industries are more important than food or textile industries although all industries play a role in the increase in national income, productivity and employment

2. The importance of the project in national security:
Sometimes, economic and technical factors as well as the principle of profit and loss are overlooked in comparison in favor to security factor regardless the cost. For example a priority is usually given to an agricultural project for wheat production because wheat is considered as a strategic product and hence represents an important element in the nation security.

3. Project importance during use:
If creating job opportunities is regarded as one of main goals of development, then the authorities are responsible for planning to create a large number of new jobs through the use of certain quantity of the capital., In other words, it attempts to use the smallest amount of the capital necessary to provide new job opportunity.

2.11.1.2 The importance of the project in terms of balance of payment

Among the problems which must be looked into when comparing public sector projects is the effect on balance of payment through finding out the extent the proposed project depends on local raw materials or imported one. If the state policy is to curb the deficit in balance of payment, priority should be given to projects that depend on local services or to projects that produce imported goods or to projects that produce goods for export so that hard currency is obtained**, Nowak, Maciej, 2005.**

2.11.2 Technical Procedure

Establishing of large and modern projects not only help in developing staff's efficiency and skill but also help in changing traditional values and creates the spirit of investment and interest in setting up projects in the society. Also such projects can support the desire for improving living conditions and discipline at work, resulting in radical changes in pattern and principles of economic development.

2.11.3 Financial Procedure

In addition to comparing project based on economic and technical standards it is vital to carry out financial and audit comparison which involves calculation of cost, revenues, profit and net returns from money spent on the project. This is considered the main restriction on investment especially in private sector.

This research tackles investment projects in Iraq (housing sector) especially housing investment in Najaf Province. The map below shows the master plan of Najaf province.

3. CASE STUDY OF THE INVESTMENT REALITY AND HOUSING INVESTMENT PROJECTS DURING THE IMPLEMENTION

The housing project in Najaf Province executed in the time period from 2010 -2014. Data and information were obtained from Najaf Investment Commission and from Investment Companies which were carrying out the projects. The number of projects whose data were adopted is three housing projects. Below is a description of one sample shown table (2).

This research tackles investment projects in Iraq (housing sector) especially housing investment in Najaf Province.

3.1 Overview of Najaf Province

Najaf is a cultural, religious, commercial and agricultural center with area of 27.845 km^2. Its main cities are**, National Investment Commission, 2013.**

1. Najaf City
2. Kufa City
3. Al Manathera City

According to the Ministry of Planning, the population is between (2006-2020) and is shown in table (3).

3.2 Al- Hassan Investment Housing Projects

It is considered one of the important housing projects. The complex consists of (112) housing units in vertical buildings. Table (4) shows the building details. The project has very high technical specifications compatible with modern housing projects**, Najaf Investment Commission,2014 .**

3.1.1 Project Construction Stages

Al- Hassan Housing Project is service project financed by local and foreign investors as well as payments from prospective buyers because the units were sold out before the start of the project. Payment is paid in installments. The project is located in Al Manathera area in Najaf. It was planned to be completed within 24 months at a cost of (ID 11.647, 554,000) to be paid in two stages. The sums of stages are (ID 6.735, 000,000) and (ID 4.912, 554,000). The idea of the investor to complete the project in two stages is considered good as the investor will be able to reduce the amount he invests to half because at the end of the first stage he will be able to fund the second stage from the repayments from the first stage shown **Fig.2** investment license. The investor should carry out 70% of the housing complex infrastructure. But the project requirements should be prepared in full.

3.1.2 Specifying the Requirements and Preparation of Feasibility Study

3.1.2.1 Project Objective: Housing and real estate are considered as a fundamental sector in the economy all over world. In Iraq housing there is an urgent need for housing.

3.1.2.2 Project Description: Residential quarter and stores.

a. Houses more than (700) people with the necessary facilities.

b. Six shopping centers, a health care center, two primary schools and two secondary schools and health center, a kindergarten, a nursery and swimming pool.

3.1.2.3 Project justification: The Province stands in need of housing units to alleviate the housing problem.

Notes:

1. It does not need foreign experience nor imported raw materials. They are available in the local markets. The working days are 25 per month.
2. The project is to be completed within two years in two consecutive stages.

The project plot was received officially from Najaf Municipality on 05/03/2013 so that work could be completed within the specified time period and cost; after getting the license, the investor faced some problems among which are:

1. The complicated administrative measures in government departments especially in Najaf Municipality which result in delaying the completion of most housing projects by not proving the land for these projects.
2. The legal measures with Relics and Heritage Office as regards issuing a certificate the specified area does not contain relics
3. There are hurdles in the area represented by high tension poles and large water pipes.

3.1.3 Design and Preparation of Bills of Quantities (BOQ)

It's one of the important stages undergone by the project where was reflecting the basic needs of the project is in line with the modern with modern residential Complex.

As a consultant designed for schemes and the preparation of an initial bill of quantities as well as the contract with the consultant / University of Kufa office by the Provincial Council Resolution (17) in 2012 on the supervision, follow-up and receive the report of residential projects in the province at all stages of the project started on 10 /4/2013 and be responsible for the work because of its experience, a good reputation and rehabilitation. The firm providing engineering consultancy services for the project in three phases as follows:

3.1.3.1 Provide BOQ for construction works and project services (electrical, mechanical and health) and the actual proportions of achievement of each item.

3.1.3.2 By taking the test samples for materials used for residential project then give the results of the test and others count corresponding to international specification then re-examined again.

3.1.3.3 Daily general inspection on the progress of work at the site to secure the implementation of specifications, general designs then provide bi-monthly reports for the quality, the percentage of completion of each item and continue the process under the program for the implementation of 24 months.

3.1.4 The Investment Opportunity

Najaf Municipality advertised the project as an Investment Opportunity with area of (37,500 m^2)

A number of investors both local and foreign submitted their offers directly to the Investment Commission which checked them to find out their qualifications in terms of capability for the work, and their executive, financial, technical, and administrative abilities as well as their readiness to work within the specified time period. After the survey was completed, the license was awarded to Company.

3.1.5 Implementation

The execution style was done by general contractor method which the site has been contributed hand by hand to the contractor on 05/03/2013. The report recorded site location, advantages, limitations, the dimensions and constraints, real estate or signs or traces. The application of the time-table to examine all the items of implementation and functioning of each type of business is calculated theoretically. The plan would follow the imposition of labor, tools and materials are all equipped to work without interruption and crises fills in the site according to the effective functioning of the stages of implementation, work progress and steps under the supervision of engineer as well as the actual daily stop and delayed of construction such as materials, supplies, rainy days, holidays and emergency conditions. After the location have been taken then the preparing of the construction will start immediately by testing the soil to determine soil effort and bearing degree of soil surface pressure at a certain level loads, the contractor begins work by construction the overnight engineers and workers living sites then identify suitable locations for the raw materials storage and leaves enough space for the passage of motor vehicles which will supply raw materials of the site the Contractor shall take the necessary procedures to deliver water and electricity to the site. The researcher tried to record the most prominent obstacles and problems through in site study of the project, the Investment Authority, the project manager and site engineers in order to identify the problems which occur during the implementation, resulting from both the administration and planning in the first phase that precedes the implementation process and the following are some points:

1. When an investor for investment opportunity has been relying on the BOQ while this is not true of the fact that the real amounts vertebrae work is matching to the first phase, which applied to 70% the proportion of the infrastructure of the project is during the implementation period.
2. Work programs progress made by the investor are not dependable, because there is a difference between programs progress and the fact the port of residential project.
3. Despite the presence of a permanent contract between the investor competent laboratory tests, but the committee did not adopt these tests while investment correspondence immediate and pay wages at the same time, causing a waste of time, effort and reduces the interest point of the tests.
4. Delay from some directories approvals for the implementation of the project including the general department of housing, the municipality of Najaf, the General Authority for Antiquities and Heritage, Department of Education, Najaf Health directory, so provide all the paperwork for the project.

4. FIELD SURVEY

4.1 EVM performance analysis and forecasting

Table (5) shows what EVM performance measures indicate about a project in regard to its planned work schedule and resource budget. It will examine **Global standard, 2005**.

1. Variances: schedule variance (SV); (CV); and Variance at completion (VAC).
2. Indices: schedule performance index (SPI); cost performance index (CPI); to complete performance index (TCPI).
3. Forecasts: Time Estimate at completion (EAC t); Estimate at completion (EAC); and Estimate to complete (ETC).

From the basic three values three kinds of deviation can be calculated from the following equations, **PMI, 2011.**

Cost variance CV= EV - AC (1)

Cost performance index (CPI) = $\frac{EV}{AC}$ (2)

Schedule variance SV= EV -PV (3)

Schedule performance index (SPI) =$\frac{EV}{PV}$ (4)

where:
CV: Cost variance.
EV: Earned value.
AC: Actual cost.
CPI: Cost performance index.
SV: Schedule variance.
PV: Planned value.
SPI: Schedule performance index.

4.2Analysis of data information about the cost and time of housing projects

After data on the cost of project with the research sample was collected, their cost was analyzed by using earned value and illustrative drawing by using Sigma Plot program to find out the magnitude of deviation between the planned cost and planned percentage of performed work for every activity through the main three values of (planned, earned, and actual) after the Cumulative total is obtained as shown in Table (6), (7) results of calculation of basic values acquired by the percentage of completion. Tables (8) as well as the balance value set for the first stage of the project (BAC)**, Global, 2005.** The percentage of deviation in every housing project is shown in **Fig.3** with the estimated cost of planned work. The reduction in cost appears in the first stage of project. This is the difference between the planned value and actual cost. The percentage of the work performed for each project (27%) respectively. The amount of money spent is not compatible with planned cost. The reason for this is financing the project depends on the deposits which were drawn from the purchasers' monthly installments. Even so the investor cannot receive any money unless Investment Commission agrees and special committee decides on the project performed work.

4. 3 Cost variance (CV) and Cost performance indicator (CPI)

The ratio of deviation in cost is positive because it ranges between (6% - 22%) in table (5) and **Eq.** (1) and (2). This deviation is an example to show that the contractor had to wait for long time to get machinery or raw materials because they were unavailable at the time they were

needed, therefore the volume of work increased in general. The deviation shows less was spent than what was expected in the project, **Fig.4** Cost performance index of the project.

4. 4 Schedule variance (SV) and Schedule performance index (SPI)

It can be seen that time deviation (SV) is negative and ranges between ((-20) % - 16%) for project shown table (9) and **Eq.** (3) and (4). The survey has shown that among the major reasons for time deviation is the increase in work volume in some areas under study, making it difficult to get machinery and workforce, resulting in long wait to get them. Because of sudden stoppage in work either on order of Investment Commission being a representative of the Government in these buildings or because of security situation in addition, foundations cannot be cast without making sure of the accuracy of their reinforcement which the consultant or his representative should endure the compatibility of design with reality. This applies also to the project planning because reducing the period for items completion during project planning will certainly cause confusion in work.

Thus time performance index SPI is less than in project. The means that there is time delay from what is expected but the spending is less than what is expected on the work in project while the actual cost has exceeded what is planned in project, **Fig.5** is a graph of the time performance index for the first stage in housing project.

The estimated values of the remaining works (ETC) in housing project executed and from **Fig.6** graph of estimated value of the remaining works in project .The worst estimated value table(9) used **Eq.**(5),(6**) , Art Gowan,2006.**They were calculated by using the following equations.

$$\textit{Estimate To Complete (ETC1)} = \frac{BAC-EV}{CPI} \quad (5)$$

$$\textit{Estimate To Complete (ETC2)} = \frac{BAC-EV}{CPI*SPI} \quad (6)$$

Where:

ETC1: Estimate To complete (the most likely)

ETC2: Estimate To complete (the worst)

BAC: Budget At completion.

EV: Earned value.

CPI: Cost performance index.

SPI: Schedule performance index.

5. CONCLUSIONS

1. Prepare a dedicated staff of residents with experience in various engineering disciplines and who have extensive experience in their field of specialty.
2. The exchange of experiences between projects and programs through the data and information assessment, especially the rare cases of a failure of the project or implementation of the project as planned in absolute terms and for the purpose of benefiting from lessons learned from the projects implemented.
3. The issuance of legal legislation imposing the existence of evaluation systems for projects and accompany it to all stages of the implementation of the project.
4. In order to achieve the quality specifications of the housing project and get the project advanced degrees in the evaluation of the quality, the parties involved are characterized in the project competence and expertise needed to achieve those standards, and this was confirmed by the answers to the questionnaire categories through the granting of this factor is the degree of high importance.
5. weak role of supervision and follow-up on residential projects in the progress of work in residential projects as well as related activities oversight role in planning and guessing for business projects.

6. RECOMMENDATIONS

1. Reconsider manner hauling projects up costs and extended implementation.
2. The middle and senior management of the executive branch on the transfer of residential projects in accordance with the standards of good.
3. The need to apply strict supervision by supervisors during execution.
4. Focus on the receiving process to be procedures in advance and specific enough to ensure the lowest level allowed flaws and mistakes.
5. Development of laws relating to land acquisition and transfer of ownership.
7. Activating proliferation policy in the implementation of the residential cities to include all provinces.
8. Organizing efforts of the various agencies involved in housing activity and activation of coordination among them for future planning.
9. Inactive the tax system at the companies in the construction works.
10. Authentication board of investment plans and maps for residential projects before beginning construction work so as to avoid any failures and overlaps in business.

7. SUGGESTIONS FOR FUTURE STUDIES

1. Assessment of construction projects and their impact on long-term (value-added of the project).
2. A detailed study to assess the actual costs of the project and compare cost planned and the various phases of the project.
3. The adoption of modern concepts in the development of evaluation systems, as an application of neural networks in building evaluation systems.

REFERENCES

- Art Gowan, J., 2006, Richard G. Mathieu, and Mark B. Hey. *Earned value management in a data warehouse project*, Information management & computer security 14.1.
- Global standard, 2005, *practice standard for earned value management*. Newtown square, PA19073-3299 USA.
- Law No. 8 of 1997, *investment guarantees and incentives*, Official Journal, No. 19 repeater, Cairo, Egypt.
- Simon, Schuster, H., 1994, *Rise and fall of strategic planning*, New York: Free Press.
- Najaf Investment Commission,2014 , *Investment projects in the Commission investment data*, Records and data investors, Archive.
- National Investment Commission of Iraq, 2013, *investment map Iraq*, page 60.
- Nowak, Maciej., (2005), *Investment projects evaluation by simulation and multiple criteria decision aiding procedure*, Journal of civil engineering and management 11.3.
- O'Reilly, J. J. W., 2005, *Project Evaluation*, Building Research Establishment of the Department of the Environment.
- PRESIDENTIAL. M. D , 2002, *Investment Guarantees and Incentives* , No.1144.
- PMI. , 2011, *Practice Standard for Earned Value Management*, Second edition.
- -RPS and INAC, R.,2000, *Project Management Manual*, Technical Information Document, page 6.

- Smith, Nigel J., Engineering *project management*. Black well, 2002.
- The Investment Egypt law. , 1977, law No.93, No.47 years1984.
- The Investment Iraqi law, 2006, *Iraqi newspaper events*, years 2007/01/17, Bagdad, Iraq, No.13, Vol. 4031.
- Vorster, Michael C., 2005, *Process Support for Requirements Engineering-A Requirement Engineering Tool Evaluation Approach*, Ph. D. Thesis., Department of Computer and Information Science Norwegian University of Science and Technology.
- Weick, K. E., 1995, *Sense making in organizations*, (Vol. 3).
- Westal, Joy Frechtling., 2002, *the 2002 User Friendly Handbook for Project Evaluation*, the National Science Foundation.
- Westland, Jason, 2006, *The project management life cycle*. ISBN 749445556.

NOMENCLATURE

A= area, acre, m2, km^2.

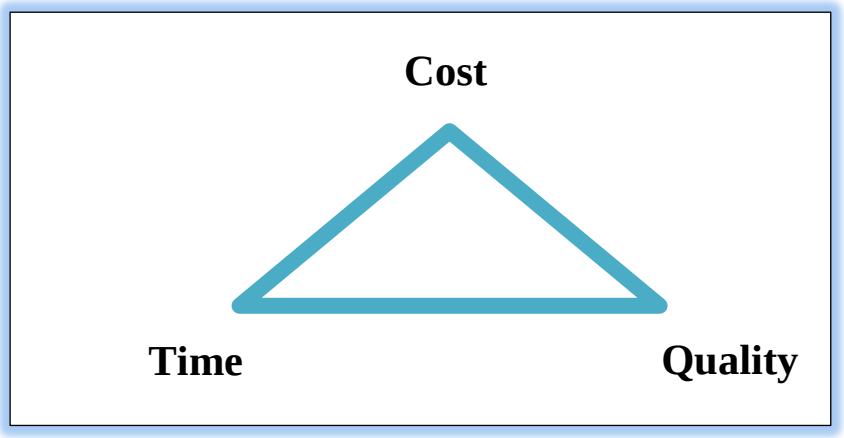

Figure 1. Success factors of project management.

Republic Of Iraq
Al-Najaf Investment Commission

جمهورية العراق
هيئة استثمار النجف الاشرف

إجازة إستثمار رقم (٦٤)
Investment License No. (64)

استناداً إلى الصلاحية المخولة لنا بموجب الفقرة (أ) من المادة (٧) والبند ثانيا من المادة (١٩) من قانون الاستثمار رقم ١٣ لسنة ٢٠٠٦ النافذ. وبعد الإطلاع على ما ورد في طلبكم وبعد إستحصال موافقة الجهات ذات العلاقة فقد قررت الهيئة منح الترخيص لحضرتكم بالإستثمار وعلى الوجه التالي :

In accordance with Article (7), paragraph (a) and Article (19), paragraph (first) within the Investment Law No.13/2006, and after favorable review of your request and after obtaining the approved of all concerned entities, the commission hereby grants a license to invest in the following project:

اسم المستثمر	Moufaq Kazim Abbas AL-Jewahiry	Name of investor
جنسيته	عراقي	Nationality
أسم المشروع	مجمع سكني	Project name
نوع الاستثمار	إسكان	Type of investment
رأس مال المشروع كتابة	خمسة مليار واربعمائة مليون دينار عراقي [written]	5.400.000.000 ID [typed] Project value
مدة تنفيذ المشروع	٢٤ شهر	24 months Project achievement period
الجهة المنفذة للمشروع	موفق كاظم عباس الجواهري	Moufaq Kazim Abbas AL-Jewahiry Project investment lead

تاريخ منح الترخيص: اليوم Day 6 الشهر Month 4 السنة Year 2010 Date of issuance:

رئيس هيئة استثمار النجف الأشرف / وكالة
By proxy/Chairman
Najaf Investment Commission

هيئة استثمار النجف رئيس الهيئة

م. سامر منهل / منتصر محمد . شرشام تحسين ٢٠١٠/٧/١١

Email : admin@investnajaf.com
Web : www.investnajaf.com
Email : investnajaf@yahoo.com

النجف الأشرف – حي الأمير – مقابل رئاسة جامعة الكوفة
Cell : + 964 219236 - 07601504342

Figure 2. Investment license.

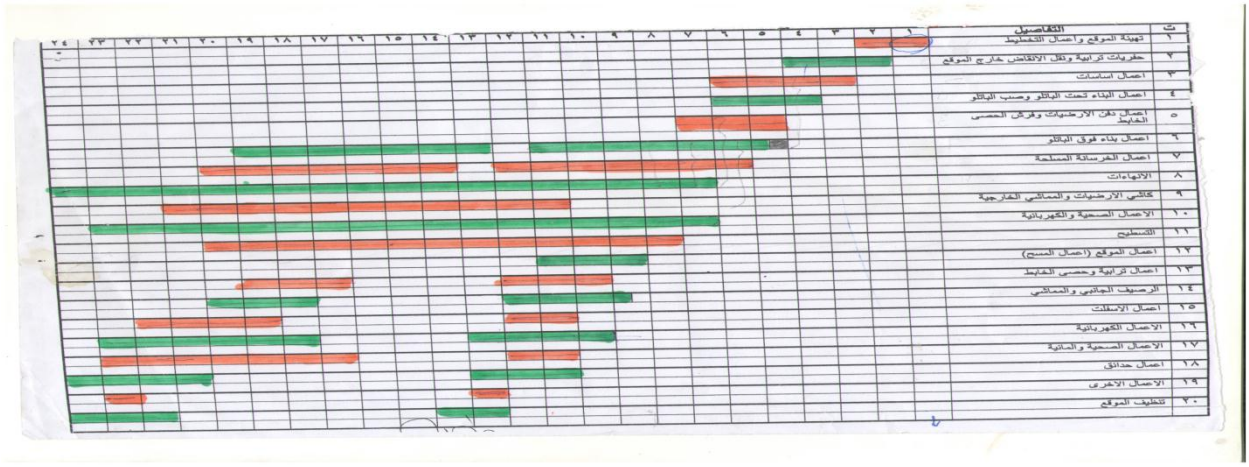

Figure 3. Provides work for the project

Figure 4. Main three values of (PV, EV, and AC) for the first housing project.

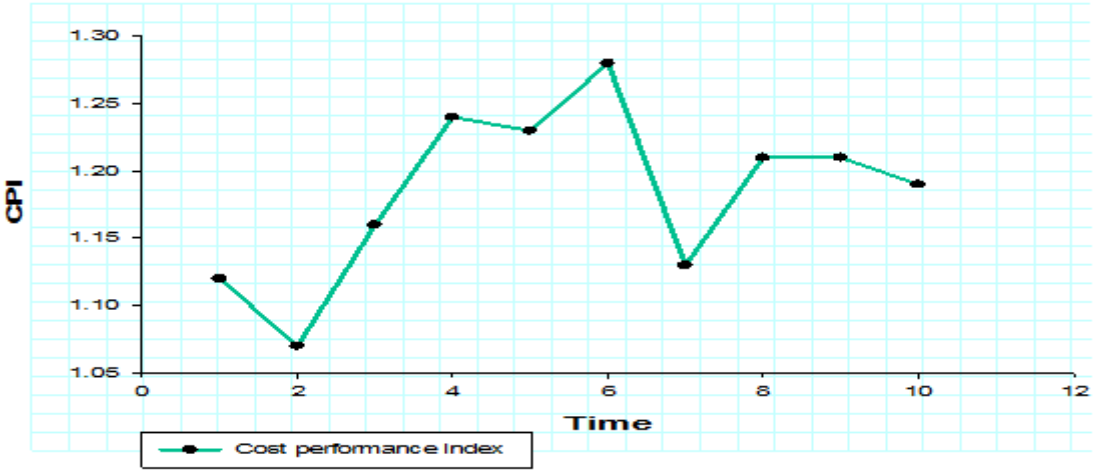

Figure 5. Cost performance index of the project.

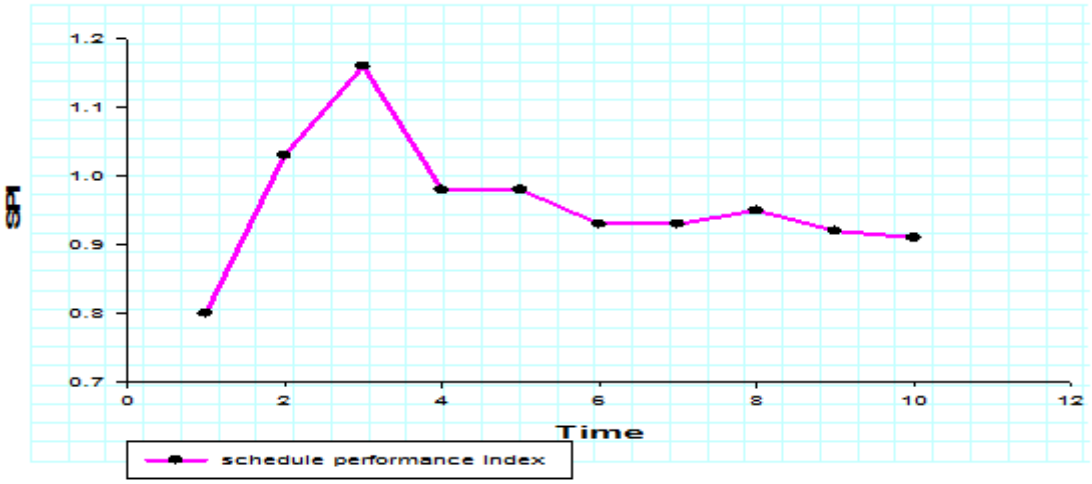

Figure 6. Schedule performance index for the first stage in housing project.

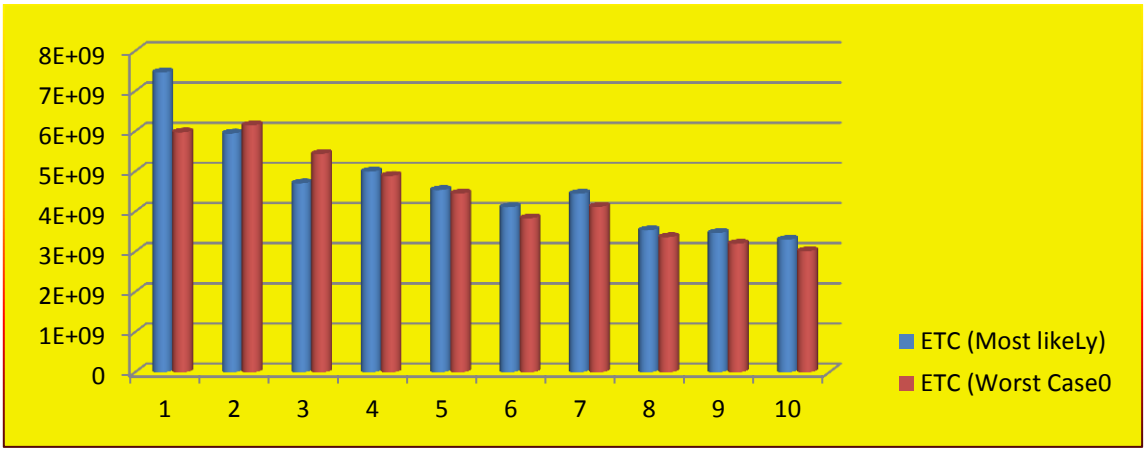

Figure 7. Graph of estimated value of the remaining works (ETC) in project.

Table 1. Reasons of project failure and the percentage of their effects.

Cause of Failure	Percentage of effect on project
Lack in integration of project requirement.	13.1%
Opinion of project users is not considered	12.4%
Insufficient resources	10.6%
Unrealistic estimations	9.9%
Inefficient administrative support	9.3 %
Changing in requirements	8.7%
Poor planning	8.1%
Real need is not well estimated	7.4%

Table 2. Description of research sample.

Project	NO. unit	Building material type	Cost ID	Investment License NO.	Achievement period	Achieved rate	Area	Date started	No of laborers. Local & foreign
Hussein complex	112	Traditional building	11,086,020,000	2010/4/6 (64)	24 MONTH	%27	15 acre	/2/18 2013	%100 Local

Table 3. Showing the population between (2006-2020) in Najaf.

Year	Population
2006	1, 081, 210
2010	1,204,730
2020	1,574,201

Table 4. The type of building, number of units and built area.

Type	Area	No. Unit	Unit area	Floor area			Building area
				Ground	1st	Total	
A	250	38	9,500	177	31	208	7,904
B	250	38	9,500	177	0	177	6,726
C	200	18	3,600	138	33	171	3,078
D	200	18	3,600	138	0	138	2,484
						SUM	20,192

Table 5. Interpretations of Basic EVM performance Measures.

Performance Measures		Schedule		
		SV>0 & SPI>1.0	SV=0 & SPI = 1.0	SV<0 & SPI< 1.0
Cost	CV > 0 & CPI > 1.0	Ahead of schedule under Budget	On schedule under Budget	Behind schedule under Budget
	CV = 0 & CPI = 1.0	Ahead of schedule on Budget	On schedule on Budget	Behind schedule on Budget
	CV < 0 & CPI < 1.0	Ahead of schedule over Budget	On schedule over Budget	Behind schedule over Budget

Table 6. The results of calculation of basic values acquired by the percentage of completion.

Measurement Time	Activity	Baseline Data			Performance Data		Actual Cost	
		% Complete	Budget Cost	PV (BCWS)	% Complete	EV (BCWP)	Actual Cost	AC (ACWP)
MONTH (1)	A	50%	85560000	42780000	40%	34224000	76308000	30523200
Accumulative				42780000		34224000		30523200
MONTH (2)	A	100%	85560000	85560000	90%	77004000	76308000	68677200
	B	33.3%	195660000	64567800	40%	78264000	191263000	76505200
Accumulative				150127800		155268000		145182400
MONTH (3)	A	100%	85560000	85560000	100%	85560000	76308000	76308000
	B	66.6%	195660000	129135600	80%	156528000	191263000	153010400
	C	25%	550000000	137500000	30%	165000000	402165000	120649500
Accumulative				352195600		407088000		349967900
MONTH (4)	A	100%	85560000	85560000	100%	85560000	76308000	76308000
	B	100%	195660000	195660000	90%	176094000	191263000	172136700

	C	50%	550000000	275000000	45%	247500000	402165000	180974250
	D	33.3%	455952000	150464160	40%	182380800	325952000	130380800
Accumulative				706684160		691534800		559799750
MONTH (5)	A	100%	85560000	85560000	100%	85560000	76308000	76308000
	B	100%	195660000	195660000	100%	195660000	191263000	191263000
	C	75%	550000000	412500000	60%	330000000	402165000	241299000
	D	66.6%	455952000	300928320	75%	341964000	325952000	244464000
	E	33.3%	501490000	165491700	35%	165491700	381490000	133521500
	F	7%	1688800000	118216000	8%	135104000	1647800000	131824000
Accumulative				1278356020		1253779700		1018679500
MONTH (6)	A	100%	85560000	85560000	100%	85560000	76308000	76308000
	B	100%	195660000	195660000	100%	195660000	191263000	191263000
	C	100%	550000000	550000000	80%	440000000	402165000	321732000
	D	100%	455952000	455952000	90%	455952000	325952000	293356800
	E	66.6%	501490000	330983400	75%	376117500	381490000	286117500
	F	14%	1688800000	236432000	12%	202656000	1647800000	197736000
	G	7%	1706738000	119471660	5%	85336900	1542481000	77124050
Accumulative				1974059060		1841282400		1443637350
MONTH (7)	A	100%	85560000	85560000	100%	85560000	76308000	76308000
	B	100%	195660000	195660000	100%	195660000	191263000	191263000
	C	100%	550000000	550000000	90%	495000000	402165000	361948500
	D	100%	455952000	455952000	100%	455952000	325952000	325952000
	E	100%	501490000	501490000	90%	451341000	381490000	343341000
	F	21%	1688800000	354648000	20%	337760000	1647800000	329560000
	G	14%	1706738000	23894220	12%	20480760	1542481000	185097720
	H	5.5%	1550800000	85294000	3%	46524000	1317811000	39534330

Accumulative				**2252498220**		**2088277760**		**1853004550**
MO (NTH 8)								
	A	**100%**	**85560000**	**85560000**	**100%**	**85560000**	**76308000**	**76308000**
	B	**100%**	**195660000**	**195660000**	**100%**	**195660000**	**191263000**	**191263000**
	C	**100%**	**550000000**	**550000000**	**95%**	**522500000**	**402165000**	**382056750**
	D	**100%**	**455952000**	**455952000**	**100%**	**455952000**	**325952000**	**325952000**
	E	**100%**	**501490000**	**501490000**	**95%**	**476415500**	**381490000**	**362415500**
	F	**28%**	**1688800000**	**472864000**	**25%**	**422200000**	**1647800000**	**411950000**
	G	**21%**	**1706738000**	**358414980**	**20%**	**341347600**	**1542481000**	**308496200**
	H	**11%**	**1550800000**	**170588000**	**10%**	**155080000**	**1317811000**	**131781100**
Accumulative				**2790528980**		**2654715100**		**2190222550**
MONTH (9)	**A**	**100%**	**85560000**	**85560000**	**100%**	**85560000**	**76308000**	**76308000**
	B	**100%**	**195660000**	**195660000**	**100%**	**195660000**	**191263000**	**191263000**
	C	**100%**	**550000000**	**550000000**	**100%**	**550000000**	**402165000**	**402165000**
	D	**100%**	**455952000**	**455952000**	**100%**	**455952000**	**325952000**	**325952000**
	E	**100%**	**501490000**	**501490000**	**100%**	**501490000**	**381490000**	**381490000**
	F	**35%**	**1688800000**	**591080000**	**29%**	**489752000**	**1647800000**	**477862000**
	G	**28%**	**1706738000**	**477886640**	**23%**	**392549740**	**1542481000**	**354770630**
	H	**16.5%**	**1550800000**	**255882000**	**13%**	**201604000**	**1317811000**	**171315430**
Accumulative				**3113510640**		**2872567740**		**2381126060**
MONTH (10)	**A**	**100%**	**85560000**	**85560000**	**100%**	**85560000**	**76308000**	**76308000**
	B	**100%**	**195660000**	**195660000**	**100%**	**195660000**	**191263000**	**191263000**
	C	**100%**	**550000000**	**550000000**	**100%**	**550000000**	**402165000**	**402165000**
	D	**100%**	**455952000**	**455952000**	**100%**	**455952000**	**325952000**	**325952000**
	E	**100%**	**501490000**	**501490000**	**100%**	**501490000**	**381490000**	**381490000**
	F	**42 %**	**1688800000**	**709296000**	**40%**	**675520000**	**1647800000**	**659120000**
	G	**35%**	**1706738000**	**597358300**	**25%**	**426684500**	**1542481000**	**385620250**

	H	22%	1550800000	341176000	16%	248128000	1317811000	210849760
Accumulative				3436492300		3138994500		2632768010

Table 7. Values of the acquired values, with values related in cost deviation.

Month	Baseline Metrics Measurement Cumulative			Cost variance			BAC
	PV	EV	AC	CV	CV%	CPI	
				EV-AC	CV/ EV	EV/ AC	
1	42780000	34224000	30523200	3700800	11%	1.12	6735000000
2	150127800	155268000	145182400	10085600	6%	1.07	6735000000
3	352195600	407088000	349967900	57120100	14%	1.16	6735000000
4	706684160	691534800	559799750	131735050	19%	1.24	6735000000
5	1278356020	1253779700	1018679500	235100200	19%	1.23	6735000000
6	1974059060	1841282400	1443637350	397645050	22%	1.28	6735000000
7	2252498220	2088277760	1853004550	235273210	11%	1.13	6735000000
8	2790528980	2654715100	2190222550	464492550	17%	1.21	6735000000
9	3113510640	2872567740	2381126060	491441680	17%	1.21	6735000000
10	3436492300	3138994500	2632768010	506226490	16%	1.19	6735000000

Table 8. Deviations show cost, time and overall performance index.

Month	EV deviation				EV Index	
	SV	CV	SV%	CV%	SPI	CPI
	EV-PV	EV-AC	SV/PV	CV/EV	EV/PV	EV/AC
1	-8556000	3700800	-20%	11%	0.80	1.12
2	5140200	10085600	3%	6%	1.03	1.07
3	54892400	57120100	16%	14%	1.16	1.16
4	-15149360	131735050	-2%	19%	0.98	1.24
5	-24576320	235100200	-2%	19%	0.98	1.23
6	-132776660	397645050	-7%	22%	0.93	1.28
7	-164220460	235273210	-7%	11%	0.93	1.13
8	-135813880	464492550	-5%	17%	0.95	1.21
9	-240942900	491441680	-8%	17%	0.92	1.21
10	-297497800	506226490	-9%	16%	0.91	1.19

Table 9. Remaining business value (ETC) in the project each quarter for estimating the most likely, and estimate the worst for the Estimate to complete of project

Month1	Estimate To Complete ETC		To Complete Performance Index TCPI (BAC)
	1	2	
1	5976189984	7470237480	1.00
2	6152338429	5948663170	1.00
3	5440018065	4706477288	0.99
4	4892205437	4999378324	0.98
5	4453419332	4540714300	0.96
6	3836865821	4113545938	0.92
7	4123205073	4447450557	0.95
8	3366361987	3538583361	0.90
9	3201643596	3470188453	0.89
10	3016076723	3301925006	0.88

Prediction of Monthly Fluoride Content in Tigris River using SARIMA Model in R Software

Asst. Prof. Dr. Awatif Soaded Alsaqqar
Department of Civil Engineering
College of Engineering
Baghdad University
Email: d.alsaqqar@yahoo.com

Asst. Prof. Dr. Basim Hussein Khudair
Department of Civil Engineering
College of Engineering
Baghdad University
Email: basim22003@yahoo.com

Asst. Lect. Rasha Attwan Faraj
Department of Civil Engineering
College of Engineering
Baghdad University
Email: rashaatwan@yahoo.com

ABSTRACT

The need to create the optimal water quality management process has motivated researchers to pursue prediction modeling development. One of the widely important forecasting models is the sessional autoregressive integrated moving average (SARIMA) model. In the present study, a SARIMA model was developed in R software to fit a time series data of monthly fluoride content collected from six stations on Tigris River for the period from 2004 to 2014. The adequate SARIMA model that has the least Akaike's information criterion (AIC) and mean squared error (MSE) was found to be SARIMA (2, 0, 0) (0,1,1). The model parameters were identified and diagnosed to derive the forecasting equations at each selected location. The correlation coefficient between the actual and predicted values for fluoride concentration at the six locations, Al-Karakh, East Tigris, Al-Wathbah, AL-Karamah, Al-Rashid and Al-Wahda WTP intakes, was 0.93, 0.82, 0.86, 0.90, 0.83 and 0.89, respectively. Model verification results indicated that the model forecasting outputs rationally estimated the actual monthly fluoride content in the selected locations.

Keywords: water quality management, time series analysis and prediction, SARIMA model, R software.

التنبؤ بمحتوى الفلورايد الشهري في نهر دجلة باستخدام (SARIMA) موديل في برنامج (R)

أ.م. د. عواطف سؤدد عبدالحميد
قسم الهندسة المدنية
كلية الهندسة/جامعة بغداد

أ.م.د. باسم حسين خضير
قسم الهندسة المدنية
كلية الهندسة/جامعة بغداد

م.م. رشا عطوان فرج
قسم الهندسة المدنية
كلية الهندسة/جامعة بغداد

الخلاصة

الحاجة لابتكار نظام افضل لادارة نوعية المياه قد حفزت الباحثين لمواصلة تطوير نماذج التنبؤ. واحد من نماذج التنبؤ المهمة والواسعة الانتشار(SARIMA). في هذه الدراسة, تم تطوير نموذج (SARIMA) بأستخدام برنامج (R) لموافقة السلاسل الزمنية لمحتوى الفلورايد الشهري لستة مواقع في نهر دجلة خلال الفترة الزمنية من (2004-2014). وقد وجد النموذج الأنسب لاحتوائه على أقل قيمة (AIC) و قيمة معدل مربع الخطأ (MSE) وقيمة (SARIMA) لتكون (0،1،1) (2،0،0). معالم النموذج قد عرفت وشخصت لاشتقاق معادلات التنبؤ في كل المواقع المحددة. معامل الارتباط بين القيم الفعلية والمتوقعة لتركيز الفلوريد في المواقع الستة، مآخذ الكرخ، شرق دجلة، الوثبة، الكرامة، الرشيد و الوحدة كان 0.93، 0.82، 0.86، 0.90 ، 0.83 و 0.89 على التوالي. قد بينت نتائج أختبار النموذج بأن نتائج التنبؤ للنموذج قد قدرت محتوى الفلورايد الشهري الفعلي في المواقع المختارة جيدا.

الكلمات الرئيسية: ادارة نوعية المياه، تحليل والتنبؤ للسلاسل الزمنية ، نموذج SARIMA، برنامج R .

1. INTRODUCTION

Water quality is a critical subject of the ongoing environmental concerns. Impairment of water quality has motivated researchers to develop methods to monitor water characteristics. Usually monitoring water quality in lakes, streams and rivers is performed through the conventional methods which involve field measurements and laboratory analysis. The conventional methods are useful for small water surfaces. However, for large areas, the conventional methods are expensive and incapable for monitoring and evaluating of regional water quality when numerous sampling locations need to be evaluated periodically , **Hirsch et al., 1982**. Therefore, thoughtful water quality management efforts have been taken into consideration in many countries to be utilized in conjunction with conventional methods.
Water quality management includes modeling, forecasting and analysis of water bodies' quality. Developing precise forecasting model of future water parameter is the essence of optimal water quality management. Modeling methods have been improved with the continued development of computer science and statistics particularly for discovering time series data patterns. Time series prediction is ongoing area of forecasting approaches. Past collected observations of the same parameter are investigated to create a model that describes the underlying relationship. Afterwards, the developed model is used to estimate the parameter in the future.

One of the most useful and important time series prediction models is the autoregressive integrated moving average (ARIMA) model , **Sowell, 1992**. The advantages of the ARIMA model can be attributed to its statistical characteristics, represented by the famous Box–Jenkins methodology ,**Harvey, 1990** in the model building process. Moreover, ARIMA models can be performed to represent several exponential smoothing applications including environmental applications ,**Williams** and **Hoel, 1999**. The development of ARIMA models have continued over decades. The basic ARIMA model has been implemented to include pure autoregressive (AR) or pure moving average (MA). Then, it was developed to combine both autoregressive and moving average (ARMA) compounds. To implant this model for non-stationary time series data, the integrated compound was included in the model to be the ARIMA model. Afterwards, studies have investigated the effect of seasonality on fitting an accurate ARIMA model and found that seasonality causes weakly stationary condition. Therefore, seasonal compound was added to the original ARIMA model to decompose a time series data uniquely into equally independent additive seasonal, trend, and irregular noise components **Hillmer** and **Tiao, 1982, Williams** and **Hoel, 2003**. Recently, the seasonal ARIMA (SARIMA) model has been used for water quality management applications**, Lehmann** and **Rode, 2001, Kurunç et al., 2005**.

Various programing languages and statistical software were utilized to build SARIMA models such as Matlab language, SAS and Stata software. To date, R software is rarely used in modeling processes of water management applications. R is a language and environment similar to the S language which is used for statistical applications. R offers a variation of statistical techniques that can be utilized for linear and nonlinear modelling, statistical tests and time series analysis. Unlike the other statistical software and environments, R software is a free software which gives the advantage of being an open source in the modeling methodology.

In the present study, Time series analysis of monthly fluoride content was carried on using R software. Also, R software was used to code and construct a SARIMA model to forecast monthly fluoride concentration in Tigris River.

2. MATERIALS AND METHOD

2.1 Study Area and Data Collection

The study area in this work is Tigris River in Baghdad City. This river is considered the main source for Baghdad City water supply systems. Sample collection locations were chosen to represent water quality in the main flow stream, including upstream, downstream and between at different water treatment plant intakes. Al-Karakh and East Tigris WTP intakes represent the upstream flow locations, Al-Wathbah and AL-Karamah WTP intakes represent in between upstream and downstream location, and Al-Rashid and Al-Wahda WTP intake represent downstream locations. The data used in this study were provided from Baghdad Mayoralty (Amanat Baghdad)–Water office which represents the fluoride content at the selected locations which were measured monthly according to the standard methods for water and wastewater examination , **APHA et al., 2005**. Monthly time series data of fluoride concentration from 2004 to 2014 was used in this study.

3. MATHEMATICAL STRUCTURE OF SARIMA MODEL

This model assumes that the predicted value of a variable is a linear function of multi previous observations with random errors, **Box et al., 2011**. The model structure is identified as the below expression:

ARIMA $(p, d, q)(P, D, Q)_s$

This expression can be broken down into two terms, non-seasonal and seasonal terms and the mathematical formula of a SARIMA is presented in Eq. (1):

$$\varphi_p(B)\emptyset_P P(B^s)\nabla^d\nabla_s^D y_t = \vartheta_q(B)\theta_Q(B^s)e_t \quad (1)$$

Where:

p and φ_p: the order of auto-regressive (AR) and the AR operator of order p, respectively.

P and $\emptyset_P$: the order of seasonal auto-regressive and the seasonal AR parameter of order P, respectively.

B: the backshift operator of y_t.

d and ∇^d: the order of integration and the differencing operator, respectively.

D and ∇_s^D: the order of seasonal integration and the seasonal differencing operator, respectively.

q and ϑ_q: order of moving average and the MA operator of order q, respectively.

Q and θ_Q: order of seasonal moving average (MA) and the seasonal MA parameter of order Q, respectively.

s : The seasonal period.

y_t : The value at time point t.

e_t : The white noise (random walk) of the stochastic model.

To fit predictive equations for fluoride content in the selected locations, a SARIMA model was constructed by proceeding multi steps, model identification, parameter estimation, diagnostic checking and model validation.

3.1 SARIMA Model Development

As mentioned above a SARIMA model was constructed for fluoride concentration at each location. An R software code was developed to construct the SARIMA model. Time series inputs for fluoride concentration from 2004 to 2012 were used to develop the SARIMA model. Data from 2013 to 2014 was used to validate the constructed model. To fit the optimal SARIMA, model parameters, *p, P, d, D, q, Q, s,* were identified. Parameter identification was performed based on examining the autocorrelation (ACF) and partial autocorrelation (PACF) functions of the transformed data. Additionally, it was examined to give the minimum Akaike's information criterion (AIC) and mean squared error (MSE). After identifying the model, the model was diagnosed and verified for being appropriately fitting the series. The diagnostic process was conducted by examining the model residuals based on its ACF, normal quantile-quantile plot (Q-Q plot) and Ljung–Box statistics results (**Box et al., 2011**). Validation of the model was performed by running correlation analysis to determine whether predicted and actual data are significantly different or not.

4. RESULTS AND DISCUSSION:

Fig. 1 shows monthly data variation of fluoride concentration at each location for the study period. The monthly data was examined for its stationary condition. This was achieved by performing Augmented Dickey-Fuller test to decide if transformation of the data is neede , **Harvey, 1990**. The time series input was found to be not stationary (p>0.05). Seasonality could result in nonstationary condition. Mainly, this is possible due to the difference between the average values at some particular times within the seasonal period and the average values at other times. Therefore, the monthly data was differentiated to yield stationary input series with respect to yearly periodicity by seasonally transformation.

4.1 SARIMA model construction

To fit the optimal SARIMA model parameters for fluoride data series, several trails were performed. The model parameters were chosen based on the statistical residual diagnostic test. Time series inputs from 2004 to 2012 were used for model calibration and to find the adequate model that fits fluoride content in each location. Data from 2013 to 2014 were used for model verification. The data was differentiated to overcome seasonal effects.

To identify and find the persistence model structure, the ACF, PACF, MSE and AIC were tested. The best fitted model was chosen to give the least ACF, PACF, MSE and AIC values. The most appropriate SARIMA model included non-sessional and sessional compounds. The model parameters, *p, d, q, P, D, Q, s,* were 2, 0, 0, 0, 1, 1, 12, respectively, for all locations. The

SARIMA (2, 0, 0) $(0, 1, 1)_{12}$ equation was derived from equation 1 based on the selected model compounds. Equation 2 is the SARIMA (2, 0, 0) $(0, 1, 1)_{12}$ equation

$$y_t=\varphi_1 y_{t-1}+\varphi_2 y_{t-2}+y_{t-12}-\varphi_1 y_{t-13}- \quad \varphi_2 y_{t-14}+e_t+\theta_1 e_{t-12} \qquad (2)$$

To compute the model parameters, the computational steps proposed by **, Box** and **Jenkins, 1976**. were followed. The residuals of the computed parameters were diagnostic to make sure that the adequate model was selected for their independence, constant variance and normality. **Fig. 2** shows the results of the statistical residual diagnostic test for the selected model of the monthly fluoride content collected at the East Tigris WTP intake. This test showed similar results for the other locations. According to, **El-Din** and **Smith, 2002**, to estimate a decent prediction model, the residuals of the fitted model should satisfy the white noise method requirements which should be uncorrelated and normally distributed around a zero mean. The statistic test showed that the ACF values of the residuals and *p* value were adequately distributed within confidence limits (98%) and no significant "spikes" among 35 lags which confirms the normality of the residuals. Also, the results exhibited no significant correlation between the residuals of the fluoride content at each location. Moreover, the normal quantile-quantile plot (Q-Q plot) exhibits that the residuals were laying closely on the theoretical line, which obviously supports the normality of the residuals. The diagnostic test showed that the selected SARIMA model is appropriately fitting the time series data.

Based on the above analyses, the model parameters were selected. **Table 1** demonstrates the sessional compounds as well as the MSE and AIC for the selected model at each location. The results exhibit that the fitted model for fluoride content at Al-Wathbah WTP intake has the highest MSE among the other location. The forecasting equation for each location can be determined by substituting the corresponding computed parameters to each location from **Table 1** in Eq. (2).

4.2 Monthly Fluoride Content Prediction and Verification

Using the fitted SARIMA model, monthly fluoride concentration at each location was predicted for the period from 2013 to 2016 as shown in **Fig. 3**. Predicted data from 2013 to 2014 was compared to the actual data to verify the fitted model. **Fig. 4** shows the correlation between the actual data and the predicted data at each location. The correlation coefficient between the actual and predicted values for fluoride concentration at Al-Karakh, East Tigris, Al-Wathbah, AL-Karamah, Al-Rashid and Al-Wahda WTP intakes was 0.93, 0.82, 0.86, 0.90, 0.83 and 0.89, respectively. These values are acceptable in common model applications, **Faruk, 2010**, **Zhang, 2003**, **Nourani et al., 2011**. Model verification results state that the model forecasting outputs reasonably estimated the actual monthly fluoride content in the selected locations.

5. CONCLUSIONS

In the last few decades, time series analysis and prediction have been considered a dynamic study area. Researchers have never stopped to improve the accuracy efficiency of prediction models of water quality. Using R software, an effective SARIMA model was

developed for monthly fluoride concentration in Tigris River. The model validation demonstrated that the fitted model is adequately forecasting monthly fluoride content. The outcomes of this study are necessary in the environmental applications especially with the raised concerns regarding water bodies impairment phenomenon.

REFERENCES

- APHA, AWWA and WEF, 2005, *Standard methods for the examination of water and wastewater*, American Public Heath Association, Washington, DC.

- Box, G.E. and Jenkins, G.M., 1976, *Time series analysis: forecasting and control*, revised ed, Holden-Day.

- Box, G.E., Jenkins, G.M. and Reinsel, G.C., 2011, *Time series analysis: forecasting and control*, John Wiley & Sons.

- El-Din, A.G. and Smith, D.W., 2002, *A combined transfer-function noise model to predict the dynamic behavior of a full-scale primary sedimentation tank*, Water Research 36(15), 3747-3764.

- Faruk, D.Ö., 2010, *A hybrid neural network and ARIMA model for water quality time series prediction*, Engineering Applications of Artificial Intelligence 23(4), 586-594.

- Harvey, A.C., 1990, *Forecasting, structural time series models and the Kalman filter*, Cambridge university press.

- Hillmer, S.C. and Tiao, G.C.,1982, *An ARIMA-model-based approach to seasonal adjustment*, Journal of the American Statistical Association 77(377), 63-70.

- Hirsch, R.M., Slack, J.R. and Smith, R.A., 1982, *Techniques of trend analysis for monthly water quality data*, Water resources research 18(1), 107-121.

- Kurunç, A., Yürekli, K. and Çevik, O., 2005, *Performance of two stochastic approaches for forecasting water quality and streamflow data from Yeşilırmak River, Turkey*, Environmental Modelling & Software 20(9), 1195-1200.

- Lehmann, A. and Rode, M., 2001, *Long-term behaviour and cross-correlation water quality analysis of the river Elbe, Germany*, Water Research 35(9), 2153-2160.

- Nourani, V., Kisi, Ö. and Komasi, M., 2011, *Two hybrid Artificial Intelligence approaches for modeling rainfall–runoff process*, Journal of Hydrology 402(1–2), 41-59.

- Sowell, F., 1992, *Modeling long-run behavior with the fractional ARIMA model*,

Journal of Monetary Economics 29(2), 277-302.

- Williams, B.M. and Hoel, L.A., 1999, *Modeling and forecasting vehicular traffic flow as a seasonal stochastic time series process*.

- Williams, B.M. and Hoel, L.A., 2003, *Modeling and forecasting vehicular traffic flow as a seasonal ARIMA process: Theoretical basis and empirical results*. Journal of transportation engineering 129(6), 664-672.

- Zhang, G.P., 2003, *Time series forecasting using a hybrid ARIMA and neural network model*, Neurocomputing 50, 159-175.

Table 1. Summary of the statistical parameters of the selected SARIMA model fitted to fluoride concentration at all locations.

Plant	φ_1	φ_2	θ_1	AIC	MSE
AL_KARAKH	0.4974	0.3788	-1	-7.0644	0.000261
EAST TIGRIS	0.4413	0.327	-0.9999	-6.5953	0.00041
AL-WATHBAH	0.4458	0.2069	-1	-4.8524	0.00235
AL-KARAMAH	0.461	-0.0879	-0.7834	-6.0299	0.00074
AL_RASHID	0.2707	0.0539	-0.7947	-6.0299	0.0013
AL_WAHDA	0.3943	-0.0758	-0.775	-6.1358	0.00082

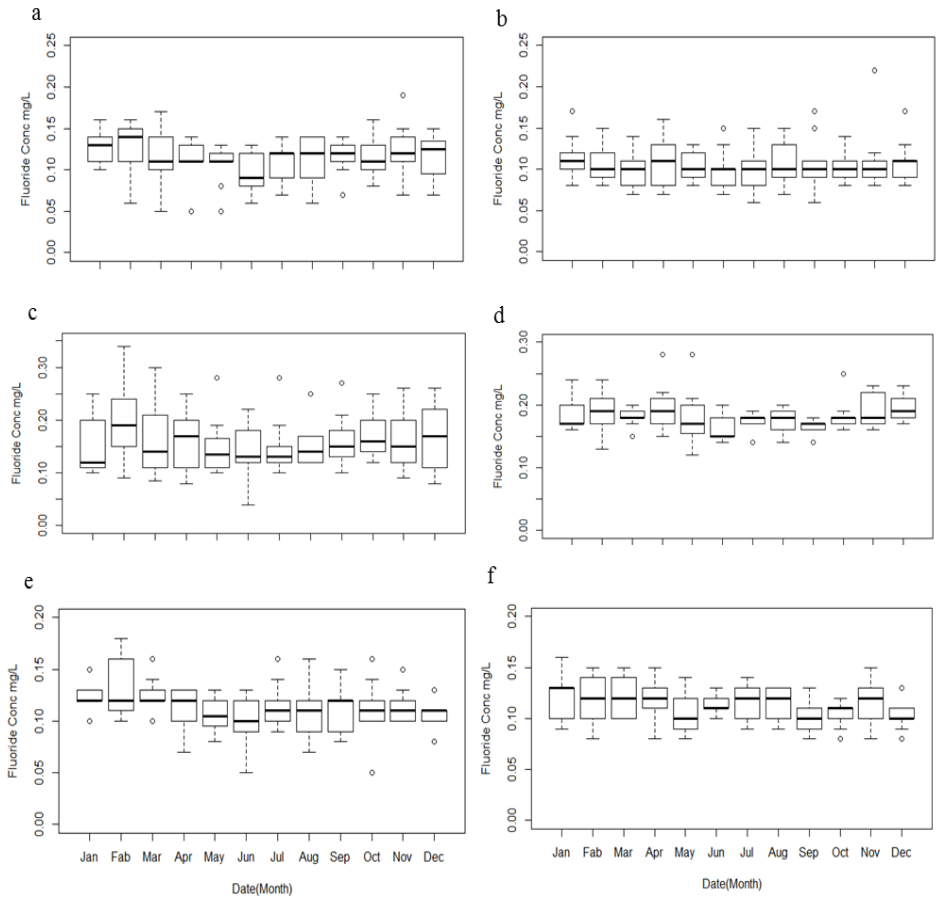

Figure 1. Box plots of monthly fluoride concentration data from 2004 to 2014 at different WTP intakes. a) Al-Karakh WTP intake. b) East Tigris WTP intake. c) Al-Wathbah WTP intake. d) Al-Karamah WTP intake. e) AL-Rashid WTP intake. f) Al-Wahda WTP intake.

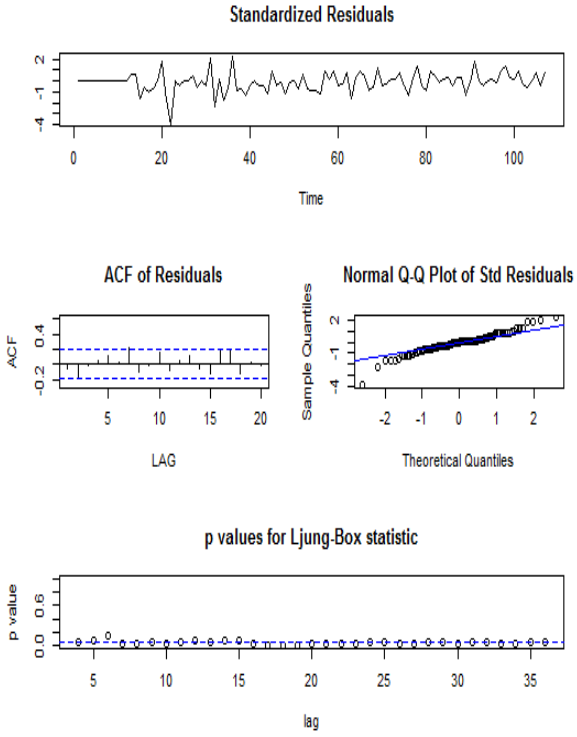

Figure 2. The residual statistical results of the fitted model for monthly fluoride content at the East Tigris WTP intake.

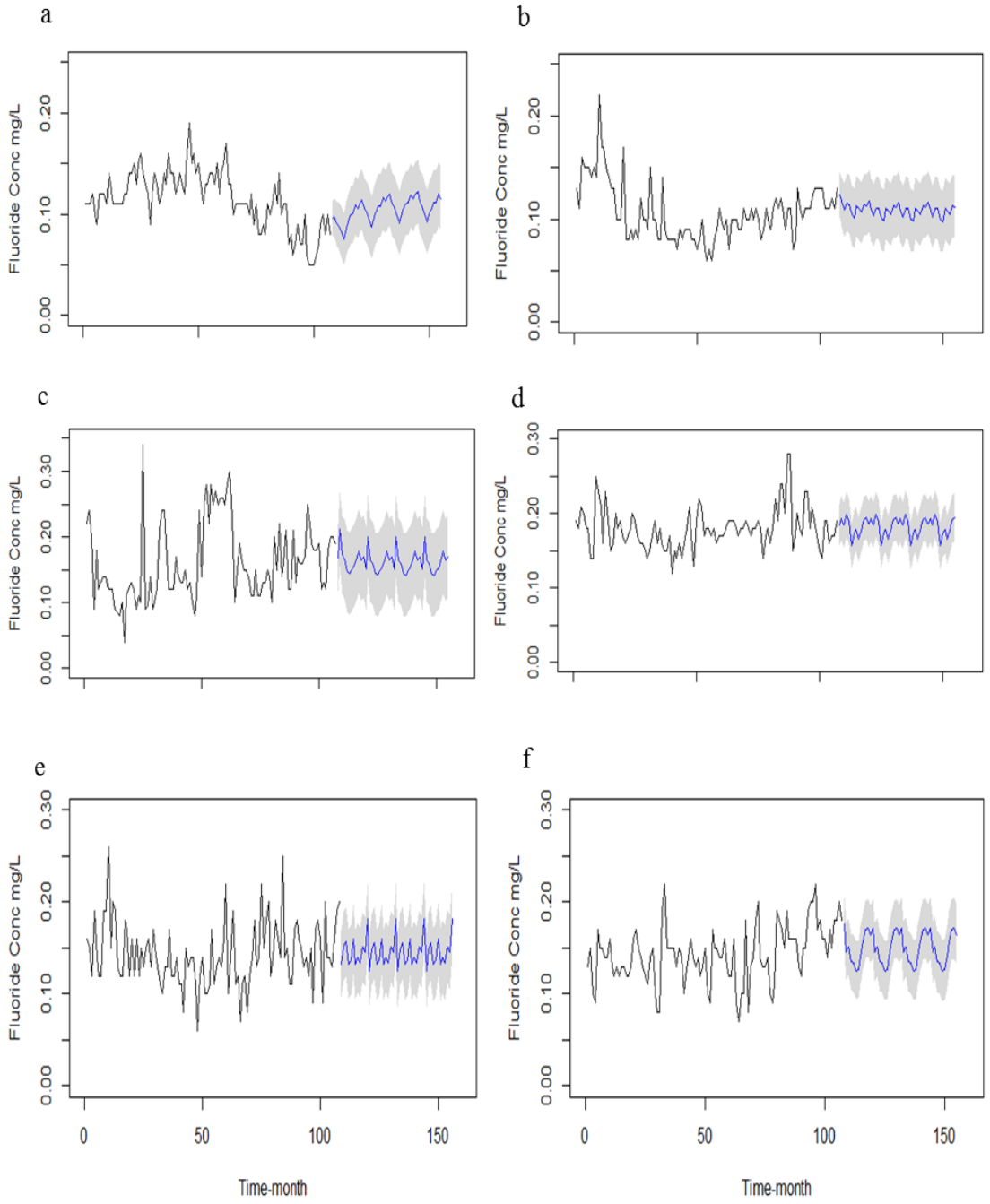

Figure 3. Prediction of monthly fluoride content at various locations in Tigris River. Black solid line is the actual data from 2004 to 2012 used to calibrate the model. Blue solid line is the predicted data for the period from 2013 to 2016. Gray areas shows the upper and lower limits of the predicted values based on 95% confidence intervals. a) Al-Karakh WTP intake. b) East Tigris WTP intake. c) Al-Wathbah WTP intake. d) Al-Karamah WTP intake. e) AL-Rashid WTP intake. f) Al-Wahda WTP intake.

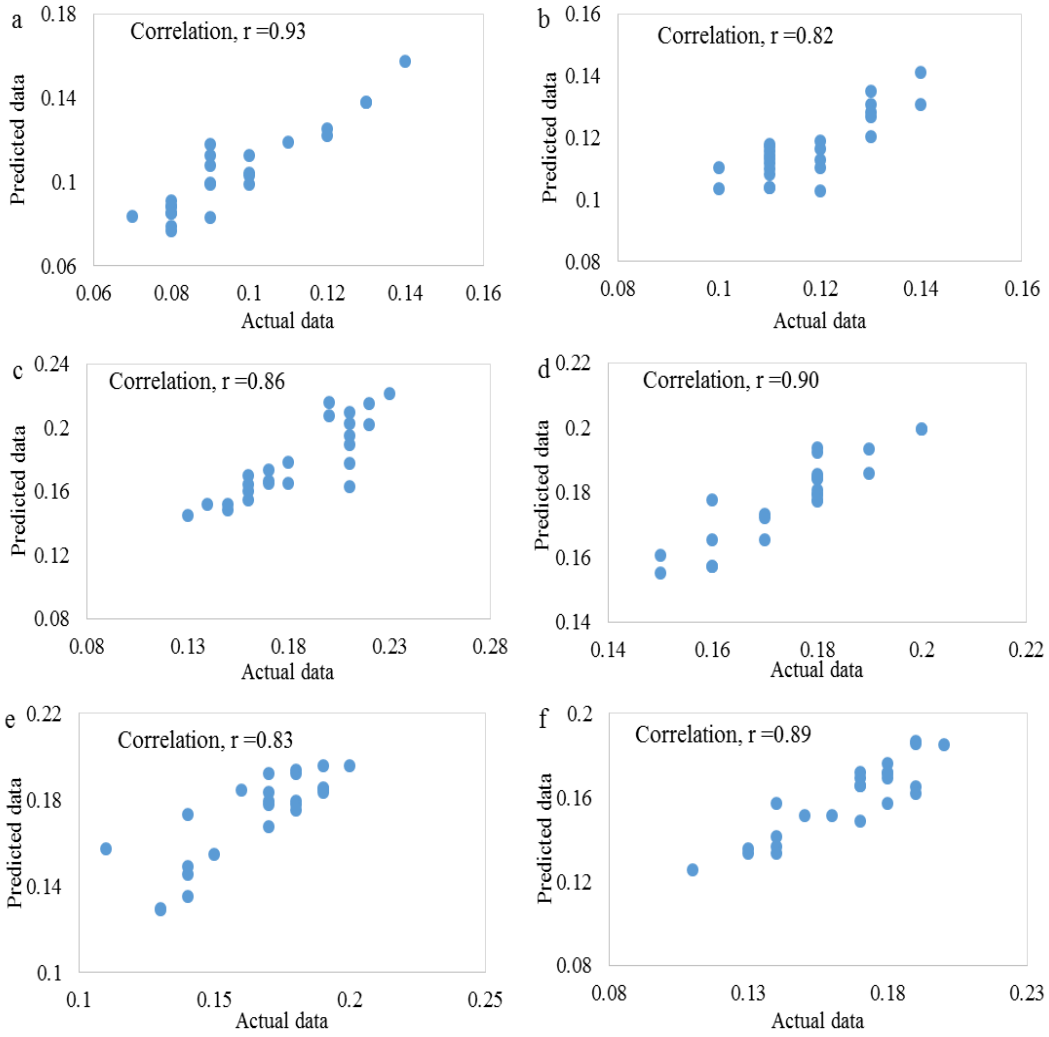

Figure 4. Actual versus predicted fluoride concentration data for correlation analysis at the selected locations. a) Al-Karakh WTP intake. b) East Tigris WTP intake. c) Al-Wathbah WTP intake. d) Al-Karamah WTP intake. e) AL-Rashid WTP intake. f) Al-Wahda WTP intake.

Evaluation of Bearing Capacity of Strip Foundation Subjected to Eccentric Inclined Loads Using Finite Element Method

Ahmed Majeed Ali
Assistant Lecturer
Building and Construction Engineering Department, University of Technology/ Baghdad
Ama.civil85@gmail.com

ABSTRACT

In real conditions of structures, foundations like retaining walls, industrial machines and platforms in offshore areas are commonly subjected to eccentrically inclined loads. This type of loading significantly affects the overall stability of shallow foundations due to exposing the foundation into two components of loads (horizontal and vertical) and consequently reduces the bearing capacity.
Based on a numerical analysis performed using finite element software (Plaxis 3D Foundation), the behavior of model strip foundation rested on dry sand under the effect of eccentric inclined loads with different embedment ratios (D/B) ranging from (0-1) has been explored. The results display that, the bearing capacity of strip foundation is noticeably decreased with the increase of inclination angle (α) and eccentricity ratio (e/B). As well as, a reduction factor (RF) expression was appointed to measure the degree of decreasing in the bearing capacity when the model footing is subjected to eccentric inclined load. It was observed that, the (RF) decreases as the embedment ratio increases. Moreover, the test results also exhibit that, the model footing bearing capacity is reduced by about (69%) when the load inclination is varied from (0° to 20°) and the model footing is on the surface. While, the rate of decreasing in the bearing capacity was found to be (58%), for both cases of footing when they are at embedment ratios of (0.5 and 1.0). Also, a comparative study was carried out between the present results and previous experimental test results under the same conditions (soil properties and boundary condition). A good agreement was obtained between the predicted bearing capacities for the two related studies.

Keywords: strip foundation, inclined loads, eccentricity ratio, finite element method.

تقييم قابلية تحمل الأساس الشريطي المُعرَض لأحمال مائلة غير مركزية بأستخدام طريقة العناصر المحددة

احمد مجيد علي
مدرس مساعد
قسم هندسة البناء والإنشاءات, الجامعة التكنولوجية/ بغداد

الخلاصة

في الظروف الحقيقية لأسس المنشآت مثل الجدران الساندة, المكائن الصناعية و منصات في مناطق بحرية تكون مُعرضة إلى أحمال مائلة بشكل غير مركزي. هذا النوع من التحميل يؤثر بشكل مهم على كامل إستقرارية الأسس الضحلة نتيجة تعرُض الأساس إلى مركبتين من الأحمال (أفقية وعمودية) وبالتالي تقلل من قابلية التحمل.
إعتماداً على تحليل عددي أُنجز بأستخدام برنامج يعتمد على طريقة العناصر المحددة (Plaxis 3D Foundation), فإن تصرف نموذج الأساس الشريطي المستند على رمل جاف و تحت تأثير أحمال مائلة غير مركزية وبنسب غرز (D/B) مختلفة تتراوح من (0-1) قد تم التحري عنه. تظهر النتائج بأن قابلية تحمل الأساس الشريطي تقل بشكل ملحوظ بزيادة زاوية الميلان و نسبة اللامركزية. أيضاً, مصطلح معامل التقليل قد أُعتمد لقياس درجة النقصان في قابلية التحمل أثناء تعرض الأساس إلى حمل مائل غير مركزي. وقد لوحظ إن معامل التقليل يقل عندما تزداد نسبة الغرز. علاوة على ذلك, تظهر نتائج الفحوصات بأن قابلية تحمل نموذج الأساس يقل بنسبة حوالي (69%) عندما يتغير ميلان الحمل من (0-20 °) ونموذج الأساس يكون على السطح. بينما, وُجِد أن نسبة النقصان في قابلية التحمل هي (58%) وذلك لكلا الحالتين والذي عندما يكون فيها الأساس عند نسب غرز (0.5- 1.0).

أُنجزت دراسة مقارنة بين النتائج الحالية ونتائج فحوصات مختبرية سابقة تحت نفس الظروف (خواص التربة, حالة الحدود). تم الحصول على توافق جيد بين قابليات التحمل المخمنة للدراستين المقصودتين.
الكلمات الرئيسية: أساس شريطي, احمال مائلة, نسبة اللامركزية ,طريقة العناصر المحددة

1. INTRODUCTION

Based on the review of the existing literatures related to the bearing capacity of shallow foundations, it seems a limited attention has been paid to predict the ultimate bearing capacity when the foundation is subjected to eccentric and inclined loads. Hence, the paucity of the numerical and experimental studies concerning the eccentrically inclined loads gives the impulsion to carry out numerous researches in this field.

However, loads on footings are normally eccentric and inclined, as shown in **Fig 1**. Loading a footing eccentrically will reduce the bearing capacity of the footing. An off-center load will increase the stress (edge stress) on one side and decrease it on the opposite side. **Purkayastha and Char**, **1977** analyzed the method of the stability of slip surfaces that used for computing the bearing capacity of eccentrically loaded footing. A close agreement was noticed between the theoretical and experimental values for the plane strain case.

Saran and Agarwal, 1991 theoretically assessed the bearing capacity of strip footing under eccentricity and inclined loads. The derived equation from that analysis is expressed as:

$$q_{(e/B,\alpha)} = D\,\gamma\,N_{q\,(e/B,\alpha)} + 1/2\,B\,\gamma\,N\gamma_{(e/B,\alpha)} \quad (1)$$

Where

$N_{q\,(e/B,\alpha)}$ and $N\gamma_{(e/B,\alpha)}$ are the bearing capacity factors which are in terms of inclination angle (α) and eccentricity load (e). They are available in tubular and graphical form in the original paper.

Gottardi and Butterfield, **1993** used an alternative approach using "interaction diagram" to relate different loading components at failure for strip footing subjected to eccentrically inclined load on sand. They revealed that, the sign of the eccentricity is important in relation to the direction of the horizontal load.

Loukidis et.al, 2008 employed the finite element method to determine collapse load of a rigid strip footing placed on a uniform layer of purely frictional soil subjected to inclined and eccentric loading. Two series of analyses were performed, one using an associated flow rule and the other using a non-associated flow rule. The results showed that, the inclination factor depends on the value of the friction angle, whereas the effective width (B′) does not. Also, laboratory model tests were carried out by **Pritam Dhar et.al, 2013** to investigate the load-inclined and eccentric load under different shapes of model footing.

2. FINITE ELEMENT ANALYSIS AND MESH DESICRETIZATION

A numerical analysis using (Plaxis 3D Foundation) software has been employed to separately characterize the load- settlement relationships of model strip footing. Geometry of mesh generated has planer dimensions of 0.5m (width), 1m (long) and 0.65m in depth. The model foundation dimensions are (500mm) in length and (100mm) in width and has a thickness of (30mm), simulated as mild rigid steel material. The type of soil element used is 15-nodes wedge element, composed of 6- triangular nodes in horizontal direction; and 8- quadrilateral nodes in vertical direction.

The mesh modeled in this case consists of (4026 and 1316) for number of nodes and elements respectively. The choice of 15-noded wedge element was made because the later demonstrates a higher rate of convergence and superior numerical performance than the other types of nodes (i.e. 6

node elements) especially for the dense sand where the intense of strain localization exists, **Loukidis et.al, 2008**. Layout of mesh geometry at different positions of footing is illustrated in **Fig. 2**.
Plaxis automatically imposes a set of general fixities to the boundaries of geometry model. These conditions are generated according to the following rules:
Vertical model boundaries with their normal to x-direction (parallel to y-z directions) are fixed in x-direction and free in y and z directions. Also, vertical model boundaries with their normal in z-direction are fixed in that direction and free in xy plane. While model boundaries neither in x- nor in z- direction are fixed in x and z- direction (displacements in these direction equal to zero) and free in y- direction. The model boundaries for bottom and ground surface are fixed and free respectively in the all directions.
To get a better representation of the interaction between the soil and the foundation, reduction factor R_{int} was used as a value of (0.8). The soil mechanical behavior is modeled using an elastic – perfectly plastic constitutive model following the Mohr– Coulomb failure criterion. Since all the calculations are based on the main input parameters; stiffness and shear strength materials, it can be emphasized in **Table 1**.

2.1 Definition of Problem to be analyzed

This research is concerned with the study of the bearing capacity of a model strip footing of width B, supported by dense sand and located at different depths (D_f/B i.e. 0, 0.5 and 1) at and below the ground level, under the action of eccentric inclined loads. The effect of inclination angles which are varied from (α=0, 5, 10, 15 to 20). Eccentricity ratio (e/B) was chosen as (0, 0.05, 0.1 and 0.15) to satisfy the safe design criterion (e< B/6) so as to avoid tension between the foundation and soil. All soil properties and foundation details used and the boundary condition in this study have been adopted from **Atalar et.al**, **2013.**

3. COMPARATIVE STDY WITH PREVIOUS EXPERIMENTAL RESULTS

Since, the present study has employed the same boundary conditions and the soil properties that were used by **Atalar et.al. 2013** but, the objective is extremely different. So, the comparison between the present numerical test results and the experimental ones in the form of ultimate bearing capacity has been done and listed in Table 2. In most cases, the deviations as demonstrated in col. (3) are less than ±15. The summation of these deviations value was about (7.65%), which is mean the degree of convergence between the numerical and experimental results is (92.35%) and provided an excellent agreement in estimating the ultimate bearing capacity of model strip footing subjected to eccentrically inclined load. The correlation between the previous experimental work and the present numerical is better clarified in **Fig.3**.

4. ANALYSIS AND DISCISSION OF TEST RESULTS

Bearing capacity of model strip footings for all tests conducted in this study has been obtained. The coupled effect of combined loads and the eccentricity on the behavior of footing was clarified. As well as, the mechanism of failure under different conditions of loading has also been implied. The criterion adopted in this study is that proposed by **Terzaghi, 1943** by which the failure load is defined as the load required to cause a settlement corresponding to 10% of footing width.

4.1 Effect of Load Eccentricity

Obviously when the load is directly applied at the center of footing, it will be subjected to a vertical displacement almost equal at each point below the footing (i.e. footing is rigid). **Fig. 4** represents the relationship between the pressure and settlement for centrally loaded footing at different embedment ratio (D_f/B).

As shown in **Fig. 4**, it can be observed that, as the eccentricity ratio increases the bearing capacity of model footing to sustain the imposed loads decreases. This issue is true for all off-centrally loaded footing, at which the model footing is confronted to rotating moment about the edge. The model footing will tilt toward the side of the eccentricity and the contact pressure increases on the side of tilt and decreases on the opposite side. As though the failure resulted in the supporting soil on the side at which the load is acted. The ultimate capacities of model footings for different cases are presented in **Fig.5.**

It is noticed that, and according to the loading curves explained above, the type of failure is general shear failure even for the tests carried out at off-central loading. This observation is compatible with **Murthy**, **2002** who stated that if the eccentricity is small (e<B/6), the load required to produce this type of failure is almost equal to the load desired for producing a symmetrical general shear failure. However, the moment counteracted about the foundation has a direct proportion with the eccentricity value and its effect is listed in **Fig. 6**.

Clearly, the values of moment that work against rotating action is increased as the distance from the center of gravity of foundation is increased. Since, the mobilized moment which tries to prevent the footing to topple is a function of vertical component of inclined load (i.e. M= v. e) thus, it is deduced that, the increase in moment when the model footing was placed at embedment ratio of (0.5 to 1) at eccentricity ratio of (0.15) was (80 and 136%) respectively in the comparison with the case of surface footing (D_f/B= 0).

This condition is justified to the fact that, installing the footing at a nominated depth and restricted by surrounding soil and which the footing will be resisted by the passive forces exerted by soil bounded the footing. Therefore, presence of the soil at the both sides of footing causes to intensify the passive region which in turn push against the active region below the footing directly and consequently, the footing will contain more external loads, than of the case when the model footing is placed on the surface. **Fig. 7** is presented to understand the failure mechanism and what happens when the model footing is loaded by a vertical eccentric loading (e> 0 and α= 0).

According to **Bransby and Randolph, 1998** the collapse mechanism when the footing is loaded by off-center vertical load consists of wedge and rotation parts. The wedge has two components: a passive wedge and a fan region. The wedge part lies to the side of footing, on the side upon which the load is applied. Plastic shearing occurs in side of the fan and the passive wedge. In contrast, the plastic strains in the rotation part located on the other side of mechanism tends to occur along the single shear band bounding the rotating part, with only minimal plastic deformations developing inside the rotating part.

4.2 Effect of Load Inclination

Exactly (15) model tests were conducted to investigate the influence of centrally inclined loads (e/B=0) at different inclination angles (α) changing from (0°, 5°, 10°, 15° to 20°) and embedment ratio (D_f/B= 0, 0.5 and 1.0). The effects of these parameters on the values of bearing capacity are shown in **Fig. 8**. As was expected, the maximum value of load that the model footing can be reached is at the case of (i.e. α=0). It is noticed that, the ultimate bearing capacity decreases as the inclination angle increases.

The test results also exhibited the model footing bearing capacity is minimized by about (69%) when the load inclination is varied from (0° to 20°) and the model footing is on the surface. However, the rate of decreasing in the bearing capacity was recorded as (58%), for the both cases of footing when they are at embedment ratios of (0.5 and 1.0). From the findings mentioned above, it is

observed that, the bearing capacity of footing is affected with the embedment ratio in addition to the inclination angle. This justification is attributed to the fact that, the amount of reduce in the bearing capacity of surface footing is larger than that of the cases when the model footing is installed at deeper distance ($D_f/B > 0$).

Normally, the surface footing that subjected to inclined load will be exposed into two components of loads, vertical and horizontal forces. The vertical component is already checked for the bearing capacity purposes. As for the horizontal force, the model footing will be subjected to sliding effect, causing to reduce of entire stability of footing. Since the footing on the surface is free and unbounded from all the direction of the planer area, the horizontal resistance is a function of vertical load according to the expression ($H= V \tan\delta$), meaning that horizontal force is mainly dependent on the friction between the soil and the foundation and the vertical component of loading.

When the model footing is constructed at a certain depth into the ground, the model footing will be confined by the surrounding soil, and the footing will be considerably withstand against sliding action. This may refer to the presence of passive forces exerted on the footing base resulting from the adjacent soil. Therefore, the horizontal force beneath the footing base can be formulated as shown:

$$H= V \tan\delta+ P_p \quad (2)$$

Where the (H) is the horizontal resistance of footing, (V) is the vertical component of loading, (δ) is a coefficient of friction and (P_p) is the passive force exerted on the footing which depends upon the friction angle **(**φ) and the soil density (γ). For these reasons, it may be said that, the sliding action is started to minimize as the embedment ratio increases.
In the case of central inclined loading ($e= 0, \alpha> 0$) as shown in **Fig. 9**, there is no rotation part in the failure mechanism, which is largely one-sided containing a passive wedge, fan and a rigid tapered wedge below the footing base that pushes against the fan region. A very small passive wedge is observed on the side of mechanism opposite the side of footing where the inclined load points.

4.3 Effect of Eccentrically Inclined Load on Bearing Capacity

In this section, the combined effect of the inclination angle and eccentricity ratio at different embedment ratios was together analyzed. A total of 31 model tests were performed (with regardless of the cases of eccentric and inclined vertical loading which have been mentioned before) for identifying the coupled influence of eccentrically inclined load on the behavior of bearing capacity of model strip footing. The influence of these factors is illustrated in **Fig. 10**.
As seen in these plots, the bearing capacity of footing has an inverse proportion with the eccentricity ratio and the angle of inclination. This principle is consistent for all the values of embedment ratio. The complicated interaction between these parameters is required using reduction factor concept. The term "RF" is used to express and compare the test data from different loading condition. So, the change in the term of bearing capacity is expressed and displayed as the following:

$$RF=1 - \frac{q_{(\frac{Df}{B}, \frac{e}{B}, \alpha)}}{q_{(Df/B,\ e/B= 0,\ \alpha=0)}} \quad (3)$$

Where RF is reduction factor, $q_{(Df/B,\ e/B,\ \alpha)}$ is the ultimate bearing capacity of footing with different values of eccentricity ratio and the angle of inclination at a specific embedment ratio, $q_{(Df/B,\ e/B=0,\ \alpha=0)}$

is a bearing capacity of footing subjected to centric vertical load and placed at a certain depth. A reduction factor has been proposed to estimate the variation of the bearing capacity when the model footing is exposed to eccentrically inclined load and the degree of reduction with respect to the reference case (e= 0, α= 0) at similar embedment ratio.

It can be noted that, the embedment ratio has a significant effect on the bearing capacity of model footing at different values of the eccentricity and inclination. All curves nearly trend to have the same behavior when the footing is loaded under eccentrically inclined loads. According to calculations which have been carried out to assess the decrease of bearing capacity using RF, the magnitude of reduction in the bearing capacity starts to increase with the increase of eccentricity ratio.

Also, in general speaking, the reduction factor is decreased as the depth where the model footing placed is increased especially for the case of load inclination of (10°) and thereafter to (20°). Details of the reduction factor of the model footing at different conditions are displayed in **Table 2**. It is found that, the decreasing of bearing capacity is raised as the eccentricity and the inclination angles are increased. As well as, attaining from the (α= 10), the reduction factor at an eccentricity ratio of (0.15) is converted from (63.8 to 49.3%) when the embedment ratio increased from (0 to 1), and for the same ratio, the reduction factor is varied from (73.0 to 61.2%) and (82.9 to 65.6%) when the load is applied at an angles of 15° and 20°) respectively.

This state can be justified to placing the model footing at a certain depth will increase the bearing capacity by reducing the ability of model footing to slide or to overturn due to the eccentric inclined load. Therefore, presence of the footing below the ground level can minimize these effects by the increase of base resistance to the horizontal forces and reduce the upheaval of soil at the side of footing where the point of load is applied at which the model will be supported by stronger region. Consequently, the amount of decreasing in the bearing capacity or by other words the reduction factor is decreased.

5. CONCLUSIONS

Based on the results of this investigation, the following main conclusions can be drawn:

1. Bearing capacity of model footing is separately reduced with both of the inclination angle (α) and eccentricity ratio (e/B), and this effect appears largely when the model footing is exposed to eccentrically inclined load directly.
2. A pronounced influence of the inclination angle on the ultimate capacity of footing presents that, the footing capacity is decreased by (8, 31, 51 and 70%) for (α=5°, 10°, 15° and 20°) respectively and at D_f/B= 0 and e/B=0. For the case of D_f/B= 0.5 and e/B=0, the ultimate capacity is minimized by (8, 25, 39 and 58%) for D_f/B= 0.5 and e/B=0. Also, the footing capacity is reduced by (9, 30, 50 and 57%) for the case of D_f/B= 1 and e/B=0.
3. The increase of mobilized moment (M= v. e) was obtained about (80 to 136%) at maximum eccentricity ratio (0.15) and embedment ratio of (0.5 to 1.0) respectively, as compared with the surface footing case.
4. The reduction factor (RF) trends to decrease as the embedment ratio increases, and decrease significantly with the eccentricity ratio and inclination angle.
5. The effects of sliding and overturning due to eccentric inclined load are minimized when the model footing is placed at a certain depth below ground level.

REFERENCES

- Atalar, C., Patra C.R., Das B.M., and Sivakugan N., 2013, *Bearing Capacity of Shallow Foundation Under Eccentrically Inclined Load*, Proceedings of the 18th International Conference on Soil Mechanics and Geotechnical Engineering, Paris.

- Bransby, M.F., and Randolph, M.F., 1998, *Combined Loading of Skirted Foundations*, Geotechnique, vol. 48, issue (5), PP. 637–655.

- Gottardi, G., and Butterfield, R., 1993, *on The Bearing Capacity of Surface Footings on Sand Under General Planar Loads*, Soils and Foundations, vol. 33, issue (3), PP. 68–79.

- Loukidis D., Chakraborty T., and Salgado R., 2008, *Bearing Capacity of Strip Footings on Purely Frictional Soil Under Eccentric and Inclined Loads*, Canadian Geotechnical Journal, vol. 45, PP. 768-787.

- Pritam D., Soumya, R., and Bikash, C.C., 2013, *Behavior of Rigid Footing Under Inclined and Eccentric Loading*, Journal of Annals of Pure and Applied Mathematics, Vol. 5, issue (1), PP. 71-81.

- Purkayastha, R.D. and Char, R.A.N., 1977, *Stability Analysis for Eccentrically Loaded Footings*, Journal of the Geotechnical Engineering Division, ASCE, vol. 103, issue (6), PP. 647-651.

- Saran, S. and Agarwal, R.K., 1991, *Bearing Capacity of Eccentrically Oblique Loaded Foundation*", Journal of Geotechnical Engineering, ASCE, vol.117, issue (11), PP. 1669-1690.

- Murthy, V.N.S., 2002, *Principles and Practices of Soil Mechanics and Foundation Engineering*, Marcel Dekker Inc., New York.

NOMENCLATURE

B and B^{-}= actual and effective footing width, m.
Cu= cohesion of soil, kPa.
D_f = excavated footing depth, m.
D_f/B = embedment ratio, dimensionless.
E_s = modulus of elasticity, kPa.
e = eccentricity, m.
e/B = eccentricity ratio, dimensionless.
H = horizontal resistance of footing, kN.
M = applied moment, kN.m.
N_q and N_γ = bearing capacity factors, dimensionless.
P_p = passive force of soil, kN.
RF = reduction factor in bearing capacity, dimensionless.
R_{int} = interface reduction factor, dimensionless.
R^2 = coefficient of regression, dimensionless.
V = vertical applied load, kN.
α = inclination angle, degree.

γ = unit weight of soil, kN/m^3.
δ = angle of wall friction, degree.
φ = angle of internal friction, degree.
ψ = angle of dilation, degree.

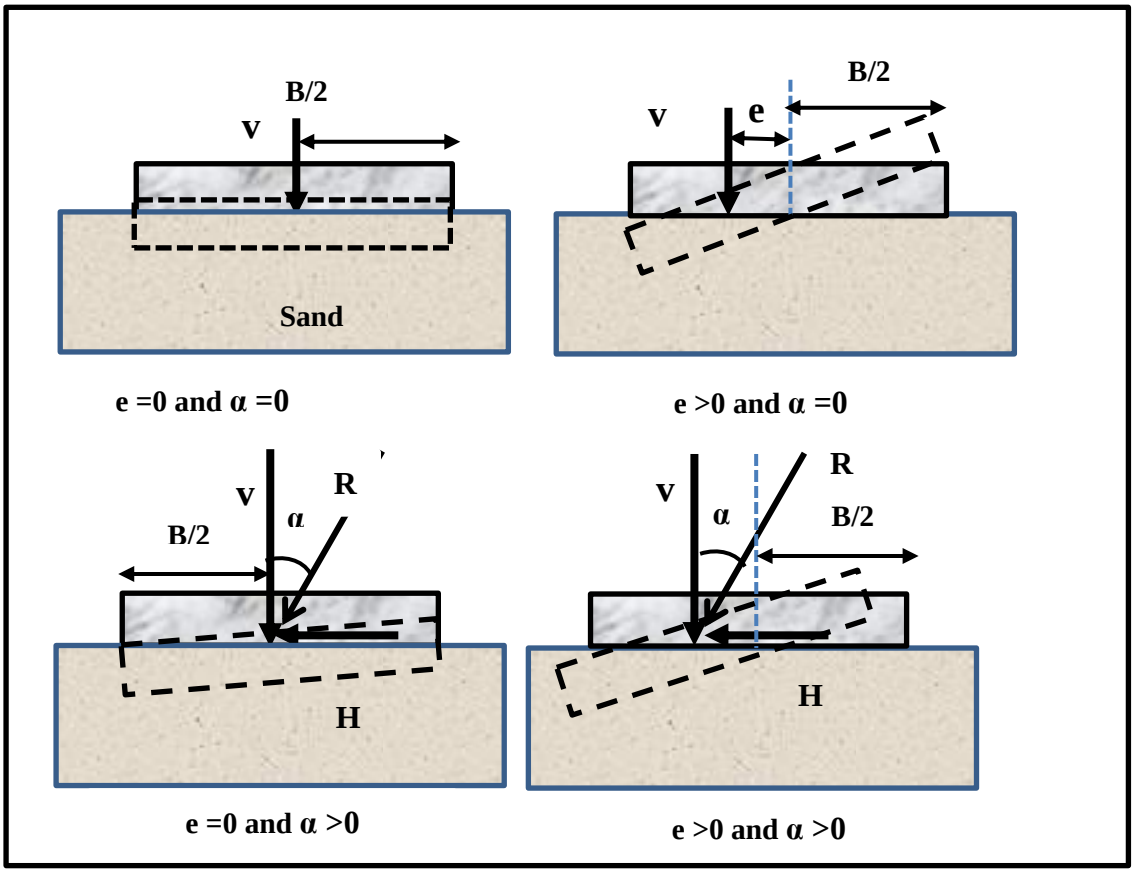

Figure 1. Footing loading condition where R, V and H are resultant, vertical and horizontal loads respectively.

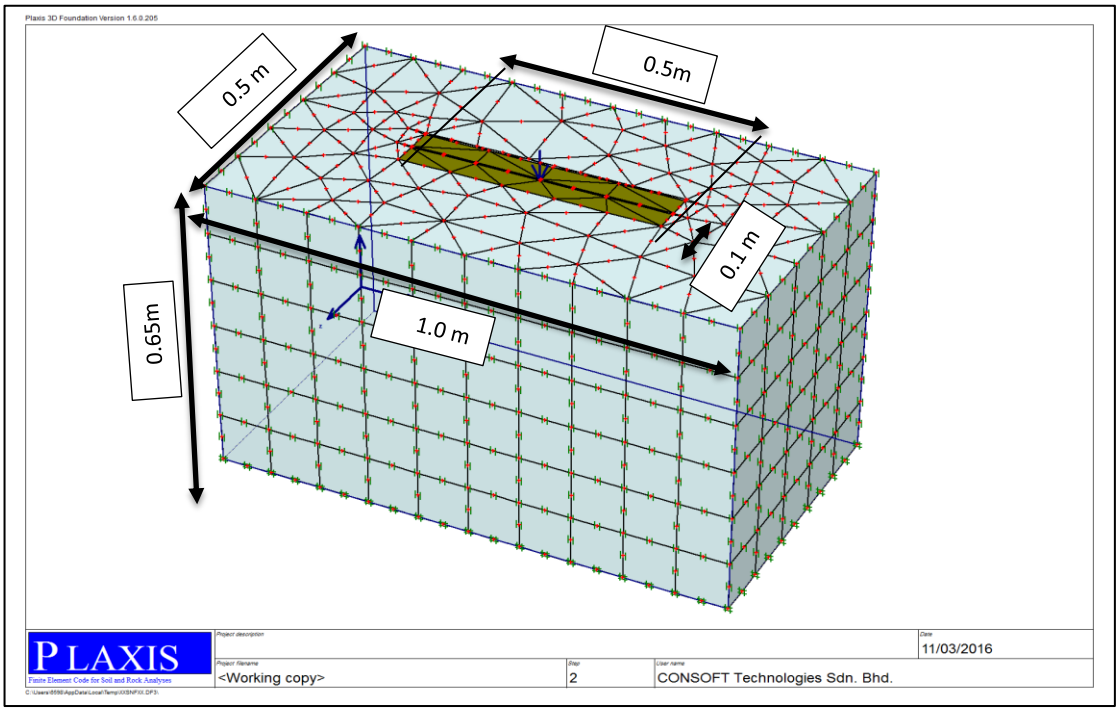

Figure 2a. Geometry of mesh boundary when footing is installed at $D_f/B=0$

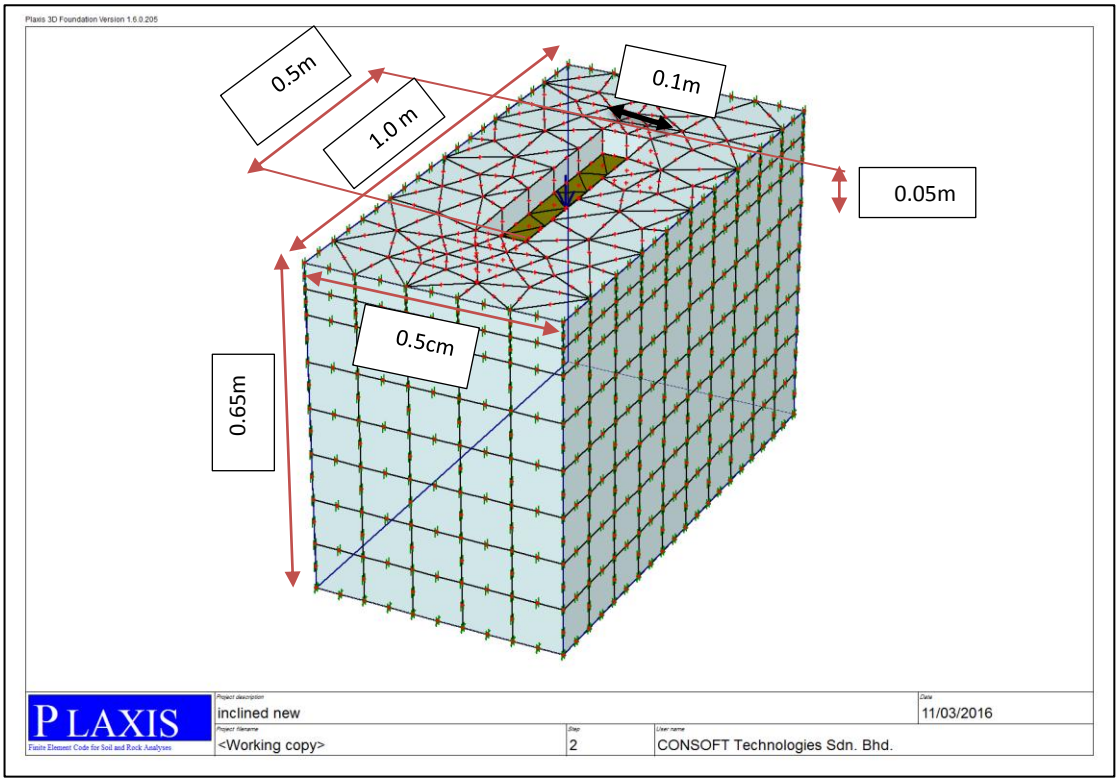

Figure 2b. Geometry of mesh boundary when footing is installed at $D_f/B=0.5$

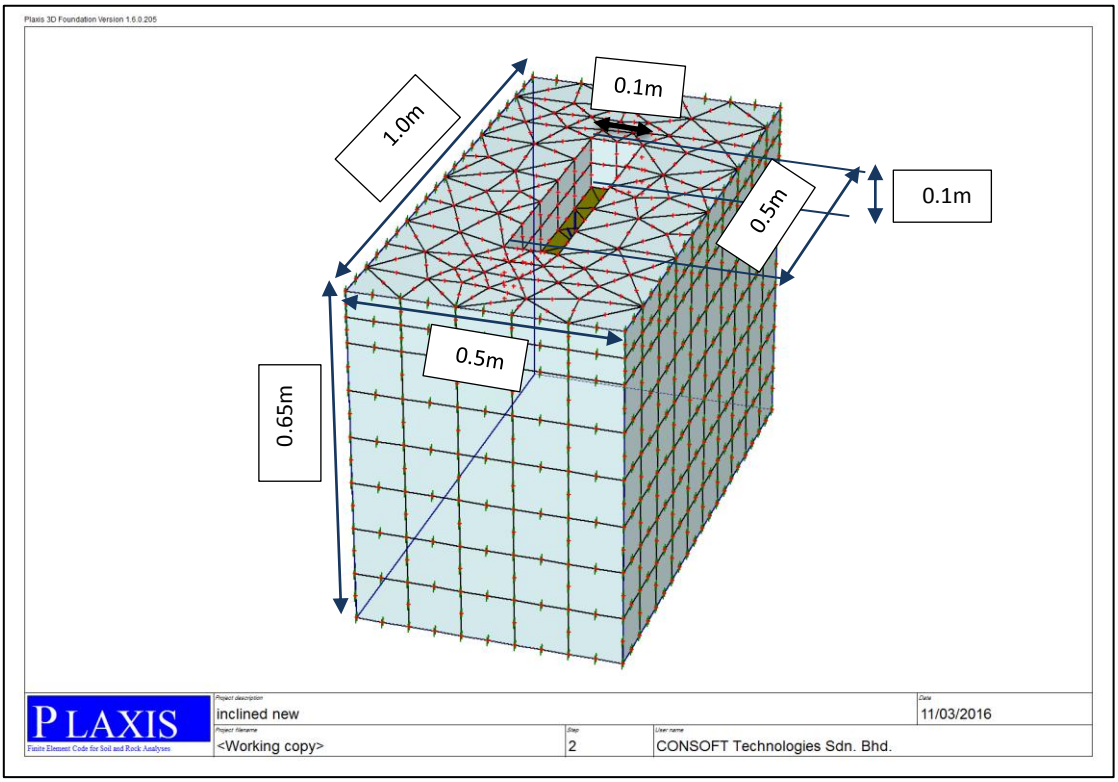

Figure 2c. Geometry of mesh boundary when footing is installed at A) $D_f/B=1$

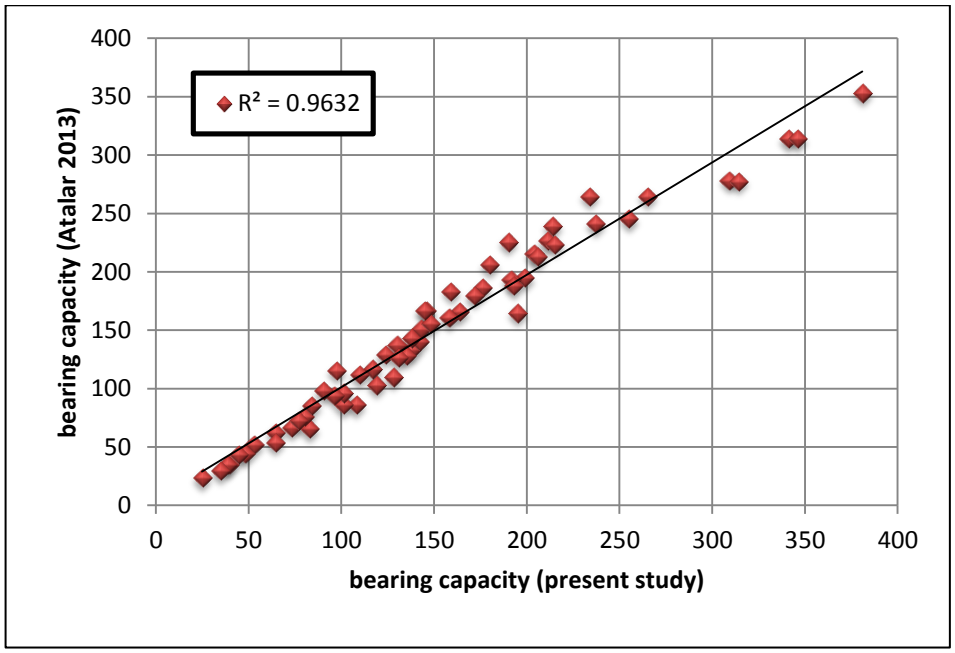

Figure 3. Comparison between bearing capacity values for present and previous studies.

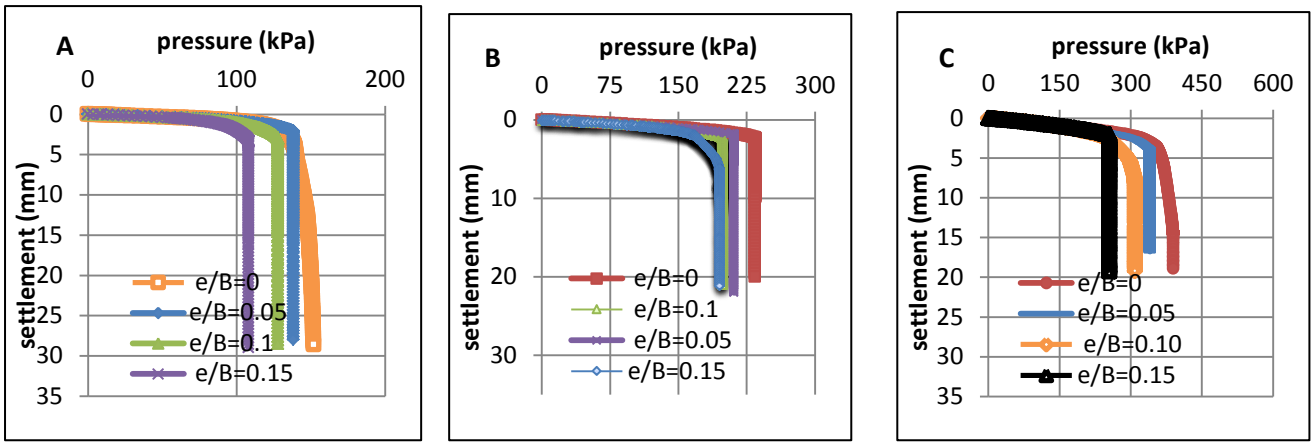

Figure 4. Pressure-settlement relationship of eccentrically vertical loaded model footing at values of embedment ratio of A) D_f/B =0, B) D_f/B =0.5 and C) D_f/B =1.0.

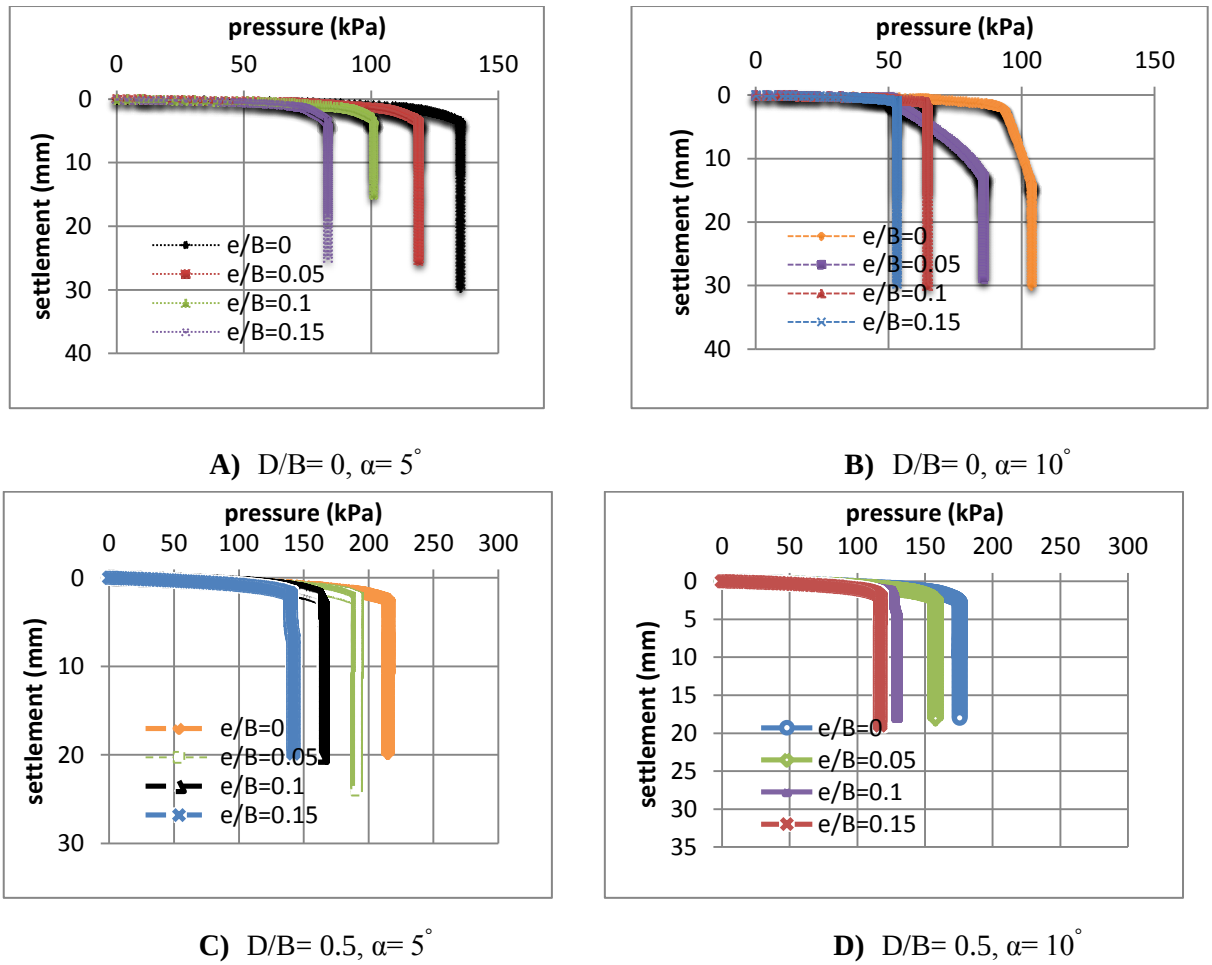

A) D/B= 0, α= 5°

B) D/B= 0, α= 10°

C) D/B= 0.5, α= 5°

D) D/B= 0.5, α= 10°

Figure 5. Stress- settlement curves for all models that have been analyzed at different conditions of loading.

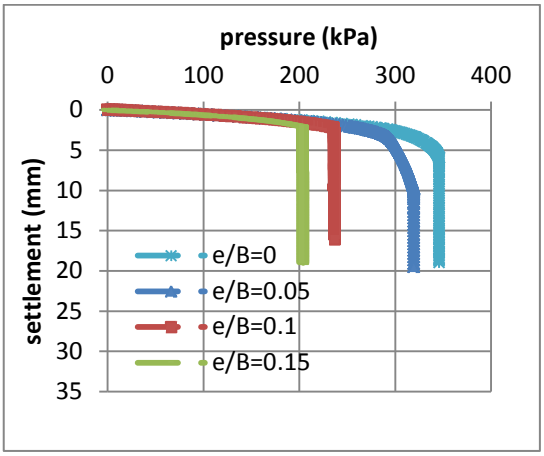

E) D/B= 1.0, α= 5°

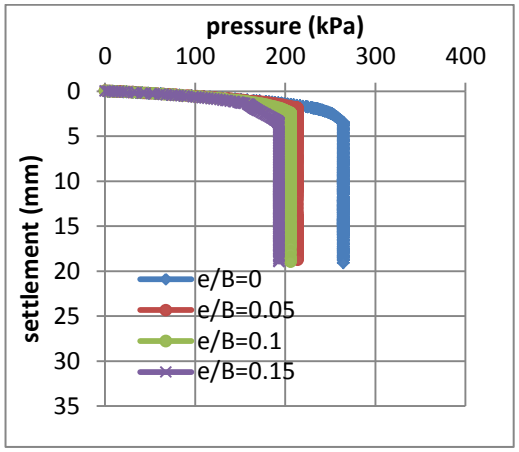

F) D/B= 1.0, α= 10°

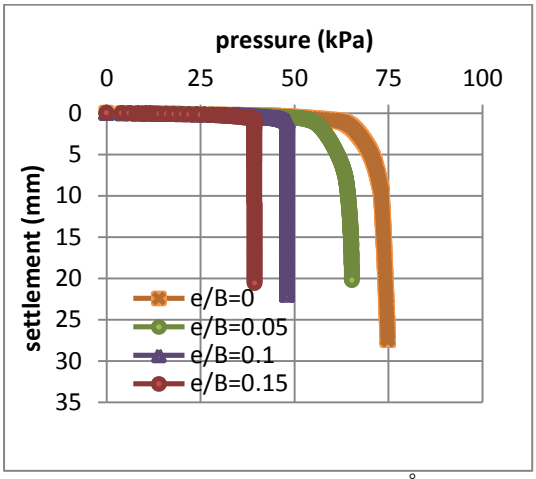

G) D/B=0, α= 15°

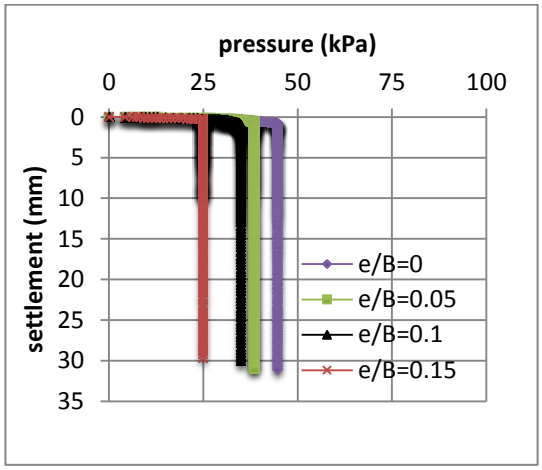

H) D/B=0, α= 20°

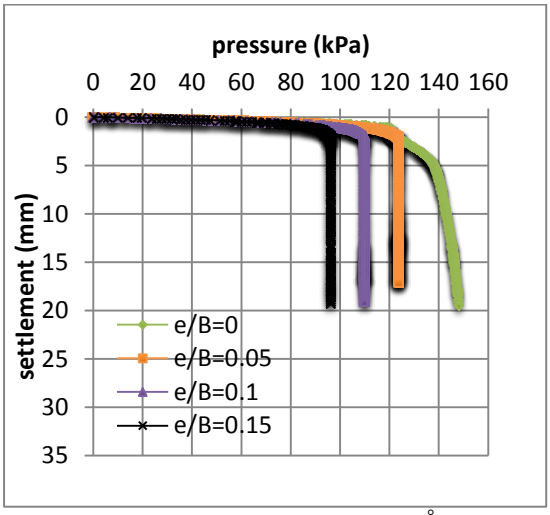

I) D/B=0.5, α= 15°

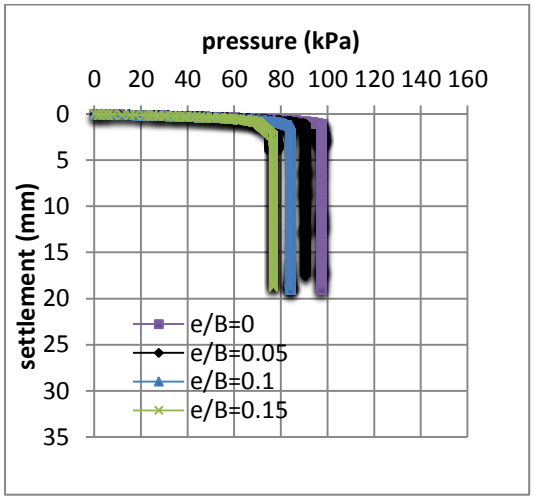

J) D/B=0.5, α= 20°

Figure 5. Continue.

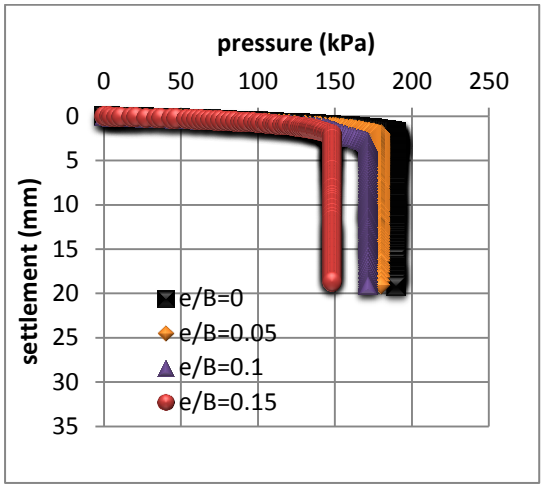

K) D/B= 1.0, α= 15°

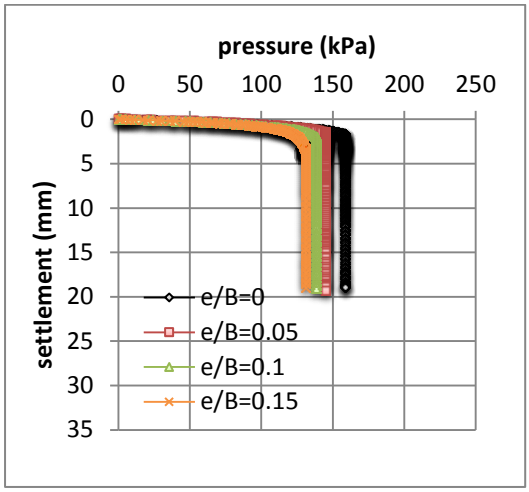

L) D/B= 1.0, α= 20°

Figure 5. Continue.

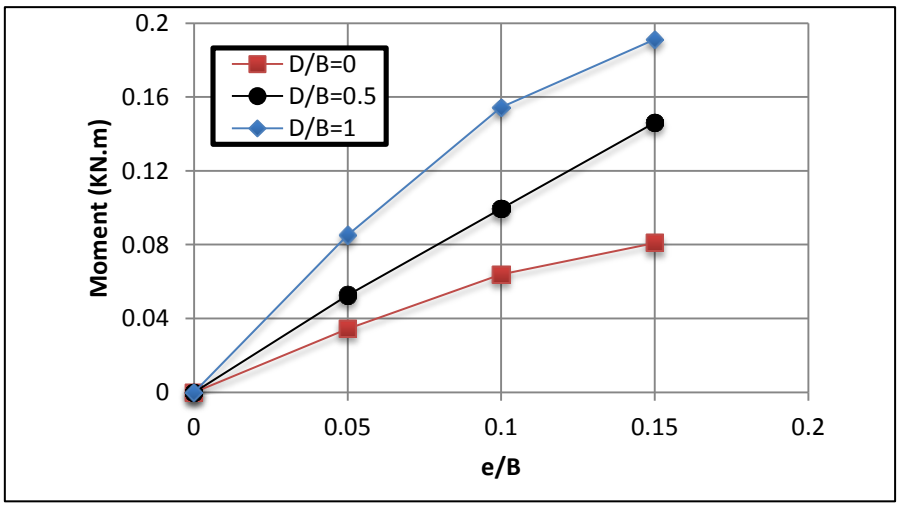

Figure 6. Maximum moment vs. eccentricity ratio relationship of vertically eccentric footing.

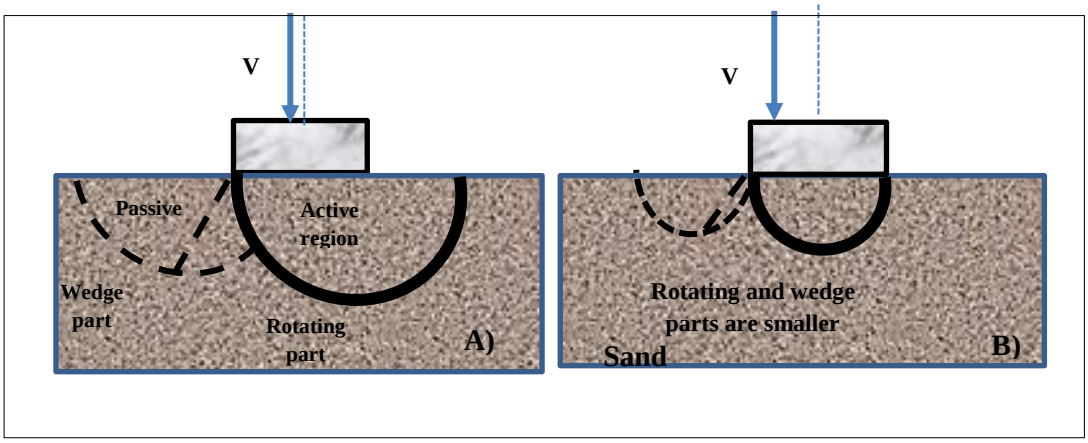

Figure 7. Mechanism of failure of eccentric vertical loaded footing A) e<B/6 and B) e>B/6.

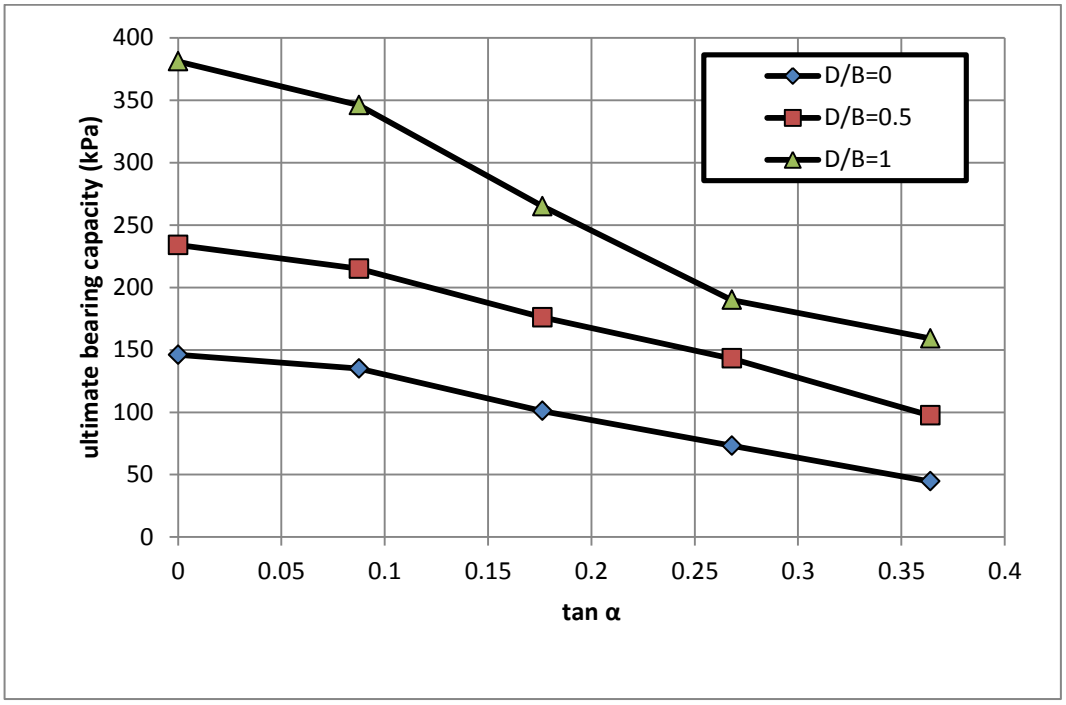

Figure 8. Effect of load inclination on the bearing capacity at different embedment ratio.

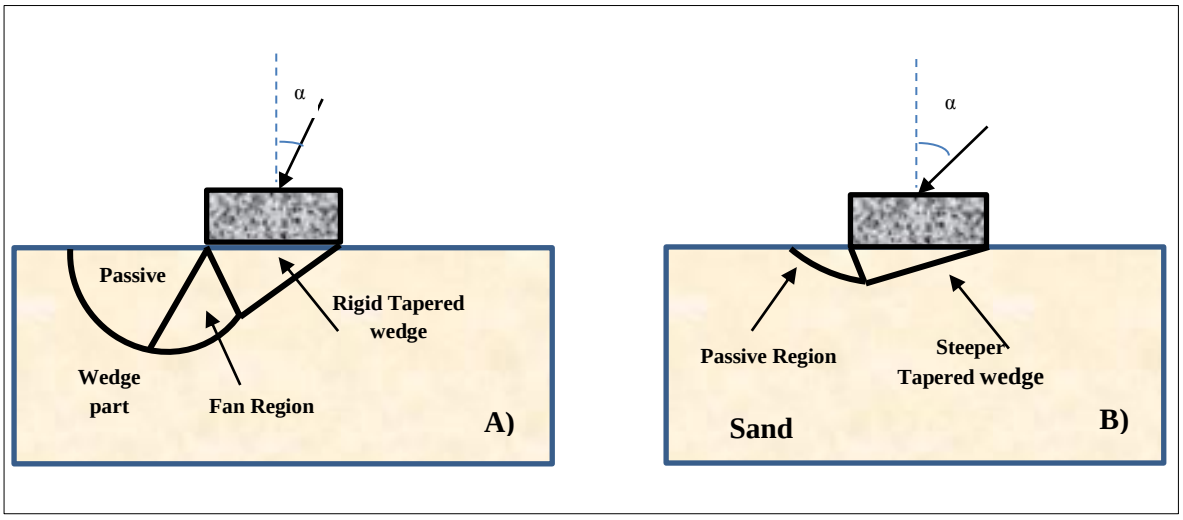

Figure 9. Mechanism of failure of centric inclined loaded footing A) α= 10° and B) = 20°.

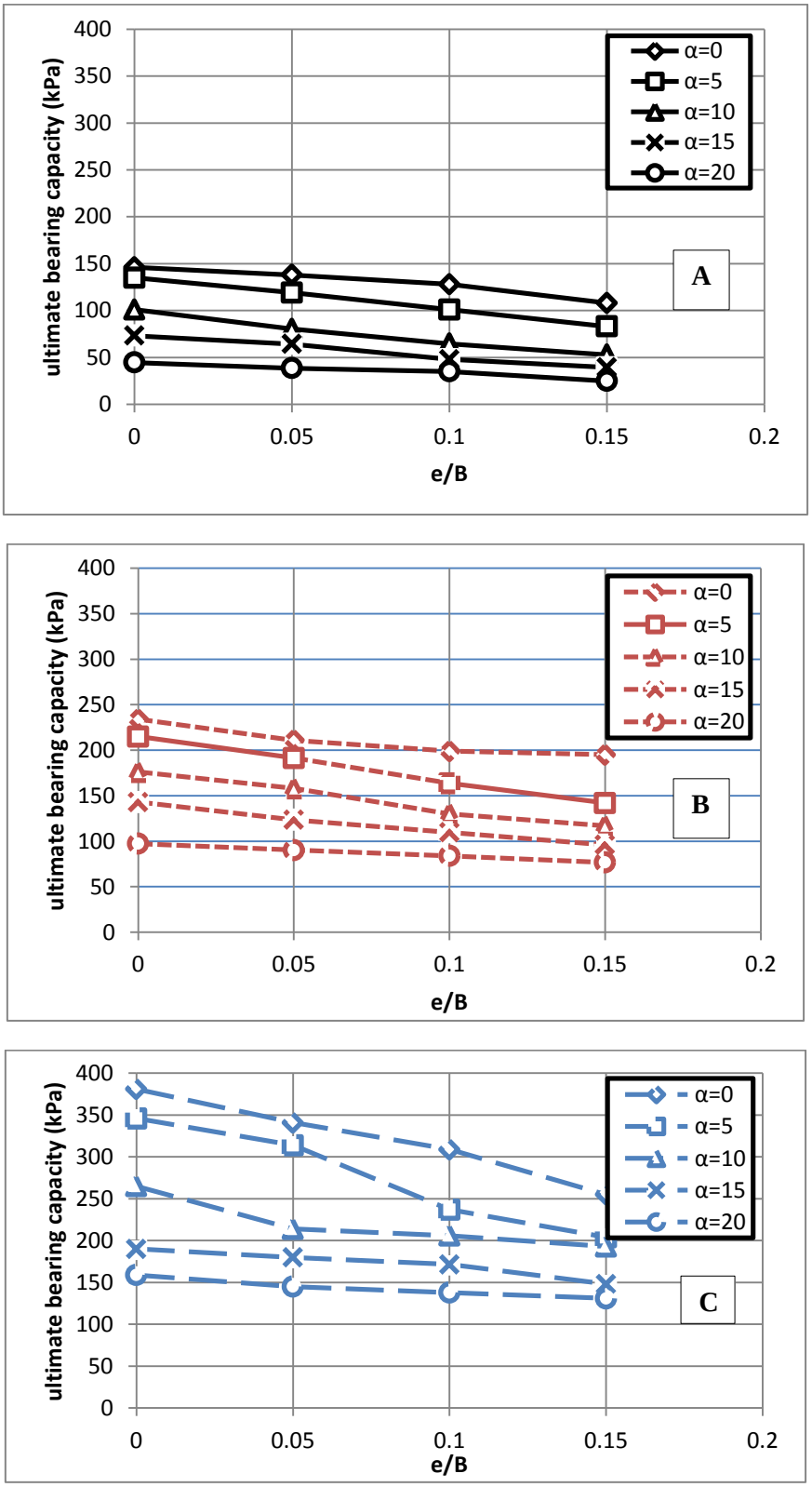

Figure 10. Effect of inclination angle and eccentricity ratio on the bearing capacity of model footing at different embedment ratios A) $D_f/B = 0$, B) $D_f/B = 0.5$ and C) $D_f/B = 1.0$.

Table 1. Parameters of soil model adopted in present study.

parameter	Index
Type of Material	Sand
Material Model	Mohr coulomb
Modulus of elasticity $\mathbf{E_S}$ (kN/m^2)	36000
Poisson's ratio, ν	0.30
Angles of internal friction φ	41°
Angle of Dilatincy ψ	11°
Cohesion $\mathbf{C_u}$ (kN/m^2)	0.001
Dry unit weight γ (kN/m^3)	14.36
Interface reduction factor $\mathbf{R_{int}}$	0.8
Stiffness of footing material (kN/m^2)	65000000

Table 2. Reduction factor and bearing capacities obtained from the present and previous studies at different cases.

No.	D_f/B	α	e/B	q_u (present study) (kPa) (1)	q_u (Atalar. et. al., 2013) (kPa) (2)	(Col.1-co12)/col.2 Deviation (3)	(RF) %
1	0	0	0	146	166.77	-12.45	**0**
2	0	0	0.05	138	133.42	3.43	**5.5**
3	0	0	0.1	128	109.87	16.50	**12.3**
4	0	0	0.15	108	86.33	25.10	**26**
5	0	5	0	135	128.51	5.05	**7.5**
6	0	5	0.05	119	103.01	15.52	**18.5**
7	0	5	0.1	101	86.33	16.99	**30.8**
8	0	5	0.15	83	65.73	26.27	**43.2**
9	0	10	0	101	96.14	5.06	**30.8**
10	0	10	0.05	80.4	76.52	5.07	**44.9**
11	0	10	0.1	64.6	62.78	2.89	**55.8**
12	0	10	0.15	52.9	51.99	1.75	**63.8**
13	0	15	0	73.2	66.71	9.72	**49.9**
14	0	15	0.05	64.3	53.96	19.16	**56**
15	0	15	0.1	48	44.15	8.72	**67.1**
16	0	15	0.15	39.4	35.12	12.18	**73**
17	0	20	0	44.6	43.16	3.33	**69.5**
18	0	20	0.05	38.5	34.83	10.53	**73.6**
19	0	20	0.1	35	29.43	18.92	**76.02**
20	0	20	0.15	24.9	23.54	5.77	**82.9**
21	0.5	0	0	234	264.87	-11.65	**0**
22	0.5	0	0.05	211	226.61	-6.88	**9.8**
23	0.5	0	0.1	199	195.22	1.93	**15**
24	0.5	0	0.15	195	164.81	18.31	**16.7**
25	0.5	5	0	215	223.67	-3.87	**8.1**
26	0.5	5	0.05	191.5	193.26	-0.91	**18.2**
27	0.5	5	0.1	163.8	165.79	-1.20	**30**
28	0.5	5	0.15	142	140.28	1.22	**39**
29	0.5	10	0	176	186.39	-5.57	**24.8**
30	0.5	10	0.05	158	160.88	-1.79	**32.5**
31	0.5	10	0.1	130	137.34	-5.34	**44.4**
32	0.5	10	0.15	117	116.74	0.22	**50**
33	0.5	15	0	143	151.07	-5.34	**38.9**
34	0.5	15	0.05	123.6	129.49	-4.54	**47.2**

35	0.5	15	0.1	109.8	111.83	-1.81	**53.1**
36	0.5	15	0.15	96	94.18	1.93	**59**
37	0.5	20	0	97.4	115.76	-15.86	**58.4**
38	0.5	20	0.05	90.3	98.1	-7.95	**61.4**
39	0.5	20	0.1	84	85.35	-1.58	**64.1**
40	0.5	20	0.15	76.8	72.59	5.79	**67.2**
41	1	0	0	381	353.16	7.88	**0**
42	1	0	0.05	341	313.92	8.62	**10.5**
43	1	0	0.1	309	278.6	10.91	**18.9**
44	1	0	0.15	255	245.25	3.97	**33.1**
45	1	5	0	346	313.92	10.21	**9.2**
46	1	5	0.05	320	277.62	15.26	**17.6**
47	1	5	0.1	237	241.33	-1.79	**37.8**
48	1	5	0.15	204	215.82	-5.47	**46.5**
49	1	10	0	265	264.87	0.04	**30.4**
50	1	10	0.05	214	239.36	-10.59	**43.8**
51	1	10	0.1	206	212.88	-3.23	**45.9**
52	1	10	0.15	193	188.35	2.46	**49.3**
53	1	15	0	190	225.63	-15.79	**50.13**
54	1	15	0.05	180	206.01	-12.62	**52.8**
55	1	15	0.1	171.6	179.52	-4.41	**55**
56	1	15	0.15	148	155.98	-5.11	**61.2**
57	1	20	0	159	183.45	-13.32	**58.2**
58	1	20	0.05	145	166.77	-13.05	**61.9**
59	1	20	0.1	138	143.23	-3.65	**63.8**
60	1	20	0.15	131	126.55	3.51	**65.6**
						∑|value|=7.65% =0.9235	

Some Properties of Carbon Fiber Reinforced Magnetic Reactive Powder Concrete Containing Nano Silica

Zain El-Abdin Raouf
Professor
Engineering College-
Baghdad University

Rafia H. Al-Suhaili
Professor
Engineering College
Baghdad University

Zainab H. Mahdi
Lecturer
Technical Engineering College Baghdad
Middle Technical University email:
zainabhashim@itbaghdad.net

ABSTRACT

This study involves the design of 24 mixtures of fiber reinforced magnetic reactive powder concrete containing nano silica. Tap water was used for 12 of these mixtures, while magnetic water was used for the others. The nano silica (NS) with ratios (1, 1.5, 2, 2.5 and 3) % by weight of cement, were used for all the mixtures. The results have shown that the mixture containing 2.5% NS gives the highest compressive strength at age 7 days. Many different other tests were carried out, the results have shown that the carbon fiber reinforced magnetic reactive powder concrete containing 2.5% NS (CFRMRPCCNS) had higher compressive strength, modulus of rupture, splitting tension, stress in compression and strain in compression than the corresponding values for the carbon fiber reinforced nonmagnetic reactive powder concrete containing the same ratio of NS (CFRNRPCCNS). The percentage increase in these values for CFRMRPCCNS were (22.37, 17.96, 19.44, 6.44 and 25.8) % at 28 days respectively, as compared with the corresponding CFRNRPCCNS mixtures.

Key word: nano silica, magnetic water, reactive powder concrete, carbon fiber, tap water

بعض خواص خرسانة المساحيق الفعالة الممغنطة المسلحة بألياف الكاربون الحاوية على النانو سيليكا

زين العابدين رؤوف
استاذ
كلية الهندسة-جامعة بغداد

رافع هاشم السهيلي
استاذ
كلية الهندسة-جامعة بغداد

زينب هاشم مهدي
مدرس
الكلية التقنية الهندسيةبغداد-الجامعة التقنية الوسطى

الخلاصة

تضمنت هذه الدراسة تصميم 24 خلطة من خرسانة المساحيق الفعالة الممغنطة المسلحة وغير المسلحة بألالياف، حيث تم أستخدم ماء الإسالة في اعداد 12 خلطة منها أما الـ 12 خلطة الأخرى فقد أستخدم الماء الممغنط في خلطها ، تم استخدام النانو سيليكا بنسب (1، 1,5، 2، 2,5 و3)% من وزن السمنت لجميع الخلطات وبينت النتائج إن الخلطة الحاوية على 2,5% نانو سيليكا أعطت أعلى مقاومة انضغاط بعمر 7 أيام. أجريت فحوصات أخرى مختلفة على النماذج، وبينت النتائج أن فحوص مقاومة الانضغاط , الانثناء, شد الانفلاق, إجهاد الضغط وانفعال الضغط, لخرسانة المساحيق الفعالة الممغنطة المسلحة بالياف الكاربون والحاوية على 2,5 % نانو سليكا أعلى من الخرسانة

الغير ممغنطة حيث أبدت النتائج زيادة في قيم الفحوصات للخرسانة الممغنطة بنسب (22,37, 17,96, 19,44, 6,44 و 25,8) % عند العمر 28 يوم على التتابع مقارنة بنفس الخلطات الخرسانية الغير ممغنطة.
الكلمات الدالة: نانو سليكا، الماء الممغنط، خرسانة المساحيق الفعالة, الياف الكاربون, ماء الاسالة

1- INTRODUCTION

1-1 General

Recently, nano technology attracted considerable scientific interest due to the new potential uses of particles in nano (10^{-9} m) scale. The use of nano-scale size of particles can result in dramatically improved properties from conventional grain-size materials of the same chemical composition. Thus, industries may enable to reengineer many existing products and design new and novel ones that function at unprecedented levels. Few researches are available in literature about mixing nano particles in cement- based building materials, **Bauer, et al**., 1996, **Lau** and **Hui**, 2002, **Fuji Chimera Research Institute**, 2002 and **Li et al**., 2004.

Qing et al., 2006, stated that the pozzolanic activity of nano-SiO_2 was much greater than that of silica fume and with a small amount of nano-SiO_2, the $Ca(OH)_2$ crystal at the interface between hardened cement paste and aggregate at early ages may be effectively absorbed in high performance concrete.

Collepardi et al., 2002, investigated the combination of silica fume, fly ash and amorphous nano silica in super-plasticized high performance concretes. They found that concrete with ternary combination of silica fume, fly ash and amorphous nano silica reduced amount of silica fume about 15 to 20 kg/m^3 perform as well as silica fume alone content 60 kg/m^3 in result of strength and durability

An investigation was carried out by **Jo et al**., 2007 to study the characteristics of cement mortar with nano-SiO_2 particles. Five different water/cementitious ratios were used, including 0.23, 0.25, 0.32, 0.35, and 0.48 with four contents of NS (3, 6, 9, and 12) % by weight of cement. The compressive strengths of cement mortar specimens with the addition of silica fume were also evaluated at w/cm ratio of 0.35 to compare with mortar containing nano silica particles and three contents of silica fume 5, 10, and 15% by weight of cement. The experimental results showed that the compressive strengths of mortars with NS were all higher than those of mortars containing silica fume at 7 and 28 days.

Remzi. and **Meral**., 2008, had studied the effect of nano powders on cement paste, mortar and concrete and found that the use of nano powders in concrete technology affects the cement kinetics and accelerates hydration significantly due to larger surface area, stronger electrostatic forces of nano powders, and improvement in the microstructures of concrete having nano powders.

Roddy et al., 2008, applied particulate NS in oil well cementing slurries in two specific ranges of particles sizes, one between 5 to 50 nm, and the other between 5 to 30 nm. Also they used NS dry powders in encapsulated form and concentrations of 5 to 15%

by weight of cement. The respective test results for the slurries demonstrated that the inclusion of NS reduced the setting time and increased the strength (compressive, tensile, Young's modulus and Poisson's ratio)

Abbas, 2009, carried out an investigation to study the influence of nano-silica addition on properties of conventional and ultra-high performance concretes and found that the addition of both silica fume and nano-silica by total amount of 10%, may lead to an increase in the 28-day compressive strength of low cement content and high cement content concretes up to 40% and 50%, respectively, over the strength of comparable concretes. It was observed that the pozzolanic contribution of nano-silica becomes significant from the very early age, compared to silica fume, which begins its pozzolanic reactivity at the age of 7 days or later. This mechanism explained the outstanding mechanical performance of nano-silica concrete.

An experimental work was carried out by, **Skripkiunas**, and **Javavicius**, 2010, on the effect of nano $Na_2O{\cdot}nSiO_2$ dispersion on the strength and durability of Portland cement matrix and the principles of nanostructures formation in the cementitious materials consisting of several binding components. Three-component binding system consisting of colloidal sodium silicate solution, super-plasticizer suspension and Portland cement was used. The different contents of nano sodium silicate, namely (0, 0.2, 0.5 and 0.8) % by weight of cement were used. They observed that hardened cement with 0.5% nano sodium silicate admixture have high amount of amorphous (irregular shape) phases, which are coating the C-S-H and CH crystals. This factor has high influence on the porosity of hardened cement by the increasing of hardened cement close porosity. The capillary pores are closed with amorphous masses in the hardened cement paste.

Furthermore, the most important challenge for concrete technologists is to improve the properties of concrete. In Russia and China, a new technology, called magnetic water technology, was used in the concrete industry. In this technology, passing water through a magnetic field, some of its physical properties change and, as a result of such changes, the number of molecules in the water cluster decrease from 13 to 5 or 6, which causes a decrease in the water surface tension. Using magnetized water in concrete mixtures causes an improvement in the workability and compressive strength of concrete, **Afshin et al**, 2010.

Ahmed, **2009**, investigated the influence of magnetic water on compressive strength and workability of concrete. The results showed that the compressive strength of concrete samples prepared with magnetic water increases 10-20% more than that of the tap water samples. The results also showed that an increase in compressive strength of concrete is achieved when the magnetic strength of water is 1.2 T, and velocity of water current that passes through magnetic field is of 0.71 m/s. He also found that magnetic water improves the workability of fresh concrete.

Afshin et al., 2010, had studied the effects of magnetic water on some mechanical properties of high strength concrete, such as workability and compressive strength. For the production of magnetic water, a magnetic treatment device was used.

The results of tests showed that, in most cases, concrete made with magnetic water (magnetic concrete), has higher slump values than those of control concrete (up to 45%). Also in some cases, the compressive strength of the magnetic concrete samples was higher than that of the control concrete samples (up to 34%), but in other cases, with the same slump and compressive strength, cement content can be reduced by 28% in the case of magnetic concrete.

Arabshahi, 2010, investigated to examine the effect of magnetic water on concrete parameters. Strength parameters of concrete were obtained for more than 104 concrete samples, (including the ordinary water) and magnetic samples (made by magnetic water), with slump and compressive strength experiments. Based on slump experiments, magnetic samples were 7 centimeters more than nonmagnetic group and the average compressive strength of samples made by magnetic water was 23% more than that of samples made by ordinary water. The experimental results show the advantages of magnetic samples in concrete industry because of increase in plasticity, the efficiency and quality of concrete boosts in comparison with nonmagnetic samples.

1-2 Research Significance

The use of nano silica with 99.8% SiO_2 content in nano scale and average particle size 12 nm is a new approach. The nano silica reacts rapidly with the calcium hydroxide in the cement paste converting it into stable cementitious compounds. These refinement processes will strengthen the micro structure and reduce the micro cracking. On the other hand, the use of magnetic water and high range water reducing admixture (HRWRA) with nano silica is expected to improve the properties of concrete due to substantial water reduction of the nano silica – cement mixtures, which improves the dispersion of cement and other material particles with the breakdown of their agglomerations by the action of HRWRA and magnetic water.

1-3 Objectives

The Primary objectives of this research are:

- To present the possibilities of using nano silica for reactive powder concrete including micro materials. Due to unavailability of studies that tackled the effect of nano silica in RPC.
- To evaluate the effect of water dosage, nano silica (NS), micro carbon fiber addition, and technical requirements for reactive powder concrete. The key factors of materials proportion are investigated systematically through a series of experiments to investigate the influence of each the individual constituent material properties on overall behavior.

- To investigate the effect of magnetic water on the mechanical properties of reactive powder concrete containing NS with and without micro carbon fibers. Because of unavailability of research about using magnetic water in reactive powder concrete.
- To understand the axial stress-strain relationship of RPC reinforced with micro carbon fibers in compression. Due to rarity of research that investigated the axial stress-strain relationship of reactive powder concrete reinforced with micro carbon fibers.

2- MATERIALS

2-1 Cement

Ordinary Portland cement (Lebanon cement, Torabat Alsabia) type I was used throughout this research. It was stored in a suitable way to avoid any exposure to hazard conditions. The chemical properties of cement used throughout this research are shown in **Table 1**. Test results were indicated that the adopted cement was conformed to the **Iraqi specification** No.5/1984.

Particles size distribution was acquired by a SHIMADZU SALD-2101 LASER DIFFRACTION PARTICLE SIZE ANALYSIS instrument. The instrument used is attached to a computer that gives data about the amount of particles according to the diameter and plot as shown in **Fig**. **1**.

From **Fig**. **1**, it can be seen that 90% of particle is less than 8 μm.

2-2 Natural Sand

Al-Ekhaider natural sand was used throughout this research as the fine aggregate with particle size distribution smaller than 600 μm and greater than 150 μm.

2-3 Nano Silica (NS)

The nano silica used in this research named as **CAB-O-SIL** is made in Germany. It has a specific surface area 200 m^2/g. The chemical composition of this material is shown in **Table 2**. The NS used in this work conforms to the chemical and physical requirements of **ASTM** C1240-03. **Tables 3** and **4** show the chemical and physical requirements, respectively. According to the manufacture company average primary particle size is 12 nanometers. X-ray diffraction diagram shows that nano silica amorphous and has the ability to reacts as shown in **Fig**. **2**.

2-4 Mixing water

Two types of water were used in this research, the first one is tap water and the second is magnetized water. The magnetized water was produced by passing the tap water in a magnetic funnel

2-5 High Range Water Reducing Admixture

The super-plasticizer used was a modified polycarboxylates based polymer manufactured and supplied by **SIKA**® under the commercial name Sika® Viscocrete® Hi-Tech 36.

2-6 Carbon Fibers

The micro Carbon fibers used in this research was brought from **Alibaba Company**. It has small diameter 0.001mm and a length 8.5mm.

2-7 Materials Proportion

To determine the optimum mixtures of the RPC that give compressive strength higher than 100MPa, various mixtures were tried by using Al-Ekhaider natural sand, glass sand, tap or magnetized water as follow:

1- The first stage

Sand to cement ratio (S/C) in mortar and type of sand were expected to have significant effect on compressive strength. Hence, it^{s} effect was investigated using five mixtures;

a- Sand to cement ratios (S/C) was (2:1, 1.75:1, 1.5:1, 1.25:1 and 1:1).
b- Al-Ekhaider natural sand and glass sand.
c- Water cement ratio W/C of 0.44.

Results indicated that the mixture with S/C (1:1) using Al-Ekhaider natural sand gave compressive strength higher than other mixtures containing glass sand as shown in **Fig. 3**. This may be due to the roughness of surface texture of Al-Ekhaider sand that lead to a stronger bond between this sand and the cement paste than the bond between smooth surface texture of glass sand and the cement paste.

2- The second stage

The optimum ratio of the nano silica (NS) additive was obtained as follows:

1-By using tap water;

a- The used ratios of the additive NS are (1, 1.5, 2, 2.5 and 3) % by weight of cement.
b- S/C ratio of 1.
c- W/C ratio of 0.17.
d- Dosage of super-plasticizer of 7% by weight of cement.
e- Dosage of super-plasticizer of 7.3% by weight of cement for mixtures incorporated micro-carbon fibers.

The results indicated that the compressive strength increases with NS increase up to 2.5%, while it decreases when the NS increased to 3% as shown in **Table 5**. This can be justified by the fact that the additional quantity of NS particles (pozzolan) present in the mixture is higher than the amount required to combine with the liberated lime during the process of hydration, this leads to leaching out of non-reactive silica, leave space which causes a lack in strength.

2- By using magnetized water:

Using the same previous procedure but with magnetized water, the results indicated increasing in compression strength. It was obvious that the percentage increase varies from 17.8% to 23.3% as shown in **Table 6**. This is mainly due to the fact that the magnetic field has a considerable effect on clusters of water molecules which causes the decrease of such a mass from 13 molecules to 5 or 6 molecules. Such a decrease of

molecules causes more participation of water molecules in the cement hydration reaction. When water is mixed with cement, cement particles are surrounded by water molecule clusters. In the case of magnetic water in which the clusters have a smaller size and lower density, the thickness of the water layer around the cement particle is thinner than in the case of normal water.

2-8 **Casting and Curing of Test Specimens**

The specimens were demoulded after 1 day immersion in tap water saturated with $Ca(OH)_2$ at laboratory temperature (20-23)^o C up to test.

3- RESULTS AND DISCUSSION

A parametric study was carried out to investigate the effect of HRWRA (SV-Hi-Tech-36), 2.5% of nano silica, 2 % of micro carbon fibers by weight of cement, tap and magnetic water, on properties of reactive powder concrete.

3-1 Compressive Strength

The compressive strength values of various types of RPC are given in **Table 7** and **Fig. 4**. It can be seen that the compressive strength considerably increases with the age progress up to 90 days, with slight increase at ages between 180 and 360 days. The compressive strength improvement of a nonmagnetic reactive powder concrete containing HRWRA (SV-Hi-Tech-36) is also shown, whereas that the percentages of increase were 68.2% and 34.73% at 28 and 360 days respectively with respect to reference RPC. This behavior is mainly due to the significant water reduction caused by incur-porating HRWRA which leads to the reduction in capillary porosity. In addition, the super-plasticizer surfactant tends to disperse the cementitious particles uniformly throughout the mix, therefore improving the uniformity of the microstructure.

The compressive strength of a nonmagnetic mixture containing 2.5%NS-HRWRA reactive powder concrete is higher than that of reference RPC, the percentages of increase were 88.4% and 52.1 % at 28 and 360 days respectively. This can be explained by the high pozzolanic reaction of NS, particles with calcium hydroxide released from cement hydration leading to pore size and grain size refinement processes which can strengthen the microstructure and reduce the micro cracking. The compressive strength of the 2.5%NS-HRWRA-CF nonmagnetic reactive powder concrete with respect to reference RPC was 92.2% and 55.38% at 28 and 360 days respectively. It is well known that the fibers embedded inside a cement mortar or concrete act as a link among the cracks caused by heavier loads and, as a consequence, this leads to an increase in the materials strength. This may also be related to the uniform dispersion of micro Carbon fibers throughout reactive powder concrete.

The influence of magnetic water on compressive strength is also illustrated in **Table 7** and **Fig. 4**. The results show that when using magnetic water in mixing materials of RPC, RPC-HRWRA, 2.5%NS-HRWRA, 2.5%NS-HRWRA-CF reactive powder concrete, it causes significant increase in the compressive strength. The percentages of increase in compressive strength were (16.04, 13.38), (21.51, 21.76), (24.0, 22.33) and (22.37,

21.99)% at 28 and 360 days respectively, compared to the same mixtures using tap water, This is mainly due to the reasons mentioned in article 2-7.

3-2 Modulus of Rupture

The modulus of rupture for each of the RPC mixtures was determined; results are shown in **Table 8** and **Fig. 5**.

These results indicated that all types of RPC exhibit continuous increase in modulus of rupture with age progress. However, the rate of modulus of rupture gain of concretes at early ages is higher than those at later ages.

HRWRA (SV-Hi-Tech-36) nonmagnetic reactive powder concrete shows a significant improvement in modulus of rupture at all ages relative to the reference RPC. The percentages of increase were 37.1% and 41.60% at 28 and 360 days respectively, this behavior is as mentioned above.

Nonmagnetic 2.5%NS-HRWRA reactive powder concrete demonstrates further increase in modulus of rupture. The percentages of increase relative to reference RPC were 66.74% and 69.2 % at 28 and 360 days, respectively. The results indicated also a considerable increase in modulus of rupture due to the adding of micro carbon fibers to the nonmagnetic 2.5%NS-HRWRA reactive powder concrete. The percentages of increase in modulus of rupture with respect to the same unreinforced mixtures were 62.97% and 60.82% at 28 and 360 days, respectively. This behavior may be due to the chopped fibers reinforcing the RPC at the micro-crack stages and enhances the response during crack-initiation whereas the large fibers provide the toughness at the stages of larger crack opening.

The influence of magnetic water on modulus of rupture of various types of RPC is illustrated also in **Table 8** and **Fig. 5**. The results show that the use of magnetic water in mixing will cause a significant increase in the flexural strength. From **Table 9**, it can be observed that the percentages increase in the modulus of rupture at all ages for all various types of magnetic RPC with and without micro carbon fibers with respect to the same nonmagnetic mixtures.

3-3 Splitting Tensile Strength

The effect of HRWRA (SV-Hi-Tech-36), NS, MCF and the age using tap or magnetic water on the splitting tensile strength for various types of RPC are presented in **Table 10** and **Fig. 6**.

The results indicate that all types of RPC show continuous increase in splitting tensile strength up to 360 days, but this increase is extremely slight at ages above 90 days. This may be attributed to the increased fineness which leads to increased activity at early ages. Additionally, because of (SV-Hi-Tech-36), a good dispersion of the cement grains throughout the mixing conduces to gain strength at early ages. The percentages of increase in splitting tensile strength of nonmagnetic HRWRA-RPC calculated with respect to reference RPC were 79.35% and 28.97 % at 28 and 360 days respectively. This behavior may be ascribed to the significant reduction in capillary porosity of the cement matrix because of the reduction in water/cementious ratio.

The percentages of increase in splitting tensile strength for 2.5%NS-HRWRA nonmagnetic reactive powder concrete with respect to reference RPC at 28 and 360 days were 158.15% and 87.16% respectively. 2.5%NS-HRWRA-nonmagnetic reactive powder concrete reinforced with 2% micro carbon fibers show continuous improvement in tensile strength at all ages. The percentages of increase in splitting tensile strength with respect to the same unreinforced mixtures were 50.00% and 48.14% at 28 and 360 days respectively. This increase in splitting tensile is attributed to the nature of binding fiber available in concrete. When the reinforced concrete is forced to split apart in the tensile strength test, the load is transferred into the fibers as pullout behavior when the concrete matrix begins to crack as it exceeds the pre-crack state.

The effect of using magnetic water in all types of the RPC mixtures is presented in **Table 10** and **Fig. 6**. The results revealed that for various types of the magnetic RPC mixtures an increase was observed in splitting tensile strength at all ages with respect to the same nonmagnetic mixtures. The percentages of increases in the splitting tensile strength relative to the same nonmagnetic mixtures are illustrated in **Table 11**.

3-4 The Axial Stress-Strain Relationship of RPC in Compression

This research shows the actual effect of age and the main variables (HRWRA (SV-Hi-Tech-36), nano silica admixture, 2% micro carbon fibers and magnetic water) on the axial stress-strain relationship of RPC in compression. The effect of each variable is shown in a separate figure that contains a set of curves constructed to cover all ages of test.

The compression stress-strain curves for various types of magnetic or nonmagnetic reactive powder concrete are shown in **Figs. 7**, **8** and **Table 12**

Fig. **7** (a and b) shows that the ascending portion of the stress-strain curves of the reference RPC and HRWRA-RPC specimens is steep and almost a straight line at later ages, whereas the descending portion has almost vanished. Therefore, plain composite reactive powder concrete fails violently and suddenly.

For 2.5%NS-HRWRA nonmagnetic reactive powder concrete, the shape of the ascending portion of the stress-strain curve is steeper than that of HRWRA-RPC at all ages as shown in **Fig**. **7 (c)**. This may be attributed to the ability of NS to produce high strength concrete. Consequently more brittleness is produced by the addition of this admixture to HRWRA-RPC.

Fig. **7** (d) shows the effect of the micro carbon fibers on the compression stress-strain curve of 2.5%NS-HRWRA nonmagnetic reactive powder concrete with age progress. The figure shows only slightly variations during the ascending portion while the descending portion is modified significantly.

At 28 days, the maximum strain reached at the peak stress was 0.00357 for 2.5%NS-HRWRA-CF-RPC-TW and decreased with age progress to reach 0.00349 at 360 days as shown in **Fig. 7** and **Table 12**. This behavior may be attributed to the ability of micro carbon fibers to arrest and slow down the progress of propagation of micro cracks, thus producing noticeable increase in the strain at the peak stress, ductility and improve the integrity of the composite

The effect of magnetic water on the compressive stress-strain curves of various types of reactive powder concrete is shown in **Fig.8** from (a to d). It can be seen that by using magnetic water two advantages were achieved. First, it increases compressive strength for various types of reactive powder concrete at all ages. Second, it reduces the slope of the descending portion and results in an increase in ductility as seen in **Fig. 8 (d**). The percentages increase for stress and strain of various types of magnetic composite reactive powder concrete in comparison with the same nonmagnetic mixtures at 28 and 360 days are shown in **Table 13**.

4- CONCLUSIONS

According to the results obtained from the experimental work of this investigation, the following conclusions can be deduced:

HRWRA-RPC, 2.5%NS-HRWRA and 2.5%NS-HRWRA-CF nonmagnetic RPC have shown considerable increase in compressive strength, modulus of rupture and splitting tensile strength. The percentages increase relative to reference RPC were (68.2, 34.9 and 79.35), (88.4, 66.74 and 158.15) and (88.4, 62.97 and 52.67) % at 28 days respectively.

Two advantages of magnetic water were observed. First, it increases compressive strength, modulus of rupture and splitting tensile strength for various types of RPC at all age with respect to the same nonmagnetic mixtures.. The percentages of increase range between (16.04 to 24.0), (17.96 to 18.90) and (15.30 to 19.44) % at 28 days respectively

Second, it reduces the slope of the descending portion for reinforced mixtures and results in an increase in ductility. The percentages increase in the axial stress-strain relationship in compression related to the same nonmagnetic mixtures range between 6.44 to 9.58% at 28 days.

REFERNCE

- Abbas, R., 2009, *Influence of nano-Silica addition on properties of conventional and ultra-high performance concretes*, HBRC Journal, vol.5, No. 1, pp. 18.
- Afshin, H., Gholizadeh, M., and Khorshidi, N., 2010, *Improving mechanical properties of high strength concrete by magnetic water technology* , Sharif University of Technology, Vol. 17, No. 1, pp. 74-79.
- Ahmed, S. M., 2009, *Effect of magnetic water on engineering properties of concrete*, Al-Rafidain Engineering, Vol.17, No.1, pp.71-82.
- *Alibaba Company*, Hong Kong Limited and licensors. www.alibaba.com/country
- Arabshahi, H., 2010, *The effect of magnetic water on strength parameters of concrete*, Alfa Universal, An International Journal of Chemistry, Vol. 1, No.,1, pp. 30-35
- ASTM C 1240–2003, *Standard specification for use of Silica fume as a mineral admixture in hydraulic-cement concrete, mortar, and grout*, Vol. 04.02, pp.1-6.
- Bauer, B. J., Liu. D., and Jackson, C. L., 1996, *Epoxy/SiO_2 Interpenetrating polmer networks, polym*, Adv. Technol. pp. 333-339.

- Collepardi, M., Ogoumah, J. J., Troli, R., Simonelli, S., and Skarp, U., Collepardi, S., 2002, *Combination of Silica fume, Fly ash and amorphous nano-Silica in superplasticized high-performance concretes*, Proceeding of First International Conference on Innovative Materials and Technologies for construction and Rehabilitation, Lecce, Italy, pp. 459-468.
- Fuji chimera Research Institute Inc., 2002,*Fine (Impalpable) powder market 2002-present and future outlook*, Skripkiunas, G., and Javavicius, E, 2010, *Effect of $Na_2O{\cdot}nSiO_2$ Nano dispersion on the strength and durability of portland cement matrix*, Materials Science, ISSN 1392–1320, Vol. 16, No. 1.
- Iraqi specification, No.5/1984., Portland *cement*, Ministry of Planning, Central Organization for Standardization and Quality Control.

- Jo, B. W., KIM, C. H., and Lim, J. H., 2007, *Characteristics of cement mortar with nano-SiO_2 particles*, ACI materials journal, Aug. vol. 104, No. 4, pp. 404-407.
- Li, H., Xiao, H., Yuan, J., and Ou, J., 2004, *Microstructure of cement mortar with nano-particles composites*, Part B, Vol. 35, No. 2, pp.185-189.
- Lovelya, J.O., and Chandrasekaran, P., 2014, *Study on chemical resistance property of concrete with silica fume*, International Journal of Innovative Research in Science, Engineering and Technology, Volume 3, PP.102-109.
- Rahmani, R., Shamsai, A., Saghafian, B., and Peroti, S., 2012, *Effect of water and cement ratio on compressive strength and abrasion of micro silica concrete*, Middle-East Journal of Scientific Research, Vol. 12, No. 8, PP. 1056-1061
- Rathi1, V.R., and Modhera, C.D., 2014, *An overview on the influence of nano materials on properties of concrete*, International Journal of Innovative Research in Science, Engineering and Technology, Vol. 3, Issue 2, PP. 9100-9105.
- Remzi, S., and Meral, Q., 2008, ***New*** *materials for concrete technology*: *nano powders*, 33rd conference on our world in concrete & structures, Singapore, pp 399-406.
- Roddy, G., Chatterji, J., and Cromwell, R., November 2008, *Well treatment composition and methods utilizing nano-particles*, Halliburton Enery Services, United States of America Patent Application no 20080277116 A1, Vol. 13, pp 1-12.
- Qing, Y., Zhang, Z. N., Li, S., and Chen, R. S., 2006, ***A comparative*** *study on the pozzolanic activity between nano SiO_2 and Silica fume*, Journal of Wuhan University of Technology Materials , Vol.21, pp. 153-157.
- *Sika® ViscoCrete® Hi-Tech 36*, Product Data Sheet, Turkey, pp. 1-3, www.sika.com.tr.
- Yu, R., Spiesz, P., and Brouwers, H.J.H., 2013, *Effect of colloidal nano-silica on the hydration of Ultra-High Performance Concrete (UHPC)*, Eindhoven

University of Technology, Eindhoven, the Netherlands,1st International Conference on the Chemistry of Construction Materials pp.269-272

Table 1. Chemical composition and main compounds of cement*

Oxides composition	Content %	Limits of Iraqi specification No.5/1984
CaO	62.2	---
SiO_2	20.1	---
Al_2O_3	5.89	---
Fe_2O_3	3.08	---
MgO	2.31	<5.00
SO_3	2.01	<2.80
L.O.I.	2.53	<4.00
Insoluble residue	1.03	<1.5
Lime Saturation Factor, L.S.F.	0.87	0.66-1.02
Main compounds (Bogue's equations)		
C_3S	50.68	-
C_2S	19.474	-
C_3A	10.3	-
C_4AF	9.55	-

* Chemical analysis has been conducted by the National Center for Construction Laboratories and Researches.

Table 2. Chemical analysis of nano Silica *

Oxide composition	Oxide content %
SiO_2	99.8
Al_2O_3	0.05
Fe_2O_3	0.003
Na_2O	0.05
K_2O	0.03
MgO	0.01
TiO_2	0.03
HCl	0.025

*Chemical analysis has been conducted by National Center for Geological Survey and Mining.

Table 3. Chemical requirements of nano Silica ASTM C 1240-03

Oxide composition	NS	Limit of specification requirement ASTM C 1240
SiO_2, min. percent	99.8	85.0
Moisture content, max. percent	1.5	3.0
Loss on ignition, max	1	6.0

Table 4. Physical requirements of nano Silica ASTM C 1240- 03

Physical properties	NS	Limit of specification requirement ASTM C 1240
Percent retained on 45-µm (No.325) sieve, max.	-	10
Accelerated pozzolanic Strength Activity Index with Portland cement at 7 days, min. percent of control	210.58	105
Specific surface, min., m^2/g	200	15

Table 5. Details of the RPC mixtures proportion (kg/m^3) used throughout this investigation using tap water

Mixtures	**Cement**	**Sand**	**Additive Material**	**Water**	**HRWRA**	**Fiber**	**Comp. Strength (MPa), 7days**
RPC Tap Water (TW)	875	875	_	385	_	_	42.6
HRWRA-RPC-TW	1100	1100	_	188.7	61	_	85.32
1% NS–HRWRA–RPC–TW	960	960	9.6	164.81	67.86	_	92.3
1% NS–HRWRA–CF–RPC–TW	950	950	9.5	163.1	70	19	94
1.5% NS–HRWRA–RPC-TW	920	920	13.8	158.74	65.36	-	93.78
1.5 NS–HRWRA–CF–RPC–TW	910	910	13.65	157	67.4	18.2	95.2
2% NS–HRWRA–RPC-TW	880	880	17.6	152.59	62.83	_	94.88
2% NS–HRWRA–CF–RPC-TW	870	870	17.4	150.85	64.78	17.4	96.41

2.5% NS–HRWRA–RPC-TW	840	840	21	146.34	60.27	_	95.92
2.5% NS–HRWRA–CF–RPC-TW	830	830	20.75	144.6	62.1	16.6	97.84
3% NS–HRWRA–RPC-TW	810	810	24.3	141.83	58.4	_	95.2
3% NS – HRWRA–CF– RPC -TW	800	800	24	140	60	16	96.9

Table 6. Details of the RPC mixtures proportion (kg/m^3) used throughout this investigation using magnetized water

Mixtures	**Cement**	**Sand**	**Additive Material**	**Water**	**HRWRA**	**Fibers**	**Comp. Strength (MPa), 7days**
RPC Magnetic Water (MW)	875	875	-	385	-	-	48.9
HRWRA -RPC- MW	1100	1100	-	188.7	61	-	99.45
1% NS -HRWRA - RPC - MW	960	960	9.6	164.81	67.86	-	108.1
1% NS-HRWRA - CF- RPC- MW	950	950	9.5	163.1	70	19	110.64
1.5% NS - HRWRA - RPC- MW	920	920	13.8	158.74	65.36	-	109.5
1.5 NS - HRWRA - CF - RPC- MW	910	910	13.65	157	67.4	18.2	112
2% NS - HRWRA - RPC- MW	880	880	17.6	152.59	62.83	-	110.9
2% NS - HRWRA - CF- RPC - MW	870	870	17.4	150.85	64.78	17.4	113.76
2.5% NS - HRWRA - RPC- MW	840	840	21	146.34	60.27	-	113.05
2.5% NS - HRWRA - CF - RPC- MW	830	830	20.75	144.6	62.1	16.6	115.9
3% NS-HRWRA-RPC- MW	810	810	24.3	141.83	58.4	-	112.86
3% NS - HRWRA - CF - RPC - MW	800	800	24	140	60	16	114.43

Table 7. Compressive strength for various types of mixtures

Mixtures	Compressive strength MPa				
	7 days	28 days	90 days	180 days	360 days
RPC Tap Water (TW)	42.6	57.48	72.24	73.3	74
HRWRA-RPC-TW	85.32	96.7	99.4	99.66	99.7
2.5%NS-HRWRA-RPC-TW	95.92	108.3	111.86	111.95	112.56
2.5%NS-HRWRA-2%CF-RPC-TW	97.84	110.48	114.6	114.84	114.98
RPC Magnetic Water (MW)	48.9	66.7	82.9	83.2	83.9
HRWRA-RPC-MW	99.45	117.5	120.77	120.9	121.4
2.5%NS-HRWRA-RPC-MW	113.05	134.3	136.7	136.9	137.7
2.5%NS–HRWRA-2%CF-RPC-MW	115.9	135.2	140.3	141.5	142.2

Table 8. Modulus of rupture for various types of mixtures

Mixtures	Modulus of rupture (MPa)				
	7 days	28 days	90 days	180 days	360 days
RPC Tap Water (TW)	6.45	9.2	10.2	10.23	10.24
HRWRA-RPC-TW	9.69	12.61	13.84	14.2	14.5
2.5%NS-HRWRA-RPC-TW	12.6	15.34	16.7	17.1	17.33
2.5%NS-HRWRA-2%CF-RPC-TW	20.45	25	26.69	27.1	27.87
RPC Magnetic Water (MW)	7.65	10.88	12.05	12.08	12.11
HRWRA-RPC-MW	11.49	14.95	16.4	16.81	17.15
2.5%NS-HRWRA-RPC-MW	14.99	18.24	19.85	20.26	20.51
2.5%NS–HRWRA-2%CF-RPC-MW	24.1	29.49	31.38	31.78	32.63

Table 9.The percentages increase in the modulus of rupture for various types of magnetic mixtures with respect to the same nonmagnetic mixtures

mixtures	The percentages of increase in the modulus of rupture				
	Age(days)				
	7	28	90	180	360
RPC Magnetic Water (MW)	18.60	18.26	18.14	18.08	18.26
HRWRA -RPC- MW	18.58	18.56	18.50	18.38	18.28
2.5% NS - HRWRA - RPC- MW	18.97	18.90	18.86	18.48	18.35
2.5% NS–HRWRA–2% CF–RPC-MW	17.85	17.96	17.57	17.27	17.08

Table 10. Splitting tensile strength for various types of magnetic and nonmagnetic mixtures.

mixtures	Splitting tensile strength (MPa)				
	Age(days)				
	7	28	90	180	360
RPC Tap Water (TW)	2.13	3.68	5.16	5.42	5.45
HRWRA-RPC-TW	5.78	6.6	6.96	7.02	7.029
2.5% NS-HRWRA-RPC-TW	8.6	9.5	10.11	10.2	10.2
2.5% NS-HRWRA-2%CF-RPC-TW	12.9	14.25	14.98	15.11	15.11
RPC Magnetic Water (MW)	2.476	4.28	6.01	6.32	6.36
HRWRA-RPC-MW	6.65	7.61	8.03	8.11	8.13
2.5% NS-HRWRA-RPC-MW	10.23	11.31	11.85	11.96	11.97
2.5% NS-HRWRA-2%CF-RPC-MW	15.4	17.02	17.53	17.67	17.69

Table 11. The percentages increase in the splitting tensile strength for various types of magnetic mixtures with respect to the same nonmagnetic mixtures.

Mixtures	The percentages of increase in splitting tensile strength %				
	Age(days)				
	7	28	90	180	360
RPC Magnetic Water (MW)	16.24	16.30	16.47	16.61	16.69
HRWRA -RPC- MW	15.05	15.30	15.37	15.53	15.66
2.5% NS - HRWRA - RPC- MW	18.95	19.05	17.21	17.25	17.35
2.5% NS–HRWRA–2% CF–RPC-MW	19.38	19.44	17.02	16.94	17.06

Table 12. Peak Compression Stress and Strain values for various types of mixtures

Mixtures		Age (days)				
		7	28	90	180	360
RPC Tap Water (TW)	**C**	**35**	**48.4**	**61.5**	**62.4**	**62.9**
	S	**0.0029**	**0.00271**	**0.00263**	**0.00258**	**0.00254**
HRWRA-RPC-TW	**C**	**73.72**	**85.5**	**88.5**	**88.74**	**90.36**
	S	**0.00271**	**0.00265**	**0.00258**	**0.00256**	**0.00255**
2.5% NS–HRWRA–RPC-TW	**C**	**83.42**	**96**	**99.76**	**99.85**	**100.5**
	S	**0.0026**	**0.00255**	**0.0025**	**0.00245**	**0.00241**
2.5% NS–HRWRA–2% CF–RPC-TW	**C**	**85.14**	**98.08**	**102.3**	**102.54**	**102.88**
	S	**0.0036**	**0.00357**	**0.00348**	**0.00345**	**0.00349**
RPC Magnetic Water (MW)	**C**	**40.5**	**58.5**	**74.8**	**75.15**	**75.9**
	S	**0.0031**	**0.0029**	**0.00286**	**0.0028**	**0.00272**
HRWRA -RPC- MW	**C**	**86.15**	**104.4**	**107.72**	**107.9**	**108.3**
	S	**0.0031**	**0.002845**	**0.00283**	**0.00278**	**0.00274**
2.5% NS - HRWRA - RPC- MW	**C**	**98.6**	**117.3**	**122.8**	**123.9**	**124**
	S	**0.0028**	**0.00275**	**0.0027**	**0.00268**	**0.0026**
2.5% NS–HRWRA–2% CF–RPC-MW	**C**	**101.1**	**120.8**	**126**	**137.4**	**128.1**
	S	**0.0039**	**0.0038**	**0.00379**	**0.00375**	**0.00373**

Compressive strength (MPa) = C, Strain = S

Table 13. The percentages increase in stress-strain for various types of magnetic mixtures with respect to the same nonmagnetic mixtures

Mixtures		The increasing percentage at age (days) %	
		28	360
RPC Magnetic Water (MW)	C	20.87	20.67
	S	7.01	7.08
HRWRA -RPC- MW	C	22.11	19.85
	S	7.36	7.45
2.5% NS - HRWRA - RPC- MW	C	22.19	23.38
	S	7.84	7.88
2.5% NS–HRWRA–2%CF–RPC-TW	C	23.16	24.5
	S	6.44	6.88

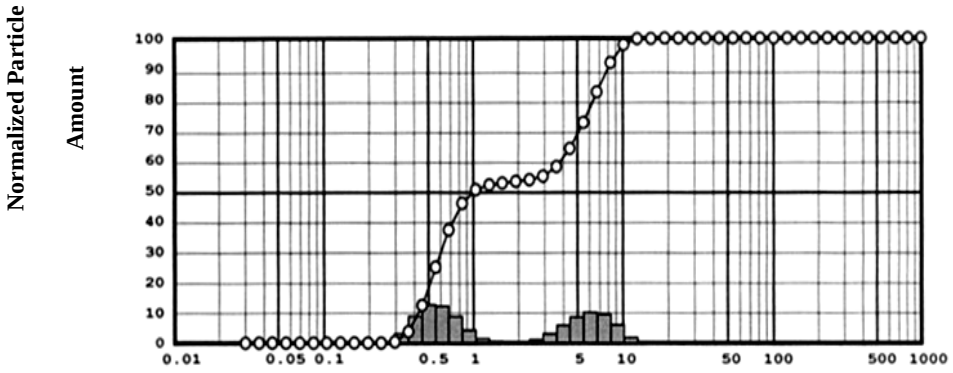

Figure 1. Particle size distribution of cement.

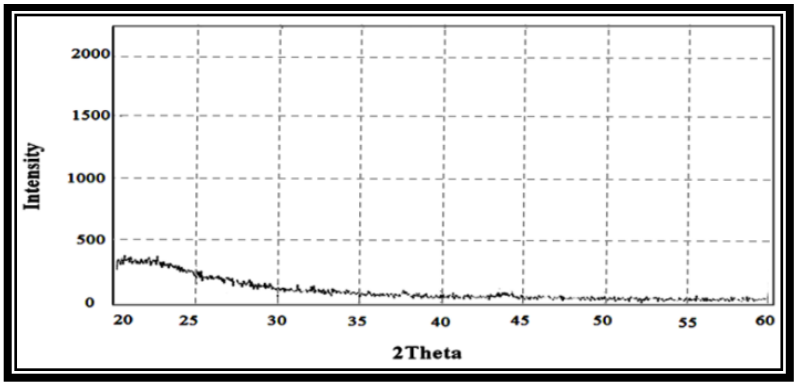

Figure 2. X-Ray diffraction patterns of NS.

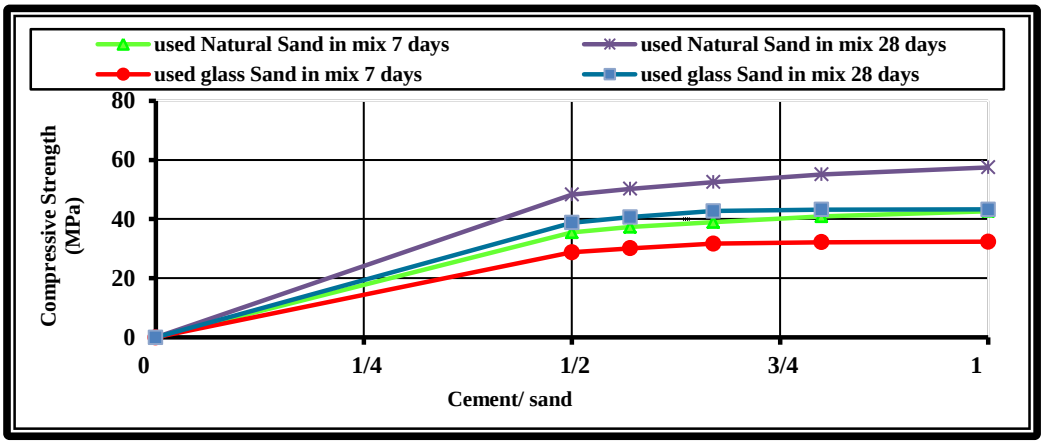

Figure 3. Relationship between compressive strength and percent of Cement/ Natural or Glass sand.

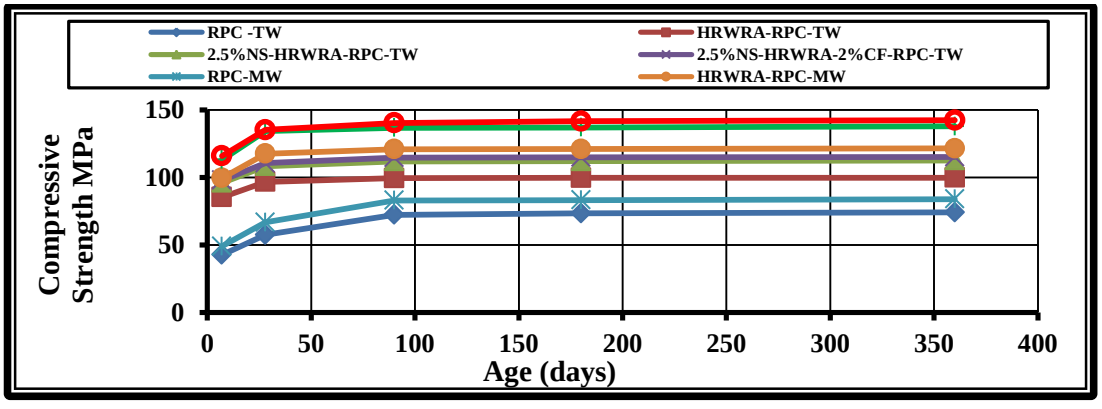

Figure 4. Effect of magnetic and nonmagnetic mixtures containing HRWRA, 2.5%NS-HRWRA and 2.5%NS-HRWRA on the compressive strength with age.

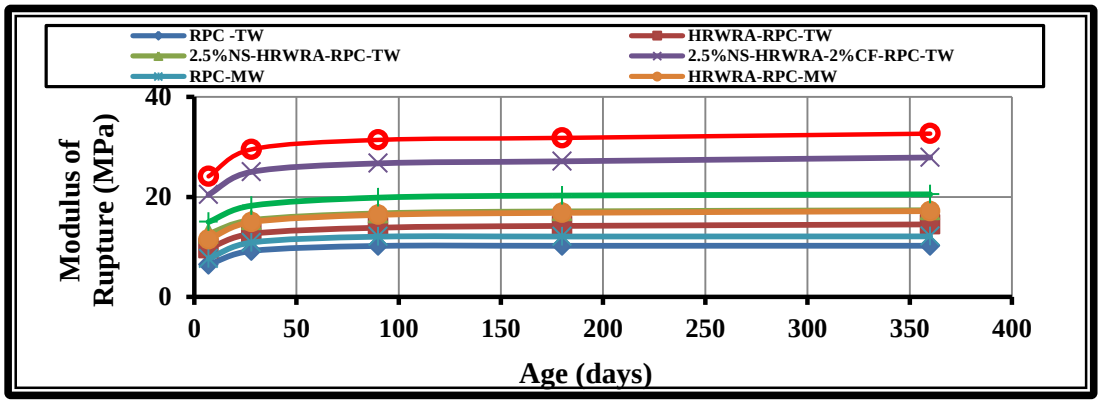

Figure 5. Effect of magnetic and nonmagnetic mixtures containing HRWRA, 2.5%NS-HRWRA and 2.5%NS-HRWRA on the Modulus of Rupture with age.

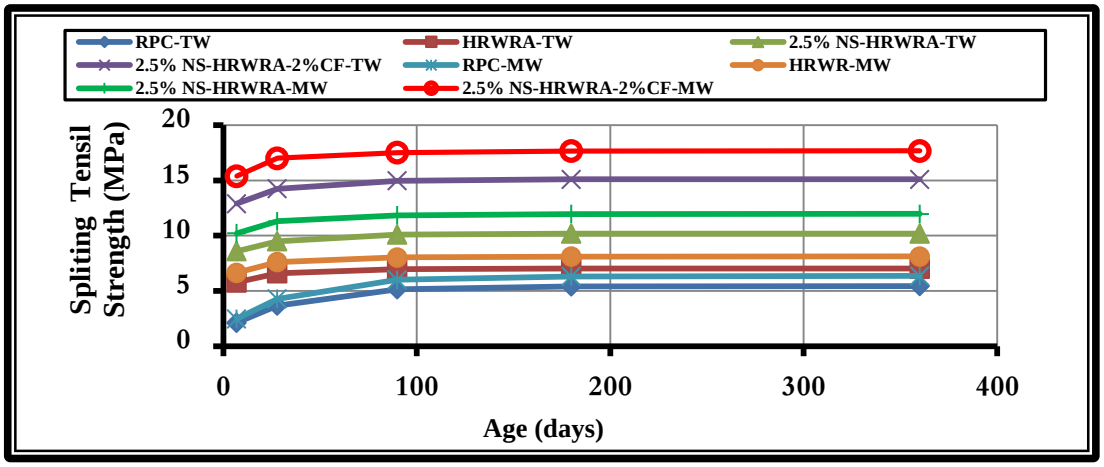

Figure 6. Effect of magnetic and nonmagnetic mixtures containing HRWRA, 2.5%NS-HRWRA and 2.5%NS- HRWRA-MCF on the splitting strength with age.

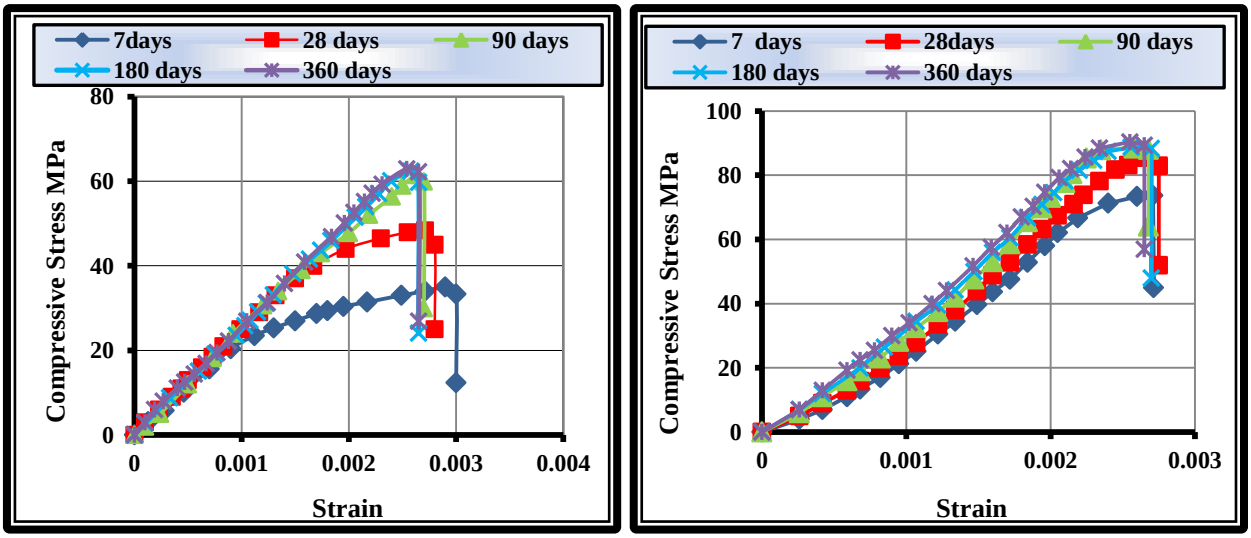

(a) RPC **(b)** HRWRA-RPC

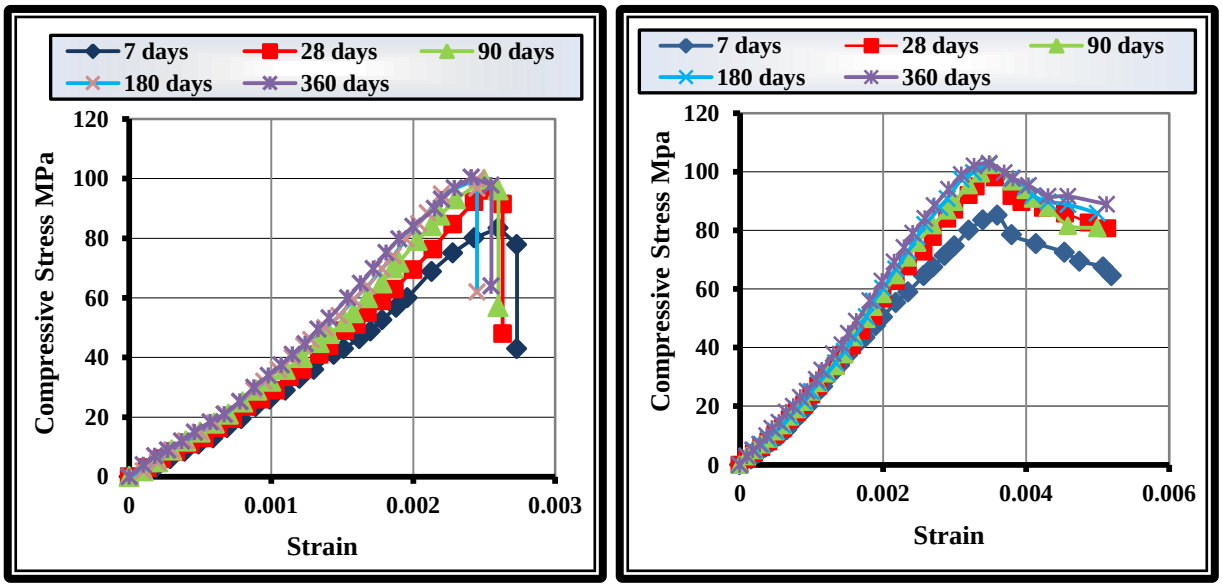

(c) 2.5% NS-HRWRA-RPC-TW **(d)** 2.5% NS-HRWRA-2%CF-RPC-TW

Figure 7. Effect of nonmagnetic mixtures (a) RPC, (b) HRWRA, (c) 2.5% NS-HRWRA and (d) 2.5% NS-HRWRA-2%CF on the axial stress – strain behavior with age progress.

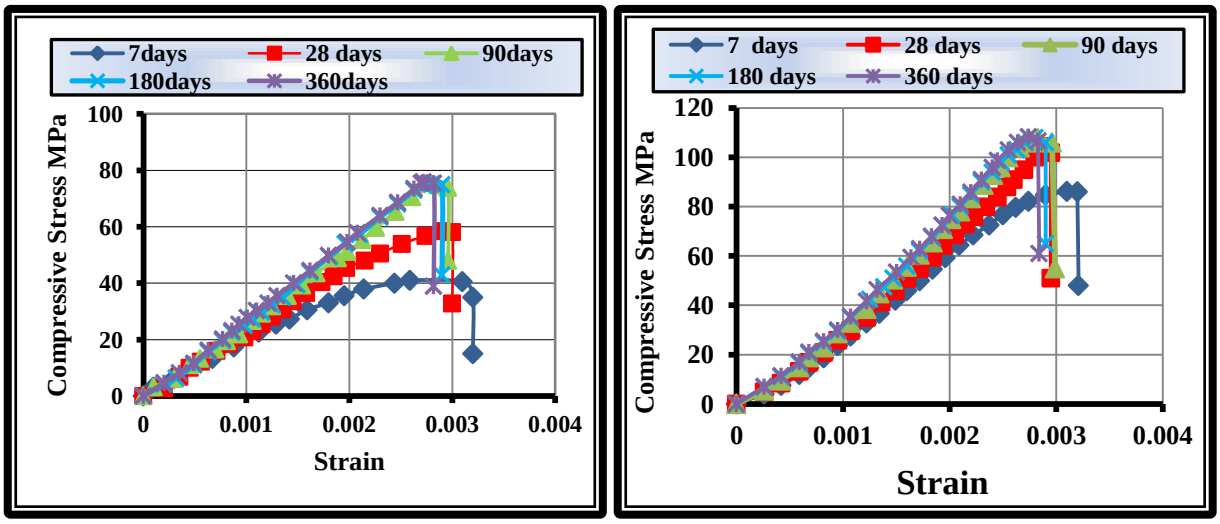

(a) RPC (b) HRWRA-RPC

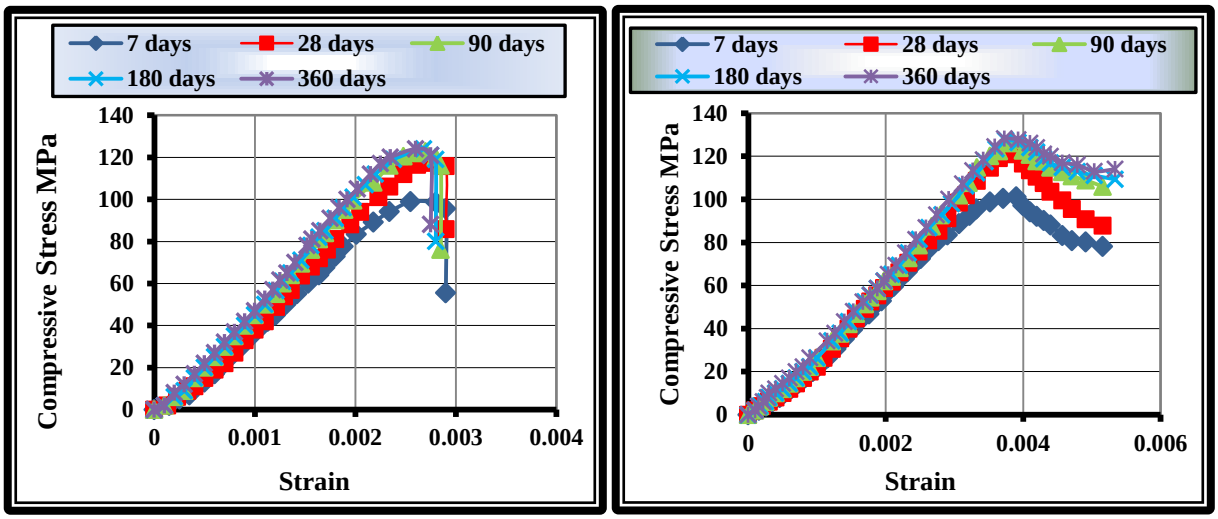

(c) 2.5% NS-HRWRA-RPC-MW (d) 2.5%NS-HRWRA-2%CF-RPC-MW

Figure 8. Effect of magnetic mixtures (a) RPC, (b) HRWRA, (c) 2.5% NS-HRWRA and (d) 2.5% NS-HRWRA-2%CF on the axial stress – strain behavior with age progress.

Structural Behavior of Confined Concrete Filled Aluminum Tubular (CFT) Columns under Concentric Load

Ahmad Jabbar Hussain Alshimmeri
Instructor
Civil Engineering Department-Engineering College-Baghdad University
Email: dr.ahmadalshimmeri@yahoo.com

ABSTRACT

This paper introduces an experimental study on the behavior of confined concrete filled aluminum tubular (CFT) column to improve strength design, ductility and durability of concrete composite structures under concentrically loaded in compression to failure. To achieve this: seven column specimens with same concrete diameter 100mm and without steel reinforcement have been examined through experimental testing, which are used to study the effects of the thickness of the aluminum tube encased concrete (thickness : 0mm, 2mm, 3mm, 4mm and 5mm with same length of column 450mm), length of column (thickness 5mm and length of column 700mm) and durability (thickness 5mm and length of column 450mm) on the structural behavior of (CFT) columns.

It is concluded from this work that the compression force capacity is affected by thicknesses of the aluminum tube with respect to reference specimen. Where the used of aluminum tube thicknesses in column specimens led to increased in load carrying capacity in range (16% for C2 -224% for C5). The specimen has a length of 700mm with 5mm thickness the decreased of strength was 0.06% than the specimen with 5mm thickness and length 450mm. For slender column the overall buckling was observed while the local buckling for the short column is the dominant failure shape. Regarding durability, no apparent difference has been found between the structural behavior of the specimen that immersed in aggressive solution and specimen in air.

Keywords: circular, column, aluminum, CFT, confinement

السلوك الإنشائي للأعمدة الخرسانية الدائرية والمحاطة بالألمنيوم تحت تأثير حمل محوري

م.د. احمد جبار حسين الشمري
قسم الهندسة المدنية
كلية الهندسة / جامعة بغداد

الخلاصة

يقدم هذا البحث دراسة عملية لتصرف الأعمدة الدائرية المكونة من انبوب الألمنيوم ذو املاء خرساني لتحسين المقاومة التصميمية والمطيلية و الديمومة تحت حمل انضغاط محوري. لتحقيق ذلك تم فحص سبع عينات مختبريا بقطر خرساني ثابت 100ملم وبدون حديد تسليح لدراسة تأثيرات سمك انبوب الألمنيوم المغطي للخرسانة (سمك :0 ملم , 2 ملم ,3 ملم ,4 ملم و 5 ملم بطول ثابت 450 ملم) , طول العمود (سمك 5 ملم وطول 700 ملم) والديمومة (سمك 5 ملم وطول 450 ملم) على التصرف الإنشائي للأعمدة.

النتائج المختبرية بينت أن مقاومة الأعمدة للانضغاط تعتمد على سمك أنبوب الألمنيوم، حيث عند استخدام سمك انبوب الالمنيوم الاقل 2 ملم لعينات العمود أدى إلى زيادة في التحميل بمقدار من 16% وعند استخدام سمك انبوب الالمنيوم الاعلى 5 ملم لعينات العمود أدى إلى زيادة في التحميل بمقدار 224% . العينة التي طولها 700ملم و ذات السمك 5ملم انخفضت القوة بمقدار 0.06% عن العينة التي يبلغ طولها 450ملم و ذات السمك 5ملم.

تم ملاحظة أن العمود النحيف يكون الفشل فيه بانبعاج كلي بينما العمود القصير يعاني من انبعاج محلي. وفي ما يتعلق بالديمومة, لم يظهر فرق بين التصرف الإنشائي للعينة المغمورة في المحلول الملحي القاسي والعينة في الهواء.

1. INTRODUCTION

Concrete-filled steel tubes (CFTs) are practical and economical structural elements that permit rapid construction because the steel tube serves as formwork and reinforcement to the concrete fill, negating the need for either. The deformation capacity of the system is increased by the combined action of the concrete fill with the thin steel tube. The concrete fill significantly increases inelastic deformation capacity and the compressive stiffness and load capacity of the CFT member. The fill also increased global buckling resistance by increasing the slenderness ratio; KL/r value, where K is effective length factor, L is the column length and r is the radius gyration of the column section. This increased deformation capacity benefits the use of CFT components for blast resistance and seismic design, **Roeder, et al., 2010** also durability of concrete.

It is well understood that lateral confinement can enhance both the strength and ductility of concrete. CFTs owe their improved deformation capacities to the confinement action provided by the surrounding FRP tube, **Ozbakkaloglu, 2013**.

CFTs are circular or rectangular composite members. Shear stress transfer is needed between the steel and concrete to develop composite action. Researches, **Yu, et al., 2007 and Han, and Yao,2004** showed that circular CFTs provide greater bond stress transfer, better confinement, and greater shear reinforcement to the concrete fill than rectangular CFTs.

Confining reinforced concrete (RC) columns can significantly increase their strength and ductility **Wu and Jiang, 2013**. There are a number of situations where it may become necessary to increase the load-carrying capacity of a structure in service. These situations include change of loading or usage, and the cases of structures that have been damaged. Deterioration of reinforced concrete (RC) columns due to corrosion of the reinforcing steel and spalling of concrete has been a major problem for the aging infrastructure, **Arya, et al, 2002.** In this study aluminum alloy 6061- T6 was used as a circular tube to confining column concrete. The strength to unit weight ratio of the aluminum alloys is more than of the steel, the aluminum alloy 6061- T6 have good resistance to corrosion without any protective covering, the aluminum structure are light in weight and the column structure have better appearance and require less maintenance, **Kissell and Ferry 2002.**

To study the effects of thickness, length and durability on the structural behavior of column, seven concrete-filled aluminum tubes (CFT) column specimens with same concrete diameter 100mm and without steel reinforcement were examined through experimental testing.

2. ADVANTAGE OF CONCRETE - FILLED ALUMINUM TUBE

The concrete-filled aluminum tube (CFT) column system has many advantages compared with the ordinary steel or the reinforced concrete system. The main advantages are:

- The strength of concrete is increased by the confining effect of aluminum tube.
- The aluminum tubes can be used as the formwork for casting concrete and the shoring system in construction, thus labor for forms and reinforcing bars is omitted. This efficiency leads to a cleaner construction site and a reduction in manpower, construction cost, and project length.
- Better cost performance is obtained by replacing reinforced concrete column with a concrete filled aluminum tubular CFT column.
- The environmental burden can be reduced by omitting the formwork.

3. EXPERIMENTAL PROGRAM

3.1 Materials:

3.1.1 Aluminum

Concrete filled aluminum tubes (CFT) are composite structures of aluminum tube and in filled concrete. The combination is ideal since concrete core has high compressive strength and

stiffness while the aluminum tube has high strength and ductility **Mursi, and Uy, 2004.** The CFT columns have high strength, high ductility and high energy absorption capacity.
One myth is that aluminum is not sufficiently strong to serve as a structural metal. The fact is that the most common aluminum structural alloy, 6061-T6, has a minimum yield strength of 35 kpsi [240 MPa], which is almost equal to that of A36 steel. This strength, coupled with its light weight (about one-third that of steel), makes aluminum particularly advantageous for structural applications where dead load is a concerned, **Kissell and Ferry 2002.** In this study circular tube made of aluminum alloy; 6061- T6 was used to encase column concrete. The aluminum alloy; 6061- T6 and A36 steel were tested in the laboratory by taking the specimens according to **ASTM E8, 2003,** which is a standard test method for tension testing of metallic materials and **ASTM B557, 2003,** which is standard test methods of tension testing wrought and cast aluminium and magnesium alloy products. The tensile testing is carried out by applying axial load at a specific extension rate to a standard tensile specimen till failure. **Fig. 1** shows the results of the stress strain curves for A36 steel and 6061-T6 and this figure showed converge between two metals especially in the elastic region between them. **Table 1** shows the properties of the aluminum alloy 6061-T6
Aluminum is inherently corrosion-resistant. Carbon steel has a tendency to self-destruct over time by virtue of the continual conversion of the base metal to iron oxide, commonly known as rust, **Kissell and Ferry 2002.** Properties that affect the performance of the aluminum alloy; 6061- T6 and A36 steel of structural members are summarized in **Table 2**.

3.1.2 Concrete material properties and mix proportions
Type I Portland cement, fine aggregate with (4.75mm) maximum size, coarse aggregate with (10mm) maximum size, water are used in casting columns. All the concrete of column are made from a single mix proportion (Cement: Sand: Gravel) of 1:1.5:3 by weight with a water /cement ratio 0.45, average compressive strength of concrete for three cylinder (150mmx300mm) at the time of column tests was 28.5 Mpa.

3.2 Test Specimens
A series of tubular concrete columns were manufactured and tested under concentric compression. The columns were prepared from the same batch of concrete. The experimental program is consisted of testing seven column specimens with same concrete diameter 100mm and without steel reinforcement and have been examined through experimental testing. Details of the columns are given in **Table 3**; four of them have aluminum tube thicknesses 2mm (C1), 3mm (C2), 4mm (C3) and 5mm (C4) which have the same length 450mm and the fifth specimens (CR) unconfined concrete column which is the reference specimen to study the effect of the thicknesses on the structural behavior of column as shown in **Fig. 2** and **Fig. 3**, the sixth specimens has thickness 5mm and length 700mm C7 to study the effect of length on the structural behavior of column as shown in **Fig. 4(a)** and the seventh specimen has thickness 5mm and length 450mm to study the effect of durability on the structural behavior of column the specimen exposed to aggressive solution for 120 days as shown in **Fig. 4(b)**. For the study the effects length and durability on the structural behavior of column the reference specimen was C5 which has thickness 5mm and length of 450mm.

3.3. Instrumentation and Testing
A total of 7 test specimens were constructed and tested under concentric axial compression loads. The columns were instrumented with dial gauges to measure axial deformation as well as circumferential strains.

Six electrical strain gauges were placed on the exterior surfaces of each column specimens to measure the vertical deformations and the perimeter expansion of the aluminium tubes in the mid-height region at symmetric locations, bonded either on the concrete surface in the case of unconfined column or on aluminium tubes in the case of confined columns, as shown in **Fig.5**.
The column specimens were placed directly into the testing machine for compression tests. A typical column test layout and instrumentation location is shown in **Figs. 6 and 7**. Prior to testing, all columns were capped with wood - bearing plate at both ends to ensure uniform distribution of the applied pressure. The columns were tested under axial compression using a 5000 kN-capacity universal testing machine. The specimens were loaded continuously until failure. A load interval of less than one-tenth of the estimated carrying load capacity was used. The progress of deformation, the mode of failure and the maximum load taken by the specimens were recorded.

4. TEST RESULTS AND DISCUSSION

The variable parameters in this study are the aluminum thickness that covered the columns from outside, the length of the column and durability

4.1 Aluminum Thickness

Five column specimens with same length 450mm are used to study the effect of the thicknesses on the structural behavior of column, four specimens have aluminum tube thicknesses 2mm (C1), 3mm (C2), 4mm (C3) and 5mm (C4) and the fifth specimen (CR) unconfined concrete column which is the reference specimens. For all five column specimens axial deformation and ultimate load were measured. **Table 4 and Fig. 8** show the ultimate load - axial deformation curves. These curves and table show that the strength of concrete is increased by the confining effect of aluminum tube for C2, C3, C4, C5 by 16%, 74%, 105%, 224% with respect to reference specimens CR respectively.
To the study the effect of columns thicknesses on the strength, the impact of the failure was as follows: reference specimen CR failure was by crushing the concrete at mid height, while C3-C4-C5 specimens have failed by buckling. It is therefore concluded that the use of aluminum tube with high resistance to confine the concrete from abroad led to a column thinness affected and thus led to the failure by buckling as shown in **Figs. 9, 10, 11** and **12**.
While C2 column has 2mm thickness failed by local buckling, as shown in **Fig. 13**. This is because the thickness of aluminum tube did not achieve the width thickness ratio for the tube, which is according to **Table 5** where the sections are classified as compact, noncompact, or slender-element sections. If the width thickness ratio D/t compression elements less than λp the section is compact. If the width thickness ratio D/t compression elements exceeds λp, but does not exceed λr the section is noncompact. If the width-thickness ratio of any element exceeds λr, the section is referred to as a slender-element section, from table B4.1in the steel construction manual, **AISC MANUAL, 2014**.

4.2 Length of the Column

To the study the effect of columns length on the strength, the specimen C6 has a length of 700mm with 5 mm thickness the decreased of strength was 0.06% than the specimen C5 with 5 mm thickness and length 450mm. The failure of the specimen C6 with a length of 700 have been affected by failure buckling substantially as shown in **Figs. 14** and **15** and **Table 6**. The specimens C6 has length of 700mm with thickness 5mm, the decreased of strength was 0.01% than the specimen C5 with same thickness and 450mm length.

4.3 Durability

The specimens C7 has length of 450mm with thickness 5mm, the decrease of strength was 0.06% than the specimen C5 with same thickness and length. The failures of two specimens (C7 and C5) have been affected by buckling failure. Therefore; no apparent difference has been found between the structural behavior of the specimen C7 that immersed in aggressive solution for 120 days and specimen C5 in air as shown in **Figs. 16, 17 and 18 and Table 7**.

5. CONCLUSIONS

This study deals with seven column specimens with same concrete diameter 100mm and without steel reinforcement. From experimental test results the following conclusions can be listed:

1. The greatest increase in axial compression load at the column has tube thickness 5mm and the lower increase in axial compression load the column has tube thickness 2mm in range (16% for C2 -224% for C5) if compared with reference specimens CR.
2. The specimens C6 decreased in strength by 0.01% than the specimen C5.
3. The specimens C7 decreased in strength by 0.06% than the specimen C5.
4. Five column specimens (C3, C4, C5, C6, C7) fail by buckling, one column specimen (CR) fail by crushing in concrete at mid height and one column specimen (C2) fail by local buckling.
5. It can be found that, the deformation of the top part of aluminium tube becomes more obvious for the specimen C2 with thinner thickness 2mm, in other words the local buckling occurred in the this specimen on the position near the top to outside of the specimen, thus can be concluded that the interaction between the aluminum tube and concrete is delayed by the restraint of the concrete to inside of the specimen but it is not delayed by the restraint of the concrete to outside of the specimen; therefore, it can be concluded in CFT column, local buckling may occur but in the research of, **Morino and Tsuda ,2014, it was** concluded that the local buckling of the steel tube is delayed by the restraint of the concrete to outside and inside of the specimen. Thus, in this work it was proved that possible occurrence of local buckling in CFT column even if there was a significant correlation between the concrete and material blocking confined.
6. The aluminum ratio in the filled aluminum tubular CFT cross section is much larger than in reinforced concrete and concrete-encased steel cross sections. Because of the aluminum of the CFT section is well plastified under bending and it is located most outside the section therefore; the strength of CFT columns increase.
7. Because of the Confining concrete filled aluminum tubular (CFT) columns can significantly increase their strength, ductility and durability thus, the confining concrete filled aluminum tubular (CFT) columns may be used in marine structures, pier of bridges and bearing bored piles in sand soil.
8. The aluminum tubes can be used as the formwork for casting concrete, thus Labor for forms and reinforcing bars is omitted.

REFERENCES

- American institute of steel construction, 2014, *STEEL CONSTRUCTION MANUAL, AISC MANUAL*, fourteenth edition.

- Arya C., Clarke JL, Kay EA and O._Regan PD. TR 55, 2002, *DESIGN GUIDANCE FOR STRENGTHENING CONCRETE STRUCTURES USING FIBRE COMPOSITE MATERIALS*, Engineering Structures, 24,889–900.

- ASTM B557, 2003, *STANDARD TEST METHODS OF TENSION TESTING WROUGHT AND CAST ALUMINIUM AND MAGNESIUM ALLOY PRODUCTS.*

- ASTM E8, 2003, *STANDARD TEST METHOD FOR TENSION TESTING OF METALLIC MATERIALS.*

- Han, L-H., and Yao, G-H. , 2004, *EXPERIMENTAL BEHAVIOR OF THIN-WALLED HOLLOW STRUCTURAL STEEL (HSS) COLUMNS FILLED WITH SELF-CONSOLIDATING CONCRETE (SCC), THIN-WALLED STRUCTURES*, 42(9),1357–77.

- Kissell and Robert L. Ferry, 2002, *ALUMINUM STRUCTURES, A GUIDE TO THEIR SPECIFICATIONS AND DESIGN*, JOHN WILEY & SONS, INC., Second Edition.

- Morino and Tsuda, 2014, *DESIGN AND CONSTRUCTION OF CONCRETE-FILLED STEEL TUBE COLUMN SYSTEM IN JAPAN* , Earthquake Engineering and Engineering Seismology, Vol. 4, No. 1, p. 51-72.

- Mursi, M. and Uy, B, 2004, *STRENGTH OF SLENDER CONCRETE FILLED HIGH STRENGTH STEEL BOX COLUMN*, Journal of construction steel research, Vol.60, p. 1825-1848.

- Ozbakkaloglu, 2013, *COMPRESSIVE BEHAVIOR OF CONCRETE-fiLLED FRP TUBE COLUMNS*, School of Civil, Environmental and Engineering, University of Adelaide, Australia

- Roeder, C.W., Lehman, D.E., and Bishop, E., 2010, *STRENGTH AND STIFFNESS OF CIRCULAR CONCRETE-FILLED TUBES*, J. Struct. Eng., 136 (12), 1545-1553.

- Yu-Fei Wu and Cheng Jiang, 2013, *EFFECT OF LOAD ECCENTRICITY ON THE STRESS–STRAIN RELATIONSHIP OF FRP-CONFINED CONCRETE COLUMNS*, J. Composite Structures 98, 228-241.
- Yu, Z-w., Ding, F-x., and Cai C.S. , 2007, *EXPERIMENTAL BEHAVIOR OF CIRCULAR CONCRETE FILLED STEEL TUBE STUB COLUMN*, Journal of Constructional Steel Research, 63, 165–174.

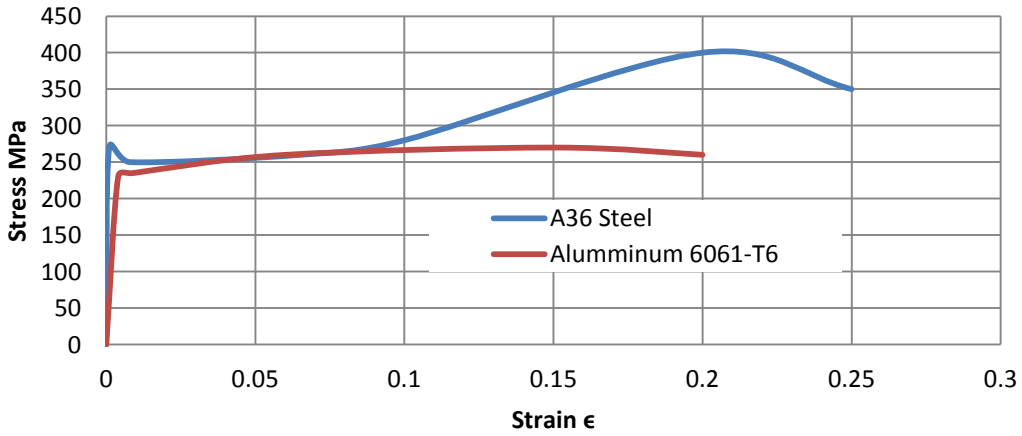

Figure 1. Comparison of the stress strain curve of A36 steel and 6061-T6

Table 1. Results of tensile test on Aluminum Alloy 6061-T6

Aluminum Alloy	Yield strength	Tensile strength	Elongation	Poisson's ratio	Unit weight	Modulus of Elasticity, E
6061-T6	230Mpa	290 Mpa	8%	0.33	27.10 kN/m^3	72000 MPA

Table 2 . Comparing common structural shapes and grades of two metals[7]&[9]

PROPERTY	ALUMINUM 6061-T6	CARBON STEEL A36
Corrosion resistance	good	fair
Tensile yield strength	230 MPa	275 MPa
Modulus of elasticity, E	72 GPa	207 GPa
Elongation	8% - 10%	20%
Density	27 kN/m^3	78 kN/cm^3
Fatigue strength (Plain metal, 5million cycles)	10.2 ksi	24 kpsi
Relative yield strength - to – weight ratio	2.8	1.0 to 1.4
Poisson s ratio	0.33	0.29
Thermal expansion coefficient, α	10^{-6} mm/(mm°C)	11.7 mm/(mm°C)

Table 3. Details of columns specimens

Specimen symbol	Aluminum tubular thickness, mm	Description	Length of columns, mm	Exposed to aggressive solution Yes
CR	0	Plain concrete	450	-
C2	2	Plain concrete - Aluminum tube	450	-
C3	3	Plain concrete - Aluminum tube	450	-
C4	4	Plain concrete - Aluminum tube	450	-
C5	5	Plain concrete - Aluminum tube	450	-
C6	5	Plain concrete - Aluminum tube	450	Yes
C7	5	Plain concrete - Aluminum tube	700	-

(a) (b)

Figure 2. Mould for specimens: (a) – CR and (b) - C2, C3, C4, C5, C6, C7.

Figure 3. Specimens CR, C2, C3, C4, and C5

(a) (b)

Figure 4. Specimens: (a)-C6 and (b)- C7.

Figure 5. Test for columns

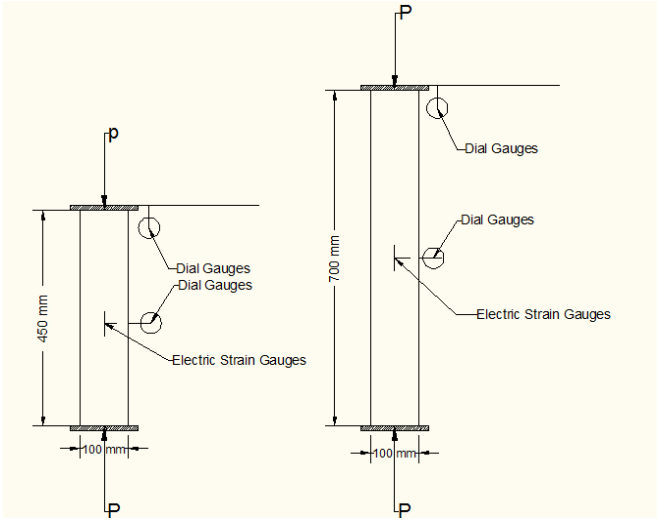

Figure 6. A typical column test layout and instrumentation

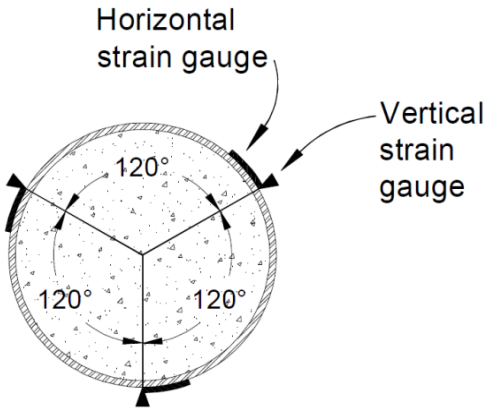

Figure 7. Longitudinal and transverse electric strain gauges

Table (4). Ultimate Load and mode failure for column specimens C2,C3,C4,C5 and CR

Specimen symbol	**Ultimate Load (kN)**	**C2,C3,C4,C5 / CR** ***Pu / Pco***	**Mode failure**
CR	190*	190/190=1.00	crushing
C2	220**	220/190=1.16	Local buckling
C3	330**	330/190=1.74	buckling
C4	390**	390/190=2.05	buckling
C5	426**	426/190=2.24	buckling

* *Pco* : the ultimate load of unconfined concrete.
** *Pu* : the ultimate load of the hybrid column.

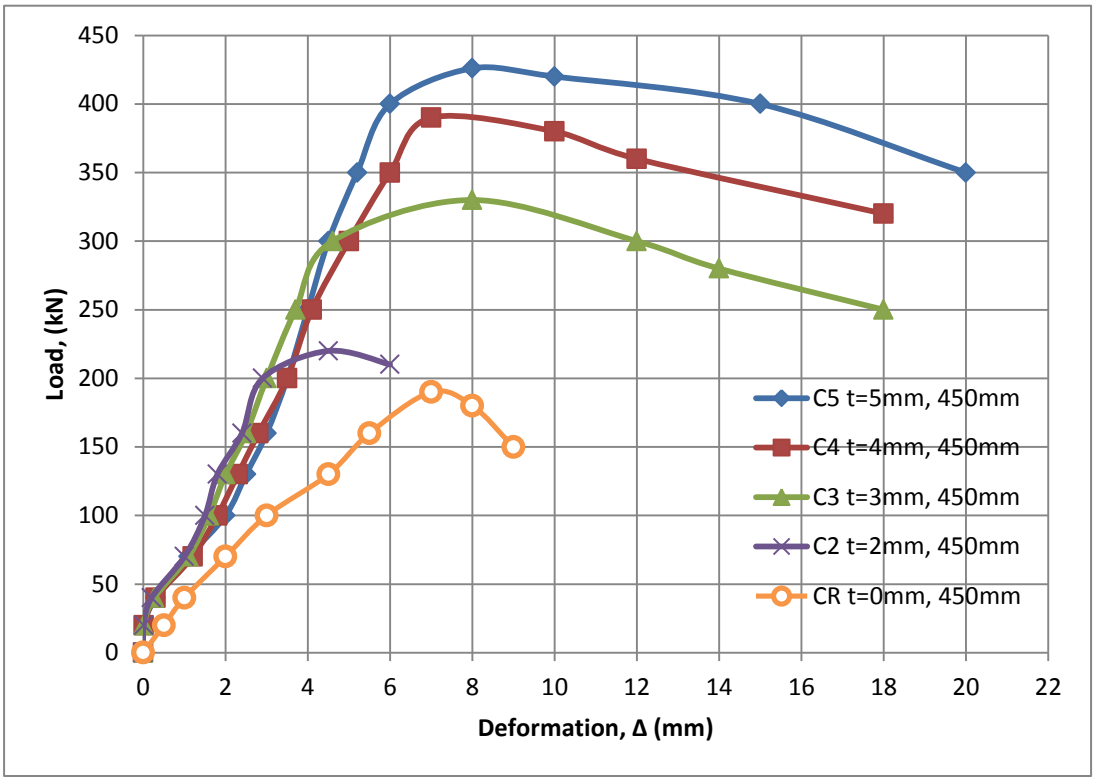

Figure 8. The ultimate load - axial deformation curves for CR, C2, C3, C4, C5.

Figure 9. Reference column CR ,t=0mm (mode failure) **Figure 10.** C3 ,t=3mm (mode failure)

Figure 11 C4 ,t=4mm (mode failure) **Figure 12.** C5 ,t=5mm (mode failure)

Figure 13. C2 ,t=2mm (mode failure)

Table 5. Limiting width-thickness ratios for compression elements

Limiting Width-Thickness Ratios for Compression Elements			
Description of Element	**Limiting Width Thickness Ratios**		
	Width Thickness Ratio	**λp (compact)**	**λr (noncompact)**
In uniform compression	D/t	NA	0.11 E/Fy
D/t =102/2=51 > λr = 0.11x E / Fy=0.11x72000/230 = 34.435 , therefore, The section is referred to as a slender-element section D = outer diameter of aluminum tube t = thickness of aluminum tube			

Table 6. Ultimate Load and mode failure for column specimens C5 and C6

Specimen symbol	Ultimate Load (kN)	C5,C6 / CR *Pu* / *Pco*	Mode failure
C5	426*	426/426=1.00	buckling
C6	422**	422/426=0.99	buckling

* *Pco* : the ultimate load of hybrid column C5.
** *Pu* : the ultimate load of the hybrid column C6.

Figure 14. C7 , t=5mmwith length 700mm (mode failure)

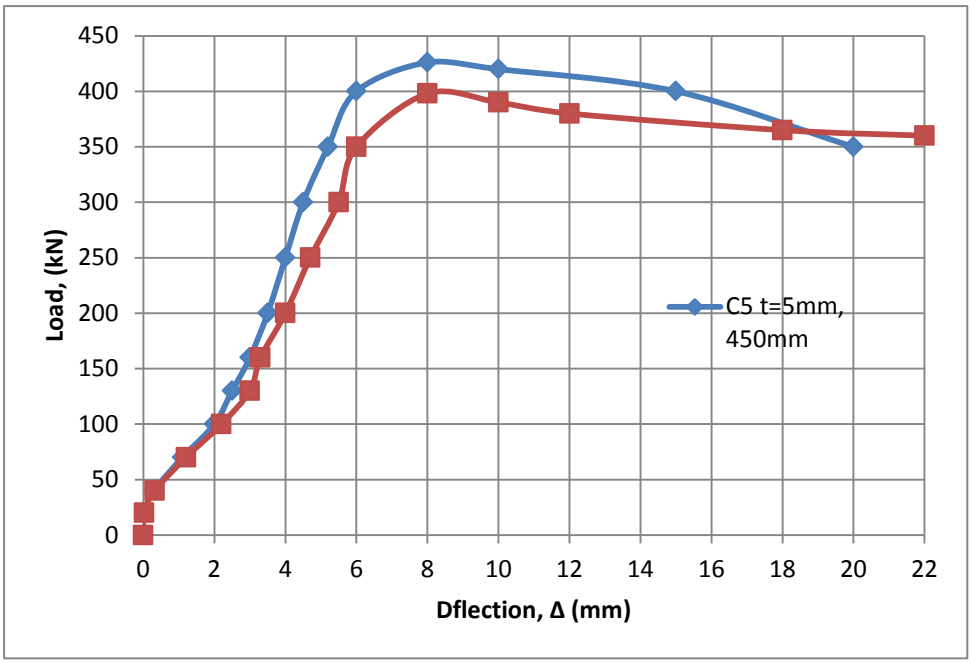

Figure 15. The ultimate load - axial deformation curves for C5 and C7.

Table 7. Ultimate Load and mode failure for column specimens C5 and C7

Specimen symbol	Ultimate Load (kN)	C5,C7 *Pu* / *Pco*	Mode failure
C5	426*	426/190=2.24	buckling
C7	398**	398/190=2.09	buckling

* *Pco* : the ultimate load of hybrid column C5.
** *Pu* : the ultimate load of the hybrid column C7.

Figure 16. C6 ,t=5mm (mode failure)

Figure 17. C6 ,t=5mm, in aggressive solution

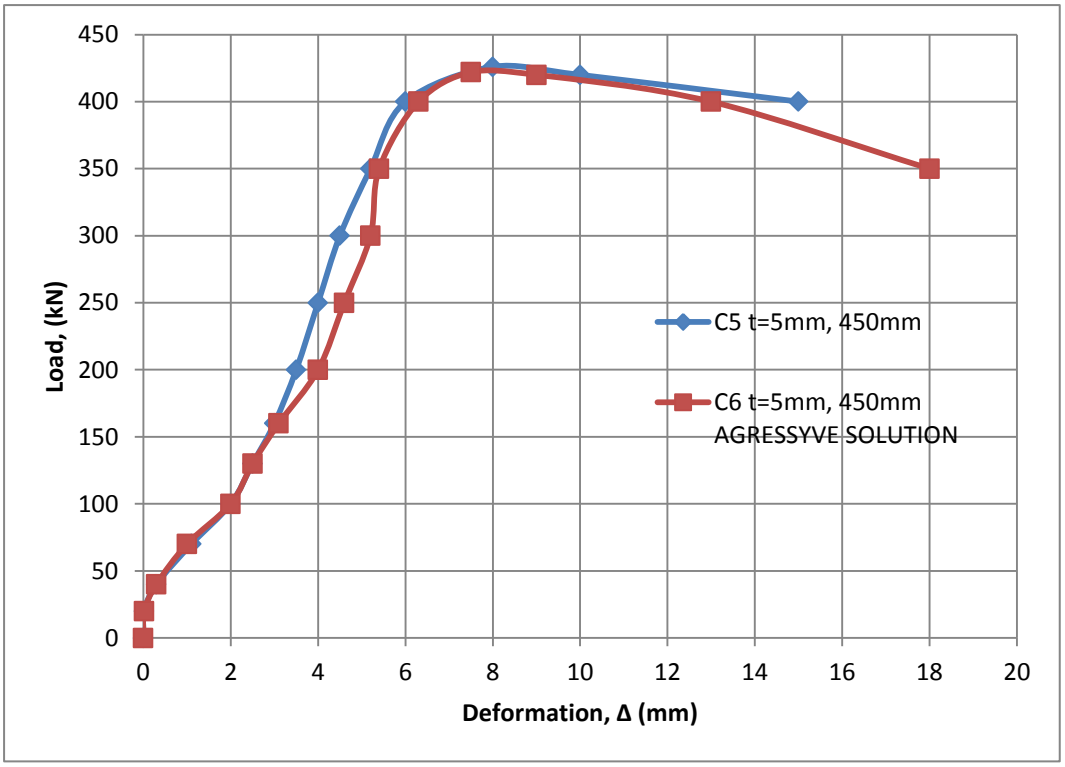

Figure 18. The ultimate load - axial deformation curves for C5 and C6.

Preparation and Characterization of Activated Carbon for Adsorption of Fluoroquinolones Antibiotics

Ammar Salih Abbas
Assistant Professor
College of Engineering-University of Baghdad
ammarabbas@coeng.uobaghdad.edu.iq

Teeba Mohammed Darweesh
Researcher
College of Engineering-University of Baghdad
teebamohammed87@yahoo.com

ABSTRACT

In this research, the preparation of a chemically activated carbon from date stones by using electric and microwave assisted K_2CO_3 activation was studied. The effect of radiation power, radiation time, and impregnation ratio on the yield and Iodine number on the activated carbons was investigated. The activated carbon characterizations were examined by its surface area, pore structure analysis, bulk density, moisture content, ash content, iodine number, FTIR, and scanning electron microscopy (SEM). The adsorption capacity was also studied by adsorption of fluoroquinolones antibiotics, CIP, NOR, and LEVO, by the prepared activated carbon.

Key words: Activated carbon, Date stones, fluoroquinolones antibiotics, Microwave.

تحضير وتوصيف الكاربون المنشط لأمتزاز ملوثات الفلوروكوينولونس

عمار صالح عباس
استاذ مساعد
كلية الهندسة-جامعة بغداد

طيبة محمد درويش
باحث
كلية الهندسة-جامعة بغداد

الخلاصة

تم تحضير الكاربون المنشط من نوى التمر بأستخدام الفرن الكهربائي و الميكروويف و باستعمال كاربونات البوتاسيوم كمادة منشطة.

تمت دراسة تاثير طاقة الاشعاع و زمن الاشعاع و نسبة التغطيس على انتاج الكاربون المنشط و قيم رقم الايودين للكاربون المنشط. خصائص الكاربون المنشط التي تمت دراستها متمثلة بالمساحه السطحية و حجم المسامات و الكثافة ومحتوى الرطوبة و محتوى الرماد و رقم الايودين و تحليل الطيفي بالأشعة تحت الحمراء و صورة المجهر الألكتروني.

تم قياس سعة امتزاز الكاربون المنشط من خلال امتزاز المضاد الحيوي الفلوروكوينولينس (السبروفلوكسن والنورفلوكسن و الليفوفلوكسن).

الكلمات الرئيسية : الكاربون المنشط, نوى التمر, مضادات الفلوروكوينولونس, مايكروويف.

1. INTRODUCTION

Many precursors can be used successfully for the preparation of low cost activated carbon such us sugar beet bagasse **Demiral, and Gündüzoğlu, 2010**, coal **Teng, et al., 1998**, fruit peel **Kartika, et al., 2008**, Waste tea **Yagmu, et al., 2008**, olive stone **Blázquez, et al., 2005**, date stone **Foo, and Hameed, 2011**, and rice husk **Tyagi, et al., 2011**. Two processes are used for preparation of activated carbon: physical activation and chemical activation. Physical activation includes carbonization of carbonaceous content and then activation of resulting char by activation agent such as steam or CO_2 **Bouchelta, et al., 2008**. Chemical activation involves the impregnation of raw material by an activation agent such as KOH, H_3PO_4, $ZnCl_2$, etc. and then heated in an inert atmosphere. Chemical activation is more preferred than physical activation because of the higher yield, shorter time, simplicity, and lower temperature needed for activating material **Li, et al., 2010**. The preparation of activated carbon by microwave heating has many advantages. The important one is the reduction in activation time which results in lower energy consumption. There are many applications in using microwave heating for prepared activated carbon by KOH activation **Foo, and Hameed, 2011**, $ZnCl_2$ activation **Wang, et al., 2009**, phosphoric acid activation **Liu, et al., 2010**.

The fluoroquinolones are a series of synthetic antimicrobial agents which have a broad spectrum of activity against organisms **King, and Lan, 1986**. It is used in the treatment of several infections in human and animals. Hospitals and drug manufactures are the main sources of wastewater containing drug contamination. Also in wastewater treatment plants, antibiotics are partially eliminated and their main amount kept to the aquatic ecosystem. The presence of drug antibiotics in surface water and wastewater, even at low concentrations is considered an environmental hazard and can cause antibiotic resistance in bacteria **Bhandari, et al., 2008**.

In previous century, many techniques were enhanced to get rid of contaminants from the wastewaters, where they present at high concentrations in order of $\mu g\ L^{-1}$ to $mg\ L^{-1}$. The best drinking water treatment and wastewater treatments were found on coagulation, filtration, flocculation, biological degradation, and sedimentation methods that exposed ineffective removing for drugs counting antibiotics **Chayid and Ahmed, 2015**.

The aim of this work is to prepare a low cost activated carbon from natural precursors (date stones) for the adsorption of fluoroquinolones antibiotics from aqueous solution. The effect of impregnation ratio, radiation power, and radiation time are also investigated to obtain a high yield and adsorption capacity.

2. MATERIALS AND METHODS

2.1 Materials

In this study, date stones were used as precursor for the preparation of activated carbon. Firstly the stones were washed with tap water to get rid of impurities, washed with distilled water, dried in oven for 24h at 110◦C, and crushed using disk mill, with the average particle size of 1 to 2 mm.

In this research, two chemical activators for preparation two types of activated carbon, K_2CO_3 (provided by Didactic Company, Espuma) of purity 99.9%. Three types of fluoroquinolones antibiotics were used: CIP of purity 99.9% are provided by Nanjing Huaxin Biofarm. Company Ltd., China, and NOR with purity 99.9% are provided by Ajanta Pharma Limited Company, India.

2.2 Preparation and Characterization of Activated Carbon

20 g of dried date stones was put in a stainless steel reactor (3 cm diameter * 15 cm length). The reactor was closed in one end and the other end had a removable cover which contains a 1mm hole in the middle to allow the escaping of the pyrolysis gases. The reactor is put in the middle of an electric furnace and heated at 500° C for 1 h. After that the reactor was taken out of the furnace and allowed to cool. Each 2g of the above sample was mixed with 10ml of K_2CO_3 solution with impregnation ratio (0.4 to 1.5 g/g) for 24h at room temperature. Then, these samples were dried in an oven at 110◦C until well dried and stored in desiccators. In the activation step of dried impregnated samples, quartz glass reactor (3 cm diameter and 13 cm length) was used. The reactor closed at one end and the other end was opened to a stainless steel pipe with 5mm inside diameter. The reactor was put in a modified microwave heating oven (MM717CPJ, China), **Fig.1,** and run at different radiation power for different radiation time. At the end of activation step the samples were withdrawn from the oven and allowed to cool. After that the samples were socked with 0.1 M HCL solution (10ml/g liquid to solid ratio). The mixture left at room temperature for 24 h and then filtered and washed with distilled water until the pH of solution reaches (6.5-7). Finally dried for 24h at 110◦C and then the samples were weighed to calculate the yield of product and finally the activated carbon was stored in tightly closed bottles. The yield of prepared activated carbon is equal the ratio of final weight of product to the weight of precursor initially used which is based on this equation:

$$yield = \frac{\mathrm{Wf}}{\mathrm{W_o}} * 100 \qquad (1)$$

where Wf and W_o are the weight of activated carbon product g and the weight of date stone, g, respectively.

The characterization of activated carbon was represented by surface area, bulk density, ash content, moisture content, iodine number.

A set of batch mode experiments were carried out to study the uptakes of each antibiotics. 0.1g of prepared activated carbon was mixed with 100 ml samples of CIP, NOR, and LEVO with initial concentration 150 mg/l. The mixtures were shaken at 200 rpm for 24hours, and then the mixtures filtered. The concentrations of each antibiotic in filtrate was analyzed using UV- Visible Spectrophotometer with wave length 274, 272, and 290nm for CIP, NOR, and LEVO respectively. The adsorbed capacity or uptake of antibiotics q_t was calculated by:

$$qt=\frac{(C_o-Ce)V}{W} \quad (2)$$

where Ce (mg/l) is the concentration of antibiotics at equilibrium, mg/l, V (ml) is volume of antibiotic solutions, and W (mg) is weight of activated carbon.

2.2.1 Bulk density

Apparent or bulk density was determined by this simple method, a 10 ml cylinder filled to a specified volume with prepared activated carbon that had been dried in an oven at 80◦C for 24 h **Ahmedna, et al., 1997**, and then calculated as follows:

$$bulk\ density = \frac{Wc}{Vc} \quad (3)$$

where Wc is the weight of dried carbon (g), and Vc is the cylinder volume (ml) filled with dried carbon.

2.2.2 Ash content

The ash content was calculated as follows: 0.1 g of activated carbon with particle size of 250µm was dried at 80◦C for 24h and put into weight ceramic crucibles. The sample was heated in an electric furnace at 650◦C for 3h. Then it was left to cool to room temperature and then weighed. Then by using this equation, the percent of ash was determined **ASTM Standard, 2000**.

$$ash\% = \frac{Ws3-Ws2}{Ws1} * 100 \quad (4)$$

where Ws_1 is the weight of activated carbon (g), Ws_2 is the weight of ceramic crucible (g), and Ws_3 is the weight of ceramic crucible containing ash (g).

2.2.3 Moisture content

Oven drying method was used to calculate moisture content **Adekola, and Adegoke, 2005**. 0.1 g of prepared activated carbon with particle size 250µm was put into weighed ceramic crucible. The sample were dried at 110◦C to constant weight, and then cooled to room temperature and weight.

$$moisture\% = \frac{Wm3-Wm2}{Wm1} \quad (5)$$

where W_{m1} is the weight of activated carbon sample (g), W_{m2} is weight of ceramic crucible with dried sample (g), and W_{m3} is the weight of ceramic crucible with original activated carbon used (g).

2.2.4 Iodine number

It is a measure of micropore content of activated carbon. It was calculated by standard method **Lubrizol Standard Test Method, 2006**. 10ml of 0.1 N iodine solution in a conical flask was titrated with 0.1N sodium thiosulfate solution with two drops of 0.1N starch solution as indicator, until the color of solution become colorless. 0.1g of activated carbon was added to 15ml of 0.1N iodine solution, and then the solution was shaken for 4minutes and then filtered. 10 ml of the filtered solution was titrated with 0.1N sodium thiosulfate in the presence of two drops of 0.1N starch solution as indicator. Then by using this equation:

$$Iodine\ number = \frac{(\mathrm{Vb}-\mathrm{Vs}).\mathrm{N}.(126.9).(\frac{15}{10})}{\mathrm{M}} \quad (6)$$

where Vb (ml) is the volume of blank sodium thiosulfate solution, Vs (ml) is the volume of titrated sodium thiosulfate solution, N1 (mol /L) is the normality of sodium thiosulfate solution, and M (g) is the mass of activated carbon used.

3. RESULTS AND DISCUSSION

3.1 Characteristics of Activated Carbon

The characteristics of prepared activated carbon were shown in Table 1. The surface area is the most important characteristics, 852 m^2/g for activated carbon impregnated with K_2CO_3. This result may be in agreement with that prepared by **Foo, and Hameed, 2011**, who prepared an activated carbon from date stones by microwave induced chemical activation with surface area of 856 m^2/g, **Bamufleh, 2009**, prepared activated carbon from date stones by chemical activation with $ZnCl_2$ with surface area 802- 1270 m^2/g, and **Hameed, et al., 2009**, who showed a surface area of activated carbon by chemical activation of KOH of date stones was 763.4 m^2/g. This may be due to the ability of K_2CO_3 to produce an activated carbon which had high micropore content.

3.2 SEM Image

The scanning electron microscope image in **Fig.2** of activated carbon with optimum operating conditions (t=8min, P=540W, IR=0.8g/g) for activated carbon activated by K_2CO_3. From SEM image, there were clear changes in the surface of date stones particles before and after chemical activation. It can be found that the surface of date stone is very flat and dense with loss of any pore, while the microwave irradiation forms a lot of pores structure with thin boundary.

3.3 FT-IR Analysis

Fourier transform infrared spectroscopy (FTIR) was used to show the carbons of any adsorbent in the range of (400-4000) cm^{-1} wave number to get information about functional group and chemical

structure **Speight James, 2005**. **Fig. 3** shows the FT-IR analysis of activated carbon, from this figure the band between the range (3400-3500) cm^{-1} for prepared activated carbon is assigned to the O-H hydroxyl groups, the hydrogen bonding may be because of the adsorbed water from the surroundings **Vinke, et al., 1994**. The double peak at (2850–2950) cm^{-1} may be due to the C-H stretching vibrations **Jia, and Thomas, 2006**. The band at (1050–1200) cm^{-1}regin is probably assigned to C-O stretching in phenols and alcohols **Phussadee, et al., 2008**. Also the peak at 1650 is the (-COOH and $–COOCH_3$) stretching vibration of nonionic carboxyl group, this may be due to carboxylic acids or esters **Li, et al., 2007**. The peak near 2360 cm^{-1} may be due to the band consideration of CO_2 **Gascoin, et al., 2008**. The bond occurring near 1400 cm^{-1} due to C=O stretching, C–O stretching in carboxylate moieties and carboxylic **groups Lua, et al., 2005**. The bands near 1750 cm^{-1} C=O group in configurations such as Quinone, lactones, and COOH groups which indicates the presence of ester and acetyl group that present in hemicelluloses **Chandrasekaran, et al., 2014**.

4. IODINE NUMBER, YIELD AND UPTAKE OF ACTIVATED CARBON

4.1 Effect of Radiation Time

The relation between the yield and time is shown in **Fig. 4**. From this figure the yield of activated carbon decreases when time increases from 4 to 12 minutes. After 10 min, a slow decrease occurred in yield during activation because of rapid formation of volatile material which form stable structure **Foo, and Hameed, 2012a.**

Fig. 5 also shows the relation between iodine No. and time. The iodine no. range 631.89 to 854.91 for prepared activated carbon. The optimum time of 8 min gave a higher iodine no. for activated carbons. It's higher than prepared by **Haimour, and Emeish, 2006**, 495mg/g for activated carbon that prepared from date stones and phosphoric acid by chemical activation. This is may be because of the ability of K_2CO_3 to form high micropore content in the active carbon.

The adsorption of fluoroquinolones antibiotics, CIP, NOR, and LEVO by activated carbon are shown in **Fig. 6**, where the uptake of all antibiotics increase when time increases and reach maximum at time of 8 min, then decreases until the time increase. The maximum uptake of fluoroquinolones antibiotics were 97.4, 93.9, 99.8 mg/g for CIP, NOR, and LEVO respectively. In this study the activation time of 8 min may be considered as a best time for preparation of both type of activated carbon. **Ahmed and Thydan, 2013**, showed that 8 min is the best time for preparation of activated carbon prepared from albizia lebbeck seed pods by microwave activation.

4.2 Effect of Radiation Power

The yield of activated carbon versus radiation power is shown in **Fig. 7.** From this figure it can be see that the yield decreased with the increase in power from 380-700W. This decrease may be due to loss in volatile materials with high power value. Also, after 620W a steep decrease in yield

occurs because of formation of stable structure. **Fig. 8** also shows the relation between Iodine no. and radiation power. 540W power gave higher iodine no. for activated carbon activated by K_2CO_3. The antibiotics uptake, **Fig. 9**, also shows the similar behavior as above. Its increase with increase in radiation power, reached maximum at 540 W for activated carbon promoted by K_2CO_3 and then increased with increasing radiation power. The maximum uptake of fluoroquinolones antibiotics were 97.4, 93.9, 99.8 mg/g for CIP, NOR, and LEVO respectively. This decrease at high power may be due to sintering effect followed by the shrinkage of the char, then realignment in the structure of the carbon that lead to reduce the pore areas and then volume **Foo, and Hameed, 2012b**.

4.3 Effect of impregnation ratio

Impregnation ratio of activator/precursor is an important factor in the chemical activation process **Ahmadpour, and Do, 1996**. The relation between yield and impregnation ratio is shown in **Fig. 10**. It can be seen that, as the impregnation ratio increases, the yield decreases. This is may be because of rapid removal of tar component from the pore. After 1g/g, a steep decrease in yield occurs due to stable structure. **Fig. 11** shows the relation between iodine no. and impregnation ratio. 0.8g/g ratio gave a higher iodine no. for activated carbon. The uptake of fluoroquinolones antibiotics also increases with increasing impregnation ratio, and reached maximum uptake at 0.8 g/g then decreased as shown in **Fig. 12**. The maximum fluoroquinolones antibiotics uptake were 97.4, 93.3, 99.8 g/g for CIP, NOR, and LEVO respectively. **Foo, and Hameed, 2012c** showed the same behavior, where the yield and uptake increased when increasing the impregnation ratio (0.25 to 2) g/g , reaching a maximum value, then decreased for their prepared activated carbon from empty fruit bunch waste by microwave heating.

4. CONCLUSIONS

A simple method is used in this work for preparation of activated carbon with high surface area and heterogeneous structure from date stones by conventional and K_2CO_3 microwave heating activation. The effect of different parameter such as radiation time, radiation power and impregnation ratio on the yield, iodine number, and fluoroquinolones antibiotics adsorption were studied. The maximum yield were 44%, 37.8%, 40% for optimum conditions of 8 min. radiation time, 540 W radiation power and 0.8 g/g impregnation ratio. The iodine no. for optimum condition was 854.91. The surface area is 852 m^2/g and pore volume 0.761cm^3/g. A good adsorption of fluoroquinolones antibiotics was obtained by the prepared activated carbon. CIP uptake of 97.4 mg/g, NOR uptake of 93.9 mg/g and LEVO uptake of 99.8 mg/g for AC- K_2CO_3 that obtained at optimum conditions.

REFERENCES

- Adekola, F. A., and Adegoke, H. I., 2005, Ife J. Sci., Vol.7, No. 1, PP.151–157.
- Ahmadpour, A., Do, D. D., 1996, *The Preparation Of Activated Carbon From Coal By Chemical And Physical Activation.* Carbon, Vol.34, NO.4, PP. 471-479.
- Ahmed, M. J., Thydan, S. K., 2013, *Adsorption Of P-Chlorophenol Onto Microporous Activated Carbon From Albizia Lebbeck Seed Pods By One-Step Microwave Assisted Activation*, Journal of Analytical and Applied Pyrolysis, Vol. 100, PP. 253–260.
- Ahmedna, M., Marshall, W. E., Rao, R. M., and Clarke, S. J., 1997, *J. Sci. Food Agric*. Vol. 75, NO.1, PP. 109–116.
- ASTM Standard, 2000, *Standard Test Method for Total Ash Content of Activated Carbon*, Designation D 2866-94.
- Bamufleh, H. S., 2009, *Appl. Catal*. A: Gen. Vol. 365, PP. 153–158.
- Bhandari, A., Close, L. I., Kim, W., Hunter, R. B., Kock, D. E., and Surampalli, R. Y., 2008, *Occurrence Of Ciprofloxacin, Sulfamethoxazole, And Azithromycin In Municipal Waste Water Treatment Plants. Practice Periodical of Hazardous, Toxic, and Radioactive,* Waste Management. Vol. 16, PP. 179-274.
- Blázquez, G., Hernáinz, F., and Calero, M., 2005, *Removal of Cadmium Ions with Olive Stones: The Effect of Some Parameters*, Process Biochemistry, Vol. 40, PP. 2649-2654.
- Bouchelta, C., Medjran, M. S., Bertrand, O., Bellat, J., and Anal, J., 2008, *Appl. Pyrol*. Vol. 28, PP. 70–77
- Chandrasekaran, T., Arunkumar, A., and Riaz, A. K.,, 2014, *Preparation And Characterization Of A Chemically Activated Carbon Derived From The Natural Plant Gmc*, World Journal Of Pharmacy And Pharmaceutical Sciences, Vol. 3, Issue 7, PP. 1644-1654
- Chayid, M. A., and Ahmed, M. J., 2015, *Amoxicillin adsorption on microwave prepared activated carbon from 2 Arundo donax Linn: Isotherms, kinetics, and thermodynamics studies*, Journal of Environmental Chemical Engineering JECE, Vol. 661, Issue 5, PP. 1–10.

- Demiral, H., and Gündüzoğlu, G., 2010, *Removal of Nitrate From Aqueous Solutions by Activated Carbon Prepared From Sugar Beet Bagasse*, Bioresource Technology, Vol. 101, PP. 1657-1680.

- Foo, K. Y., and Hameed, B. H., 2011, *Preparation of Activated Carbon From Date Stones By Microwave Induced Chemical Activation: Application For Methylene Blue Adsorption*, Chemical Engineering Journal, Vol. 170, PP. 338–341.

- Foo, K. Y., and Hameed, B. H., 2012a, *Coconut Husk Derived Activated Carbon Via Microwave Induced Activation: Effects Of Activation Agents, Preparation Parameters, And Adsorption Performance*, chemical Engineering Journal, Vol. 184, PP. 57-65.

- Foo, K. Y., and Hameed, B. H., 2012b, *Factors Affecting The Carbon Yield And Adsorption Capability Of The Mangosteen Peel Activated Carbon Prepared By Microwave Assisted K2CO3 Activation*, Chemical Engineering Journal, Vol. 180, PP. 66–74.

- Foo, K. Y., and Hameed, B. H., 2012c, *Preparation Of Activated Carbon By Microwave Heating Of Langsat (Lansium Domesticum) Empty Fruit Bunch Waste*, Bioresource Technology, Vol. 116, PP. 522–525.

- Gascoin, N., Gillard, P., Bernard, S., and Bouchez, M., 2008, *Fuel Process Technol*., Vol. 89,PP. 1416-1428.

- Haimour, N. M., and Emeish, S., 2006, *Waste Manage*. Vol. 26, PP. 651-660.

- Hameed, B. H., Salman, J. M., and Ahmad, A. L., 2009, *Adsorption Isotherm And Kinetic Modeling Of 2,4-D Pesticide On Activated Carbon Derived From Datestones*, J. Hazard. Mater. Vol. 163, PP. 121–126.

- Jia, Y. F., and Thomas, K. M., 2006, *Adsorption Of Cadmium Ions On Oxygen Surface Sites In Activated Carbon*, Langmuir, Vol. 16, PP. 1114-1122.

- King, A., and Lan,P., 1986, *The Comparative In-Vitro Activity Of Eight Newer Quinolones And Naliidixic Acid*, J. Antimicrob. Chemother, 18(Suppl. D.): 1-20.

- Li, F. T., Yang, H, Zhao, H., and Xu, R., 2007, Chin Chem Lett. 18,325.

- Li, Y., Du, Q., Wang, X., Xia, Y. J., 2010, *Hazard. Mater*. Vol. 183, PP. 583–589.

- Liu, Q-S, Zheng, T., Wang, P., and Guo, L., 2010, *Preparation And Characterization Of Activated Carbonfrom Bamboo By Microwave-Indesed Phosphoric Acid Activation*, Industrial Crop and Products,Vol. 31, PP. 233-238.

- Lua, A. C., Yang, T., 2005, *J. Colloid. Interf. Sci*., 290, 505.

- Lubrizol Standard Test Method, 2006, *Iodine Value*, Test Procedure AATM 1112-01, October 16.

- Phussadee, P., Apipreeya, K., and Prasert, P., 2008, *Batch Studies Of Adsorption Of Copper And Lead On Activated Carbon From Eucalyptus Camaldulensis Dehn. Bark*, J. Environ. Sci., Vol. 20, PP. 1028-1034.

- Prahas, D., Kartika, Y., Indraswati, N., and Ismadji, S., 2008, *Activated Carbon Preparation From Jackfruit Peel Waste By H_3PO_4chemical Activation: Pore Structure and Surface Chemistry Characterization*, Chemical Engineering Journal, Vol. 140, PP. 32-42.

- Speight James G. 2005, *Lange`S Handbook Of Chemistry*, McGraw – Hill, Inc., 16th ed. PP (8–41) – (8-61).

- Teng, H., Yeh, T., and Hsu, L-Y., 1998, *Preparation of Activated Carbon From Bituminous Coal With Phosphoric Acid Activation*, Carbon, Vol. 36, PP. 1378-1395.

- Tyagi, D. K., Sarita, Y., and Yadav, O. P., 2011, *Equilibrium And Kinetic Studies On Adsorption Of Aniline Blue From Aqueous Solution Onto Rice Husk Carbon*, International journal of Chemistry Research, Vol. 2, NO. 3, PP. 0976-5689.

- Vinke, P., Eijk, V., Verbree, M., Voskamp E., and Bekkum, H.V., 1994, *Modification Of The Surface Of A Gas Activated Carbon And A Chemically Activated Carbon With Nitric Acid, Hypochlorite, And Ammonia*, Carbon, Vol. 32, PP. 657-686.

- Wang, T., Tan, S., and Liang, C., 2009, *Preparation and Characterization Of Activated Carbon From Wood Via Microwave-Induced Zncl$_2$ Activation*, Carbon, Vol. 47, PP. 1880-1883.
- Yagmu, E., Ozmak, M., and Aktas, Z., 2008, *A Novel Method for Production of Activated Carbon From Waste Tea By Chemical Activation With Microwave Energy*, Fuel, Vol. 87, PP. 3278-3285.

NOMENCLATURE

Ce	Equilibrium condentration of each antibiotics, mg/l
C_o	Initial concentration of each antibiotics, mg/l
M	Mass of activated carbon, mg
N1	normality of sodium thiosulfate solution, mol/l
qt	Uptake of antibiotic at equilibrium, mg/g
V	Volume of antibiotic solutions, ml
V_b	volume of blank sodium thiosulfste solution, ml
V_c	Cylinder volume, ml
V_s	volume of titrated sodium thiosulfste solution, ml
W_c	Weight of dried carbon, mg
W_f	Weight of activated carbon product, mg
W_{m1}	weight of activated carbon sample, g
W_{m2}	weight of ceramic crucible, g
W_{m3}	weight of ceramic crucible with original activated carbon used, g
W_o	Weight of date stones, g

ABBREVIATIONS

CIP	Ciprofloxcin
LEVO	Levofloxcin
NOR	Norfloxcin

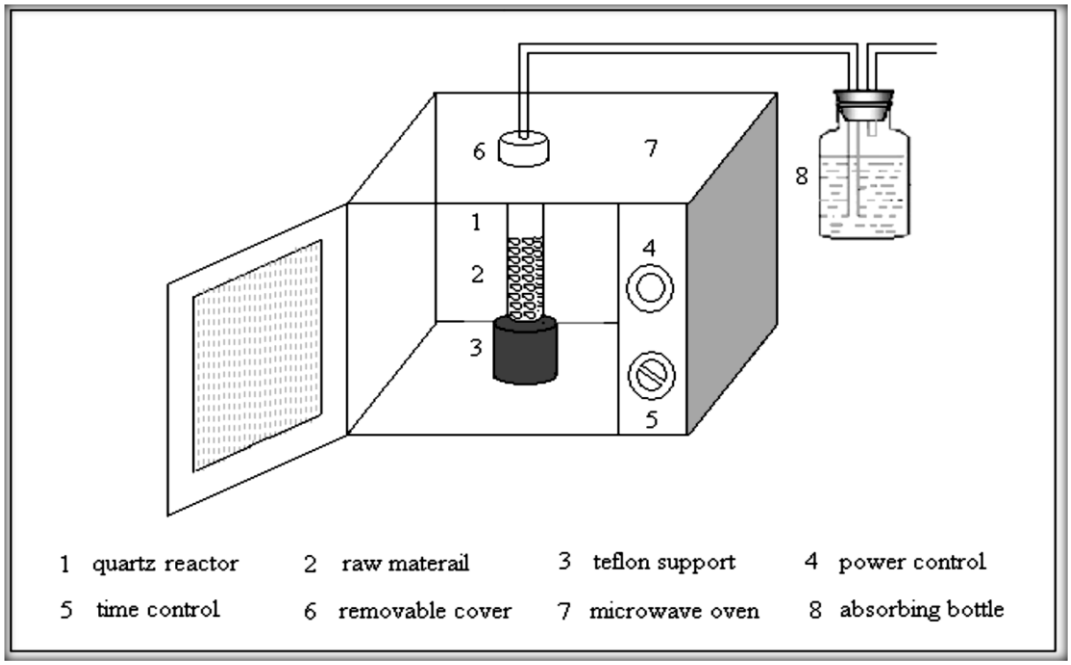

Figure 1, Schematic diagram of microwave unit for preparation of activated carbon.

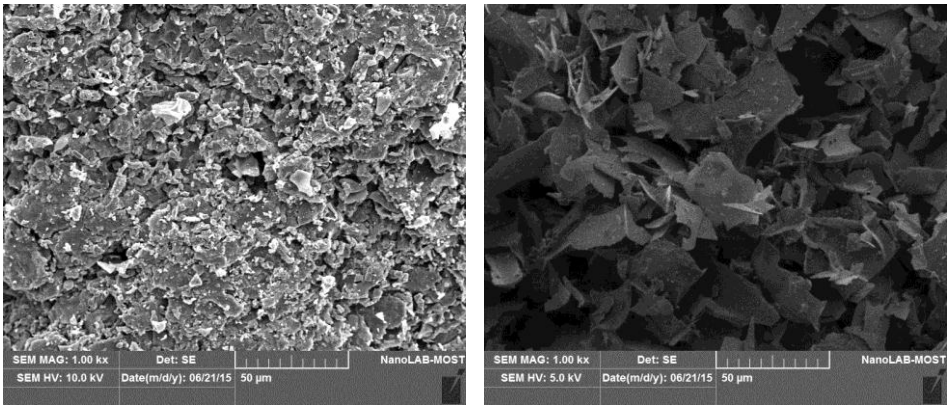

(a) (b)

Figure 2. SEM images of (a) date stone and (b) activated carbon, respectively.

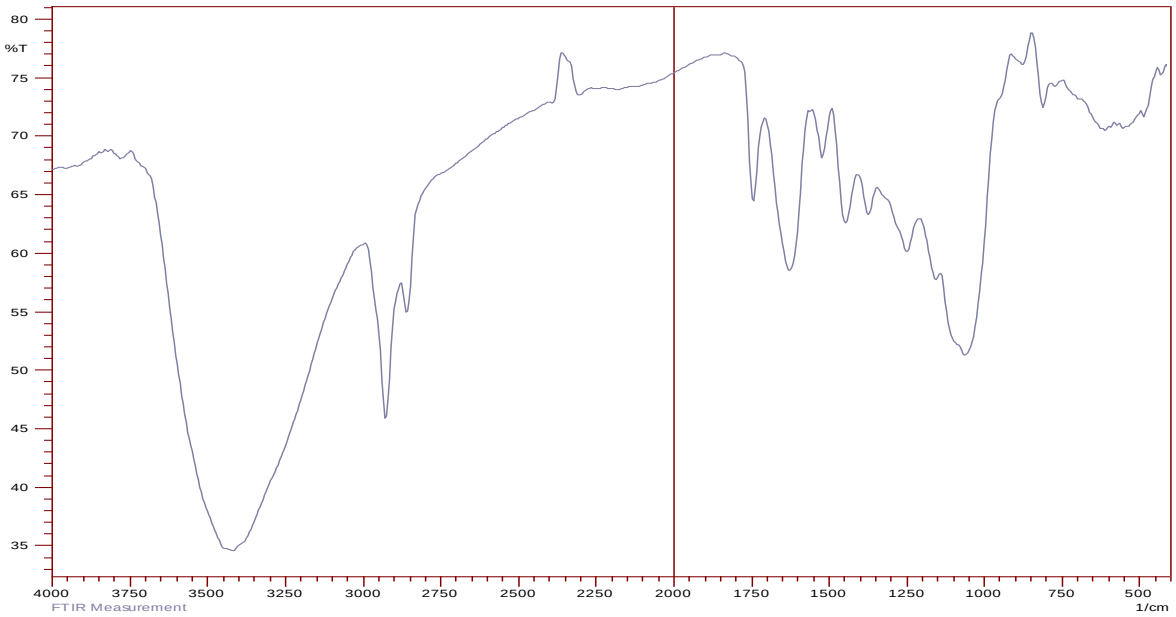

Figure 3. Activated carbon activated by K_2CO_3

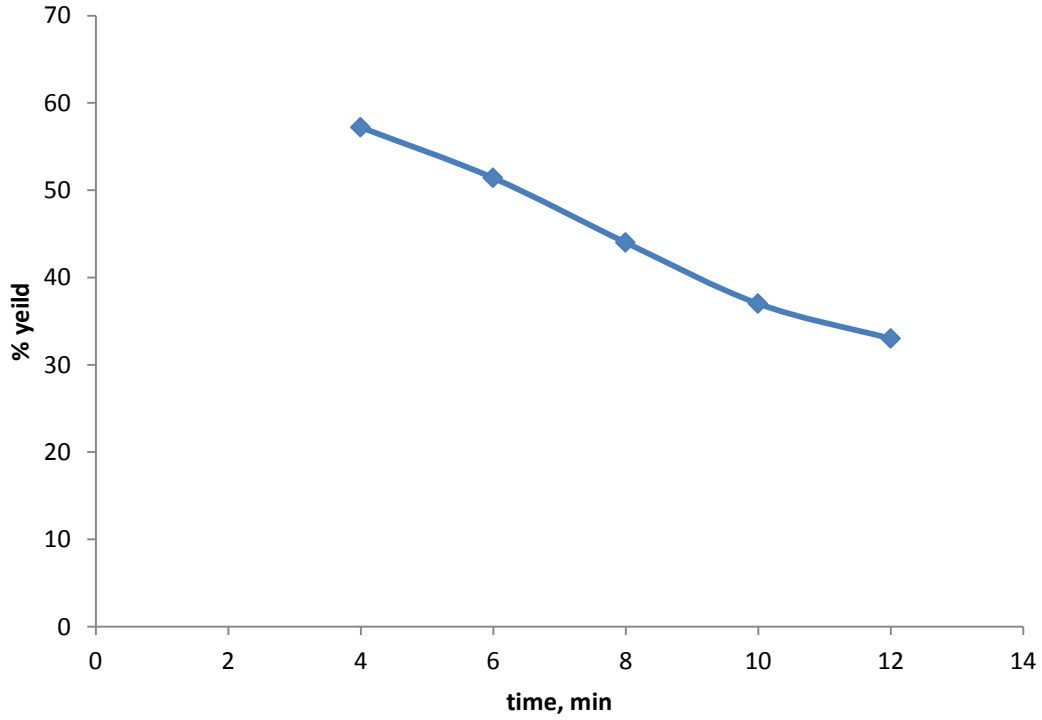

Figure 4. Effect of time on the yield of activated carbon.

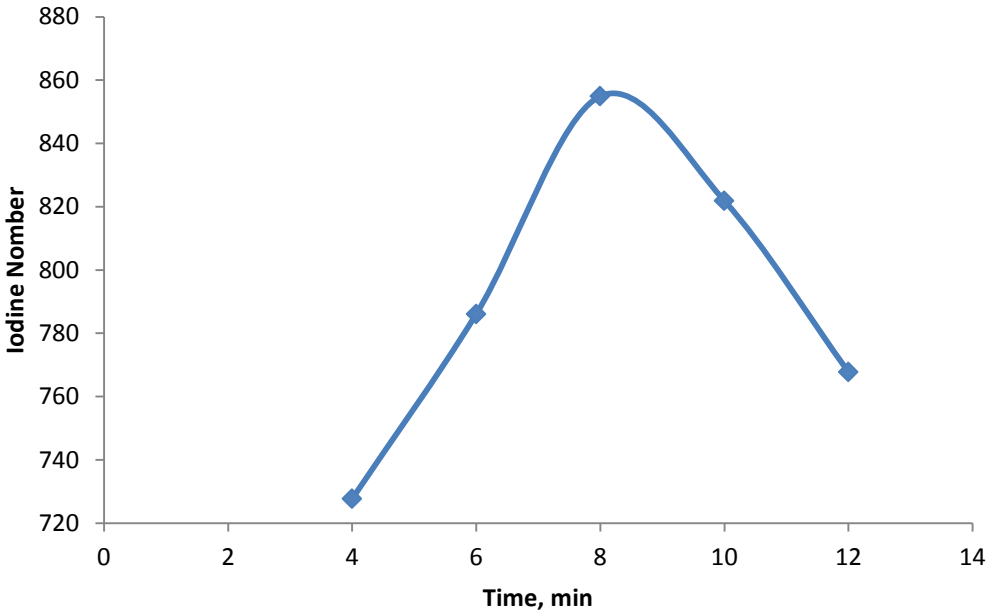

Figure 5. Effect of time on Iodine number

.

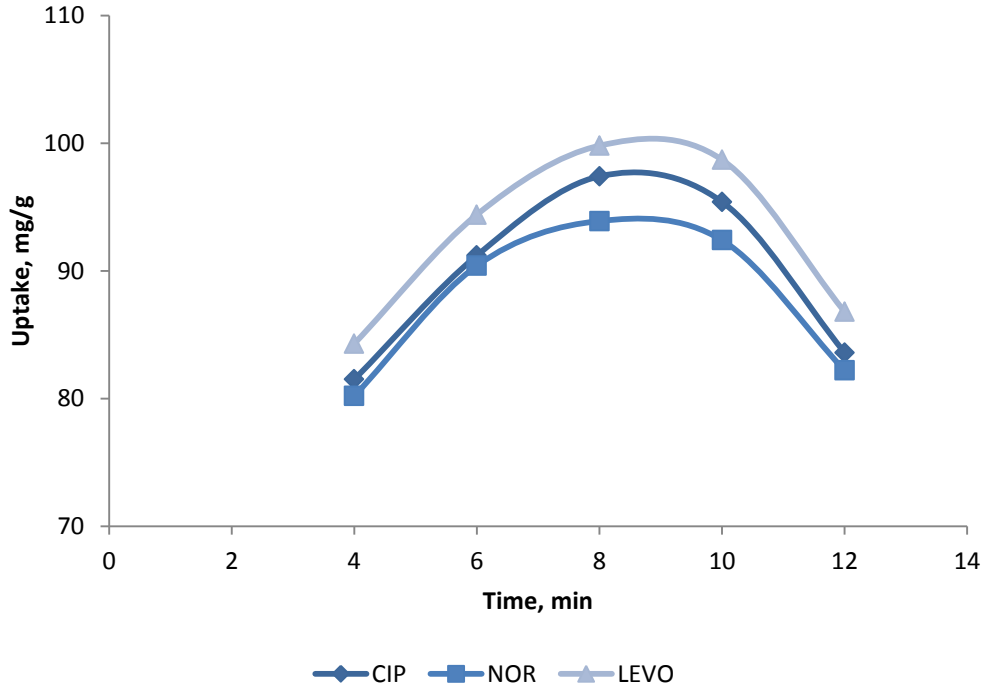

Figure 6. Effect of time on the uptake of antibiotics.

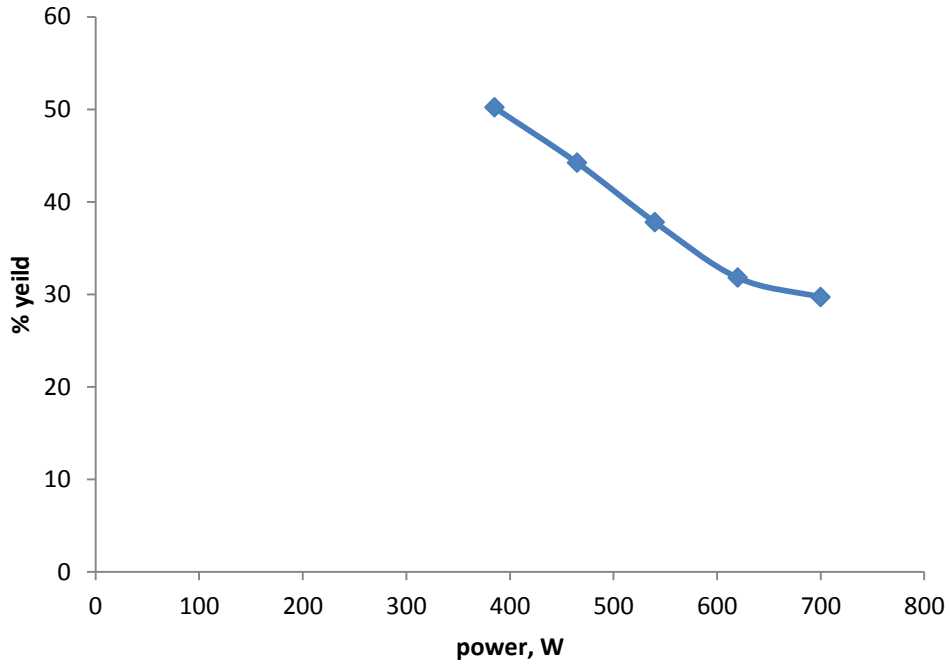

Figure 7. Effect of radiation power on the yield of activated carbon.

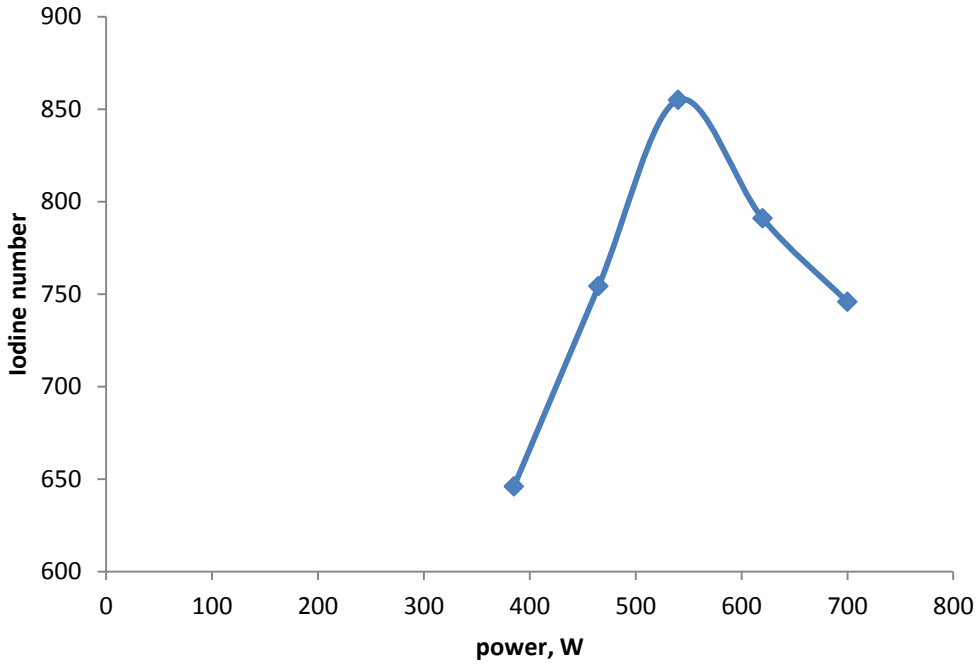

Figure 8. Effect of radiation power on Iodine number.

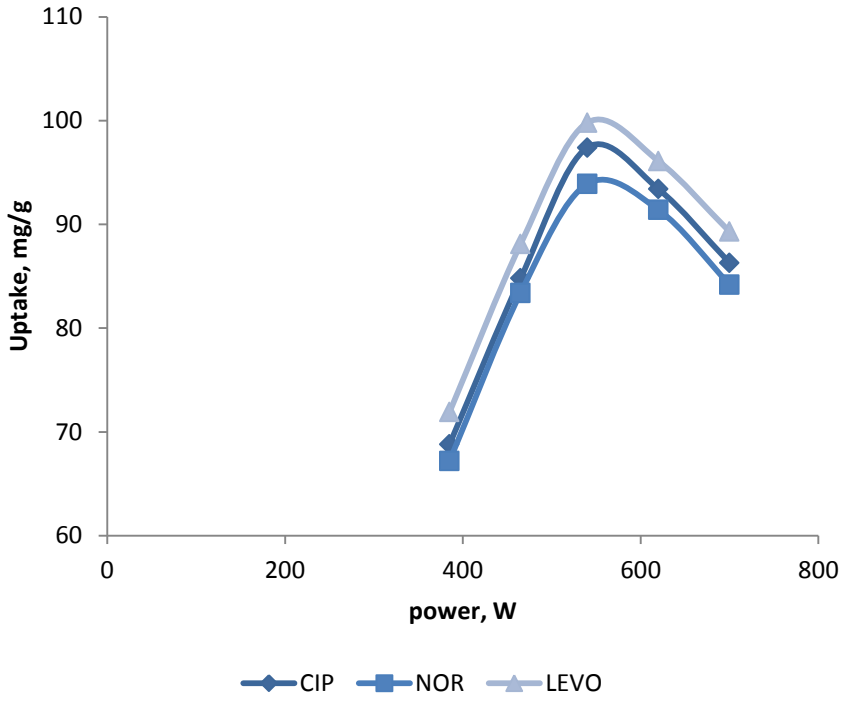

Figure 9. Effect of radiation power on the uptake of antibiotics.

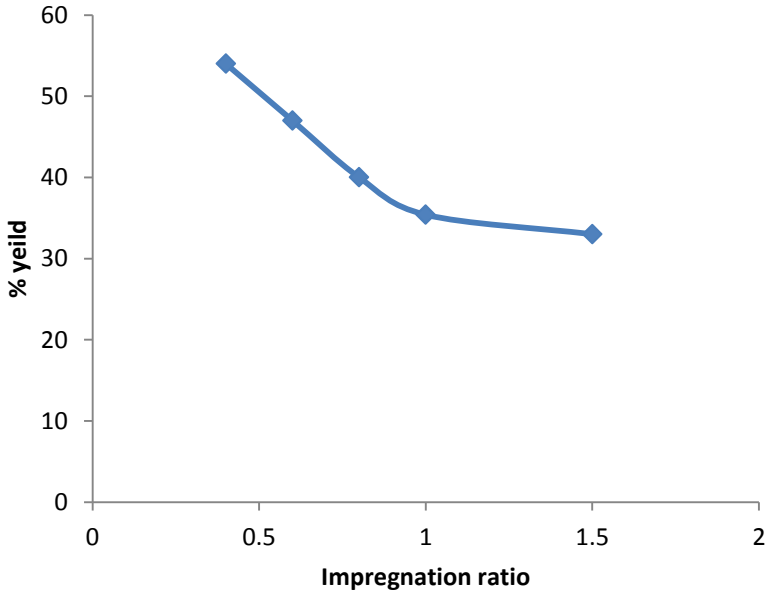

Figure 10. Effect of impregnation ratio on the yield of activated carbon.

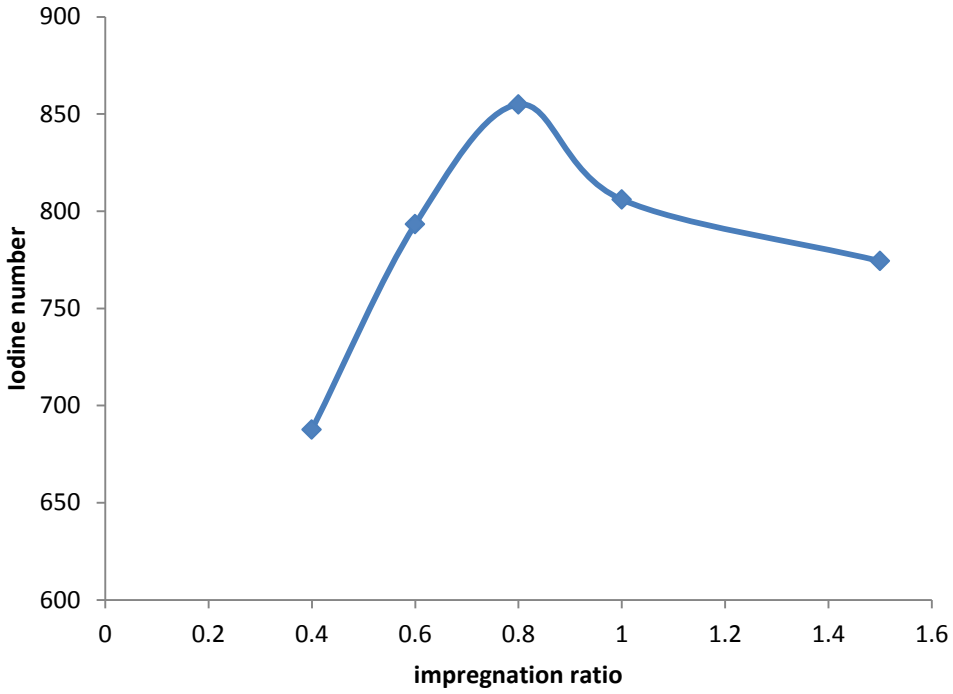

Figure 11. Effect of impregnation ratio on iodine number.

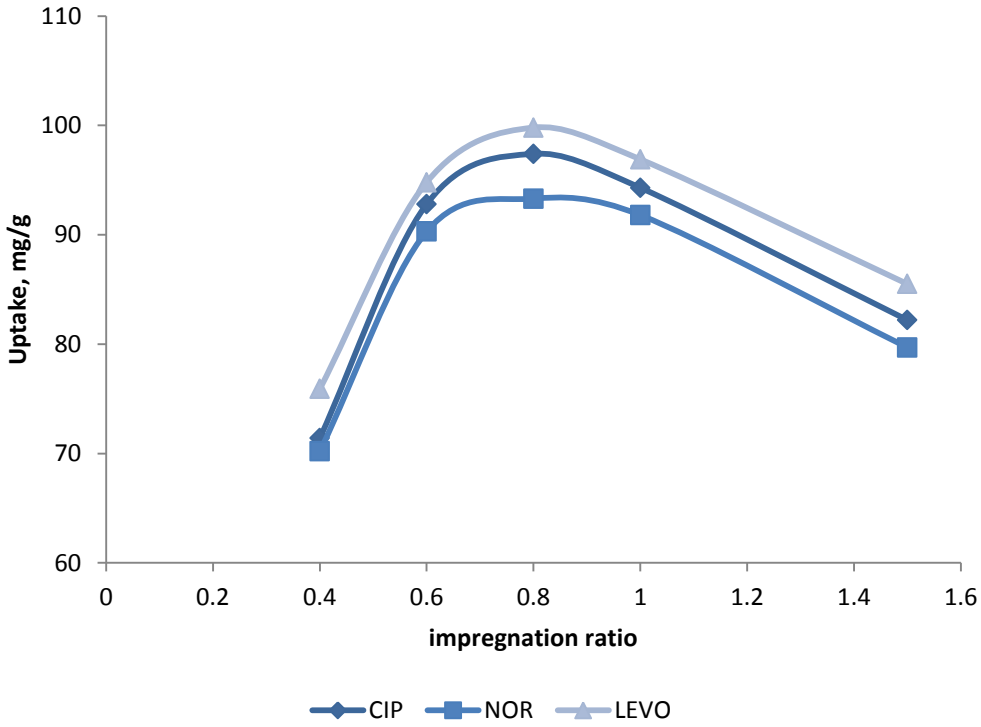

Figure 12. Effect of impregnation ratio on the uptake of antibiotics.

Table 1. Characterization of activated carbon.

Characteristics	AC-K_2CO_3
Surface area, m^2/g	852
Pore volume, cm^3/g	0.671
Ash content, %	3.88
Moisture content, %	4.9
Bulk density, g/ml	0.352

Galvanic Corrosion of Carbon Steel -Stainless Steel Couple in Sulfuric Acid under Flow Conditions

Basim Obed Hasan
Assistant Professor
Chemical Eng. –Nahrain University
Email: basimohasan13@gmail.com

Naseer Abood Al-habubi
Assistant Professor
Chemical Eng. -Nahrain University
Email: naseer@habobi.com

Samar Saadi Hussien
Ph. D student
Chemical Eng. - Nahrain University
Email: samar_saadi@yahoo.com

ABSTRACT

Galvanic corrosion of stainless steel 316 (SS316) and carbon steel (CS) coupled in 5% wt/v sulfuric acid solution at agitation velocity was investigated. The galvanic behavior of coupled metals was also studied using zero resistance ammeter (ZRA) method. The effects of agitation velocity, temperature, and time on galvanic corrosion current and loss in weight of both metals in both free corrosion and galvanic corrosion were investigated. The trends of open circuit potential (OCP) of each metal and galvanic potential (E_g) of the couple were, also, determined. Results showed that SS316 was cathodic relative to CS in galvanic couple and its OCP was much more positive than that of CS for all investigated ranges of operating conditions. A sharp increase in galvanic current from CS to SS316 was noticed in the first 20 min and then decrease with time. Increasing the agitation velocity led to increase in galvanic corrosion rate. The decrease in galvanic current is attributed to metal passivation due to the formation of a protective film which grows with time. The minus sign in galvanic current means that the current is flow from CS (anode) to SS316 (cathode). The galvanic current of CS-SS316 couple shifts to the negative direction with increase agitation velocity.

Keywords: Galvanic current; corrosion rate; potential; passivation film.

التاكل الكلفاني للحديد الكاربوني والحديد المقاوم للصدأ في حامض الكبريتيك تحت تاثير الجريان

ا. م.د. باسم عبيد حسن
هندسة كيمياوية/ جامعة النهرين

ا.م.د. نصير عبود الحبوبي
هندسة كيمياوية/ جامعة النهرين

سمر سعدي حسين
هندسة كيمياوية/ جامعة النهرين

الخلاصة

تم دراسة التاكل الكلفاني للحديد الكاربوني والحديد المقاوم للصدأ بوجود سرع في (5% wt/v) حامض الكبريتيك. السلوك الكلفاني للمعدنين ايضا درس باستعمال مقياس التيار الكهربائي ذو المقاومة صفر (ZRA) . تاثير السرعة ودرجة الحرارة والزمن على تيارات التاكل الكلفاني والوزن المفقود للمعدنين في حالة التاكل الحر والتاكل الكلفاني. حساب جهود المعادن في الحالة الحرة والربط الكلفاني. من النتائج نلاحظ ان الحديد المقاوم للصدأ هو كاثود الحديد الكاربوني هو انود في حالة الربط الكلفاني. الجهد الحر للحديد المقاوم للصدأ في جميع الظروف المدروسة كان اكثر خمولا من الحديد الكاربوني. زيادة حادة في التيار الكلفاني من الحديد الكاربوني الى الحديد المقاوم للصدأ في اول عشرين دقيقة ثم يقل مع الزمن وهذا يزداد مع زيادة السرعة. نقصان معدل التاكل الكلفاني وكذلك معدل التاكل الحر للحديد المقاوم وذلك بسبب تاثير طبقة الحماية على سطح المعدن التي تنمو مع الزمن. الاشارة السالبة في التيارالكلفاني تعني اتجاه التيار من الحديد الكاربوني الى الحديد المقاوم.تزداد قيمة التيار الكلفاني للمعدنين معا باتجاه السالب (وذلك يعني الحديد الكاربوني انود والحديد المقاوم للصدأ هو كاثود) مع زيادة السرعه.

الكلمات الرئيسية: التيار الكلفاني, معدل التاكل ,الجهد, طبقة الحماية.

1. INTRODUCTION

Galvanic corrosion occurs when two dissimilar metals, with different potentials, in electrical contact are exposed to an electrically conducting corrosive liquid, because the metals have different natural potentials in the liquid, a current will flow from the anode (more electronegative) metal to the cathode (more electropositive), the less noble metal in general suffers more corrosion and the more noble metal suffers less than if they were isolated in the same medium **Talbot**, and **Talbot, 1998**.

Acidic solutions of hydrochloride acid and sulfuric acid have wide industrial applications, the most important fields being acid pickling, acid descaling, industrial cleaning and oil-well acidizing. In aqueous solutions of acids, the surface of metals and alloys are covered with highly protective oxyhydroxide passive film affecting its corrosion behavior **Singh**, and **Ray, 2007**.

The corrosion behavior of carbon steel in acidic solution is significant considering its widespread applications, namely, in the manufactures of pipe lines for petroleum industries. Acid solutions are frequently used in the removal of rust and scale-developed in industrial process. Since the steel is the major structural material utilized in the construction industry, there have been considerable efforts focused on the prevention of steel corrosion. As most steels are stable in neutral or alkaline media, acidic environments are the major concern. However, a group of materials that could serve as substitutes of steel are the inter metallic compounds when exposed to acidic solutions because these compounds possess good corrosion and oxidation resistance in media, containing not only oxygen but also sulphur, good abrasion resistance, and small density **Greene et al, 1961; Guo et al, 1986; Higginson et al, 1989; Hermas et al, 1995**.

Since stainless steels are passive and exhibit a noble potential, they can be coupled successfully to metals that are either passive or inherently noble. This includes metals and alloys like silver; silver solder; copper; nickel; 70% Ni − Cu alloy; 76% Ni, 16% Cr, 7% Fe alloy; and, usually, aluminum in environments in which it remains passive. Stainless steels are best employed under fully aerated or oxidizing conditions, which favor the passive state. Whether used in handling chemicals or exposed to the atmosphere, the alloy surface should always be kept clean and free of surface contamination **Revie** and **Uhlig, 2008**.

Stainless steels are more resistant to concentrated sulfuric acid than carbon steels. Because the passive film on stainless steel is harder and much more resistant to flow-induced corrosion than is the iron sulfate film which form on carbon steels, use of corrosion resistant alloys for components such as valves, inlets, outlets, and wear plates is advised in the standard. Application for stainless steel in sulfuric acid production is in towers, pumps, tanks, mist eliminators, acid coolers, and piping **Grubb, 2009**.

To control the corrosion, good understanding of the effect of operating conditions on the corrosion behavior is required. Therefore, this work aims to study free corrosion and galvanic corrosion behavior of carbon steel and stainless steel in sulfuric acid for ranges of temperatures and agitation speed. Then, galvanic current between each couple of these metals will be investigated under the same conditions by using zero resistance ammeter and also by weight loss. Potential measured of each metal to study the free corrosion behavior, whereas, the galvanic currents will be measured using zero resistance ammeter (ZRA). The galvanic coupling effect on the corrosion behavior of metal is important to be investigated. The loss in weight of coupled metals is necessary to be determined before and after coupling.

2. EXPERIMENTAL WORK

The free corrosion rate for specimens CS and SS316 was determined by weight loss method under agitation velocity of 0, 400, and 600 rpm, and temperatures 30, 40, 50 and 60 ºC, in a solution of 5% wt/v H_2SO_4. And the galvanic corrosion rate of CS-SS316 couple was evaluated under isothermal (T=40 °C) and agitation velocity 0, 400, and 600 rpm.

Fig. 1 shows the connected experimental apparatus that was used in galvanic experiments. The corrosion rate for two dissimilar metals was calculated by measured weight loss before and after experiment.

The electrode specimens were mechanically press-cut into coupons of 20 mm ×40 mm dimensions with a total specimen surface area of 800 mm^2. The specimen were connected to a plastic board through a very small holes made in the center using fine screw. The effect of screw was ignored. The chemical composition of specimen is shown in **Table 1** and **2**.

Before each experiment the specimen was abraded with glass emery paper of grade numbers; 120, 180, 220, 400 and 2000 respectively, washed continuously with brushing by plastic brush in running tap water, followed by distilled water, dried with a clean tissue, followed by ethanol for 30 second dried with clean tissue, and then dried by using electrical oven to temperature of about 110 ºC for 10 minute **Mahato et al., 1980**. The specimen then was stored in the desiccator over high activity silica gel until use.

Then the specimen was weighed to the 4th decimal of gram by using digital balance. After that one face of the rectangular coupon was exposed to corrosion environment for 1 h by immersion in acid solutions, while the other face was completely insulated by insulating tape. So that the corrosion rate of each specimen was determined for two cases: free corrosion and galvanic corrosion.

At the end of weight loss experiment, the specimen was washed by tap water with brushing to remove the corrosion products that may still stick to surface, washed with distilled water, dried with clean tissue, rinsed in ethanol and dried by using electrical oven to a temperature about 110 ºC for 10 minute. Then the specimen was kept in the desiccator to cool and then weighted. The change in the open circuit potential of specimen as function of time was measured at the all weight loss experimental run.

In galvanic corrosion experiments, before each experiment, the specimens were weighed by accurate balance. After the solution had reached the required isothermal temperature and velocity, the two dissimilar metals were connected together to measure galvanic currents variation with time by using Zero Resistance Ammeter (ZRA). The carbon steel specimen was connected to the (+ve) and the stainless steel to the (-ve). The distance between the specimens in the test solution was maintained at 10 mm in all experiments. The coupons were mounted by connecting them on hold board using a small screw.

During each experimental run, galvanic potential variation with time was measured by using Saturated Calomel Electrode SCE bridged by a Luggin capillary at a distance of 1- 2 mm from the working electrode, and connected to personal computer for data recording. The specimens were immersed in the acid solution for 1 h. During this time period, the galvanic current and potential were measured with time. After each run, the couple specimens were weighed by high accuracy balance. Each run was repeated twice, a third run was conducted in case of any doubt in the results.

3. RESULTS AND DISCUSSION

3.1 Free corrosion

Fig. 2 and **3** illustrates the variation of corrosion rate of carbon steel (CS) and stainless steel 316 (SS316) that expressed in gmd with temperature and flow velocity for a 1 h of immersion time.

From **Fig. 2** it is clear that the corrosion rate increases with increasing temperature for both metals at the stationary condition. The effect of temperature on the corrosion rate is governed by changing two parameters affecting the corrosion rate in conflicting ways that are the O_2 solubility and diffusivity. Increasing the temperature will increase the rate of oxygen diffusion to the metal surface by decreasing the viscosity of aqueous solutions resulting in enhanced corrosion rate. On the other hand, increasing temperature decreases the oxygen solubility the factor that restrains the corrosion **Mahato et al, 1980**. It is also evident from **Fig. 2** that the increase in the CR of SS is very little with increasing temperature. This agrees with previous works **Okamoto, 1973; Grubb, 2009; Ibrahim et al, 2015**.

From **Fig. 3**, it is clear that increasing the flow velocity leads to an increase in the corrosion rate of CS while the influence on the SS corrosion is negligible. This can be attributed to the increase in the concentration of oxygen close to the metal surface by eddy transport. The rate of oxygen reduction reaction is generally limited by the speed at which oxygen can reach the surface of the metal. Previous studies **Foroulis, 1979; Scheers, 1992; Shreir et.al, 2000; Slaiman and Hasan, 2010; Hasan and Sadek, 2014** indicated that the greater the turbulence due to high velocities results in more uniform O_2 concentration near the surface. **Figs 2** and **3** reveal that the corrosion rate of CS exhibited high corrosion rate compared to stainless steel. In addition, their corrosion rates increased appreciably with temperature. Stainless steel exhibited a clear corrosion resistance under most investigated conditions even at high temperature and high rotational speed. This is due to the increased anodic polarization and a possibility of passivation.

Fig. 4 and **5** shows the corrosion potential (open circuit potential) versus time for carbon steel and stainless steel respectively in 0.52 M H_2SO_4 solutions at four different temperatures of 30, 40, 50, and 60 ºC, for stationary condition. From **Fig. 4** for CS, it is clear that the potential at 30 and 40 ºC shifts to more negative and reaching asymptotic values of -0.566 and -0.524 V respectively after about 10 min.

At 50 and 60 ºC, the potentials show a decrease of the corrosion potential value and then after 4 and 10 min respectively the potential shifts towards more positive until reach stable value is -0.524 and -0.507 V after 1 h. This shift can be ascribed to the formation and growth of a Fe_2O_3 film on the corroding surface. The ennoblement of the potential observed in **Fig. 4** is attributable to healing of the pre-immersion air-formed oxide film and further thickening of the oxide film as a result of the interaction between the electrolyte and the metal surface **Evan, 1960**. The growth of the oxide film continues until the film acquires a thickness that is stable in the electrolyte. During this step the alloy oxidation is under anodic control and the reduction of oxygen is the cathodic reaction **Abd El Kader**, and **Shams El Din, 1979**.

Fig. 5 for SS316, at 30 ºC the potential shifts to the negative values in the first 13 min and then slow increase in potential. At 40 ºC the potential decreases in the first 4 min and then shifts to the positive value in the four minute and tends to more positive in the 20 min. At 50 ºC the potential decrease in the first 5 min and then increases until it reaches stable value (E_{corr}= -0.46 V) in 30 min. At 60 ºC initial potential increases in the first 8 min and then reaches stable value at E_{corr}= -0.405V. The asymptotic values (steady state values) and the OCP increases with increasing temperature. The potential profiles can be explained by assuming that the potential rise indicates the formation of an insoluble layer product, probably oxide phase on the electrode surface. The anodic shifting of E_{corr} can be attributed to the product layer thickening process and to an increase in the resistance of this layer. These results are in agreement with **Alain et al., 2013** for 316L stainless steel in HCl aqueous solution, **Azambuja et al., 2003** for Fe and AISI 304 stainless steel in tungstate aqueous solution, and with **Bore et al., 2006** for 304 stainless steel in sulfuric acid.

The temperature favors the cathodic reaction and more specifically, it favors the hydrogen evolution reaction (HER) which leads to an increase of H_2 evolution. In other words, an increase of temperature decreases the cathodic overpotential as a result of decreasing the activation overpotential of hydrogen evolution reaction. Moreover, temperature also favors the kinetics of the corrosion reactions, and especially the anodic dissolution of the alloy, since the corrosion current densities are high for each alloy as temperature increases **Ibrahim et al, 2015**.

It is worth to mention that the passive region appeared on the anodic region of the polarization curves for iron and steel was due to the formation of iron oxides and/or corrosion products on their surfaces as shown by Equations (1) and (2) **Sherif, 2014**.

$$Fe + ½\ O_2 + H_2O = Fe(OH)_2 \quad (1)$$

$$3Fe(OH)_2 + ½\ O_2 = Fe_3O_4 + 3H_2O \quad (2)$$

where, the formed ferrous hydroxide reacted with more oxygen to form the top layer of magnetite corrosion product, Fe_3O_4. The presence of such oxide partially protects the iron surface from further dissolutions and led to the appearance of the passive region **Sherif, 2014**.

Shams El Din et al., 1994 demonstrated that the surface of high molybdenum containing stainless steel immersed in seawater at high temperatures becomes rich with molybdenum ions due to outward diffusion of molybdenum ions through the oxide film as confirmed by X-ray surface analysis. Therefore, the behavior indicated in **Fig. 6** can be attributed to the dissolution of the passive film on the steel in the temperature ranging from 30 to 40 °C and 50 to 60 °C is under mixed control (anodic and cathodic). While in the range of 40 to 50 °C, the oxygen solubility in the solution decreases with increasing temperature, so the passivation process becomes under cathodic control.

Fig. 7 and **8** shows the effect of agitation speed on the corrosion potential curves vs. time of carbon steel and stainless steel 316 respectively, in 0.52 M H_2SO_4 solution at isothermal temperature T=40 ºC for 1 h immersion time.

Fig. 7 for CS reveals that when the velocity increases from 0 to 400 rpm, the potential shifts to more negative. This is due to increased arrival O_2 to the metal surface which leads to an increase in the polarization resistance to more negative values. The corrosion potential shifts to more positive (higher than 400 rpm) when the velocity up to 600 rpm.

Fig. 8 for SS316 shows that the potential shifts to more positive values with increasing velocity due to the increased O2 transport to the surface. This agrees with previous findings **Foroulis, 1979; Mahato et al, 1980; Silverman, 1984; Hasan, 2003; Hasan et al, 2011**. Therefore, the corrosion potential in aerated and oxygen-saturated solutions is flow dependent since the cathodic process, i.e., oxygen reduction reaction, is mass transfer controlled, i.e., at a constant bulk temperature the corrosion potential (E_{corr}.) increases as the flow rate increases. The anodic kinetics (dissolution of metal) is not mass transfer dependent as it is under activation control. The oxygen reduction reaction is dictated by the limiting values of mass transfer control. This may explain the noble trend of the corrosion potential as the flow rate (rpm) is increased as in **Fig. 8**. This behavior is in agreement with previous findings **Hubbard** and **Lightfoot, 1966; Chin** and **Nobe, 1977; Nesic et.al, 1995; Ross et al, 1966**. **Ross et al., 1966**, stated that the increase in E_{corr} with velocity is due to the increase in oxygen transport to the metal surface and when the system is free from oxygen, velocity has no effect on corrosion potential (E_{corr}).

3.2 Galvanic corrosion

Fig. 9 shows corrosion potential with time of CS, SS316, and CS–SS316 couple in a H_2SO_4 solution at 40 ºC for stationary conditions (u=0 rpm). It is clear that the OCP of CS and SS316 free reveals that the corrosion potential decreases and then increases after 5 min and more increases at 20 min decreases with time while the CS-SS316 couple initial rises in first few minutes and reaching almost steady value. Some of literature found the same tendency such as **Azambuja et al., 2003** for Fe & AISI 304 stainless steel in tungstate aqueous solution, **Bore et al., 2006** for 304 stainless steel in sulfuric acid, **Alain et al., 2013** for 316L stainless steel in HCl aqueous solution. **Fig. 9** reveals that OCP of CS is nobler than SS316 in the first 5 min. and reverse after that time. However, the galvanic potential of CS–SS316 couple is nobler than OCP of CS and SS316. The degree of passivity, the nature of the redox couples in the solution, and the stability of the system, all determine the polarity and its variation with time **Gilbert, 1948**.

During the OCP test the passive film containing Cr_2O_3 grew on the electrode surface, shifting the OCP value to higher potentials **Lothongkum et al, 2003**.

Fig. 10 and **11** shows a comparison of the potential variation with time for CS, SS316, and CS- SS316 couple in H_2SO_4 solution for agitation velocity of 400 and 600 rpm at T=40ºC respectively.

Fig. 10 for CS indicates that the OCP of CS and the galvanic potential become more negative with time. It reveals that OCP of SS316 is nobler than OCP of CS, whereas the galvanic potential of CS-SS316 couple is between the OCPs of the two metals.

Fig. 11 shows the galvanic potential of CS- SS316 couple and OCP of SS316 decrease and then increase in positive direction and the values of potentials are almost equal. However, the OCP of CS shifts to more negative direction.

Fig. 12 shows the effect of agitation speed on galvanic potential (CS- SS316 couple) at T=40ºC. It is clear from figure that the galvanic potential shifts toward the negative direction with increasing agitation velocity from 0 to 400 rpm. This indicates that the E_g is affected by the CS potential more than by SS316 potential. E_g goes to the positive direction when increasing the velocity from 400 to 600 rpm and that revels the E_g is affected by the SS316 potential due to passivation layer on SS316 surface at velocity 600 rpm higher than at 400 rpm. **Table 3** shows the corrosion rate of CS when coupled with SS316, at velocity 400 rpm it is less than that at 600 rpm suggesting that due to the galvanic potential at 600 rpm higher than 400 rpm.

Fig. 13 shows the variation of galvanic current of CS-SS316 couple with time for different agitation velocity at T=40 ºC. The minus sign in galvanic current means that the current is flowing from CS (anode) to SS316 (cathode). The figure reveals that there is a sharp increase in galvanic current from CS to SS316 in the first 20 min and then it decreases with time. It can be seen that the galvanic current increase with increasing velocity. The decrease in galvanic current is attributed to metal passivation due to the formation of a protective film which grows with time **Guenbour, 2010** this film increases with velocity.

The corrosion data for carbon steel-stainless steel 316 couple are summarized in **Table 3**. The direction of the galvanic currents shows that carbon steel is anodic (electronegative or corroding) pole of CS-SS316 couples immersed in 0.52 M H_2SO_4 solution. Since the open circuit potential of SS316 is higher than the open circuit potential of CS, the current flows from CS to SS316.

Table 3 lists the values of corrosion rate obtained from weight loss of CS and SS316 in both free and coupling cases for range of agitation velocity at constant temperature T=40 ºC. The values of corrosion rate reveal that the corrosion rate of SS316 is lower than that for CS and that indicate the SS316 is cathodic and CS is anodic in the galvanic couple. In addition, when coupling CS with SS316, the corrosion rate of SS316 decreases and that of CS increases due to the galvanic action. Under flow conditions, the corrosion rate of CS increases due to the galvanic effect produced by coupling with SS316, while the SS316 is protected. Under flow conditions at 600 rpm, the corrosion rate of carbon steel coupled to stainless steel 316 is lower than free corrosion of carbon steel. This may be attributed to the formed protective oxide film on carbon steel and become the sacrificial anode. Moreover, the galvanic potential of couple at 600 rpm is higher than that at 400 rpm. That justified the decrease in the galvanic current with increased velocity (from 400 rpm to 600 rpm).

4. CONCLUSIONS

1- The free corrosion rate for SS316 is lower than CS due to its passivity.

2- The galvanic current of CS-SS316 couple shifts to the negative direction with increase agitation velocity.

3- When coupling CS with SS316, the corrosion rate of SS316 decreases while the CS increases at stationary with negligible effect at agitation velocity.

4- The open circuit potential for CS shifts to more positive with increasing temperature and time (especially at high temperature) and, in general, to more negative with increasing agitation velocity.

5- The open circuit potential for SS316 shifts to more positive with increasing temperature, time and agitation velocity.

REFERENCES

- Abd El Kader, J.M. and Shams El Din, A.M., 1979, *Film thickening on nickel in aqueous solutions in relation to anions type and concentration*, Br. Corros. J., Vol. 14, PP. 40–45.

- Alain, R., Gilbert, S., Jorge, L. R., 2013, *Corrosion Behavior of HA-316L SS Biocomposites in Aqueous Solutions*, Materials Research, Vol. 16, No. 6, PP. 1254-1259.

- Azambuja, D. S., Emilse, M. A., Martinia, and Iduvirges L. M., 2003, *Corrosion Behaviour of Iron and AISI 304 Stainless Steel in Tungstate Aqueous Solutions Containing Chloride*, J. Braz. Chem. Soc., Vol. 14, No. 4, PP. 570-576.

- Bore J., Dragutin M. D. and Jovan P. P., 2006, *Corrosion potential of 304 stainless steel in sulfuric acid*, J. Serb. Chem. Soc. Vol. 71, No. 5, PP. 543–551.

- Chin, R. J., and Nobe, K., 1977, *Electrochemical aspects of Steel Corrosion in Sea Water*, Corrosion J., vol.33, pp.364.

- Evans, U.R., 1960, *The Corrosion and Oxidation of Metals*, Edward Arnold, London, PP. 898.

- Foroulis, Z. A., 1979, *The Influence of Velocity and Dissolved Oxygen on the Initial Corrosion Behavior of Iron in High Purity Water*, Corrosion, vol. 35, pp. 340-344.

- Gilbert, P.T., Oct.–Dec., 1948. *An Investigation into the Corrosion of Zinc and Zinc Coated Steel in Hot Waters*. Sheet Metal Industries.

- Greene, N. D., Bishop, C.R., and Stern, M., 1961, *Corrosion and electrochemical behavior of chromium-noble metal alloys*, Journal of the Electrochemical Society, Vol. 108, No. 9, PP. 836–841.

- Grubb, J., 2009, *High Alloy Stainless Steels for Concentrated Sulfuric Acid*, 5D Corrosion solutions, Conference.

- Guo, J., Seo, M., Sato, Y., Hultquist, G., Leygraf, C., and Sato, N., 1986, *Electrochemical behavior and surface composition of copper containing ferritic stainless steel in sulfuric acid solution*, Corrosion Engineering, Vol.35, PP. 283–288.

- Hasan, B. O., Abdul Kader, H. D., and Abdul-Jabbar, M. F., 2011, *Experimental Study on Carbon Steel Corrosion and its Inhibition Using Sodium Benzoate Under Different Operating Conditions*, Iraqi Journal of Chemical and Petroleum Engineering, Vol.12, No.3, PP.11-24.

- Hasan, B. O., Heat, Mass, and Momentum, 2003, *Analogies to Estimate Corrosion Rates under Turbulent Flow Conditions*, Ph. D. Thesis Dept. of Chem. Eng., University of AL-Nahrain, Baghdad.

- Hermas, A. A., Ogura, K., and Adachi, T., 1995, *Accumulation of copper layer on a surface in the anodic polarization of stainless steel containing Cu at different temperatures*, Electrochimical Acta, vol.40, no.7, PP.837–844.

- Higginson A., Newman R. C., and Procter R. P. M., 1989, *The passivation of Fe-Cr-Ru alloys in acidic solutions*," Corrosion Science, Vol.29 , No.11-12, PP.1293–1318.

- Hubbard, D. W., and Lightfoot, E. N., 1966, *Correlation of Heat and Mass Transfer Data for High Schmidt and Reynolds Numbers*, Ind. Eng. Chem. Vol.5, PP.370–379.

- Ibrahim, M. A. M., Abd El Rehim, S. S. and Hamza, M. M., 2015, *Potentiodynamic polarization behavior of some austenitic stainless steel AISI samples of different molybdenum contents in H_2SO_4 solutions*, Arabian Journal of Chemical and Environmental Research, Vol.2, No.2, PP.37–50.

- Lothongkum G., Chaikittisilp S., Lothongkum A. W., 2003, *XPS investigation of surface films on high Cr-Ni ferritic and austenitic stainless steels*, Appl. Surf. Sci., 218, PP. 203-210.

- Mahato, B. K., Cha, C. Y., and Shemlit, W., 1980, Corrosion Science, Vol. 20, PP. 421-441.

- Nesic, S., Solvi, G. T., and Enerhaug, J., 1995, *Comparison of Rotating Cylinder and Pipe Flow Test for Flow-Sensitive Carbon Dioxide Corrosion*, Corrosion, Vol. 51, PP. 773-787.

- Okamoto, G., 1973, *Passive film of 18-8 stainless steel structure and its function*, Corrosion Science, Vol.13, Issue 6, PP. 471-489.

- Revie, R.W. and Uhlig, H. H., 2008, *Corrosion and Corrosion Control an Introduction to Corrosion Science and Engineering*, fourth edition, John Wiley & Sons, Inc., Hoboken New Jersey.

- Ross, T. K., Wood, G. C., and Mahmud, I., 1966, *The Anodic behaviour of Iron-Carbon Alloys in Moving Acid Media*, J. Electrochem. Soc., Vol. 113, PP. 334-345.

- Shams El-Din, A.M., Wang, L. and Saber, T. M. H., 1994, *Behaviour of High Strength Molybdenum Containing Stainless Steels in Arabian Gulf Water*. Part 1: Oxide Film Thickening. British Corrosion Journal, 29, PP. 58-64.

- Sherif El-Sayed M., 2014, *A Comparative Study on the Electrochemical Corrosion Behavior of Iron and X-65 Steel in 4.0 wt % Sodium Chloride Solution after Different Exposure Intervals*, Molecules, 19, PP. 9962-9974.

- Silverman D.C., 1984, Corrosion NACE, No. 5, Vol. 40, PP. 220.

- Singh, V.B., Ray, M., 2007, *Effect of H_2SO_4 addition on the corrosion behaviour of AISI 304 austenitic stainless steel in methanol-HCl solution*, Int. J. Electrochem.Sci., Vol 2, PP. 329-340.

- Talbot, D. E. J. and Talbot, J. D. R., 1998, *Corrosion Science and Technology, CRC series in materials science & technology*, New York.

NOMENCLATURE

Symbol	Meaning	Units
A	surface area of specimen	mm^2
CR	corrosion rate	$gm/m^2.day$
E_g	galvanic potential	V
$E_{corr.}$	corrosion potential	V
t	immersion time	h
T	temperature	^oC
u	revolution per minute	rpm

ΔW	weight loss	gm

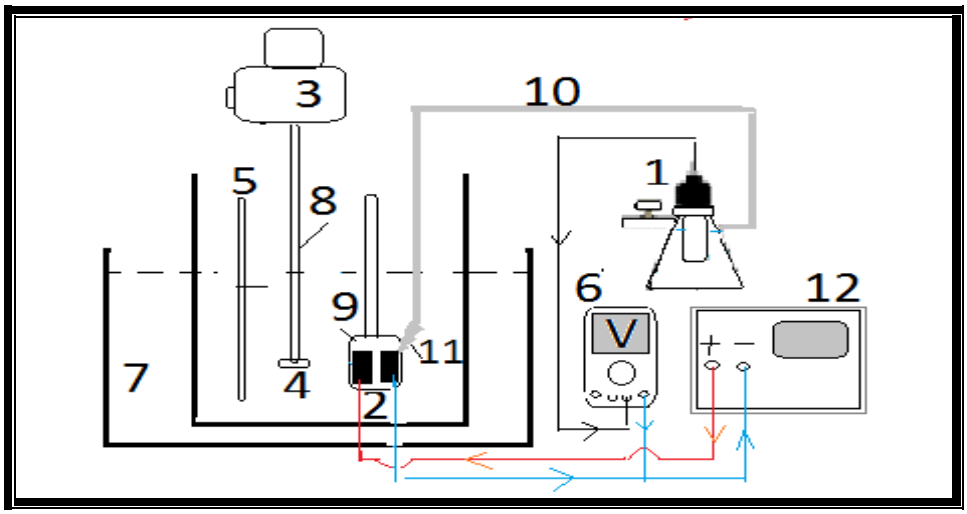

Figure 1. Galvanic experiment set-up: 1- Reference Saturated Calomel Electrode (SCE), 2- Working electrode (specimen), 3-Motor, 4- Stirrer, 5- Thermometer, 6- Voltmeter, 7- Water bath, 8- Glass shift, 9- Holder of specimens, 10- Rubber, 11- Luggen capillary tube, 12- Zero Resistance Ammeter (ZRA).

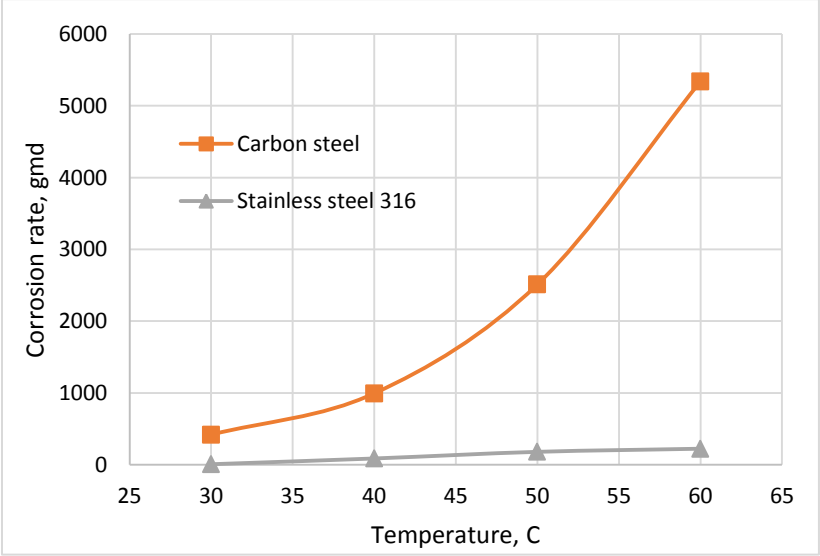

Figure 2. Variation of corrosion rate with temperature at stationary condition.

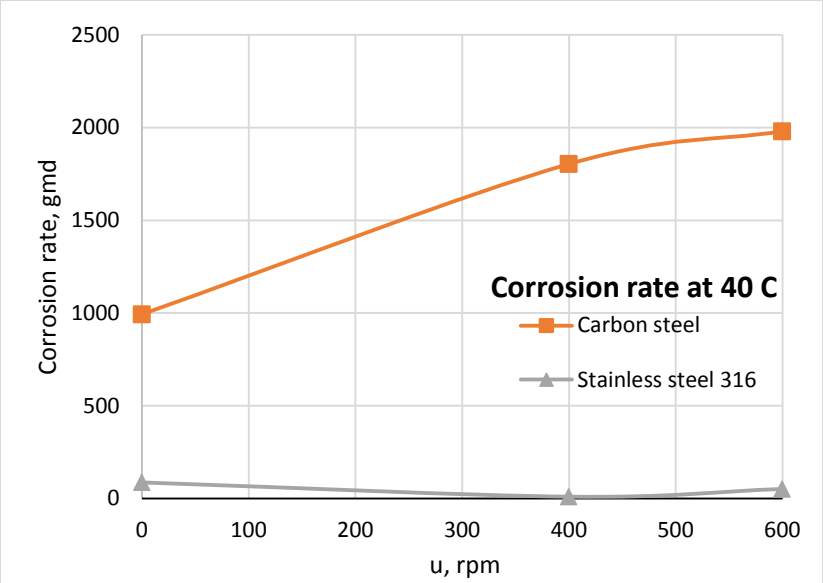

Figure 3. Corrosion rate vs. velocity of CS and SS at T=40 ºC.

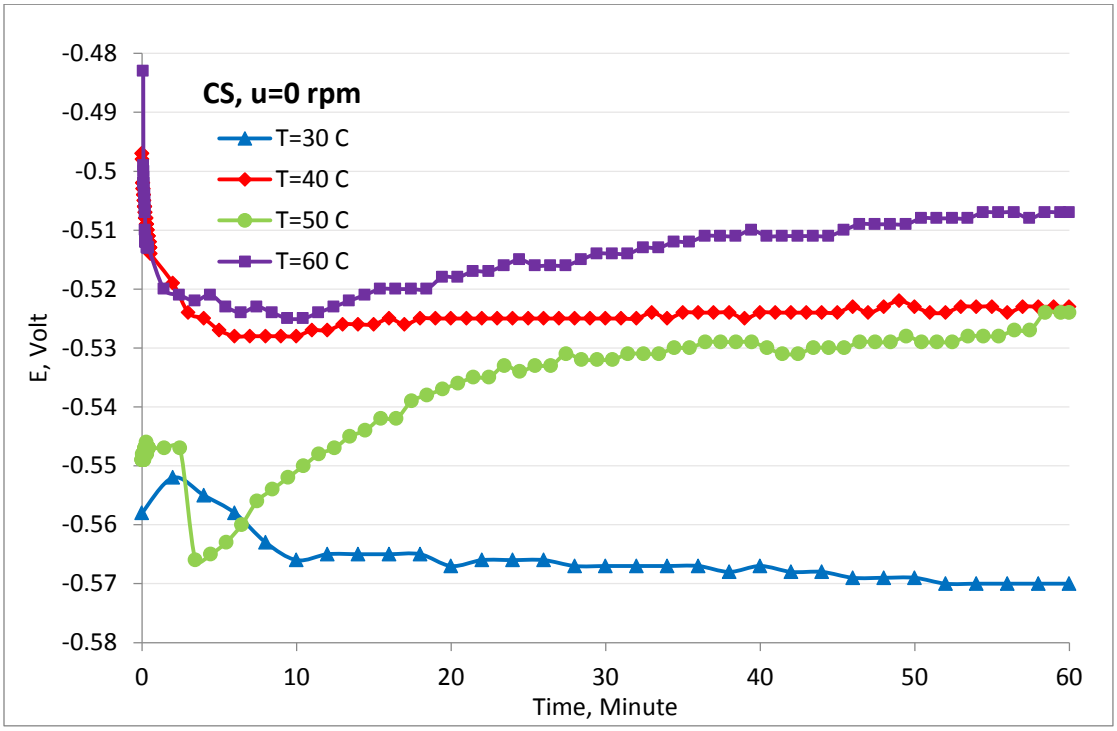

Figure 4. Corrosion potential vs. time of carbon steel specimen at stationary condition at different temperature.

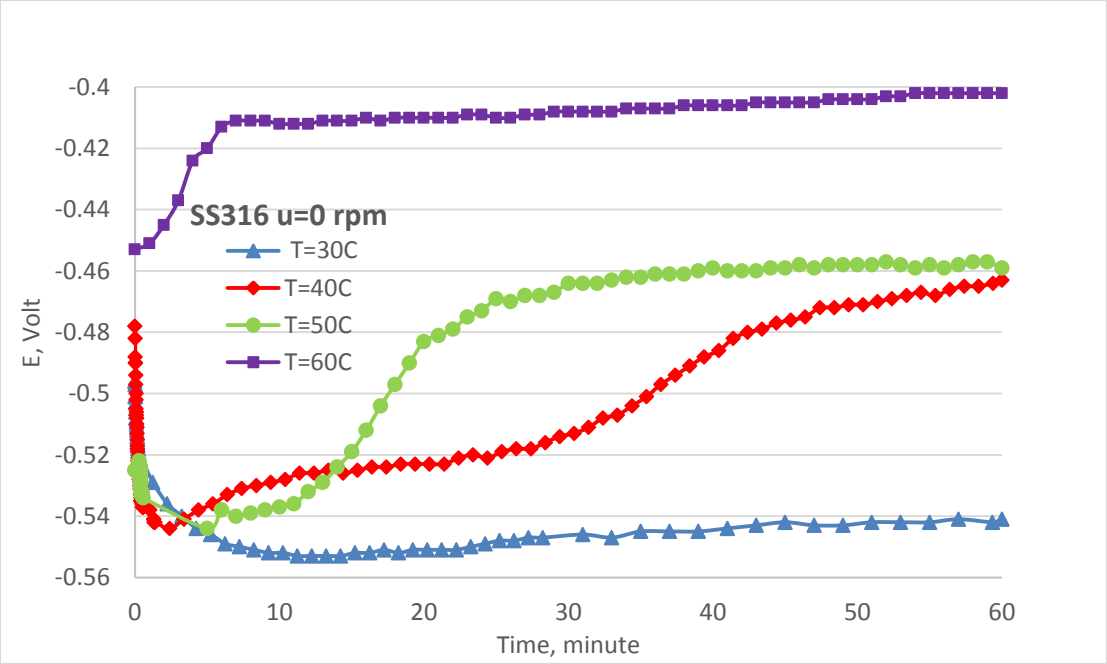

Figure 5. Corrosion potential vs. time of stainless steel specimen at stationary condition at different temperature.

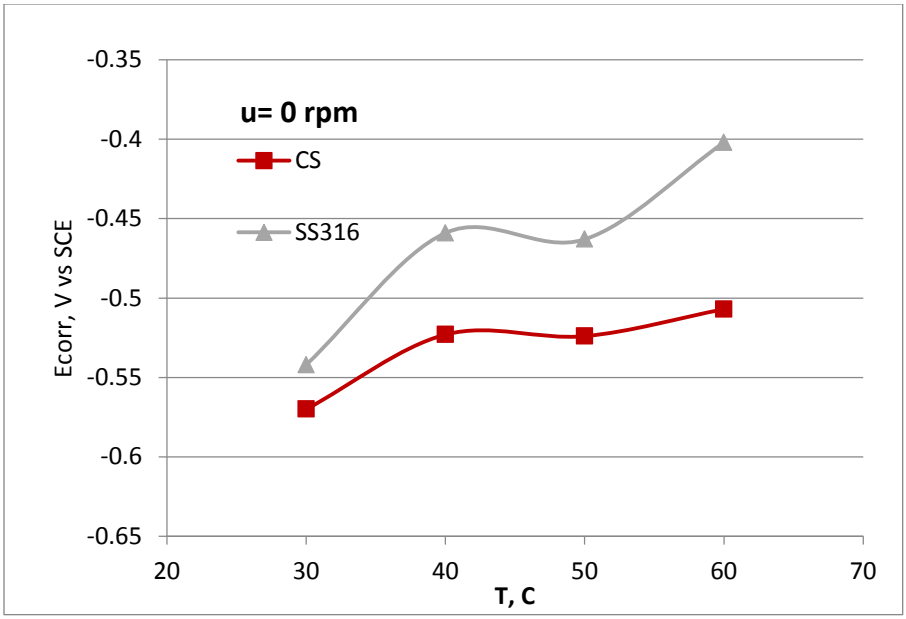

Figure 6. Variation of E_{corr} with temperature at stationary condition.

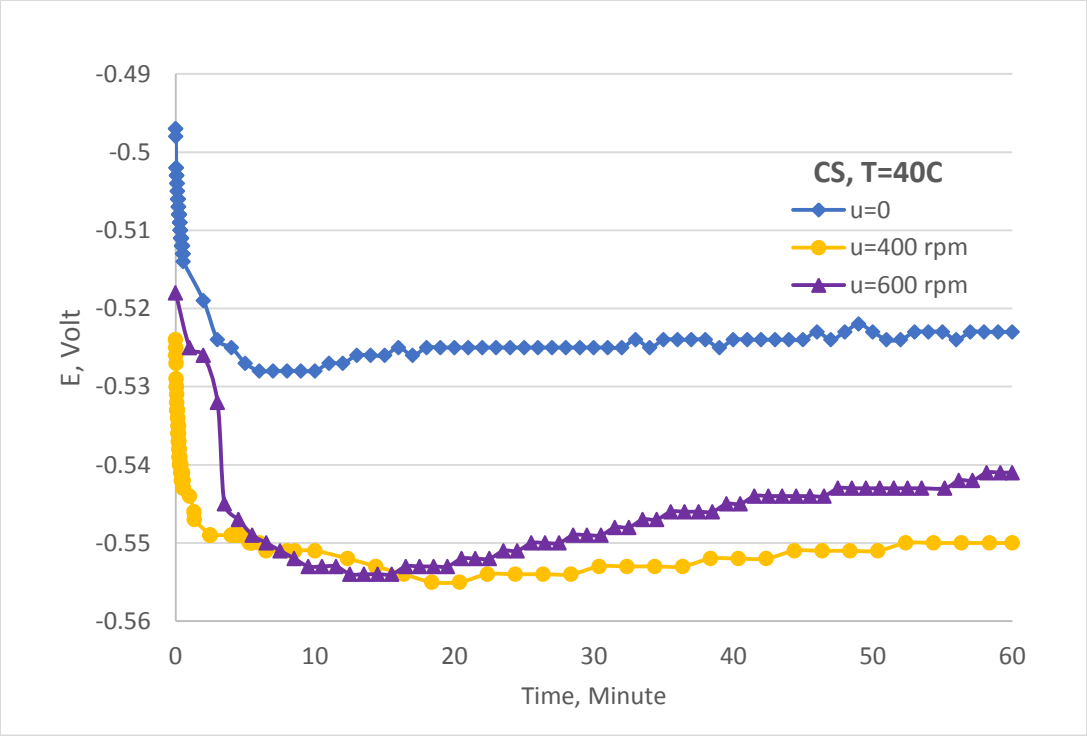

Figure 7. Corrosion potential vs. time of CS at different velocity and 40 ºC.

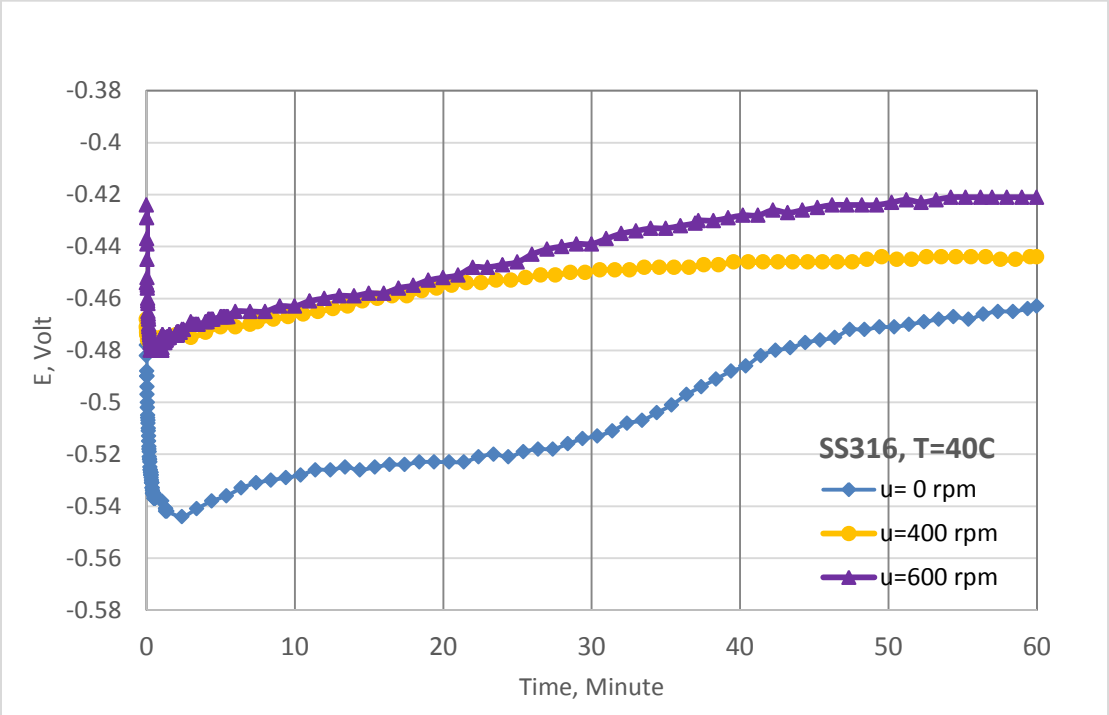

Figure 8. Corrosion potential vs. time of SS316 at different velocity and 40 ºC.

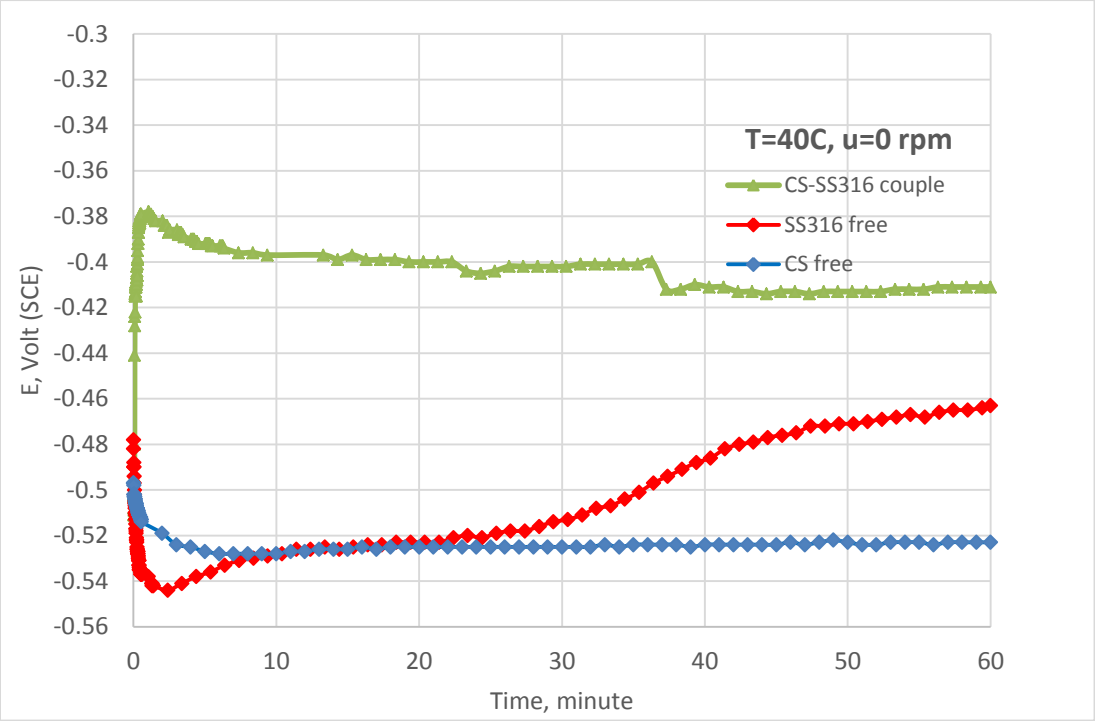

Figure 9. OCP and galvanic potential versus time of carbon steel and stainless steel at const. temperature (T=40 ºC) and stationary (u=0 rpm).

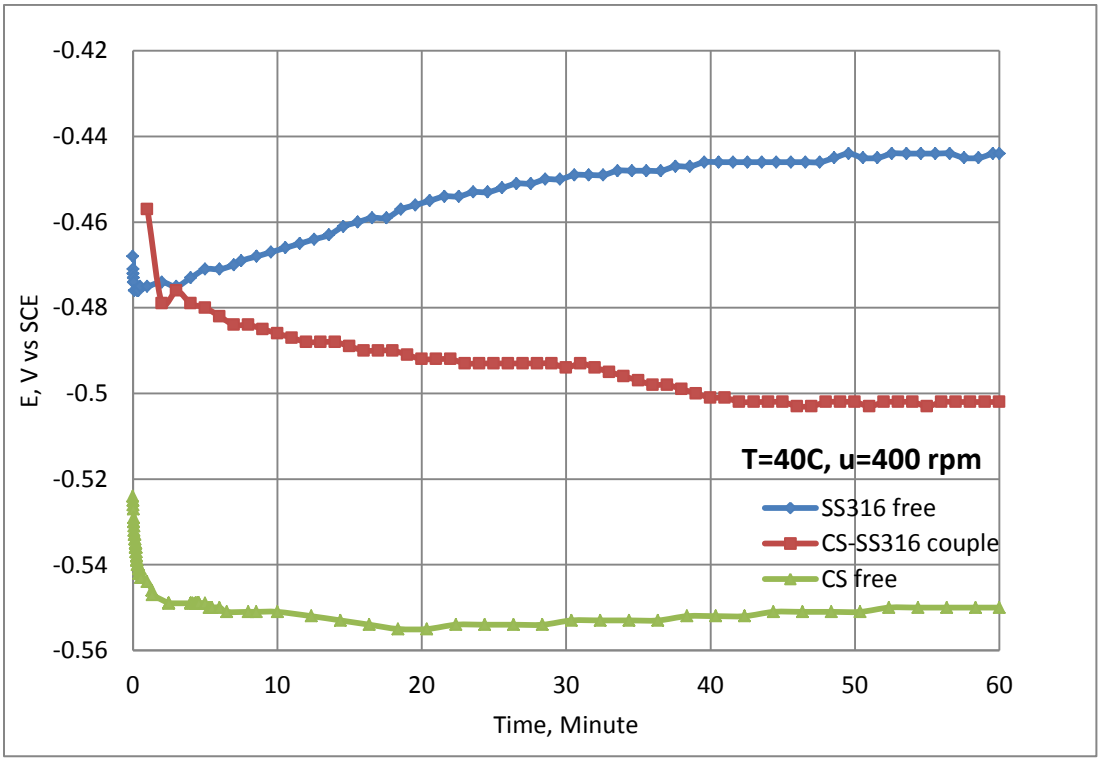

Figure 10. Potentials of CS, SS316, CS-SS316 couple under u=400 rpm.

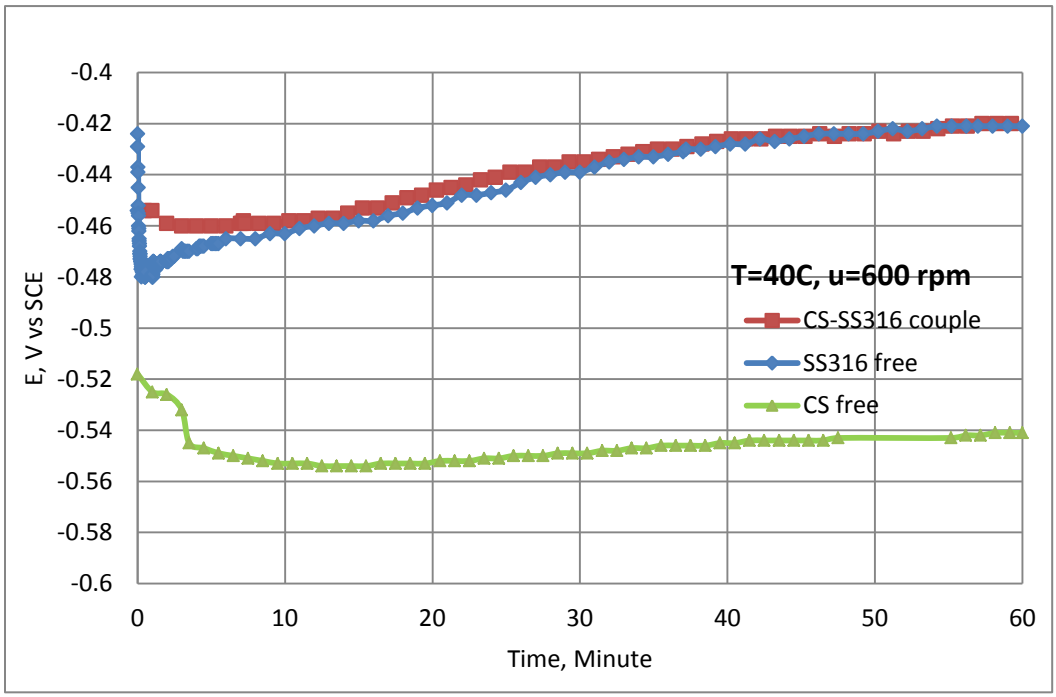

Figure 11. Potentials of CS, SS316, CS-SS316 couple under u=600 rpm.

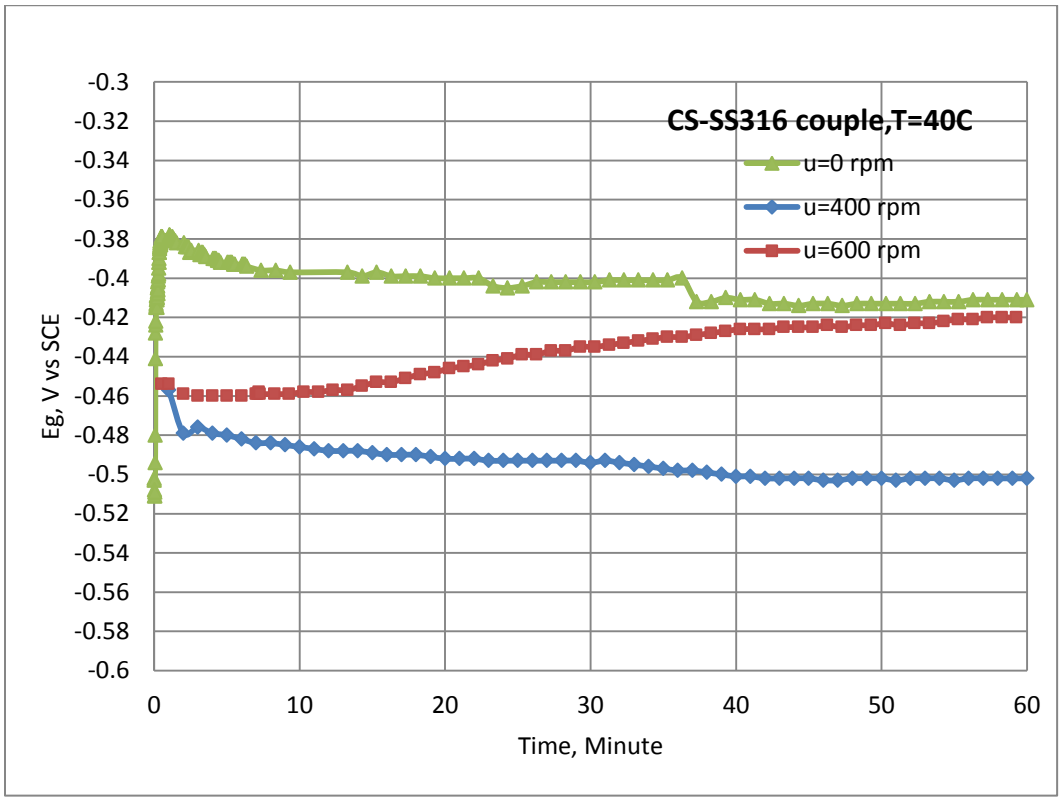

Figure 12. Effect of agitation velocity on the galvanic potential (CS-SS316).

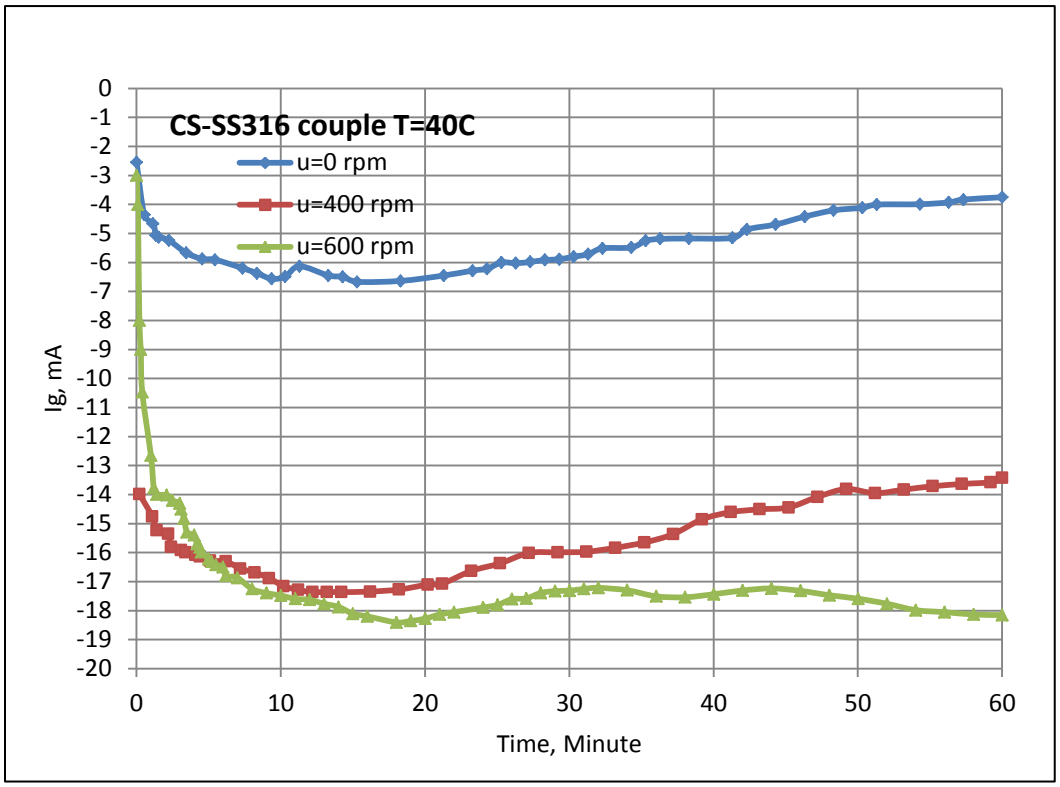

Figure 13. Effect of agitation velocity on the galvanic current (CS-SS316).

Table 1. Analysis of carbon steel specimen

Carbon steel	0.29% C	0.62% V	0.00% Cr	0.22% Mn	0.08% Cu	0.08% Mo	Balance Fe

Table 2 Analysis of stainless steel specimen

Stainless steel 316	0.08% C	2% Mo	16 % Cr	2% Mn	0.08% P	0.03% S	0.75% Si	0.1% N	Balance Fe

Table 3 Corrosion rate of carbon steel and stainless steel 316 in free and coupling at different agitation velocity and T=40 ºC.

u, rpm	***CR, gmd***			
	CS free	***SS316 free***	***Cs(coupled to SS316)***	***SS 316(coupled to CS)***
0	993.4	86.3414	1148.43	22.2996
400	1803.48	9.4736	1803.786	0
600	1980	51.2195	1896.296	8.3623

Modeling and Simulation of Thermal Performance of Solar-Assisted Air Conditioning System under Iraq Climate

Asst. Prof. Dr. Najim Abid Jassim
Department of Mechanical Engineering
University of Baghdad
E-mail: najmosawe@yahoo.com

Mohammed Abdulhassan Abid
Department of Mechanical Engineering
University of Baghdad
E-mail : mhmdabdulhassan@yahoo.com

ABSTRACT

In Iraq most of the small buildings deployed a conventional air conditioning technology which typically uses electrically driven compressor systems which exhibits several clear disadvantages such as high energy consumption, high electricity at peak loads. In this work a thermal performance of air conditioning system combined with a solar collector is investigated theoretically. The hybrid air conditioner consists of a semi hermetic compressor, water cooled shell and tube condenser, thermal expansion valve and coil with tank evaporator. The theoretical analysis included a simulation for the solar assisted air-conditioning system using EES software to analyze the effect of different parameters on the power consumption of compressor and the performance of system. The results show that refrigeration capacity is increased from 2.7 kW to 4.4kW, as the evaporating temperature increased from 3 to 18 ºC. Also the power consumption is increased from 0.89 kW to 1.08 kW. So the COP of the system is increased from 3.068 to 4.117. The power consumption is increased from 0.897 kW to 1.031 kW as the condensing temperature increased from 35 ºC to 45 ºC. While the COP is decreased from 3.89 to 3.1. The power consumption is decreased from 1.05 kW to 0.7kW as the solar radiation intensity increased from 300 W/m^2 to 1000 W/m^2, while the COP is increased from 3.15 to 4.8. A comparison between the simulation and available experimental data showed acceptable agreement.

Keywords: solar assisted air conditioning system, solar collector, thermal performance, simulation program, EES.

تقييم الاداء الحراري لمنظومة تكييف هواء تعمل بمساعدة الطاقة الشمسية في العراق نظرًياً

أ.م.د نجم عبد جاسم
قسم الهندسة الميكانيكية
جامعة بغداد

محمد عبدالحسن عبد
قسم الهندسة الميكانيكية
جامعة بغداد

الخلاصة:

معظم المباني الصغيرة والمتوسطة في العراق تعتمد على انظمة التبريد ذات الضاغط الكهربائي والذي من عيوبه الاستهلاك العالي للطاقة الكهربائية عند حمل الذروة. في هذا العمل تم التحقق نظريا من الاداء الحراري لمنظومة تكييف الهواء المركبة مع مجمع شمسي. يتكون مكيف الهواء الهجين من ضاغط شبه مقفل، مكثف نوع الاسطوانة والانبوب المبرد بالماء، صمام تمدد حراري ومبخر نوع الخزان والملف. شمل التحليل النظري محاكاة لمنظومة تكييف الهواء التي تعمل بمساعدة الطاقة الشمسية باستخدام برنامج EES لتحليل تأثير عوامل مختلفة على استهلاك طاقة الضاغط وأداء المنظومة. بينت النتائج ان سعة التثليج قد زادت من 2,7 الى 4,4 كيلو واط مع زيادة درجة حرارة التبخير من 3 الى 18 درجة مئوية وكذلك فان الطاقة المستهلكة قد زادت من 0.89 الى 1.08 كيلو واط , والذي ادى الى زيادة معامل اداء المنظومة من 3,068 الى4,117. ان

الطاقة المستهلكة قد ازدادت من 0,897 الى 1,031 كيلو واط مع زيادة درجة حرارة التكثيف من 35 الى 45 درجة مئوية. بينما معامل الاداء قد انخفض من من 3,89 الى 3,1. ان الطاقة المستهلكة قد انخفضت من 1,05 الى 0,7 كيلو واط عند زيادة الاشعاع الشمسي 300 الى 1000 واط\م^2, بينما معامل اداء المنظومة قد ازداد من 3,15 الى 4,8. واظهرت المقارنة بين النتائج التجريبية والنظرية اتفاق مقبول بينهما.

كلمات رئيسية: مكيف هواء بمساعدة الطاقة الشمسية ، مجمع شمسي , اداء حراري , برنامج محاكاة .

1. INTRODUCTION:

The increasing consumption of energy in buildings on air-conditioning systems has initiated a great deal of research for energy savings. With the consolidation of the demand for human comfort, around 48% of energy is consumed in commercial and public buildings due to air conditioners, usually by driving electrical vapour compression chillers **Lamberts, 1999**. The use of solar thermal energy for air-conditioning in hot and sunny climate is a promising application of solar collectors in buildings. The main advantage of the solar air conditioning system is that in solar air conditioning applications solar gains and cooling loads occur at the same time and on the seasonal level. Figures 1 and 2 show the main variations of solar radiation and maximum temperature and relative humidity for Baghdad station **, Al-Salihi Ali et al, 2010**. Iraq is one of the countries with the highest electricity production from oil during 2008 **IEA, 2011**. **Vakiloroaya et al. 2012** described and studied a newly-developed solar-assisted air-conditioning system. They proposed a new discharge bypass line connected with an inline solenoid valve, installed after compressor to regulate the refrigerant flow rate passing through a hot water storage tank. Experimental test results show that the daily energy saving is about 38.6%, while the indoor temperature and relative humidity are within comfort ranges. **Ha et al. 2012** analyzed the performance of a newly solar-assisted direct expansion air conditioner and demonstrate the capability of energy savings and ecological conservation. They equipped a flat collector storage system as well as immersed piped coil with the direct expansion evaporator to raise the superheat temperature entering the variable speed compressor, causing the smaller duty cycle of the compressor and the slight increase in the suction pressure, and hence, reduce the energy consumptions. Water in the solar collector is in a contact with the collector absorbing surface so the heat is transferred to the water, then to the refrigerant in an immersed heat exchanger. Once the space has achieved the desired temperature, the compressor turns off while space cooling will continue till the pressure of the refrigerant at the circulation loop fails for saving the desired temperature. The advantage of the system is that the heat can be imparted in the refrigerant via the flat plate collector and therefore the compressor can remain off longer. The process justifies up to 40% of energy savings.

In the current study the thermal performance of solar assisted air conditioning system was investigated theoretically under Iraqi climate conditions. Theoretical tests were studied by varying the parameters to investigate their effects on the thermal performance of the solar assisted air conditioning system such as cooling water flow rate, heating water flow rate, ambient temperature and solar radiation intensity.

2. THE MATHEMATICAL MODEL

The following general assumptions have been adopted: i. Quasi-steady state conditions are approximated within the chosen time interval. ii. Pressure drop and heat loss in the connecting pipes are neglected. iii. Frictional losses in the evaporator and the condenser are negligible. iv. A good thermal insulation over the refrigerant loop is assumed, i.e. thermal loss to the surroundings

is neglected. v. Kinetic and potential energy changes are assumed to be insignificant. vi. The refrigerant undergoes polytrophic compression with a constant polytrophic index (n). Vii. Isenthalpic expansion process is considered. The main components covered in the model are compressor, expansion valve, water-refrigerant condenser, evaporator and liquid solar collector. **Fig.3** shows the system configuration used in the simulation.

2.1 Compressor

The various equations are expressed as follows from **Stoecker and Jones, 1982**.

Piston Displacement volume per cylinder is calculated as:

$$V_d = \frac{\pi\, D^2\, L\, N}{4} \tag{1}$$

Volumetric efficiency of compressor is calculated as:

$$\eta_v = 1 + C - C\left(\frac{p_o}{p_i}\right)^{\frac{1}{n}} \tag{2}$$

where C is the clearance volume ratio and obtainable from the manufacturer's data.

Refrigerant mass flow rate can be evaluated such that:

$$\dot{m}_r = \frac{V_d\, N\, \eta_v}{60\, v_i} \tag{3}$$

Compressor work input can be written as:

$$W_{comp} = \frac{p_i\, v_i\, \dot{m}_r}{\eta_{mech}} \left(\frac{n}{n-1}\right)\left[\left(\frac{p_o}{p_i}\right)^{\frac{n-1}{n}} - 1\right] \tag{4}$$

where η_{mech} is the compressor mechanical efficiency.

Refrigerant discharge temperature and specific volume are determined such that:

$$T_{r,o} = T_{r,i}\left(\frac{p_o}{p_i}\right)^{\frac{n-1}{n}} \tag{5}$$

$$v_o = v_i\left(\frac{p_i}{p_o}\right)^{\frac{1}{n}} \tag{6}$$

2.2 Water Cooled Condenser

The water condenser is a shell and tube heat exchanger, with water in the tube and the refrigerant around it. Refrigerant releases heat to the water in the condenser, and becomes saturated or sub-cooled. Cold water is also supplied to the condenser and hot water flows out to maintain the water temperatures and allows for more hot water production**.**

The heat rejected by the refrigerant is given as:

$$Q_r = \dot{m}_r\left(h_{r,i} - h_{r,o}\right) \tag{7}$$

The heat absorbed by the water is given as:

$$Q_w = M\ C_{p,w}\ \frac{dT_w}{dt} + \ \dot{m}_w C_{p,w}\ \left(T_{w,o} - T_{w,i}\right) \quad (8)$$

where the first term refers to the heat gain by the water in the storage tank, while the second term refers to the heat gain by the circulating water. The first term would be zero if there is no change of water temperature in the tank over time, while the second term would be zero if there is no water supplied or discharged from the tank.

Assuming negligible heat loss from the water tank to the ambient, the heat transfer from the refrigerant to the water should be balanced as follows:

$$\dot{m}_r\left(h_{r,i} - h_{r,o}\right) = M\ C_{p,w}\ \frac{dT_w}{dt} + \ \dot{m}_w C_{p,w}\ \left(T_{w,o} - T_{w,i}\right) \quad (9)$$

The heat released by the condenser can be written as:

$$Q_{cond} = \varepsilon\ C_{min}\left(T_{h,i} - T_{c,i}\right) \quad (10)$$

where $T_{h,i}$ is the inlet temperature of the hot fluid and $T_{c,i}$is the inlet temperature of the cold fluid. In present work, $T_{h,i}$ refers to the temperature of superheated refrigerant and $T_{c,i}$ refers to the temperature of feed water. Effectiveness-NTU method is used to determine the effectiveness of condensing coil. Effectiveness, ε, is the ratio of actual heat transfer rate of a heat exchanger to the maximum possible heat transfer rate. ε can be expressed as follow:

$$\varepsilon = \frac{actual\ heat\ transfer}{maximum\ possible\ heat\ transfer} = \frac{Q_{cond,evap}}{Q_{\max(cond,evap)}} \quad (11)$$

$C_{\ min}$ is the heat capacity of the fluid with the lowest value. Two different heat capacities C_h and C_c can be defined for hot or cold circulating fluid respectively such as C_{min} is determined as follows:

$$C_h\ = \dot{m}_h C_{p,h} \quad (12)$$

$$C_c\ = \dot{m}_c C_{p,c} \quad (13)$$

If $C_h > C_c$, $C_{min}\ = C_c$ and $C_{max}\ = C_h$. However, if $C_c > C_h$, $C_{min}\ = C_h$ and $C_{max}\ = C_c$. In heat exchanger equations, it is useful to describe heat capacity ratio, C as:

$$C = \frac{C_{min}}{C_{max}} \quad (14)$$

2.3 Thermostatic Expansion Valve

The thermostatic expansion valve is used to bring the pressure and temperature of the refrigerant

from a high pressure and high temperature state to a low pressure and low temperature state. The expansion valve is also used to regulate the flow rate of the refrigerant to control the level of superheat and to ensure complete evaporation of the refrigerant in the evaporator.

An isenthalpic expansion process is assumed for the thermostatic expansion valve as there is no heat or work input or output, given as:

$$h_{r,i} = h_{r,o} \tag{15}$$

2.4 Evaporator

The heat transferred through the evaporator was determined by calculating the refrigerant enthalpy increase, and energy lost by the water as seen below:

$$Q_{evap} = \dot{m}_w cp_w \left(T_{w,i} - T_{w,o}\right) \tag{16}$$

$$Q_{evap} = \dot{m}_r \left(h_{r,o} - h_{r,i}\right) \tag{17}$$

where $T_{w,i}$ and $T_{w,o}$ correspond to the inlet and outlet temperatures of water in the evaporator, and $h_{r,o}$ and $h_{r,i}$ are the enthalpies of the refrigerant at the outlet and inlet on the refrigerant side of the evaporator. In order to find the heat transfer through the evaporator, the greatest heat transfer must be calculated, which is dependent on the greatest temperature difference between both sides of the heat exchanger, then limited by the minimum capacitance rate, i.e.,

$$q_{max} = \left(\dot{m}\, c_p\right)_{min} \left(T_{h,i} - T_{c,i}\right) \tag{18}$$

2.5 Water-in-glass Evacuated Tube Solar Collector

The heat transfer in this collector is driven purely by natural circulation of water through the single-ended tubes. Water in the tubes is heated by solar radiation, rises to the storage tank and is replaced by colder water from the tank as shown in **fig.4**.

The heat rate gained by the water is given by:

$$Q = \dot{m} c_{p,w} (T_o - T_i) \tag{19}$$

The collector efficiency can be defined as the useful heat output from the collector to the input solar irradiation (I) received on the surface of the collector, and is:

$$\eta = \frac{\dot{m} c_{p,w} (T_o - T_i)}{A_c\, I} \tag{20}$$

2.6 Cooling Tower

Cooling towers are heat exchangers which are used to dissipate large heat load to the

atmosphere. They are equipment's used to reduce the temperature of a water stream by extracting heat from water and rejecting it to the atmosphere. They are used in a variety such as power generation and refrigeration. Cooling towers are designed for industrial plants for various purposes and sizes to provide cool water.

3. EES SOFTWARE

Engineering Equation Solver is thermodynamic based software developed by William Beckman and Sanford Klein of the University of Wisconsin and is academically and commercially available from F-Chart Software. EES will solve for enthalpy. The enthalpy at the different states can be used to solve for quantities like heat transfer, power consumption and system performance as shown under the System Equations section.

Parameters of interest for solar assisted air-conditioning system: there were four system inputs that were explored when using EES. **Table (1)** below depicts all the parameters that were bracketed when exploring the possibility of the working fluids. By allowing the values to vary over a large range, the capability of the solar assisted air-conditioning system can be found.

As mentioned, the high temperature of the cycle will be determined by the performance of the solar collectors. The condenser temperature will depend on where the excess heat of the system is going to be rejected to. The program flow chart and the P-h diagram are presented in **fig.4** and **Fig.5** respectively**.**

4. RESULTS AND DISCUSSION

4.1 Effect of Evaporating Temperature on Compressor Work and Refrigerating Effect

The range of evaporating temperatures used was (3℃ to 18℃) all with constant condensing temperatures at (40℃) as shown in **figs.6 and 7**.

Fig.7 shows the relation between evaporation temperature and refrigeration capacity. It is seen that the refrigerating capacity was increased with increasing the evaporating temperature. This is due to the increase of evaporation pressure which will definitely increase the evaporator temperature the enthalpy of the refrigerant at the evaporator outlet is increased. Also the pressure ratio is decreased with increasing the evaporation pressure, which will definitely increase the volumetric efficiency and refrigerant vapour density consequently higher values of refrigerant mass flow rate was achieved.

The refrigeration capacity is increased from 2.7 kW to 4.4kW, as the evaporating temperature

increased from 3 to 18℃.

In case of studying the effect of evaporating temperature on the compressor power consumption, it was found that the power consumption increases with increasing the evaporating due to the increase of refrigerant mass flow rate as discussed in previous paragraphs which overcomes the decrease of enthalpy difference with increasing the evaporation pressure the power consumption is increased from 0.89 kW to 1.08 kW as the evaporating temperature increase from 3 to 18℃. Consequently due to the reasons the COP of the system was increased with increasing the evaporating temperature as shown in **fig.6**. The coefficient of performance of the system is increased from 3.068 to 4.117, as the evaporation temperature increased from 3 to 18℃.

4.2 Effect of Condensing Temperature on the Compressor Work and Refrigerating Effect

Condensing temperature (Tcon) is also an important operating parameter that influences the system performance. Evaporating temperature is kept constant at values of (9 ºC) and the condensing temperature was ranged from 35 ºC to 45 ºC.as shown in **figs.8 and 9**.

Fig.9 shows the relation between condensation temperature and refrigeration capacity. It is seen that the refrigerating capacity was decreased with increasing the condensation temperature. This is due to the increase of condensation pressure which will definitely increase the pressure ratio, which will definitely decrease the volumetric efficiency and refrigerant vapour density consequently lower values of refrigerant mass flow rate was achieved.

In case of studying the effect of condensing temperature on the compressor power consumption, it was found that the power consumption increases with increasing the condensing due to the increase of refrigerant mass flow rate as discussed in previous paragraphs which overcomes the decrease of enthalpy difference with increasing the evaporation pressure the power consumption is increased from 0.8966 kW to 1.031 kW as the condensing temperature increased from 35 ºC to 45 ºC as shown in **fig.8**. Consequently due to these reasons the COP of the system was decreased with increasing the condensation temperature as shown in **fig.8**. The coefficient of performance of the system is decreased from 3.89 to 3.1, as the condensation temperature increased from 35 to 45℃.

4.3 Effect of Refrigerant Mass Flow Rate on Compressor Work and Refrigerating Effect

The rate of refrigerant mass flow rate was used in all experiments (83, 75, 66, 58, 50 and 41) kg/hr, the condensing temperature was kept constant at 40℃ and the evaporating temperature was kept constant at 9℃. The results are shown in **fig.10** and **fig.11**.

Fig.11 shows the refrigerating capacity is increased with increasing the refrigerant mass flow rate. This result trend can be explained according to the **eq.16**. Also the pressure ratio is decreased, which will definitely increase the volumetric efficiency, the refrigerant mass flow rate higher values. The refrigeration capacity is increased from 1.6 kW to 3.34kW as the refrigerant mass flow rate increase from 41 to 83 kg/hr.

In case of studying the effect of refrigerant mass flow rate on the compressor power consumption, it is found that the power consumption increases with increasing the refrigerant mass flow rate, the power consumption is increased from 0.48 kW to 0.97 kW as the refrigerant mass flow rate increase from 41 to 83 kg/hr, which is in the better agreement with **eq.4**. The COP is equal theoretically as shown in **fig.10**.

4.4 Effect of the Solar Radiation on the Compressor Work and Thermal Performance

Since the solar radiation intensity plays a major role on the collector heat gain, the effect of this parameter on the system performance is analyzed and presented in this section. The solar radiation intensity was used in all experiments (300, 400, 500, 600, 700, 800, 900 and 1000) W/m^2, the condensing temperature was kept constant at 40℃ and the evaporating temperature was kept constant at 9℃. The results are shown in **fig.12** and **fig.13**.

Fig.12 shows the variation of collector useful heat gain with the radiation intensity. It is seen that as the solar radiation is increased the useful energy gain is increased.

As shown in **fig.13** the power consumption is decreased from 1.05 kW to 0.7 kW as the solar radiation intensity increased from 300 W/m^2 to 1000 W/m^2, while the COP is increased from 3.15 to 4.8.

4.5 Comparison between Theoretical and Experimental Works

Figs.14 to 16 shows comparisons between the experimental and the theoretical results of power consumption and the coefficient of performance of the system. **Fig.14** shows a comparison regarding the influence of the evaporator water temperature on the power consumption and the coefficient of performance of the system. The deviation between the experimental and theoretical power consumption and the performance of the system is about 0.03 and 0.12 respectively. As it is clear from this figure the measured and the predicted values are in a reasonable agreement.

In **Fig.15** the measured power consumption and the performance of the system regarding the variation of with condensing temperature are compared to the predicted results. The deviation between the experimental and theoretical power consumption and the coefficient of performance

of the system is about 0.17 and 0.25 respectively.

Fig.16 shows a comparison between the measured and predicted values regarding the influence of refrigerant mass flow rate on power consumption, cooling capacity and COP of the system. The deviation between the experimental and theoretical power consumption, cooling capacity and the performance of the system is about 0.35, 0.07 and 0.43 respectively.

These figures show that there is a reasonable agreement between the measured and predicted power consumption and cooling capacity as well as between the measured and predicted COP.

Generally, this theoretical work indicates that EES software is a good tool to predict the performance of solar assisted air conditioning system.

5. CONCLUSIONS

According to the discussed results, several conclusions can be extracted, these are:

1- Evaporating temperature is an important operating parameter that influences the system performance. An increase in evaporating temperature affects the COP of the system negatively. The refrigeration capacity is increased from 2.7 kW to 4.4 kW as the evaporating temperature increased from 3 to 18℃. The power consumption is increased from 0.89 kW to 1.08 kW as the evaporating temperature increased from 3 to 18 ℃. Consequently the COP of the system was increased from 3.068 to 4.117, as the evaporation temperature increased from 3 to 18℃.

2- The refrigerating capacity was decreased from 3.5 kW to 3.225 kW with increasing the condensation temperature from 35 to 45℃. The power consumption is increased from 0.897 kW to 1.031 kW as the condensing temperature increased from 35 ºC to 45 ºC. Consequently the COP of the system is decreased from 3.89 to 3.1.

3- Increasing the collector heat gain leads to decrease the compressor power consumption from 1.05 kW when the heat gain of 0.255 kW at a solar radiation of 300 W/m^2 to 0.7 kW when the heat gain of 1.9 kW at a solar radiation of 1000 W/m^2, consequently the COP increased from 3.15 to 4.8.

REFERENCES

- Ali M. AL-Salihi, Maylaa M. Kadum and Ali. J Mohammed, 2010, Estimation of Global Solar Radiation on Horizontal Surface Using Routine Meteorological Measurements for Different Cities in Iraq .Asian Journal of Scientific Research, 3 (4), PP. 240-248.

- Duffie, J., & Beckman, 2006. Solar Engineering of Thermal Processes, 3rd, Ed., Hoboken, NJ: John Wiley & Sons, Inc.

- EIA: U.S Energy Information Administration, 2011, Country analysis briefs, Saudi Arabia. Retrieved 01 2011, from EIA :U.S Energy information administration.

- Florides, G.A., Kalogirou, S.A., Tassou, S.A., Wrobel, L.C., 2002. Modeling and Simulation of Absorption Solar Cooling System for Cyprus. Solar Energy 72 (1), 43–51.

- Ha, Q.P., 2012. A Novel Solar-assisted Air Conditioner System for Energy Savings with Performance Enhancement. Procedia Engineering, 49, 116-123.

- Henning, 2007, H. Solar Assisted Air Conditioning of Buildings-an Overview. Applied Thermal Eng., vol.27, 2007, pp. 1734-1749.

- History of Air Conditioning Source: Jones Jr., Malcolm, 2007, Air-Conditioning, Newsweek. Winter 1997 v130 n24-A p42 (2).

- Lamberts, 1999, R. Energy Efficiency in Buildings in Brazil, March 1999, Towards a Standard. Report presented to the International Energy Initiative.

- Mohamed H. B. Abdul Jalil, 2012, Simulation of Performance of Air Conditioning System, Faculty of Mechanical Engineering / University Malaysia Pahang.

- Spangenberg, J. , 2004, Improvement of Urban Climate in Tropical Metropolis, Master´s Thesis University of Applied Sciences Cologne (Institute for Technologies in the Tropics).

- Solair, 2009, Requirements on The Design and Configuration of Small and Medium Sized Solar Air-Conditioning Applications – Guidelines.

- Stoecker, W. F. and J.W. Jones, 1982, *Refrigeration and Air-conditioning*, McGraw-Hill Book Company, 2nd edition, 1982. New York, p. 205-280.

- V. Vakiloroaya, , Q.P. Ha, and B. Samali, 2012, Experimental Study of A New Solar-Assisted Air-Conditioner for Performance Prediction and Energy Saving, School of Electrical, Mechanical and Mechatronic Systems, University of Technology, Sydney, Australia.

NOMENCLATURE

A= area, m^2.

C_p= specific heat at constant pressure, kJ/kg ^oC.

C= clearance volumetric ratio, dimensionless.

D= Bore of compressor, m.

F_R= collector heat removal factor, dimensionless.

H= specific enthalpy, kJ/kg.

I= solar radiation, W/m^2.

L= Stroke of compressor, m.

$\dot{m}$= mass flow rate, kg/hr.

N= Rotational speed of compressor, rpm.

n= polytropic index of compressor, dimensionless.
P= pressure, Pa.
Q_u= useful Energy gain/rejected, Watt.
T= temperature, ^oC.
W_{comp}= compressor power consumption, kW.
U = Overall heat transfer coefficient, $W/m^2\,^oC$.

Greek letter

υ= Specific volume, m^3/kg.
η= Efficiency, dimensionless.
ϵ= Effectiveness, dimensionless.
ρ= Density, kg/m^3.
τα= Transmitance – absorptance, dimensionless.

Sub-Script

i Inlet , inner
o Outlet , outer
r Refrigerant
w Water
m Mean
u Useful

Table 1. Governing Factors for Parametric Study.

Parameter to be explored	Minimum value	Maximum value	Governing element
Refrigerant mass flow rate kg/hr	40	80	Air-conditioning loop
Set room temperature ^oC	15	30	Air-conditioning loop
Ambient temperature ^oC	40	50	Air-conditioning loop
Radiation intensity W/m^2	400	1000	Solar collector

Table 2. Temperature distribution for the studying apparatus

Symbol	Meaning
1	Compressor suction
2	Compressor discharge
3	Condenser inlet
4	Condenser outlet
5	Evaporator inlet
6	Evaporator outlet
7	Water outlet of the storage tank
8	Water inlet of the storage tank
9	Water outlet of the condenser
10	Water inlet of the condenser
11	Water outlet of the evaporator
12	Water inlet of the evaporator

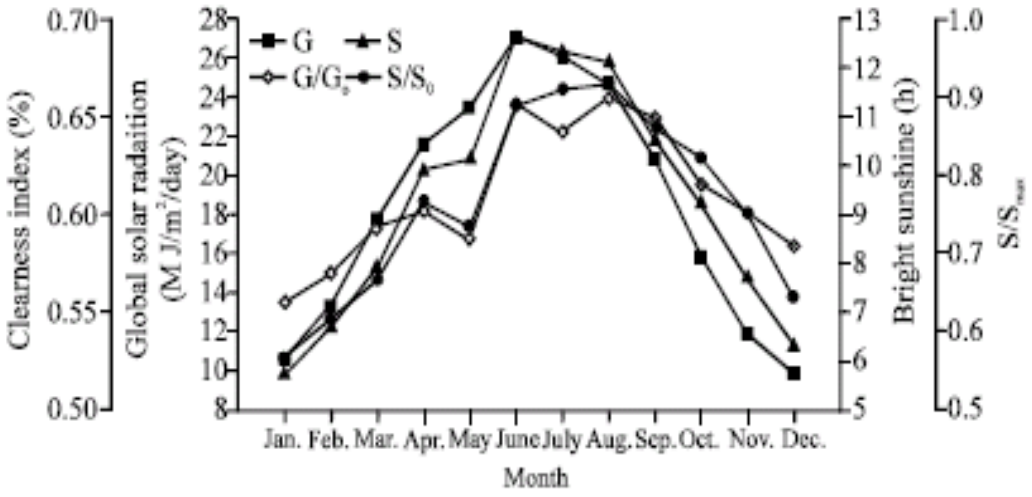

Figure 1. Monthly mean variation of a global solar radiation, bright sunshine, clearness index and S/Smax for Baghdad station

AL-Salihi Ali et al, 2010.

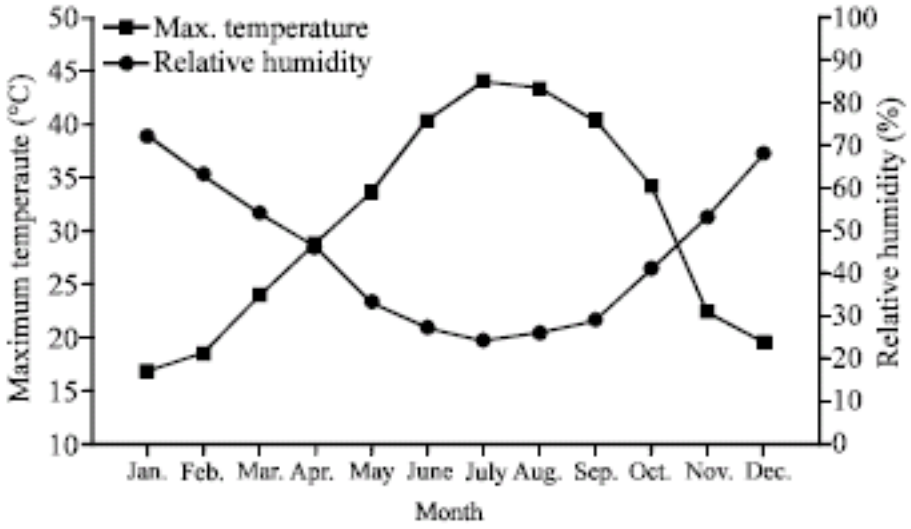

Figure 2. Monthly mean variation of maximum temperature, relative and relative humidity for Baghdad station

Al-Salihi Ali et al, 2010.

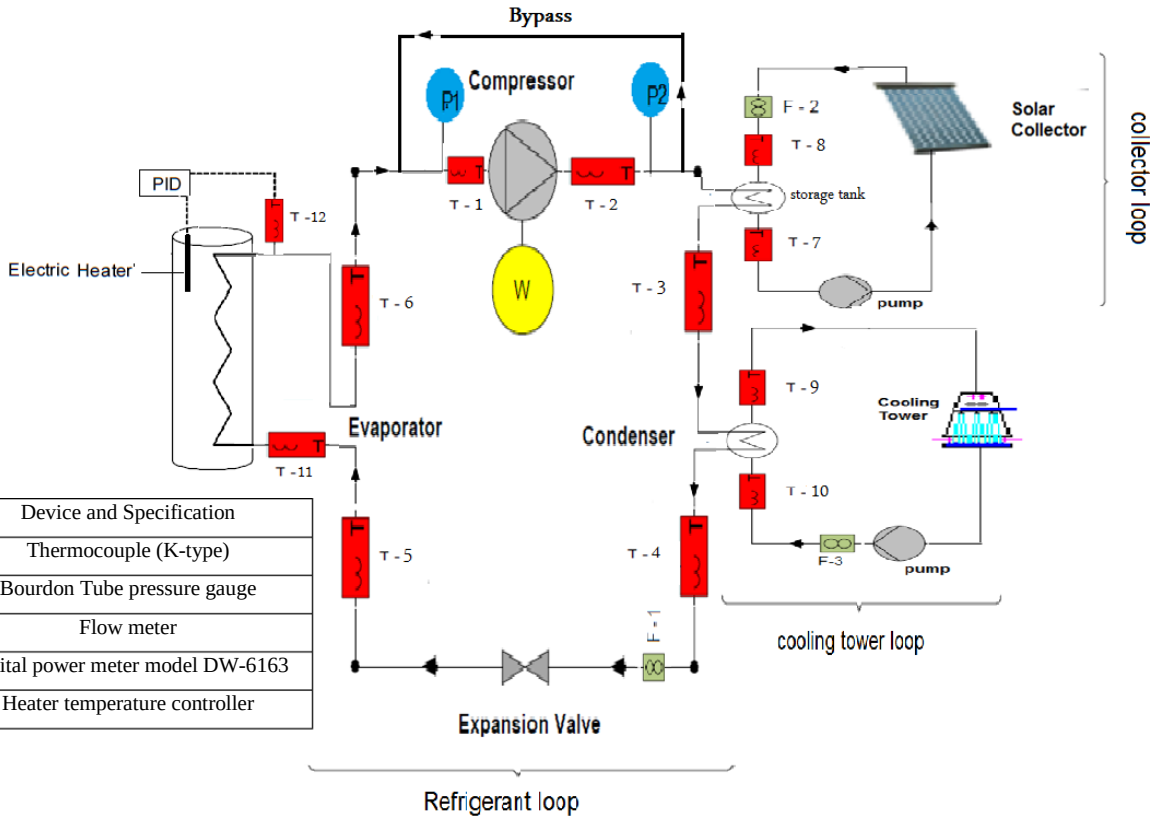

Part	Device and Specification
T_1-T_{12}	Thermocouple (K-type)
P_1,P_2	Bourdon Tube pressure gauge
F1-F3	Flow meter
W	Digital power meter model DW-6163
PID	Heater temperature controller

Figure 3. System configuration used in the simulation.

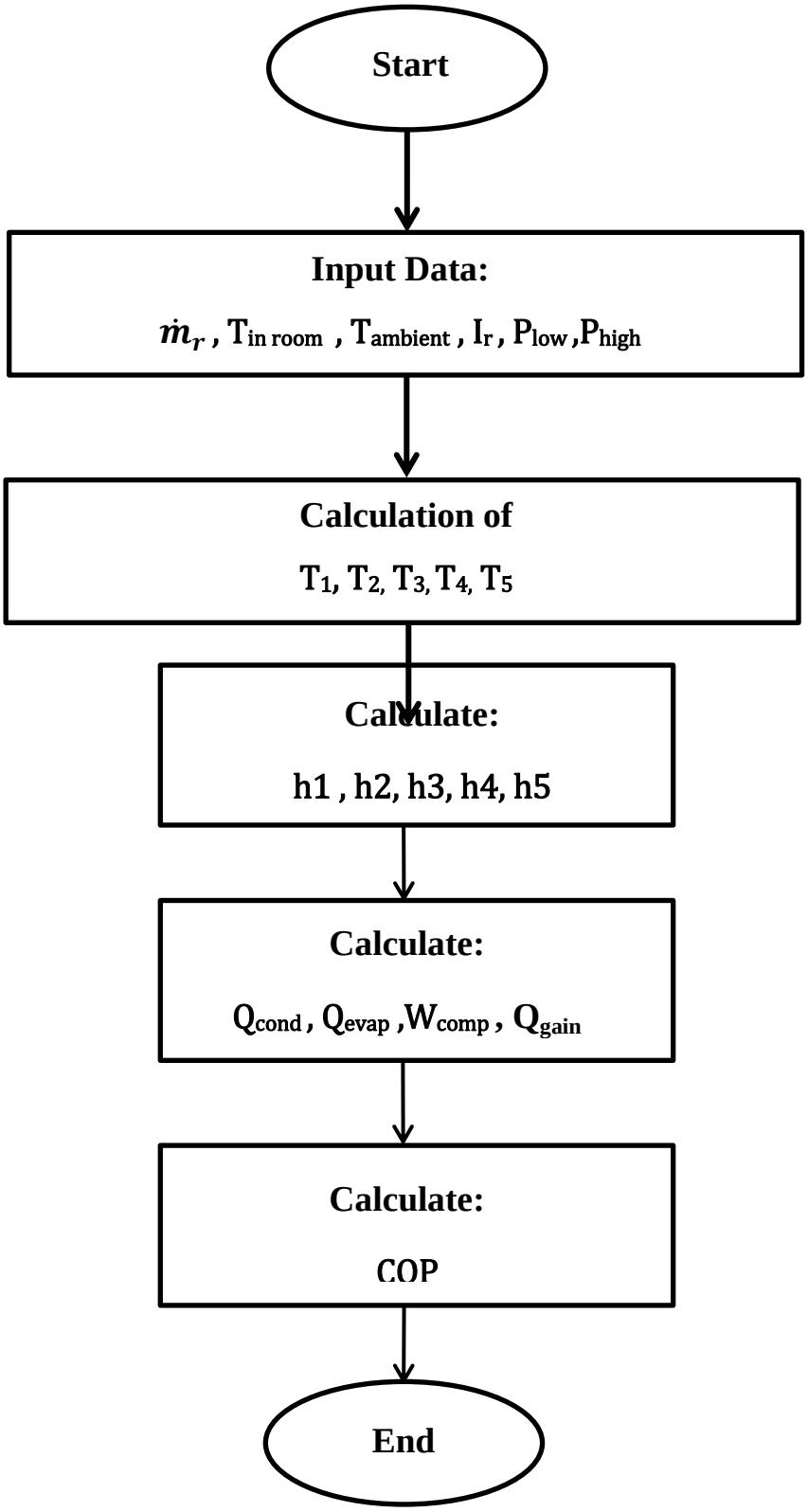

Figure 4. Program Flow Chart.

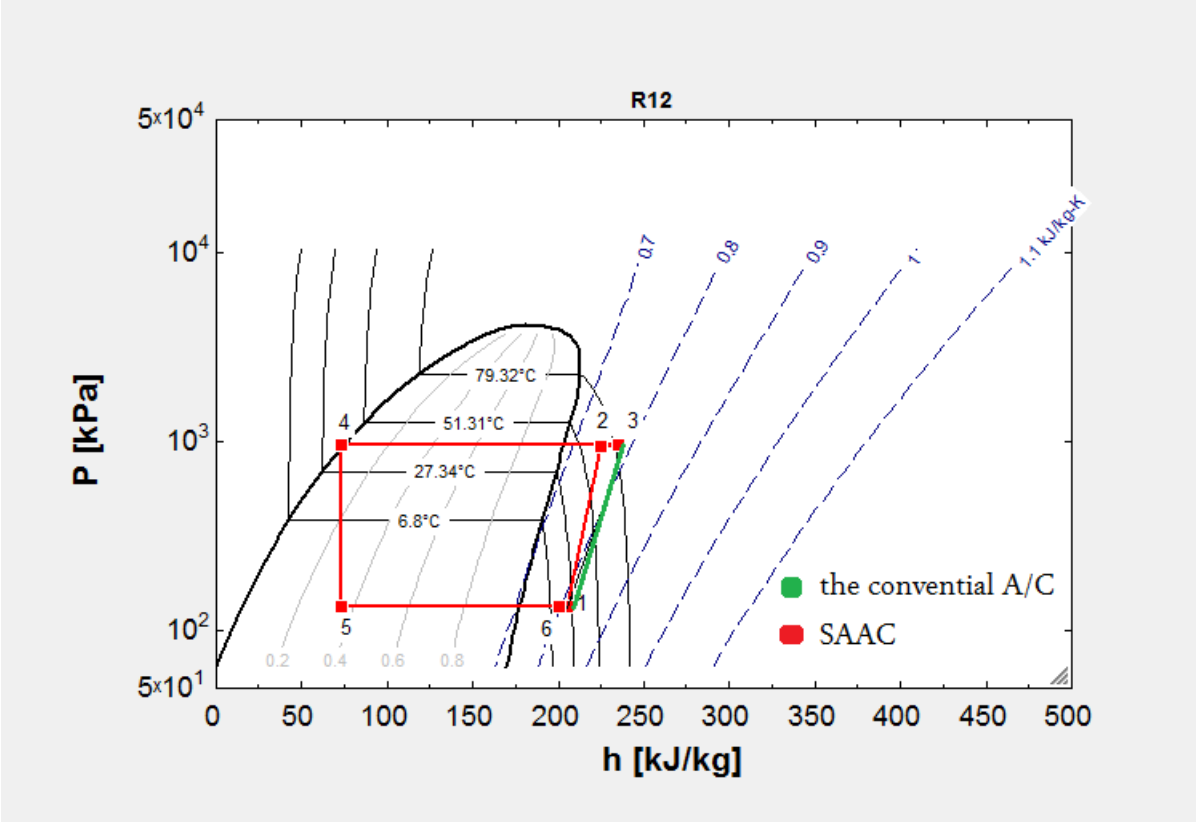

Figure 5. The P-h diagram of Solar Assisted air conditioning system

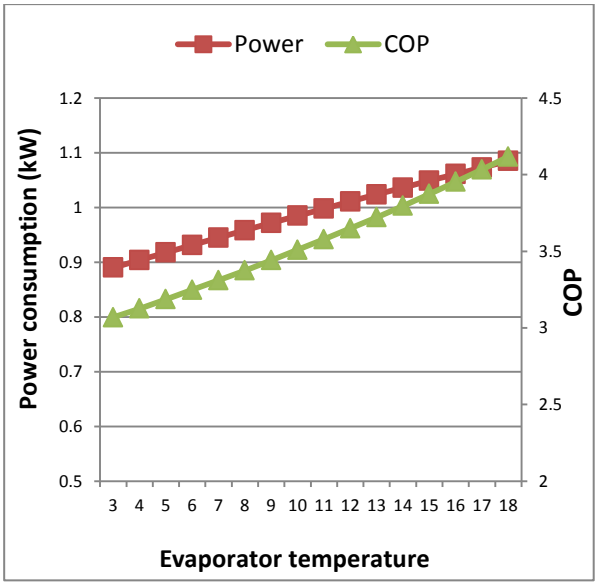

Figure 6. Variation of compressor power and COP with evaporator temperatures.

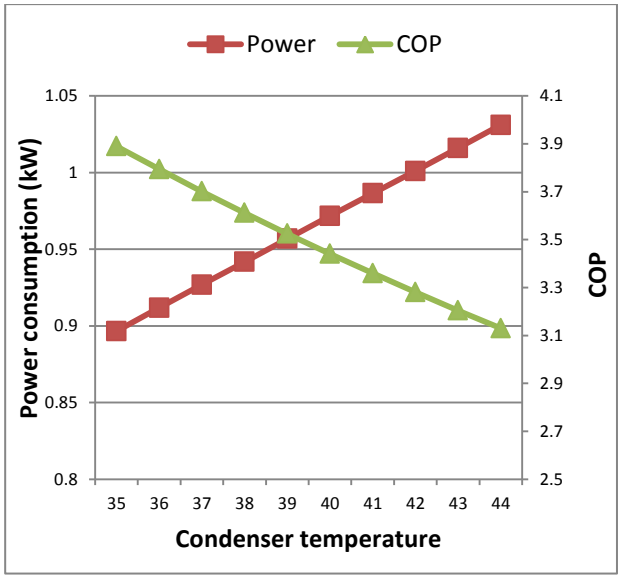

Figure 8. Variation of compressor power and COP with condensing temperatures.

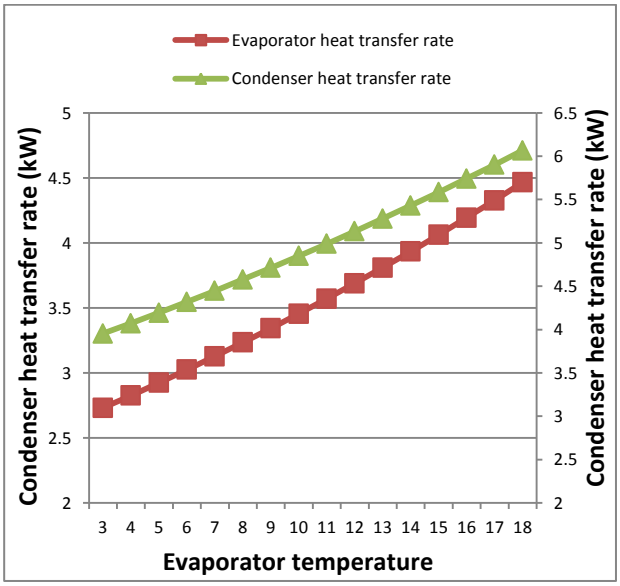

Figure 7. Variation of condenser heat transfer rate and cooling capacity with evaporator temperatures.

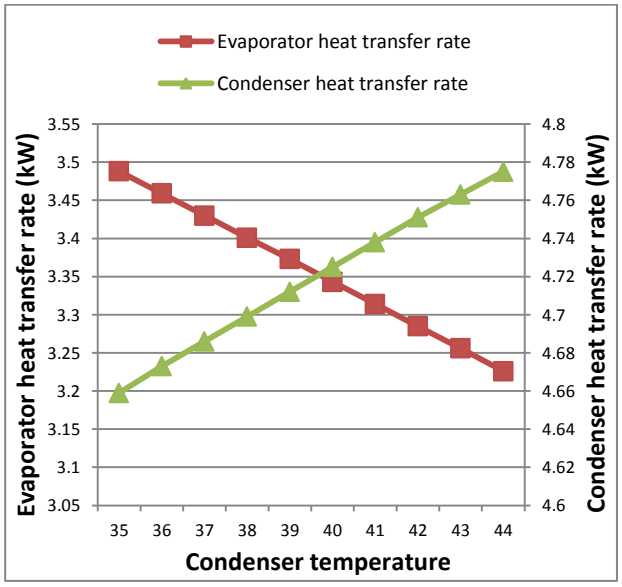

Figure 9. Variation of condenser heat transfer rate and cooling capacity with condensing temperatures.

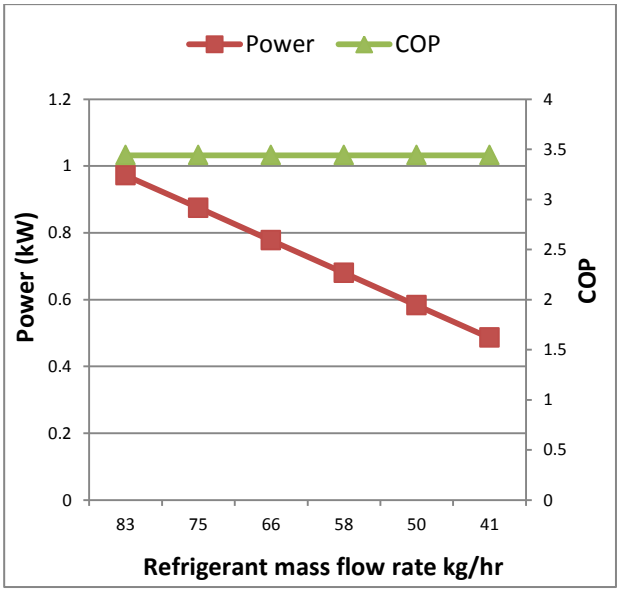

Figure 10.Variation of compressor power and COP with refrigerant mass flow rate.

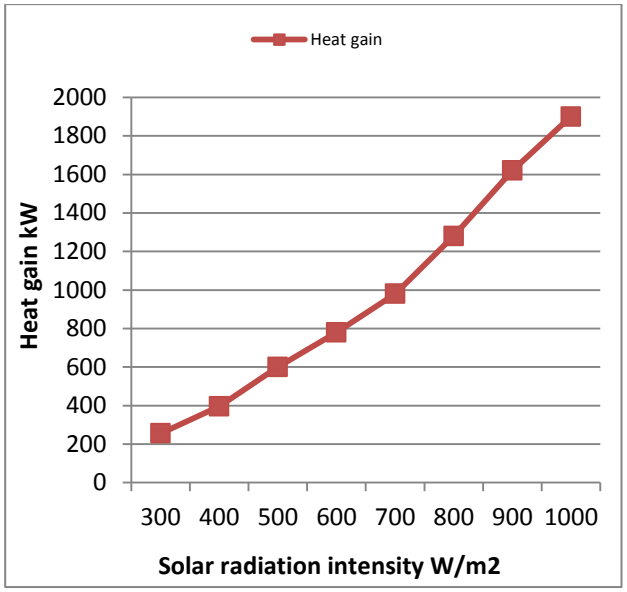

Figure 12. Variation of heat gain with solar radiation intensity.

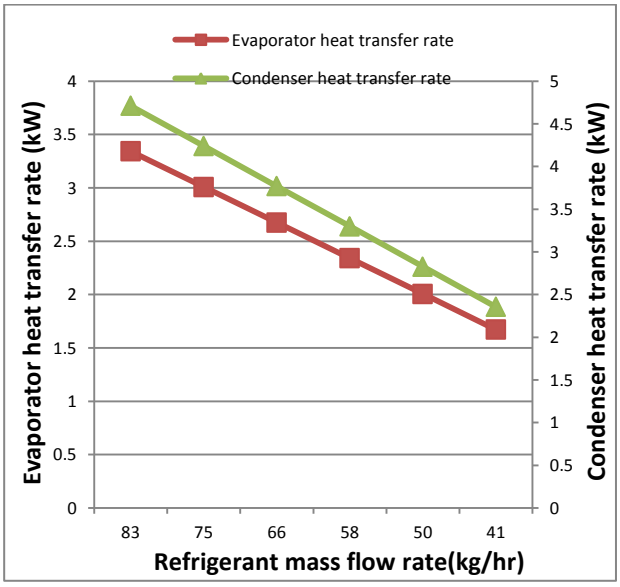

Figure 11. Variation of condenser heat transfer rate and cooling capacity with refrigerant mass flow rate.

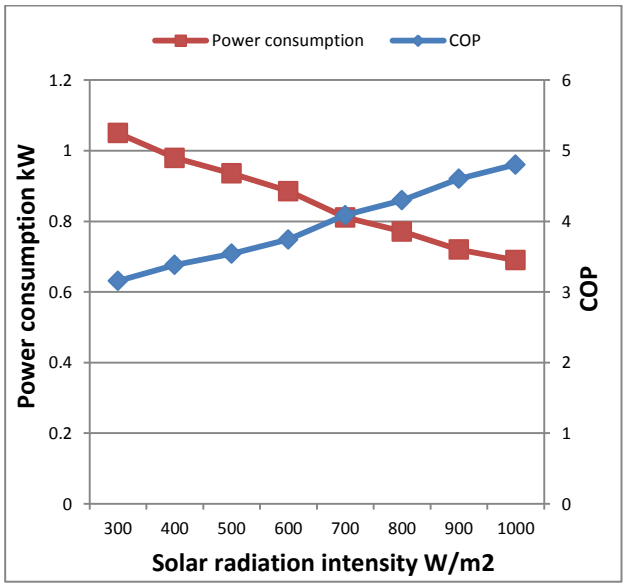

Figure 13. Variation of power consumption and thermal performance of the system with solar radiation intensity.

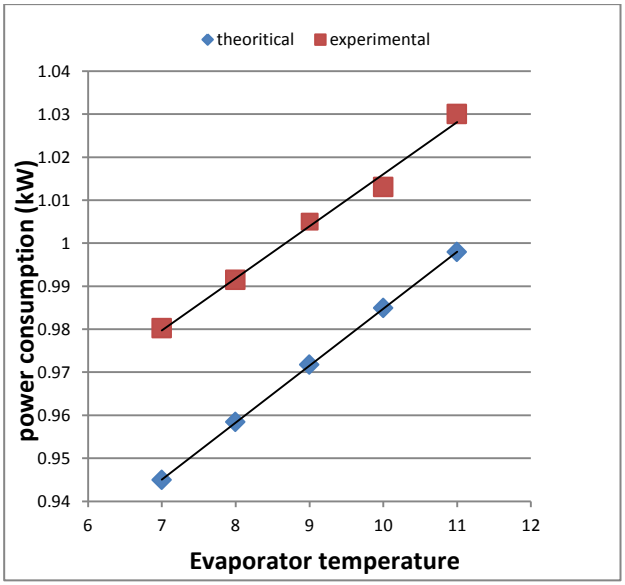

A. The power consumption

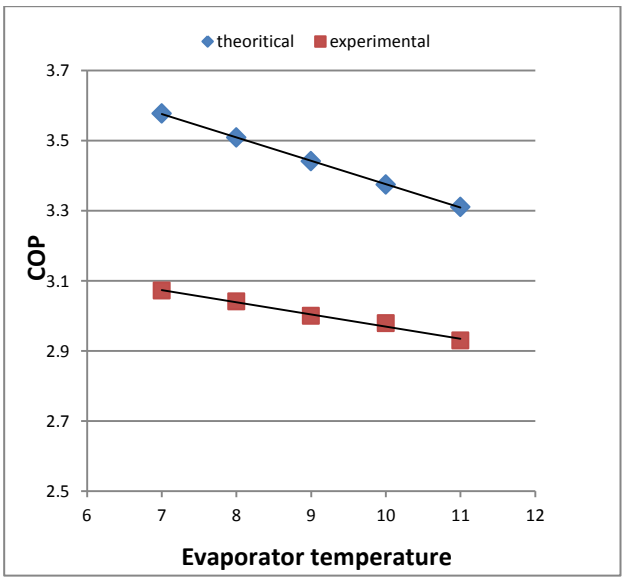

B. COP

Figure 14. Comparison between the experimental and theoretical regarding the influence of evaporator water temperature on: A. The power consumption B. COP

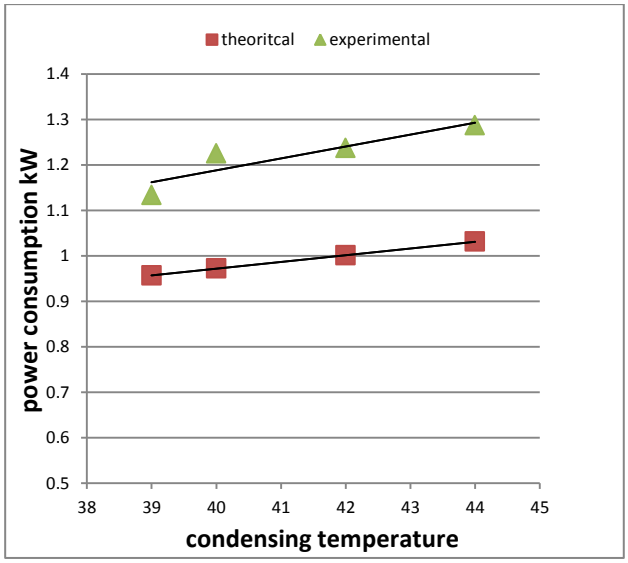

A. The power consumption

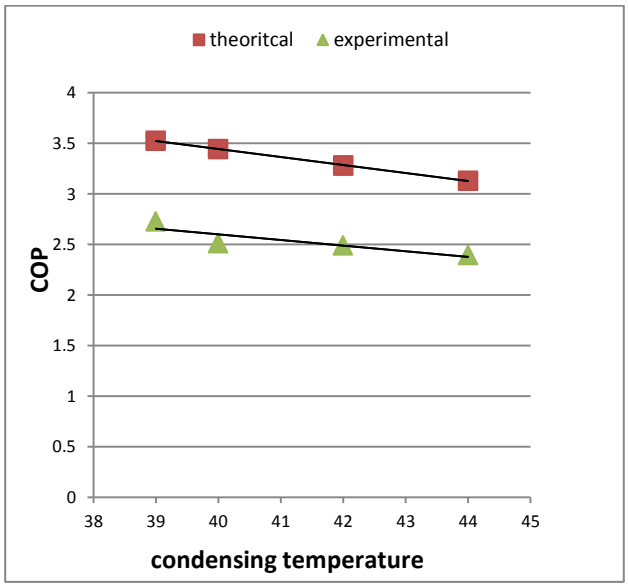

B.COP

Figure 15. Comparison between the experimental and theoretical regarding the influence of condensing temperature on: A. the power consumption B. COP

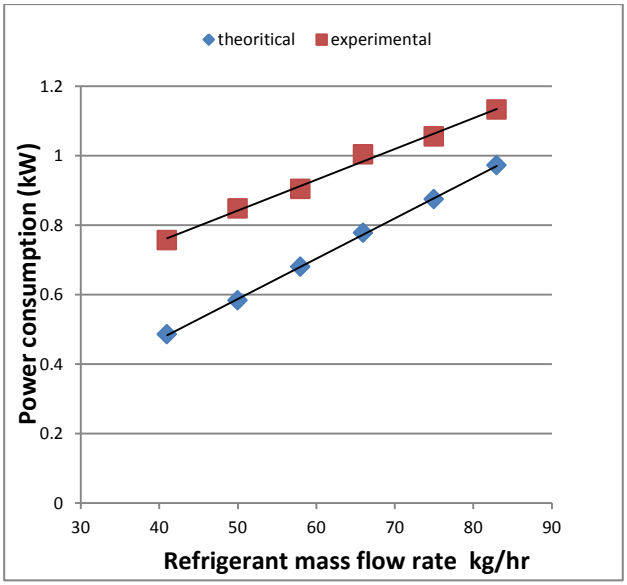

A. Power consumption

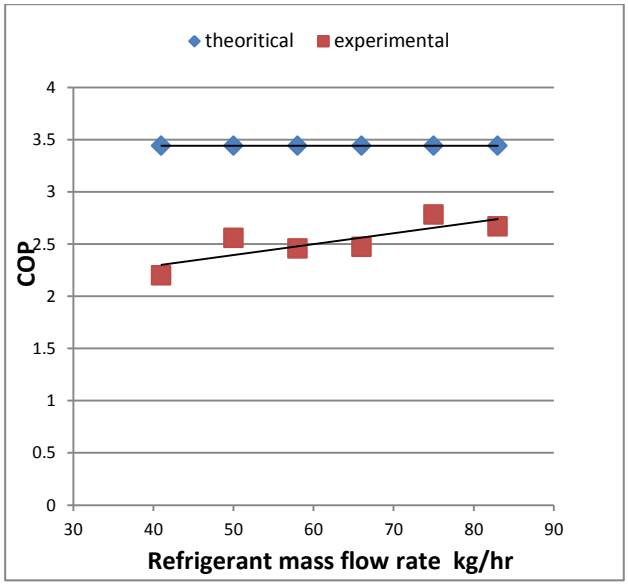

B. COP

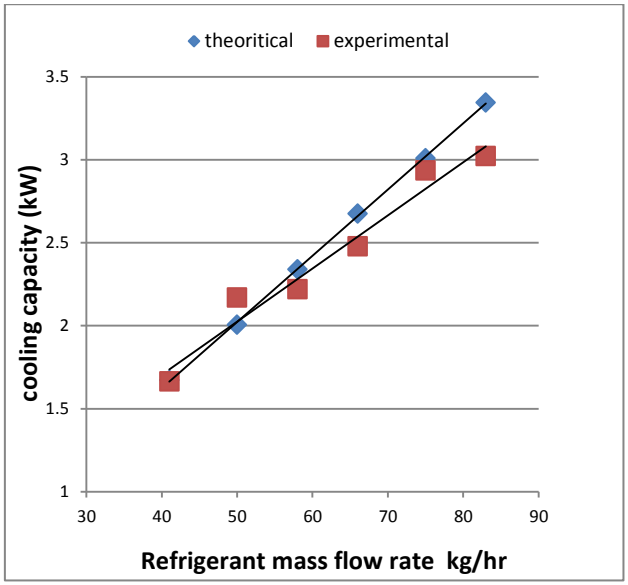

C. Cooling capacity

Figure 16. Comparison between the experimental and theoretical regarding the influence of refrigerant mass flow rate on: A. the power consumption B. COP c. the cooling capacity

Investigation of Factors Influencing Dispersion of Liquid Hydrocarbons in Porous Media

Hussain Ali Baker
Lecturer
College of Engineering-University of Baghdad
E-mail: ha.baker@yahoo.com

ABSTRACT

An experimental work has been done to study the major factors that affect the axial dispersion of some hydrocarbons during liquid-liquid miscible displacement. Kerosene and gas oil are used as displacing phase while seven liquid hydrocarbons of high purity represent the displaced phase, three of the liquids are aromatics and the rest are of paraffinic base. In conducting the experiments, two packed beds of different porosity and permeability are used as porous media.
The results showed that the displacement process is not a piston flow, breakthrough of displacing fluids are shown before one pore volume has been injected. The processes are stable with no evidence of viscous fingering.

Dispersion model as adapted by Brigham et.al (1961) is used to determine the axial dispersion coefficient of displacing fluid. The results show an increasing in dispersion coefficient as the interstitial velocity and viscosity ratio increases.

Key words: dispersion, viscosity ratio, interstitial velocity, axial

دراسة العوامل المؤثرة على تشتت الهيدروكاربونات السائلة في الوسط المسامي

حسين علي باقر
مدرس
كلية الهندسة-جامعة بغداد

الخلاصة

أجريت دراسة مختبرية لتحديد العوامل المؤثرة على تشتت بعض السوائل الهيدروكاربونية اثناء الازاحة الامتزاجية في الوسط المسامية.استخدم النفط الابيض وزيت الغاز كاطوار مزيحة وسبعة مركبات عالية النقاوة كاطوار مزاحة. اربع من هذه المركبات ذات اساس برافيني والثلاث المتبقية ذات اساس اروماتي.أجريت التجارب في وسطين مساميين ذوا قيم مختلفة للمسامية والنفاذية. اظهرت النتائج ان عملية الازاحة لاتحصل بشكل مكبسي بل يظهر اختراق للطور المزيح قبل حقن حجم مسامي واحد من ذلك الطور. كذلك بينت النتائج ان الازاحة كانت مستقرة ولايوجد دليل لحصول ظاهرة التصبع اللزج .تم حساب معامل التشتت ولوحظ زيادة في قيمة هذا المعامل بزيادة السرعة الموقعية للطور المزيح ونسبة اللزوجة بين الطور المزاح والطور المزيح.

الكلمات الرئيسية: التشتت. نسبة اللزوجة. السرعة الموقعية. المحوري.

1. INTRODUCTION

During miscible displacement a transition zone develops gradually across the sharp interface. The evolution of such zone is controlled by dispersion. Dispersion is described in terms of two components at right angel: 1-Axial dispersion. 2- Radial dispersion.
Dispersion occurs in ground water flow, chemical engineering processes and miscible displacement in enhanced oil recovery.
Von Rosenberg and **Baker** ,**1956**; **Handy**,**1959**; **Brigham et al**.,**1961**;**Perkins** and **Johnston**,**1963**; **Shengkai** and **Wojtanowicz**,**2008**; **Mostaghimi et al**.,**2010** and **Raman et al.,2011** studied dispersion mechanisms in porous media. The previous studies mostly depended on convection-dispersion equation:

$$\frac{\partial^2 c}{\partial x^2} - v\frac{\partial c}{\partial x} = \frac{\partial c}{\partial t} \quad (1)$$

Brigham, 1961 solved Eq.(1) to calculate the concentration of displacing fluid as given by Eq.(2)

$$c = \frac{1}{2} erfc\left[\frac{L.U}{2\sqrt{KTV_p}}\right] \quad (2)$$

Brigham 1961 showed that a graph of concentration of displacing fluid versus a volume modifying function U, on a probability paper yields a straight line and the dispersion coefficient K, can be determined as follows:

$$k = \frac{1}{v_p T}\left[l\frac{U_{90}-U_{10}}{3.625}\right]^2 \quad (3)$$

$$U = \frac{V_p - V_i}{\sqrt{V_i}} \quad (4)$$

2. EXPERIMENTAL APPARATUS AND TEST PROCEDURE

The equipment used to conduct the experiments is consisting of three sections. a- saturation-displacing section, this section consists of two positive displacement pumps (Ruska 2248). b- test section: two stainless-steel coils of 0.625 cm(ID) packed with glass beads of size range of 80-100 mesh as porous medium. Table 1 indicates the properties of test section. c- Concentration measurement instrument. **Fig.1** is a schematic diagram of experimental apparatus.

The testing procedures can be summarized as follows:

1- The coil is evacuated and then saturated with the desired displaced fluid.
2- The coil connected to displacing pump and the displacement process is stared with the desired flow rate.
3- The effluent sample is taken at each 0.026 of pore volume injected fore coil #1 and 0.0196 pore volume for #2.
4- The effluent is tested by Refractive index and the concentration of displacing fluid is measured, the measurements continued till the concentration become 100 % (vol/vol).

All measurements are conducted at constant temperature of 20^0 C.

3. MATERIALS USED

Kerosene and Gas oil are used as displacing fluid and seven hydrocarbon liquids of high purity (spectroscopic grade) are the displaced fluids. The properties of these fluids are given in table 2.

4. SCOPE OF THE EXPERIMENTS

Two sets of experiments have been conducted to evaluate the major factors that affect the dispersion during liquid-liquid miscible displacement. The total number of test is 103. During the first set of expriments, coil#1 represents the porous media and kerosene is the displacing fluid. The second is accomplished with coil#2 and gas oil as a displacing fluid. The concentration of kerosene and gas oil is measured by refractive index apparatus. Six flow rates were applied during the experiments which are 2.6, 5.2, 10.4, 20.8, 31, 2 and 41.6 cc/hr. The experiments covers a wide range of interstitial velocities (0.00554-0.1173 cm/sec) and viscosity ratios of (o.106-0.71).Table 3 is a sample of results for Q = 5.2 cc/hr. and kerosene as a displacing fluid.

5. RESULTS AND DISCUSSION

5.1. CONCENTRATION- TIME PROFILE

Fig.2 is a sample of displacing fluid concentration versus pore volume injected relationship. It can be considered as concentration-time profile. The main features of all concentration- pore volume injected are:

1- The transition zone between the displacing and displaced fluid follows the S-shape as the concentration increase from zero to 100%.This phenomena is attributed to continuous mixing rather than piston drive.
2- The 50% concentration of the displacing fluid corresponds to one pore volume injected.
3- The curve is symmetric around PV=1.

5.2 DETERMINATION OF DISPERSION COEFFICIENT

The volume modifying function U is calculated using Eq.(4) and correlated graphically with concentration of displacing fluid as illustrated in **Fig.3**. The dispersion coefficient is determined by Eq.(3).

5.3 EFFECT OF INTERSTITIAL VELOCITY

The results showed that dispersion coefficient increases as interstitial velocity increases due to increasing of mixing rate as viscosity ratio remain unchanged.

5.4 EFFECT OF VISCOSITY RATIO

The viscosity ratio is the ratio between viscosities of the displaced fluid to the displacing fluid. The results showed that the dispersion coefficient is influenced by this ratio. Table 4 and table 5 gave a clear ideas related to the effects of both viscosity ratio and interstitial velocity as represented by flow rates on dispersion coefficients

5.5 EFFECT OF HYDROCARBON TYPE

The results show an increase in magnitude of dispersion coefficients of both kerosene and gas oil as the molecular weight of displaced fluid of paraffinic base increase, same behavior does not appear for fluids of aromatic base.

6. CONCLUSIONS

1-Breakthrough of displacing fluid is shown before one pore volume is injected.

2-All runs result in breakthrough of 50% concentration of displacing fluid as one pore volume is injected.

3-The rate of mixing increases as the interstitial velocity of displacing fluid increases.

4-The dispersion coefficient is influenced by viscosity ratio.

REFERENCES

- Brigham W.E., Reed P.W., and Dew J.N., 1961, *Experiments on Mixing During Miscible Displacement*, Tran. AIME Vol.222.PP 1-8
- Handy L.L, 1959 , *An Evaluation of Diffusion effects in miscible displacement*, Tran. AIME Vol. 216 PP. 328-334
- Mostaghimi P, Bijeljic B, and Blunt M, 2010, *Simulation of Flow and Dispersion on Pore-Space Images*, SPE 135216.
- Perkins T.K., and Johnston O.C., 1963, *A Review of Diffusion and Dispersion in Porous Media*, SPEJ Vol.3 No.1 PP. 70-84
- Raman J K., Bryant S., Lake L.W, 2011, *Effect of Diffusion on Dispersion*, 115961-PA SPE Journal Paper – 2011
- Shengkai D., Wojtanowicz A.K. , 2008, *Theoretical and Experimental Investigation of Transverse Water in Oil Dispersion in Porous Media*, 115518-MS SPE Conference Paper – 2008.
- Von Rosenberg W.F., and Baker L.E., 1956, *Factors affecting miscible flooding dispersion coefficient*, A,I,Ch.E.J Vol.2 No.1 PP 55-58

NOMENCLATURE

C: Concentration of displacing fluid, Vol./Vol.

Erfc: Complementary Error Function.

K: Dispersion Coefficient, cm^2/s.

L: Length of Porous Media, cm.

Q: Flow Rate cc/hr.

T: Time Required to inject One Pore Volume.

T: time.

U: Volume Modifying Function,

V_i: Volume Injected, cc.

V_P: Pore volume cc.

Φ: Porosity, fraction.

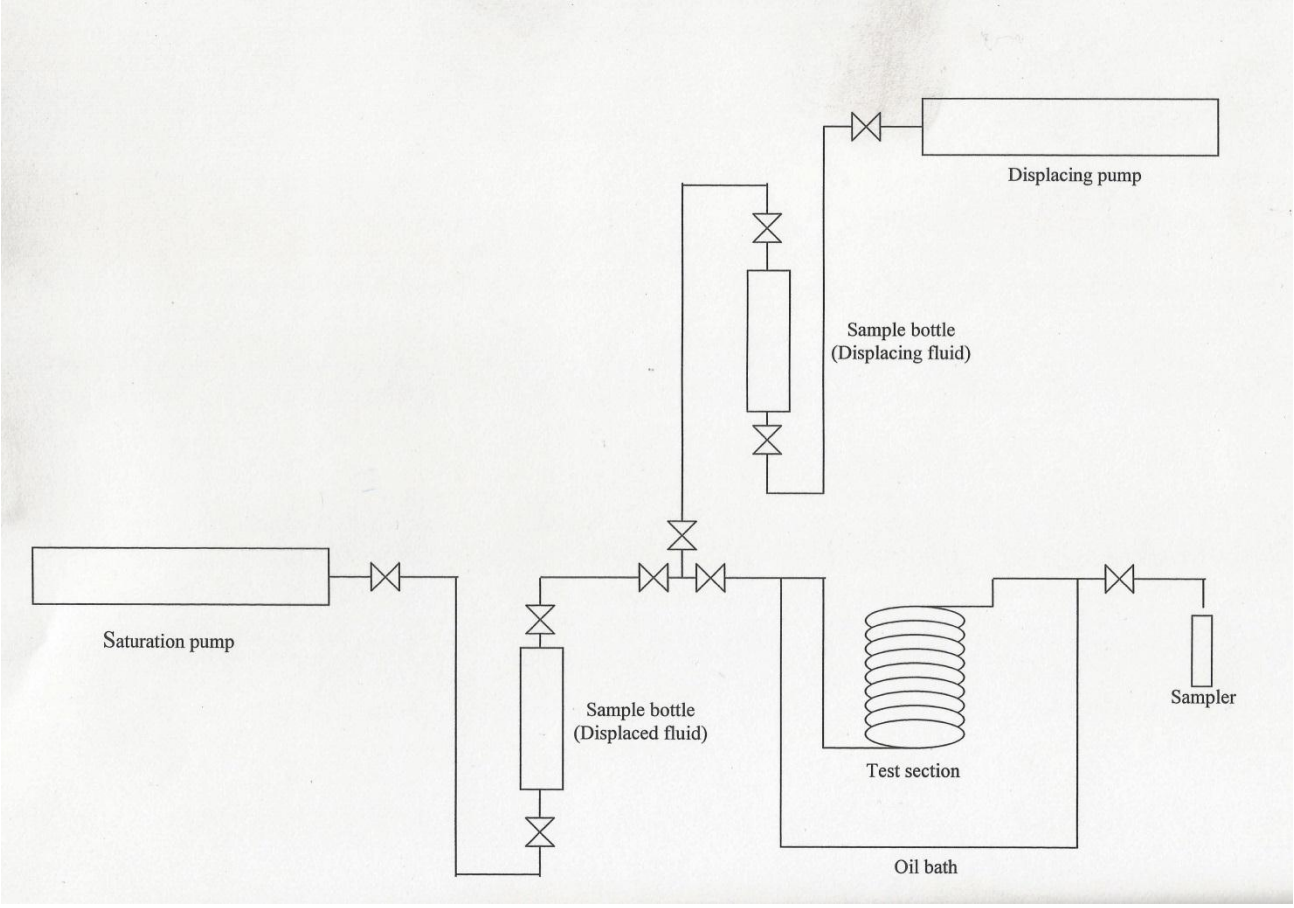

Figure 1. Schematic diagram of experimental apparatus.

Table 1. Properties of test-section

	length cm	Porosity Fraction	permeability Darcy	Pore volume cc
Coil #1	406	0.321	10	40
Coil #2	406	0.425	12	53

Table 2. Physical properties of displacing and displaced fluids at T= 20 ^{0}C.

Fluid	Dynamic Viscosity(Centi- Poise)	Refractive Index
Kerosene	1.281	1.44
Gas Oil	4.43	1.4737
n-Decane	0.91	1.411
n-Nonane	0.711	1.40561
Xylene	0.69	1.498
Benzene	0.652	1.5011
Toluene	0.59	1.497
Octane	0.542	1.39745
Heptane	0.409	1.38764

Table 3. Displacing fluid concentration (Coil #1,Q=5.2 cc/hr)

PV injected	U	Kerosene concentration(%) when the displaced fluid is						
		Heptane	Octane	n.Nonane	n.Decane	Benzene	Toluene	Xylene
0.6955	2.3092	0	0	0	0	0	0	0
0.7215	2.0736	0	0	0	0.5	0	0	0
0.7475	1.847	0	0	0.8	0.97	0.58	0	0.65
0.7735	1.6288	0	0	1.9	1.9	1.45	1	1.5
0.7995	1.4182	0.3	0.6	3	4	2.8	2.5	3.4
0.8255	1.2147	1.2	2	4.8	6.3	5.5	5	5.7
0.8515	1.0178	3	4	6.5	10	9.2	9	10
0.8775	0.827	5.9	7.65	11	15	15.1	15	16
0.9035	0.6421	11	13	17	20.9	22.8	22.15	23
0.9295	0.4625	19.1	21	24	28	31.9	30	32
0.9555	0.2879	29	30	32.4	35.25	41.95	41.8	42
0.9815	0.1181	42	41	42	44	53.4	52	54
1.0075	-0.0472	54.7	52.37	52	53.11	62	62	63
1.0335	-0.2084	66	63	62.1	61	72	71	72
1.0595	-0.3656	77.66	73	70	68.4	79	79.22	79.83
1.0855	-0.519	85	81.23	78	74	85.1	85.25	85.2
1.1115	-0.6689	90	88	84	80.6	90	90	90
1.1375	-0.8153	95	92	89	85.25	93.5	93.7	93.6
1.1635	-0.9586	97.8	95.6	93	89	96.2	96.45	96
1.1895	-1.0989	99	97.7	95	92	98	98.1	97.5
1.2155	-1.2362	99.5	99	96.6	94.5	99.2	99	99
1.2415	-1.3708	100	100	98.6	96.37	100	100	100
1.2675	-1.5027			99	97.5			
1.2935	-1.632			100	98.5			
1.3195	-1.759				99.3			
1.3455	-1.8838				100			

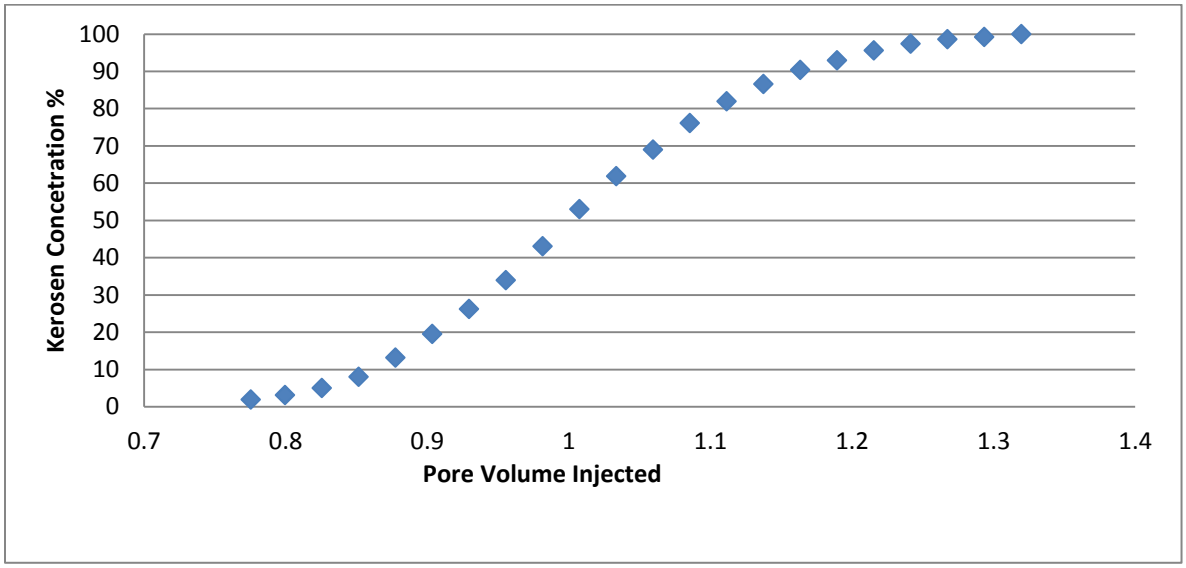

Figure 2. Kerosene concentration-pore volume injected(Coil #1-Displaced fluid n Decane – Q=2.6 cc/hr.)

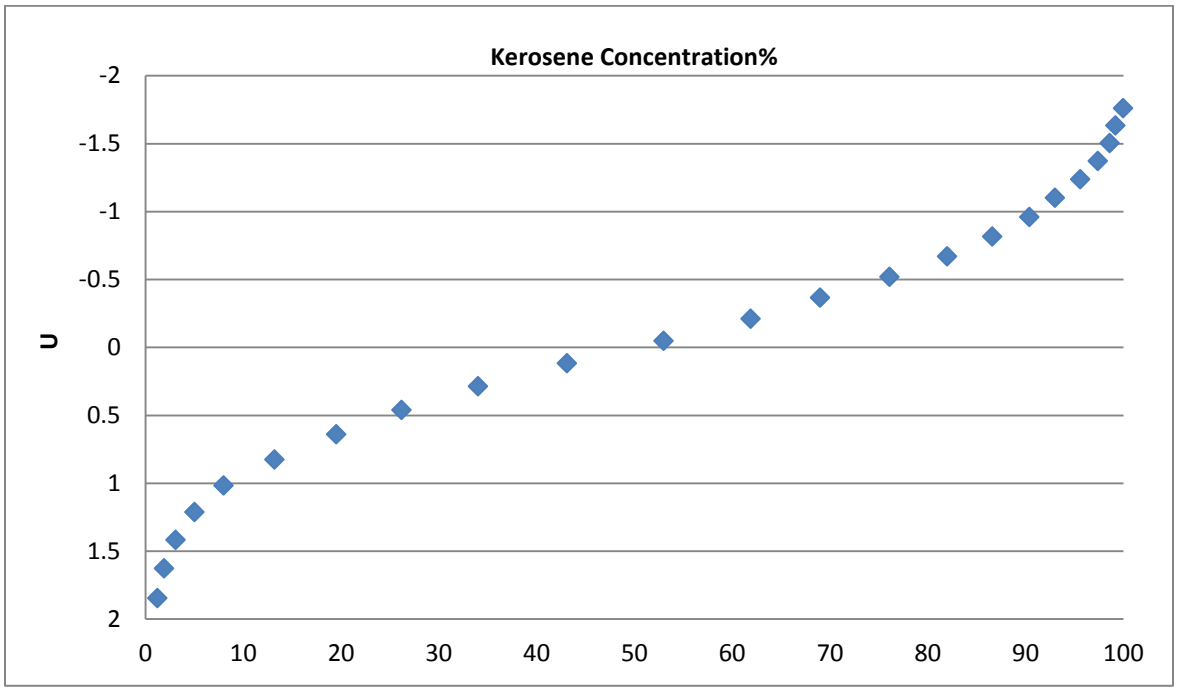

Figure 3. Volume modifying function versus kerosene concentration(coil#1,Q=2.6 cc/hr)

Table 4. Dispersion Coefficient of Kerosene (Coil#1)

Displaced Fluid	Viscosity Ratio	Dispersion Coefficient					
		Q=2.6 cc/hr	Q=5.2 cc/hr	Q=10.4 cc/hr	Q=20.8 cc/hr	Q=31.2 cc/hr	Q=41.6 cc/hr
Heptane	0.32	0.0089	0.0193	0.0416	0.0894	0.14	0.1923
Octane	0.423	0.012	0.025	0.057	0.118	0.1875	0.2621
n.Nonane	0.555	0.0157	0.0337	0.0726	0.156	0.2445	0.336
n.Decane	0.712	0.02	0.046	0.098	0.205	0.321	0.441
Benzene	0.509	0.0148	0.03	0.067	0.14	0.225	0.31
Toluene	0.46	0.0132	0.0284	0.0612	0.132	0.206	0.29
Xylene	0.538	0.015	0.031	0.071	0.15	0.2398	0.3295

Table 5. Dispersion Coefficient of Gas oil (Coil#1)

Displaced Fluid	Viscosity Ratio	Dispersion Coefficient				
		Q=2.6 cc/hr	Q=5.2 cc/hr	Q=10.4 cc/hr	Q=20.8 cc/hr	Q=31.2 cc/hr
Heptane	0.106	0.00303	0.00653	0.014	0.0302	0.0473
Octane	0.14	0.00398	0.00856	0.0184	0.0396	0.062
n.Nonane	0.1815	0.00513	0.011	0.0238	0.0511	0.08
n.Decane	0.24	0.00693	0.0149	0.032	0.07	0.1078
Benzene	0.1625	0.0046	0.01	0.0216	0.0464	0.0727
Toluene	0.1516	0.0043	0.0093	0.019	0.043	0.0673
Xylene	0.1758	0.005	0.0108	0.0232	0.049	0.0781

تحري العوامل المؤثرة على التخمين الاولي للكلف وتحليل العلاقة بينها باستخدام عملية التحليل الهرمي

د. أحمد محمد رؤوف محجوب
مدرس
جامعة بغداد/ كلية الهندسة

د. مرفت رزاق ولي
مدرس
جامعة بغداد/كلية الهندسة

هبه اكرم عطية
مدرس مساعد
الجامعة العراقية / كلية الهندسة

الخلاصة

تعتبر عملية تخمين الكلف واحدة من اهم الواجبات في ادارة المشاريع الانشائية حيث ان التخمين الدقيق لكلف الانشاء يؤثر على نجاح وجودة المشاريع الانشائية. ويعتبر التخمين الاولي مرحلة مهمة جدا لفريق المشروع لأنه يمثل أحد العناصر الرئيسية للمشروع، حيث أنه يساعد في صياغة أساس لاستراتيجيات وخطط التنفيذ للبناء والهندسة.

التخمين الاولي ، والذي يتم في مرحلة مبكرة، يقدر تكاليف البناء اعتمادا على الحد الأدنى لتفاصيل المشروع بحيث يعطي مؤشرا لمرحلة التصاميم الأولية للمشروع. يدرس هذا البحث العوامل التي تؤثر على التخمين الاولي للكلف فضلا عن العلاقة بين هذه العوامل باستخدام طريقة برنامج عملية التحليل الهرمي (AHP). تم استخراج الاستنتاجات والتوصيات النهائية لتحسين دقة التخمين الاولي في ادارة المشاريع.

الكلمات الرئيسية: - الكلفة ، التخمين، العوامل المؤثرة، عملية التحليل الهرمي

Exploring the Factors Affecting the Elemental Cost Estimation with Relationship Analysis Using AHP

Dr. Ahmed Mohammed Raoof Mahjoob
Instructor
Engineering College-Baghdad university
Mrahmed.civil@yahoo.com

Dr. Mervat Raziq Wali
Instructor
Engineering College-Baghdad university
Meervat 3@yahoo.com

Hiba Akram Atyah
Asst. Instructor
Engineering College-The Iraqi university
Hiba akrm @yahoo.com

ABSTRACT

Cost estimation is considered one of the important tasks in the construction projects management. The precise estimation of the construction cost affect on the success and quality of a construction project. Elemental estimation is considered a very important stage to the project team because it represents one of the key project elements. It helps in formulating the basis to strategies and execution plans for construction and engineering.

Elemental estimation, which in the early stage, estimates the construction costs depending on minimum details of the project so that it gives an indication for the initial design stage of a project. This paper studies the factors that affect the elemental cost estimation as well as the relation between these factors using Analytic Hierarchy Process (AHP) method. Final conclusions and recommendations were extracted for better elemental estimation accuracy in project management.

Key Words: - cost, estimation, affecting factors, AHP

المقدمة: –

تعتبر عملية التخمين الاولي للكلف ،التي تسبق عملية تقديم العطاءات، نقطة حاسمة في عملية التصميم والبناء. و تحدث هذه العملية في وقت مبكر بعد الاتصال الأولي مع صاحب العمل ، أو كجزء من عملية دراسة الجدوى أو بعد أول تصميم تصويري للمشروع يمثل الفكرة المطلوبة من قبل صاحب العمل.

تعتبر هذه المرحلة مهمة لأنها تحدد معايير التكلفة التي يجب أن تتفق مع التصميم المطلوب. فإذا كانت هذه المعايير غير صحيحة فان تقدير التكلفة قد يتجاوز الميزانية في مراحل لاحقة من مراحل المشروع إذا تم اكتشاف أن بعض عناصر التصميم اللازمة مفقودة في تقديرات المرحلة الاولية. اما المبالغة في تقدير التكلفة في مرحلة الاولية فإن هذا قد يعني أن المشروع قد لا يمضي قدما (Raisbeck and Aibinu 2010).

عادة يتم العمل على التخمين الاولي في مراحل التخطيط الأولى من المشروع المقترح لتتناسب مع احتياجات العملاء ومتطلبات البرامج المقررة، والقيود المفروضة على الميزانية من أجل تأسيس اطار وتوقعات جودة المشروع. تستخدم مقارنات التخمين في هذه المرحلة في تقييم جدوى البدائل الاستراتيجية التي يجري النظر فيها لتلبية متطلبات المساحة الحالية والمتوقعة (مثل، البناء الجديد مقابل التجديد، أو الإيجار) .

ان نجاح وجودة المشروع يعتمد على التخمين الدقيق للكلف حيث ان هذا التخمين هو أفضل مصدر للمعلومات حول اتخاذ قرار بشأن سعر لمشروع و يساعد على تخطيط وتنظيم عملية البناء بشكل صحيح. وعليه يجب ان تكون العوامل المؤثرة في اعداد هذا التخمين معرفة بشكل كامل للحصول على الدقة المطلوبة وتجنب الاخطاء التي قد تؤدي في بعض الاحيان الى فشل المشروع.

الدراسات السابقة: –

سوف يتم في هذا الجزء استعراض الدراسات والبحوث السابقة التي تناولت موضوع التخمين الاولي للكلف والتي تنوعت بين تحليل التخمين ل 181 مشروعا في سنغافورة حيث وجد الباحثون الغالبية العظمى من العوامل أثرت على دقة التخمين (Gunner. and Skitmore1999). وفي دراسة اخرى قام (Ling and Boo 2001) باستخدام بيانات من 42 مشروعا في سنغافورة وجدت نتائج مشابهة للدراسة الاولى. اما (Skitmore. and Picken 2000) درس تأثير أربعة عوامل مستقلة (نوع البناء، وحجم المشروع، قطاع المشاريع والسنة) على دقة التخمين واختبر الباحثان العوامل الأربعة باستخدام بيانات من 217 مشروعا في الولايات المتحدة الأمريكية . وفي دراسة اخرى قام (Oberlender and Trost 2001) بتحديد 45 عاملا من العوامل التي تسهم في دقة التخمين في المرحلة المبكرة

أهداف البحث: –

ان دقة تخمين التكاليف في وقت مبكر لمشاريع الهندسة والبناء مهمة لصاحب العمل وفريق المشروع للغاية. بالنسبة لصاحب العمل فان تخمين التكاليف المبكر أمر حيوي لاتخاذ قرارات الأعمال التي قد تشمل استراتيجيات الاستثمار، دراسة مشروع محتمل، و الموارد لتطوير مزيد من المشاريع. ان التخمين الأولي غير الدقيق يمكن أن يؤدي إلى إهدار الفرص، وضياع جهود التنمية ، وخفض العوائد المتوقعة. اما بالنسبة لفريق المشروع فغالبا ما يتم قياس الأداء ونجاح المشروع ككل من خلال مقدار التكلفة الفعلية مقارنة مع التكلفة التخمينية في وقت مبكر. غالبا ما يتوقع أن تتفق التخمين الأولي مع (أي تكون مساوية أو أقل من) التكلفة المستقبلية ،ومع ذلك، غالبا ما تتجاوز التكلفة النهائية التقديرات الأولية. وفي كثير من الأحيان ،هنالك تباين كبير عند المقارنة بين أهمية التخمين الأولي مع كمية المعلومات المتاحة عادة أثناء إعداد التخمين الاولي. وعليه فان هذا البحث يهدف الى ايجاد العوامل المؤثرة على التخمين الاولي للكلف وتحليل العلاقة بين هذه العناصر.

تعريف التخمين الاولي للكلف: –

اصبح من المهم في هذه المرحلة من البحث ان يكون هنالك تعريف واضح لمصطلح (التخمين الاولي للكلف). حيث ان كثير من البحوث تشير الى هذا المصطلح بـ (تقديرات أولية أو المفهومية، تخمين مبكر و تخمين التمويل الكامل). وبعد الكثير من النقاش والمداولة، خلص فريق البحث إلى أن كل شركة ومؤسسة لديها مجموعة من التعاريف والتسميات، بخصوص التخمين الأولي يتوافق مع التمويل الكامل في مراحل مختلفة من المشروع. فقد قدم (Serpell 2005) تعريفا لمرحلة التخمين المبكر للكلف على انه "التنبؤ من تكلفة المشروع خلال طور التخطيط التصميم".

اما (Oberlender and Trost 2001) فقد عرفا التخمين في وقت مبكر على انه " أي تقدير أعد من بداية المشروع وبما يصل إلى الموافقة على التمويل". اما (Oberlender 2000) فقد عرف التخمين المبكر بانه " التقدير الذي تم إعداده بعد دراسة وحدة العمل ولكن قبل الانتهاء من التصميم التفصيلي". وقد بين (Oberlender 2000) ان هنالك منظمات مختلفة قد عرفت تصنيفات لتخمين التكاليف. وكمثالين لهذه المنظمات تصنيف تخمين التكاليف من قبل الجمعية الدولية المتقدمة للتكلفة الهندسية (International Association for Advancement of Cost Engineering AACE) كما مبين في الشكل (1) ومعهد الصناعة الانشائية (Construction Industry Institute CII) وهو موضح في الشكل (2). بشكل عام، يتم تعريف التخمين الاولي على انه التخمين الذي أعد قبل الانتهاء من الأعمال الهندسية التفصيلية. وينطبق هذا التعريف على الدرجة 5، الدرجة 4، والدرجة الأولى 3 لتصنيف (AACE) الدولية. وينطبق هذا التعريف أيضا على (order–of–magnitude) ايضا على (factored estimates) الموصوفة في المنشورات (CII).

منهجية البحث : –

لغرض الوصول الى الاهداف المرجوة ، فقد تم تقسيم منهجية البحث الى ثلاثة اجزاء رئيسية

اولا : جمع وتصنيف العوامل المؤثرة على التخمين الاولي للكلف

تم انجاز هذا الجزء من خلال مراجعة البحوث والدراسات السابقة للتعرف على اهم العوامل المؤثرة التي تم جمعها من قبل الباحثين وتصنيفها الى مجموعات بحسب العلاقة بينها. فقد تم جمع (50) عاملا مختلفا من البحوث لكل من (Oberlender and Trost 2001), (Gunner and Skitmore1999), (Ling and Boo 2001), (Skitmore. and Picken 2000) و(Bhattad and Jain 2015) . ومن ثم تم تصنيفها الى اربعة محاور اساسية

ثانيا: أيجاد الاهمية النسبية لكل عامل

ولغرض انجاز هذا الجزء فقد تم اجراء استبيان مغلق يتضمن العوامل التي تم جمعها لغرض ايجاد الاهمية النسبية لكل عامل. تم اعتماد وزن افتراضي لكل عامل على مقياس اهمية ليكرت الخماسي الذي يتكون (1– 5)، وتم ايجاد الاهمية النسبية لكل عامل باستخدام المعادلة الاتية:

$$RI = \frac{\sum(fi * W)}{N}$$

حيث ان: –

RI= الاهمية النسبية لكل عامل

W= درجة تقيم الاجابة لفقرة الاستبيان (1– 5)

fi= تكرار الاجابة لفقرة الاستبيان

N= حجم عينة الاستبيان

شملت عينة الاستبيان (35) مهندسا من ذوي الخبرة ومن مختلف الاختصاصات. وبعد اجراء التحليل الاحصائي تم ايجاد الاهمية النسبية (RI) لكل عامل ضمن المحاور الرئيسية الاربعة ومن ثم اعادة ترتيب العوامل تنازليا ضمن كل فقرة. بعد الانتهاء من ترتيب العوامل المؤثرة تنازليا تم استبعاد العوامل التي حصلت على اهمية نسبية اقل من المتوسط (3) وكانت المحصلة النهائية الحصول على (38) عاملا مؤثرا على التخمين الاولي لكلف المشاريع الانشائية وكما مبين في الجدول (1).

ثالثا أجراء عملية التحليل الهرمي

تعد عملية التحليل الهرمي (AHP) إحدى الأساليب المعتمدة في اتخاذ القرارات التي تعتمد (Multi Attribute Decision Method –MADM) وفق معايير متعددة. ويمكن من خلالها وصف شكل تحديد المعايير الاساسية والمفاضلة بينها بوصفها مشكلة اتخاذ قرار متعدد المعايير. وبصفة عامة توجد خطوات اساسية لاستخدام هذا التحليل وهي :-

1- تعريف المشكلة والمعايير المؤثرة عليها وبدائلها المقترحة.

2- وجود مقارنة ثنائية بين المعايير الاساسية والمعايير الفرعية مع بعضها البعض وذلك بإيجاد وزنها نسبة للهدف.

3- اخذ رأي من الخبراء من خلال تحديدهم للأهمية النسبية الموضحة في الجدول(2) واخذ المتوسط الهندسي لكل مقارنة بين معياريين.

4- اجراء التحقق من نسبة الاتساق والتي يجب ان لا تزيد عن 10%.

5- ترتيب المعايير فيما بينها من خلال استخدام اوزان المعايير .

لغرض اجراء عملية التحليل الهرمي تم اجراء استبيان ثاني، تم فيه توزيع استمارة الاستبيان على مجموعة من الخبراء (33 مستبين) من اجل التعرف على مؤشر الأهمية لكافة العوامل قيد الدراسة, وفيما يلي اهم مراحل استخدام نظرية التحليل الهرمي للحالة التطبيقية :

المرحلة الاولى:- مرحلة تكوين الهرم الذي يضم الهدف الاساسي من التحليل مع تحديد اهم العوامل المؤثرة على ذلك الهدف وتحديد استمارة الاستبيان الخاصة بالتحليل الهرمي .ونتيجة للآراء والاجوبة الموجودة في الاستبيان تم الحصول على الشكل الهرمي المطلوب لاختيار العوامل الرئيسية في عملية التحليل.

المستوى الاول: الهدف المتمثل في اختيار العوامل المؤثرة على كلف التخمين المبكر للمشاريع الانشائية.

المستوى الثاني: المحاور الاساسية المؤثرة على كلف التخمين المبكر للمشاريع الانشائية.

المستوى الثالث: المعايير وهي المستخلصة من المحاور الاساسية المؤثرة في المستوى الثاني.

تم اعتماد تصنيف المحاور الاساسية المؤثرة على كلف التخمين المبكر للمشاريع الانشائية المبينة في الجدول رقم (1) وكما يلي:

1-العوامل المؤثرة في كيفية أعداد التخمين

2- تأثير المعلومات المتوفره عن المشروع على التخمين المبكر للكلف

3- تأثير العوامل التي تؤخذ في الاعتبار عند اعداد التقديرات على التخمين المبكر للكلف.

4- تأثير المشتركين في أعداد التخمين على التخمين المبكر للكلف.

قام فريق البحث بتطبيق نموذج التحليل الهرمي باستخدام برنامج Super Decision من خلال (WWW. Super Decision.com) لاستخدام نموذج المقارنة الثنائية النسبية لمعرفة الاهمية الخاصة بكل عنصر في كل مستوى.. وتمت هيكلة النموذج من خلال البرنامج بما يلي:

1-تكوين الشكل الهرمي من خلال تحليل المشكلة الى عناصر

2-جمع بيانات المسح الخاصة بالمقارنات الثنائية من خلال ايجاد الوسط الهندسي لكافة القيم وادخالها في المقارنات الثنائية بالبرنامج,

3-يقوم البرنامج بعمل المصفوفة وحساب قيمة ايجن لحساب الاولويات من المصفوفة الناتجة والتحقق من نسبة االاتساق المطلوبة لنجاح المقارنة الثنائية ،بمعنى عدم وجود تناقض في اراء عينة الاستبيان وهذه النسبة يجب ان لا تتعدى 10%.

وبعد اكمال هذه الاجراءات تم الحصول على النتائج التالية:

- الشكل الهرمي للتحليل الشبكي وكما مبين في الشكل رقم (3)
- المقارنات الثنائية بين المحاور الرئيسية الاربعة والهدف الرئيسي وكما مبين في الشكل رقم (4)
- المقارنات الثنائية بين المعايير الموجودة في هذه المحاور والهدف وكما مبين في الشكل رقم (5)
- مصفوفة المعايير المتعددة : حيث تم تقييم وحساب وتحليل الأولويات التي تبين العلاقة بين العوامل وذلك من اجل تحديد أهميتها النسبية إلى الهدف وكما مبين في الشكل رقم (6).
- مصفوفة المعايير الثانوية : حيث تم تقييم وحساب وتحليل الأولويات التي تبين العلاقة بين المعايير الخاصة بكل عامل على حدا وذلك من اجل تحديد أهميتها النسبية إلى الهدف وكما مبين في الشكل رقم (7) للمحور الاول كنموذج عام .
- نتائج المسح الخاص بالمقارنات الثنائية للعوامل الرئيسية واستعراض للأوليات الخاصة بها وكما مبين في الشكل رقم (8)
- الاولويات النهائية لكافة المعايير الموجودة في المحاور الرئيسية الاربعة وكما مبين في الشكل رقم (9)

مناقشة النتائج: -

بعد اكمال نتائج عملية التحليل الهرمي... توصل فريق البحث الى النقاط التالية :-

1. إن نتائج مقارنة الأهمية النسبية لمعرفة العوامل المؤثرة في التخمين المبكر تعتمد بصورة اكبر على العوامل المؤثرة على كيفية اعداد التخمين حيث بلغت مقدار اهميتها 52.25% تليها العوامل التي تؤخذ بالاعتبار عند اعداد التقديرات على التخمين المبكر وبلغت اهميتها بحدود 25,8% .اما تاثير المعلومات المتوفرة عن المشروع فبلغت اهميتها بحدود 14.95%. اما عامل تاثير المشتركين في اعداد التخمين فقد بلغت اهميته بحدود 6.97% وهي اهمية ضئيلة لاتتجاوز 13.35% من الاهمية الكلية ويعتقد الباحثان ان هذه الاهمية مناسبة لهذا المعيار الرئيسي لانه اغلب المشاركين في عمليات التخمين هم من المهندسين والمختصين بعمليات التخمين.النتائج موضحة في الجدول (3) .
2. اتفقت أغلبية أراء أفراد العينة المعتمدة في الاستبيان على ان العوامل المؤثرة على كيفية اعداد التخمين تحتل اهمية عالية ووضحت العينة ان الاجراء القياسي لتحديد المعلومات والطريقة القياسية المستخدمة في اعداد التقديرات تشكلان اهمية كبيرة في هذا المحور وحازت كل منهما على اهمية مقدارها 26.98% و 22.25% على التوالي .. اما باقي المعايير الفرعية فقد تقاسمت الاهمية فيما بينها وكما موضحة في االجدول(5) .

3. وبخصوص العوامل التي تؤخذ بالاعتبار عند اعداد التقديرات على التخمين المبكر الإنشاء التي جاءت بالمركز الثاني نظرا لاهميتها .فقد اتفقت العينة ان الخدمات اللوجستية للهندسة والانشاءات لها اهميه كبيرة بحدود 32.38% تليها العوامل المالية التي كانت اهميتها بحدود 18.13% تليها القوة العاملة بحدود 12.23% وتستمر باقي المعايير الثانوية تساوية في الاهمية وكما مبينة في الجدول(5).
4. واتضح من خلال إجابات أفراد العينة إن محور تاثير المعلومات المتوفرة عن المشروع جاء في الاهمية الثالثة وتحديد استراتيجية المشروع والتقييم البيئي لهما اهمية كبرى في هذا المحور وبنسب مقدارها 24.05% و20.35% على التوالي تليها التكنولوجيا المستخدمة وباهمية مقدارها 14.5% لتتساوى المعايير الثانوية الاخرى بالاهمية وكما موضحة في الجدول(6) .
5. اما المحور الاخير الذي حار على اهمية ضئيلة بحدود 6.97% من الاهمية الكلية الخاص بتاثير المشتركين في اعداد التخمين. فقد بينت النتائج في الجدول(7) ان الخبرة السابقة لفريق التخمين لها اهمية كبيرة تعادل 32.68% تليها اهمية الغرض من اعداد التخمين وبنسبة 20.16% ويتساوى المعيارين الفرعيين الخاص بتاثير الاطراف الاخرى وتكامل وانسجام فريق التخمين باهمية مقاربة الى 12.5% تقريبا لكل منهما.وتتدرج الاهمية الاخرى لباقي المعايير الثانوية من مراجعة وقبول التخمين بنسبة 9.15% الى اقل اهمية للمعيار الخاص بوجهة النظر حيال التغييرات الذي اعطته العينة مقدار اهمية 2.1% تقريبا.

الاستنتاجات

1- تبين لفريق البحث من خلال مقابلات العينة و نتائج البحث إن أسلوب التحليل الهرمي AHP هو من الأساليب المهمة في تقدير العوامل المؤثرة في عملية التخمين المبكر وذلك من خلال إجراء المقارنات الزوجية بين هذه المحاور الرئيسية المؤثرة.
2- عدم وجود دراسات محلية حديثة تسعى لتحقيق المتطلبات المؤثرة الحقيقية على عملية التخمين المبكر ، على الرغم من اهميتها الحقيقية في تخمين الكلفة والوقت.
3- التأكيد على الاهتمام بالعوامل التي حصلت درجة اهمية عالية عند اجراء التخمين الاولي للكلف من خلال نشر نتائج هذا البحث كواقع حال لقطاع الانشاء العراقي.
4- ضرورة مواكبة ادوات التحليل الادارية الحديثة وخاصة تقنية التحليل الهرمي AHP والتحليل الشبكي ANP , للاستفادة منها في ومساعدة متخذي القرار والباحثين في مجال التحليل الاداري.

REFERENCES

- Bhattad Parag R. and Jain R. K. 2015) "An Assessment of Factors Affecting the Accuracy of an Early Cost Estimate for Repetitive Projects" International Journal of Science and Research, Volume 4 Issue 4, April.

- Gunner, J. and Skitmore, M. (1999) "Comparative analysis of pre-bid forecasting of building prices based on Singapore data ". Construction Management and Economics **17**, 635- 646.

- Ling, Y. Y. and Boo, J. H. S. (2001) "Improving the accuracy of approximate estimates of building estimates". Building Research and Information, **29**(4), 312-318.

- Oberlender Garold D. (2000) "PROJECT MANAGEMENT FOR ENGINEERING AND CONSTRUCTION" McGraw -Hill Higher Education, second Edition.

- Oberlender Garold D. and Steven M. Trost, (2001) "PREDICTING ACCURACY OF EARLY COST ESTIMATES BASED ON ESTIMATE QUALITY" Journal of Construction Engineering and Management, Vol. 127, No. 3, May/June, ASCE.

- Raisbeck, P and Aibinu, A A (2010) "Early stage cost estimation and the relationship of architects to quantity surveyors". In: Egbu, C. (Ed) Procs 26th Annual ARCOM Conference, 6-8 September 2010, Leeds, UK, Association of Researchers in Construction Management, 53-61.

- Serpell, A. F. (2005) "Improving conceptual cost estimating performance". AACE International Transactions EST.13: EST.13.1-13.6.

- Skitmore, R. M. and Picken, D. (2000) "The accuracy of pre-tender building price forecasts: an analysis of USA data". Australian Institute of Quantity Surveyors Refereed Journal, **4**(1), 33 -39.

Estimate class	Level of project definition	End usage (Typical purpose of estimate)	Expected accuracy range
Class 5	0% to 2%	Concept Screening	−50% to 100%
Class 4	1% to 5%	Study or Feasibility	−30% to +50%
Class 3	10% to 40%	Budget, Authorization, or Control	−20% to +30%
Class 2	30% to 70%	Control or Bid/Tender	−15% to +20%
Class 1	50% to 100%	Check Estimate or Bid/Tender	−10% to +15%

شكل (1) تصنيف تخمين التكاليف من قبل الجمعية الدولية المتقدمة للتكلفة الهندسية (AACE)

Estimate class	Percent range	Description/methodology
Order-of-Magnitude	+/−30 to 50%	Feasibility study—cost/capacity curves
Factored Estimate	+/−25 to 30%	Major equipment—factors applied for costs
Control Estimate	+/−10 to 15%	Quantities from mech/elect/civil drawings
Detailed or Definitive	+/−<10%	Based on detailed drawings

شكل (2) تصنيف تخمين التكاليف من قبل معهد الصناعة الانشائية (CII)

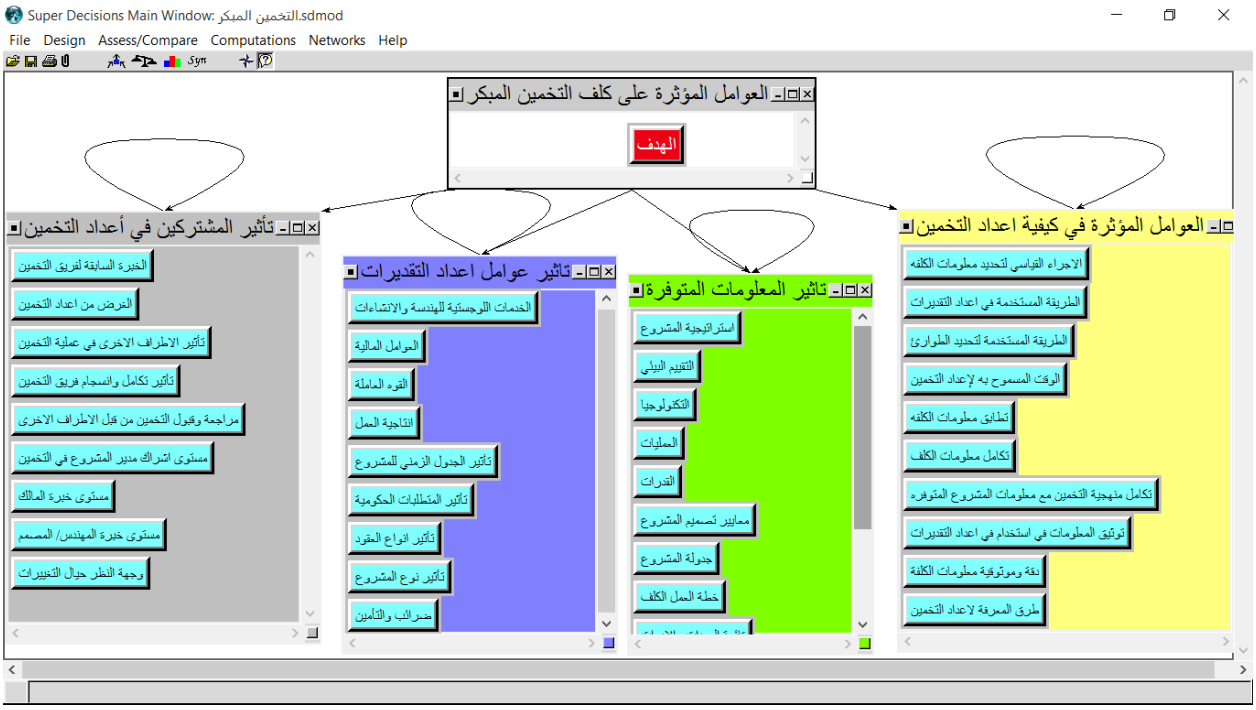

شكل (3) الشكل الهرمي للتحليل الشبكي

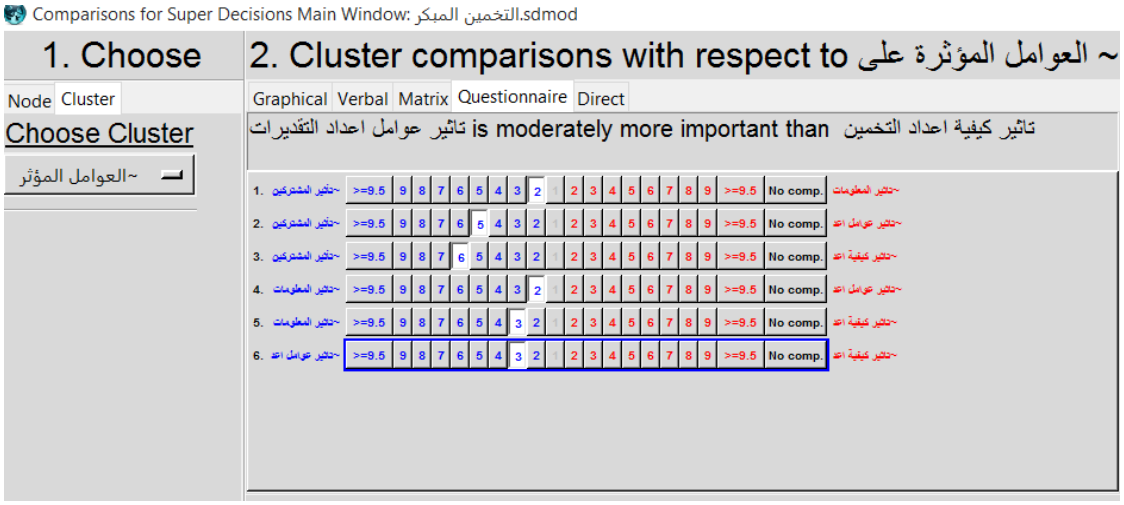

شكل (4) المقارنات الثنائية بين المحاور الرئيسية والهدف الرئيسي

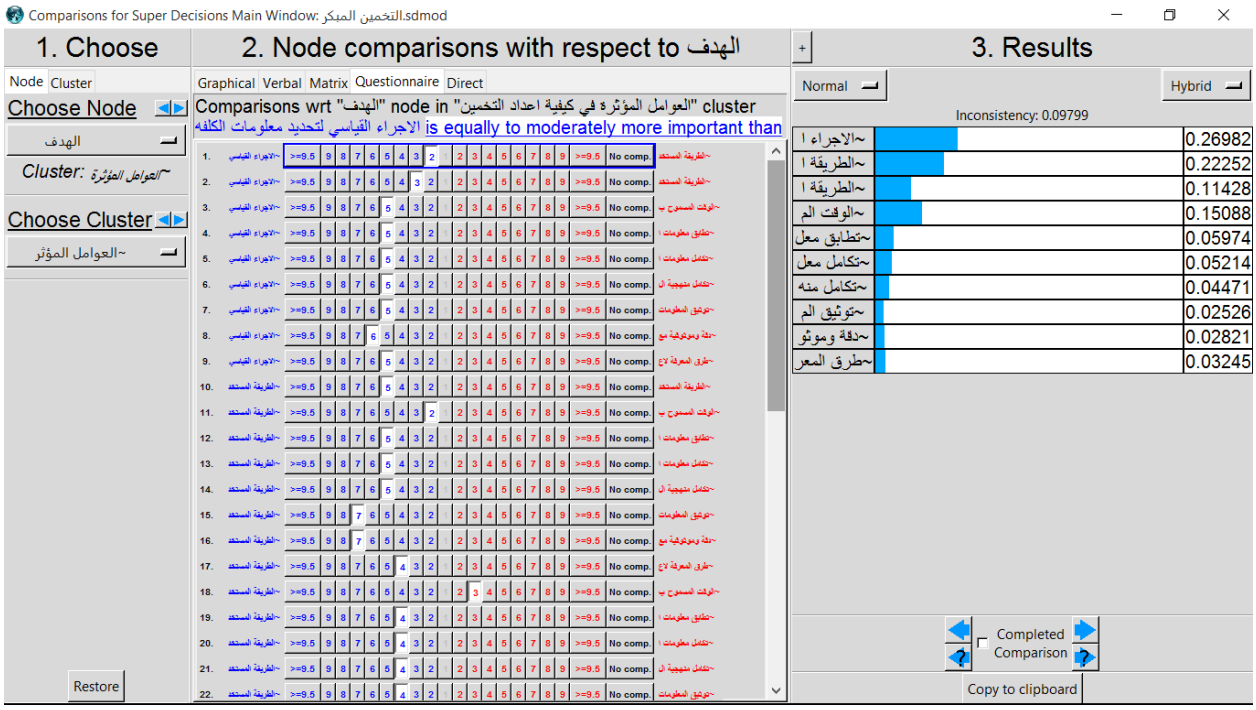

شكل (5) المقارنات الثنائية بين المعايير الموجودة في المحور الاول والهدف(مثال)

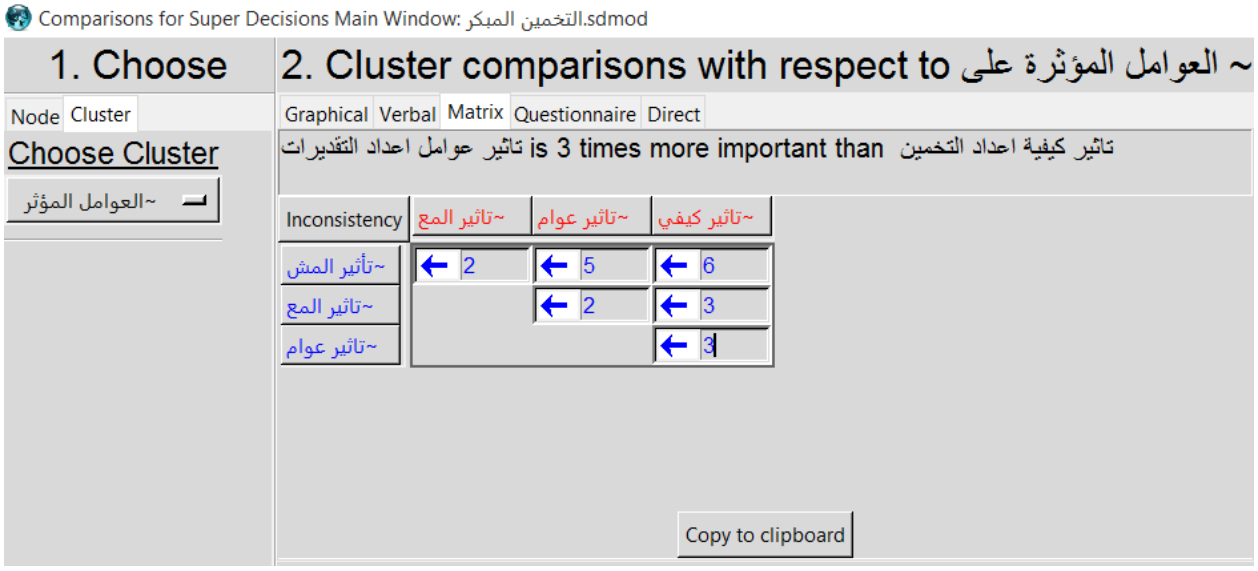

شكل (6) مصفوفة المعايير المتعددة

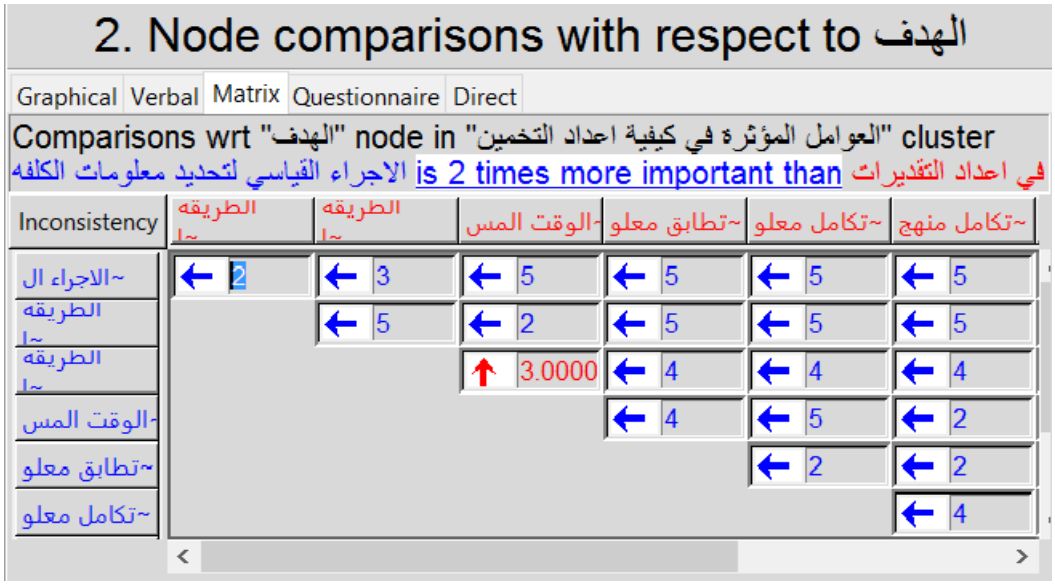

شكل (7) مصفوفة المعايير الثانوية في المحور الاول(مثال)

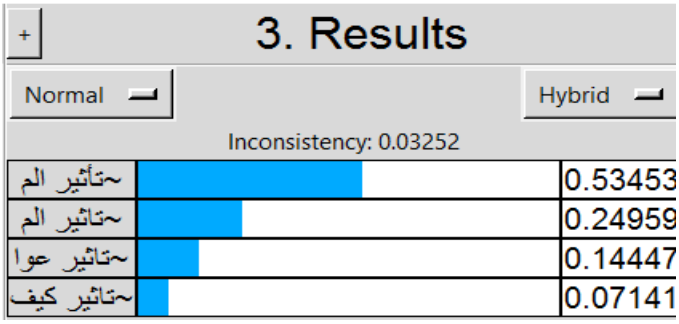

شكل (8) نتائج المسح الخاص بالمقارنات الثنائية للمحاور الرئيسية الاربعة

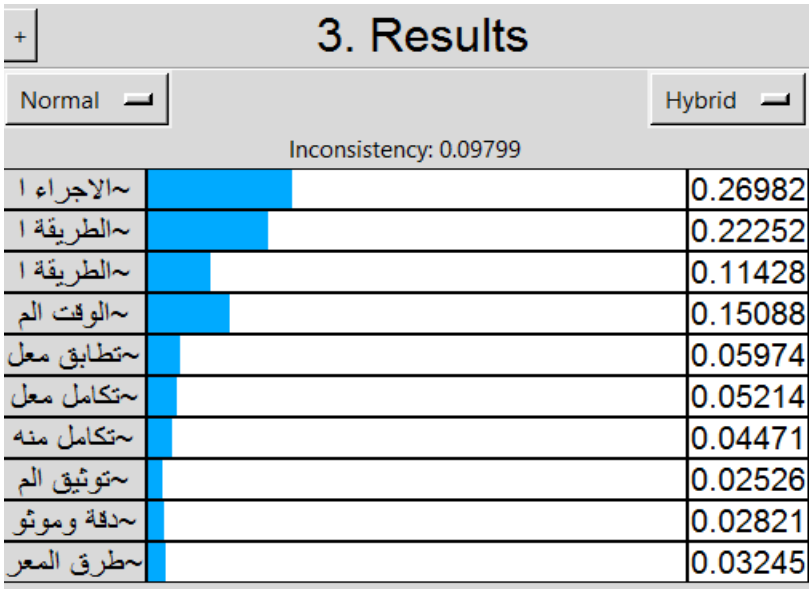

شكل (9) الاولويات النهائية للمعايير الثانوية الموجودة في المحور الاول

جدول (1) العوامل المؤثرة على التخمين الاولي للكلف

المحاور	تأثير كيفية أعداد التخمين	المعلومات المتوفره عن المشروع	أعداد التقديرات على التخمين المبكر للكلف	تأثير المشتركين في أعداد التخمين
-1	تكامل معلومات الكلف	خطة العمل الكلف	العوامل المالية	الخبرة السابقة لفريق التخمين
-2	تطابق معلومات الكلفه	جدولة المشروع	تأثير الجدول الزمني للمشروع	مستوى اشراك مدير المشروع في التخمين
-3	الاجراء القياسي لتحديد معلومات الكلفه	استراتيجية المشروع	تأثير انواع العقود	تأثير الاطراف الاخرى في عملية التخمين
-4	تكامل منهجية التخمين مع معلومات المشروع المتوفره	معايير تصميم المشروع	تأثير المتطلبات الحكومية	مراجعة وقبول التخمين من قبل الاطراف الاخرى
-5	الوقت المسموح به لإعداد التخمين	القدرات	القوه العاملة	تأثير تكامل وانسجام فريق التخمين
-6	دقة وموثوقية معلومات الكلفة	التكنولوجيا	انتاجية العمل	الغرض من اعداد التخمين
-7	الطريقة المستخدمة في اعداد التقديرات	العمليات	تأثير نوع المشروع	مستوى خبرة المالك
-8	توثيق المعلومات في استخدام في اعداد التقديرات	موقع العمل	ضرائب والتأمين	مستوى خبرة المهندس/ المصمم
-9	الطريقة المستخدمة لتحديد الطوارئ	مصادر المنفعة وحالة العرض	الخدمات اللوجستية للهندسة والانشاءات	وجهة النظر حيال التغييرات
-10	طرق المعرفة لاعداد التخمين	مخطط الاجهزة		
-11		التقييم البيئي		
-12		قائمة المعدات والادوات		

الجدول(2) المقياس الأساسي للمقارنات الثنائية

1	متساويان في الأهمية	يساهم النشاطان بنفس مقدار الاهمية للهدف
3	أهمية معتدلة	تفضيل احد النشاطين على الآخر بدرجة بسيطة
5	أهمية كبيرة	تفضيل احد النشاطين بقوة كبيرة على الآخر
7	أهمية كبيرة جدا	تفضيل احد النشاطين بقوة على الآخر بدرجة كبيرة
9	أهمية قصوى	بيان تفضيل احد النشاطين على الأخر ليمثل أعلى
2،4،6،8	اهمية وسطية	تستخدم عند الحاجة لها في المقارنة
مقلوب القيم اعلاه	إذا كان احد النشاطين له إحدى القيم الصحيحة أعلاه ، حينئذ يأخذ النشاط الاخر مقلوب تلك القيمة	لزوم إجراء مقارنة باختيار أصغر العناصر كوحدة لتقدير العناصر الأكبر باعتبارها ضعف تلك الوحدة

الجدول(3) نتائج الاولوية للمحاور الاساسية الاربعة

Name	Normalized	Idealized
العوامل المؤثرة في كيفية اعداد التخمين	0.522468	1
تاثير عوامل اعداد التقديرات	0.25825	0.494289
تاثير المعلومات المتوفرة	0.149483	0.286109
تأثير المشتركين في أعداد التخمين	0.069799	0.133594

الجدول(4) نتائج الاولوية للمعايير الثانوية الخاصة بالمحور الاول(العوامل المؤثرة في كيفية أعداد التخمين)

المعايير الفرعية	Normalized	Idealized
الاجراء القياسي لتحديد معلومات الكلفه	0.269824	1
الطريقة المستخدمة في اعداد التقديرات	0.222516	0.824673
الطريقة المستخدمة لتحديد الطوارئ	0.114281	0.423539
الوقت المسموح به لإعداد التخمين	0.150881	0.559183
تطابق معلومات الكلفه	0.059742	0.221412
تكامل معلومات الكلف	0.052136	0.193223
تكامل منهجية التخمين مع معلومات المشروع المتوفره	0.044706	0.165684
توثيق المعلومات في استخدام في اعداد التقديرات	0.025256	0.0936
دقة وموثوقية معلومات الكلفة	0.028209	0.104546
طرق المعرفة لاعداد التخمين	0.03245	0.120262

الجدول(5) نتائج الاولوية للمعايير الثانوية الخاصة بالمحورالثالث (أعداد التقديرات على التخمين المبكر للكلف)

Name	Normalized	Idealized
الخدمات اللوجستية للهندسة والانشاءات	0.323877	1
العوامل المالية	0.181356	0.559954
القوه العاملة	0.122301	0.377618
انتاجية العمل	0.0903	0.27881
تأثير الجدول الزمني للمشروع	0.101861	0.314507
تأثير المتطلبات الحكومية	0.080757	0.249344
تأثير انواع العقود	0.048394	0.149422
تأثير نوع المشروع	0.030896	0.095394
ضرائب والتأمين	0.020258	0.062547

الجدول(6) نتائج الاولوية للمعايير الثانوية الخاصة بالمحور الثاني (المعلومات المتوفره عن المشروع)

Name	Normalized	Idealized
استراتيجية المشروع	0.24052	1
التقييم البيئي	0.203595	0.846476
التكنولوجيا	0.145002	0.602869
العمليات	0.058554	0.243445
القدرات	0.080595	0.335084
جدولة المشروع	0.088186	0.366647
خطة العمل الكلف	0.044907	0.186708
قائمة المعدات والادوات	0.034133	0.141912
مخطط الاجهزة	0.038965	0.162002
مصادر المنفعة وحالة العرض	0.019942	0.08291
معايير تصميم المشروع	0.024736	0.102844
موقع العمل	0.020866	0.086753

الجدول(7) نتائج الاولوية للمعايير الثانوية الخاصة بالمحورالرابع (تأثير المشتركين في أعداد التخمين)

Name	Normalized	Idealized
الخبرة السابقة لفريق التخمين	0.3268	1
الغرض من اعداد التخمين	0.20159	0.616861
تأثير الاطراف الاخرى في عملية التخمين	0.126031	0.385653
تأثير تكامل وانسجام فريق التخمين	0.124839	0.382005
مراجعة وقبول التخمين من قبل الاطراف الاخرى	0.091519	0.280047
مستوى اشراك مدير المشروع في التخمين	0.051196	0.156659
مستوى خبرة المالك	0.03423	0.104744
مستوى خبرة المهندس/ المصمم	0.022733	0.069561
وجهة النظر حيال التغييرات	0.021062	0.06445